



# New bio-based polyesters useful in food packaging : synthesis, thermal, mechanical and transport properties

Xuelian Liu

## ► To cite this version:

Xuelian Liu. New bio-based polyesters useful in food packaging : synthesis, thermal, mechanical and transport properties. Polymers. Normandie Université, 2021. English. NNT : 2021NORMIR03 . tel-03510205

**HAL Id: tel-03510205**

**<https://theses.hal.science/tel-03510205>**

Submitted on 4 Jan 2022

**HAL** is a multi-disciplinary open access archive for the deposit and dissemination of scientific research documents, whether they are published or not. The documents may come from teaching and research institutions in France or abroad, or from public or private research centers.

L'archive ouverte pluridisciplinaire **HAL**, est destinée au dépôt et à la diffusion de documents scientifiques de niveau recherche, publiés ou non, émanant des établissements d'enseignement et de recherche français ou étrangers, des laboratoires publics ou privés.



Normandie Université

# THESE

Pour obtenir le diplôme de doctorat

**Chimie**

Préparée au sein de L'Institut National des Sciences Appliquées Rouen Normandie

## New Bio-based Polyesters Useful in Food Packaging: Synthesis, Thermal, Mechanical and Transport Properties

Présentée et soutenue par  
**Xuelian LIU**

Thèse soutenue publiquement le 9 avril 2021  
devant le jury composé de

Mme Nathalie GONTARD	Directeur de Recherche, Université de Montpellier, INRA	Rapporteur
Mme Sophie GUILLAUME	Directeur de Recherche, Université de Rennes 1, ISCR	Rapporteur
M Stéphane BRUZAUD	Professeur des Universités, Université de Bretagne-Sud, IRDL	Examineur
M Nicolas DESILLES	Maître de Conférences, INSA Rouen Normandie, PBS	Directeur de thèse
M Laurent LEBRUN	Professeur des Universités, Université de Rouen Normandie, PBS	Co-directeur de thèse

Thèse dirigée par Nicolas DESILLES et Laurent LEBRUN, Laboratoire  
Polymères, Biopolymères, Surfaces UMR6270



Polymères  
Biopolymères  
Surfaces  
UMR 6270





## Acknowledgments

My sincere acknowledgment would be first conveyed to the China Scholarship Council (CSC) for its financial support of my life in France.

It is also my honor to thank Ms. Nathalie GONTARD (research director of INRA, University of Montpellier) and Ms. Sophie GUILLAUME (research director of ISCR, University of Rennes 1), for accepting as reporters and spending their precious time on reviewing this work.

I would like to extend my gratitude to Mr. Stéphane BRUZAUD (professor, University of Bretagne-Sud), for being the president of the Jury and accessing my defense.

My heartfelt gratitude would be expressed to my two supervisors Mr. Nicolas DESILLES (assistant professor, INSA Rouen Normandie) and Mr. Laurent LEBRUN (professor, University of Rouen Normandie), whose encouragement, guidance, and support from the initial to the final level enabled me to develop an understanding of this subject. Without them, it would not have been possible to complete this project and this thesis. I enjoyed my three and half years of Ph.D. work under their supervision. I also appreciate their kindness and patience during each discussion, especially their patience with my French, certainly, without them, I would not have been progressed so much in my French. Besides, I would like to thank them for offering me not only scientific but also life suggestions.

I wish to express my appreciation to Ms. Kateryna FATYEYeva for the water permeation measurements and to Ms. Corinne CHAPPEY for gas permeation measurements. The same thanks to Ms. Nadège FOLLAIN for helping with the DVS measurements and data processing. Thanks also go to Mr. Stephane MARAIS for polarizing optical microscopy instructions and his kindly discussion about permeation results. Likewise, thanks would be conveyed to Ms. Laurence LECAMP for the guidance of the MS-TGA measurement and to Mr. Nasreddine KÉBIR for the tuition of contact angle measurement. Equally, my gratitude would be expressed to Catherine LEGRAND, Jérémy DESHAIS, Fabien BOUST, Christine DEVOUGE-BOYER and Murielle HIBLOT for their help in the lab, and especially Catherine, who is so kind to me and shows so much patience to talk with me in French and helps me a lot.

It is also my pleasure to thank all the permanents from the PBS laboratory, especially those from teams MM and MPBM, for whom supported me in any respect during the



## Acknowledgments

---

completion of this Ph.D. project: Fabrice BUREL, Gaëlle MORANDI, Daniela VULUGA-LEGROS, Boulos YOUSSEF, Louise HESPEL.

I would also like to thank all my colleagues in MM and MPBM for the daily discussions and their friendship: Amelie MARTIN, Assala SAMAD, Bassidi DIAWARA, Cyrielle IBANEZ, Duc-Trung TRAN, Guillaume Le CRAS, Guillaume BRETEL, Julien BOUILLON, Ludovic GEELHAND De MERXEM, Pi  re BOISAUBERT, Ghislain RABODON, S  bastien VOTAT, Yevhenii PRYKHODKO. And super thanks to Alice GONTIER, Naila BOU HAIDAR, Quentin LOZAY, Vincent GONNOT, Vincent VALETTE, Yaroslav KOBZAR, Yuzhen LOU, Klara JASTAK, Di WANG, who have brought me happiness inside and outside the lab as I worked on this thesis. Particularly, Yuzhen who kept me company from the beginning to the end and worked me through many problems.

I am grateful for the life joy in France from my friends: Jundong WANG, Jie XU, Jing ZHANG, Liwen CHEN, Pan XIAO, Xiaojia LU, Xuefei WANG, Yanjun WANG. Especially the happiness and support that I have received from my best friend: Yanan WANG.

I would also like to thank my master supervisor Mr. Sheng Zhang (director of CFMS, Beijing University of Chemical Technology) for his continuous attention to my research work and my life.

My deepest gratitude would be expressed to my family, especially, my dear father, life would not be so wonderful without his support and love.

Finally, unique thanks to Bo JIANG, my future lifemate, for sticking with me through every hardship and sharing with me every sweet moment.

*The best preparation for tomorrow is doing your best today.*

**To my precious memory**

## Publications

- P1      **Xuelian LIU**, Nicolas DESILLES, Laurent LEBRUN. Polyesters from renewable 1, 4: 3, 6-dianhydrohexitols for food packaging: synthesis, thermal, mechanical and barrier properties [J]. European Polymer Journal, 2020: 109846.
- P2      **Xuelian LIU**, Nicolas DESILLES, Laurent LEBRUN. Fully bio-based polyesters involving 2,6-pyridinedicarbonyl structure (In preparation)
- P3      **Xuelian LIU**, Nicolas DESILLES, Laurent LEBRUN. Tg-tunable aliphatic-aromatic copolyesters from renewable isosorbide, sebacic acid and 2,6-pyridinedicarboxylic acid (In preparation)
- P4      **Xuelian LIU**, Nicolas DESILLES, Laurent LEBRUN. 1,4:3,6-dianhydroxitols based aliphatic-aliphatic/aromatic copolyesters: synthesis, thermal, mechanical and barrier properties (In preparation)
- P5      **Xuelian LIU**, Nicolas DESILLES, Laurent LEBRUN. New bio-based polyesters containing 2,6-pyridine moiety with excellent gas barrier properties (In preparation)
- P6      **Xuelian LIU**, Nicolas DESILLES, Laurent LEBRUN. Copolyesters derived from 2,6-pyridinedicarbonyl: synthesis, thermal, mechanical and permeation properties (In preparation)

## Oral Communications

- C1      1,4:3,6-Dianhydrohexitols based polyesters useful for food packaging: synthesis, thermal, mechanical and transport properties  
**Xuelian LIU**, Nicolas DESILLES, Laurent LEBRUN  
40èmes journées GFP Grand-Ouest-Orléans, 23-24 May 2019
- C2      Bio-based polyesters for food packaging: synthesis, thermal, mechanical and permeation properties  
**Laurent LEBRUN**, **Xuelian LIU**, Nicolas DESILLES  
BIOPOL-2019, Stockholm, 17th-19th June 2019

## Poster

- Bio-based polyesters used in food packaging: synthesis and characterizations  
**Xuelian LIU**, Nicolas DESILLES, Laurent LEBRUN, Fabrice BUREL, Stephane MARIS  
Journée de l'Ecole Doctorale Normande de Chimie, Caen, 5 July 2019



## Table of contents

<b>Acknowledgments.....</b>	<b>I</b>
<b>Publications.....</b>	<b>III</b>
<b>Table of Contents .....</b>	<b>V</b>
<b>List of Abbreviations.....</b>	<b>IX</b>
<b>Chemical structures of acronyms .....</b>	<b>XIII</b>
<b>List of Figures.....</b>	<b>XV</b>
<b>List of Schemes .....</b>	<b>XIX</b>
<b>List of Tables.....</b>	<b>XXI</b>
<b>Résumé de la Thèse en Français .....</b>	<b>XXV</b>
<b>General Introduction .....</b>	<b>1</b>
<b>Chapter 1: Overview of bio-based food packaging polymers .....</b>	<b>7</b>
1.1 Definition of food packaging.....	9
1.2 Function of food packaging.....	9
1.3 Classification of food packaging materials .....	9
1.4 Plastic food packaging materials .....	10
1.5 Bio-based food packaging plastics .....	11
1.5.1 Polysaccharides .....	12
1.5.2 Proteins.....	15
1.5.3 Bio-based polyolefins.....	16
1.5.4 Bio-based polyesters .....	17
1.6 New trends in bio-based polyesters for food packaging.....	23
1.6.1 1,4:3,6-dianhydrohexitols as platforms for bio-based polyesters .....	24
1.6.2 Pyridinedicarboxylic acids as platforms for bio-based polyesters.....	30
1.7 Polymerization methods .....	33
1.8 General properties required for food packaging polyesters.....	35
1.8.1 Thermal properties .....	35
1.8.2 Mechanical properties .....	36
1.8.3 Permeation properties.....	37
1.9 Bio-based polyesters for food packaging: opportunities and challenges .....	46
1.9.1 Challenges.....	46
1.9.2 Opportunities.....	46
References .....	47
<b>Chapter 2: 1,4:3,6-dianhydrohexitols based aliphatic polyesters .....</b>	<b>63</b>

## Table of Contents

2.1	Synthesis .....	65
2.2	Characterization of polyesters .....	67
2.2.1	Structures.....	67
2.2.2	Molar masses and yields .....	68
2.2.3	Thermal degradation .....	69
2.2.4	Differential scanning calorimetry (DSC) .....	70
2.3	Characterization of films .....	71
2.3.1	Preparation of films .....	71
2.3.2	Crystallinity of films .....	72
2.3.3	XRD of films .....	73
2.3.4	Microscopy of films .....	74
2.3.5	Mechanical properties .....	75
2.3.6	Contact angle measurements .....	76
2.3.7	Liquid water sorption and water vapor sorption .....	76
2.3.8	Water vapor permeation .....	80
2.3.9	Gas permeation measurements .....	80
2.3.10	Relationship between microstructure and permeation properties .....	82
2.4	Conclusion .....	83
	References .....	84
	<b>Chapter 3: 2,6-Pyridinedicarbonyl based polyesters .....</b>	<b>87</b>
3.1	Synthesis .....	90
3.1.1	Synthesis of monomer .....	90
3.1.2	Synthesis of polyesters .....	92
3.2	Characterization of polyesters .....	95
3.2.1	Structures.....	95
3.2.2	Thermal degradation .....	99
3.2.3	Differential scanning calorimetry (DSC) .....	100
3.3	Characterization of films .....	105
3.3.1	Preparation of films .....	105
3.3.2	Crystallinity of films .....	105
3.3.3	Mechanical properties .....	108
3.3.4	Contact angle measurements .....	110
3.3.5	Liquid water and water vapor sorption .....	111
3.3.6	Water vapor permeation .....	115
3.3.7	Gas permeation.....	117

3.3.8 DMA of films .....	119
3.4 Conclusion .....	121
References .....	122
<b>Chapter 4: Copolyesters from 1,4:3,6-dianhydrohexitols or 2,6-pyridinedicarbonyl ...</b>	<b>125</b>
4.I ISC10 and IMC10 based copolyesters.....	127
4.I.1 Synthesis .....	127
4.I.2 Characterization of polyesters .....	129
4.I.3 Characterization of copolyester films .....	134
4.II PDD26-DD copolyesters .....	147
4.II.1 Synthesis.....	147
4.II.2 Characterization of copolyesters .....	147
4.II.3 Characterization of films .....	153
4.III Conclusion .....	162
References .....	163
<b>General Conclusion .....</b>	<b>167</b>
<b>Annexes .....</b>	<b>173</b>
Annex 1 Synthesis.....	175
Annex 2 Films preparation.....	181
Annex 3 Characterizations .....	183
Annex 4 SEC.....	206
Annex 5 NMR.....	214
Annex 6 DSC .....	218
Annex 7 XRD .....	223
Annex 8 POM .....	224
Annex 9 Reagents .....	225

### Attention

Two free pages of the chemical structures of the polyester acronyms in this thesis were attached for reference.



## List of Abbreviations

### Acronyms

FTIR	Fourier Transform Infrared
NMR	Nuclear Magnetic Resonance
SEC	Size Exclusion Chromatography
TGA	Thermogravimetric Analysis
DSC	Differential Scanning Calorimetry
DMA	Dynamic Mechanical Analysis
XRD	X-ray Diffraction
POM	Polarized Optical Microscopy
DVS	Dynamic Vapor Sorption
HDPE	High density polyethylene
LDPE	Low density polyethylene
LLDPE	Linear low density polyethylene
PP	Polypropylene
EAA	Poly(ethylene-co-acrylic acid)
PEVA	Poly(ethylene-co-vinyl acetate)
PVOH	Poly(vinyl alcohol)
PVC	Poly(vinyl chloride)
PVDC	Polyvinylidene chloride
PS	Polystyrene
PA	Polyamide
PAN	Polyacrylonitrile
PA6	Nylon-6
PC	Polycarbonate
PPC	Poly(propylene carbonate)
PEN	Poly(ethylene naphthalate)
PCL	Polycaprolactone
EVOH	Poly(ethylene-vinyl alcohol)
PVAc	Poly(vinyl acetate)
TPS	Thermoplastic starch
PET	Poly(ethylene terephthalate)
PTT	Poly(trimethylene terephthalate)
PBS	Poly(butylene succinate)
PEST	Poly(ethylene succinate-co-terephthalate)
PBST	Poly(butylene succinate-co-terephthalate)
PBAT	Poly(butylene adipate-co-terephthalate)
PEI	Poly(ethylene isophthalate)
PC	Polycarbonate
CA	Cellulose acetate
PLA	Poly(lactic acid)
PGA	Poly(glycolic acid)
PCTF	Poly(chlorotrifluoroethylene)



PHAs	Poly(hydroxyalkanoates)
PHB	Poly(hydroxybutyrate)
PEF	Poly(ethylene 2,5-furanoate)
PPF	Poly(propylene 2,5-furanoate)
PBF	Poly(butylene 2,5-furanoate)
PPeF	Poly(pentylene 2,5-furanoate)
PNF	Poly(neopentyl glycol 2,5-furanoate)
PPCE	Poly(propylene cyclohexanedicarboxylate)
IS	Isosorbide
IM	Isomannide
EG	Ethylene glycol
BD	1,4-Butanediol
HD	1,6-Hexanediol
DD	1,10-Decanediol
C4	Succinyl chloride
C6	Adipoyl chloride
C10	Sebacoyl chloride
PDD26	2,6-Pyridinedicarbonyl dichloride
PDD25	2,5-Pyridinedicarbonyl dichloride
PDA25	2,5-Pyridinedicarboxylic acid
IPC	Isophthaloyl chloride
Py	Pyridine
ISC4	Poly(isosorbide succinate)
ISC6	Poly(isosorbide adipate)
ISC10	Poly(isosorbide sebacate)
IMC4	Poly(isomannide succinate)
IMC6	Poly(isomannide adipate)
IMC10	Poly(isomannide sebacate)
PDD26-EG	Poly(ethylene 2,6-pyridinedicarbonate)
PDD26-BD	Poly(butane 2,6-pyridinedicarbonate)
PDD26-HD	Poly(hexane 2,6-pyridinedicarbonate)
PDD26-DD	Poly(decane 2,6-pyridinedicarbonate)
ISC10C4	Poly(isosorbide sebacate succinate)
ISC10IPC	Poly(isosorbide sebacate isophthalate)
ISC10PDD26	Poly(isosorbide sebacate 2,6-pyridinedicarbonate)
IMC10C4	Poly(isomannide sebacate-co-succinate)
IMC10IPC	Poly(isomannide sebacate-co-isophthalate)
IMC10PDD26	Poly(isomannide sebacate-co-2,6-pyridinedicarbonate)
PDD26-DD <sub>92</sub> -IS <sub>8</sub>	Poly(isosorbide-co-decane 2,6-pyridinedicarbonate) (8% mol IS)
PDD26-DD <sub>85</sub> -IS <sub>15</sub>	Poly(isosorbide-co-decane 2,6-pyridinedicarbonate) (15% mol IS)
PDD26-DD <sub>76</sub> -IS <sub>24</sub>	Poly(isosorbide-co-decane 2,6-pyridinedicarbonate) (24% mol IS)
PDD26-DD <sub>33</sub> -EG <sub>67</sub>	Poly(ethylene-co-decane 2,6-pyridinedicarbonate) (67% mol EG)

## Notations

$\bar{M}_n$	Number-average molar mass ( $\text{g}\cdot\text{mol}^{-1}$ )
$\bar{M}_w$	Weight-average molar mass ( $\text{g}\cdot\text{mol}^{-1}$ )
$\bar{D}$	Dispersity

---

$\overline{DP}_n$	Degree of polymerization
$M$	Molar mass of repeating unit ( $\text{g}\cdot\text{mol}^{-1}$ )
$T_{5\%}$	Temperature at 5% weight loss ( $^{\circ}\text{C}$ )
$T_{\max}$	Temperature at the maximum degradation rate ( $^{\circ}\text{C}$ )
$T_g$	Glass transition temperature ( $^{\circ}\text{C}$ )
$T_{g, \text{H}_2\text{O}}$	Glass transition temperature after sorbed water ( $^{\circ}\text{C}$ )
$T_m$	Melting temperature ( $^{\circ}\text{C}$ )
$T_c$	Crystallization temperature ( $^{\circ}\text{C}$ )
$T_{cc}$	Cold crystallization temperature ( $^{\circ}\text{C}$ )
$T_i$	Isothermal crystallization temperature ( $^{\circ}\text{C}$ )
$T$	Temperature <i>at</i> the maximum <i>of</i> $\tan\delta$ ( $^{\circ}\text{C}$ )
$T'_c$	Critical temperature ( $^{\circ}\text{C}$ )
$T'_c(\text{H}_2\text{O})$	Critical temperature of water ( $^{\circ}\text{C}$ )
$T'_c(\text{CO}_2)$	Critical temperature of $\text{CO}_2$ ( $^{\circ}\text{C}$ )
$T'_c(\text{O}_2)$	Critical temperature <i>of</i> $\text{O}_2$ ( $^{\circ}\text{C}$ )
$T'_c(\text{N}_2)$	Critical temperature <i>of</i> $\text{N}_2$ ( $^{\circ}\text{C}$ )
$T_{dp}$	Dew point temperature ( $^{\circ}\text{C}$ )
$\tan\delta$	Tangente delta (loss factor)
$\alpha$	Glass transition temperature detected by dynamic mechanical analysis ( $^{\circ}\text{C}$ )
$\beta$	Second glass transition temperature ( $^{\circ}\text{C}$ )
$A_n$	Normalized area by excluding the crystallinity
$\Delta H_m$	Melting enthalpy ( $\text{J}\cdot\text{g}^{-1}$ )
$\Delta H_c$	Crystallization enthalpy ( $\text{J}\cdot\text{g}^{-1}$ )
$\Delta H_{cc}$	Cold crystallization enthalpy ( $\text{J}\cdot\text{g}^{-1}$ )
$\Delta H_m^{100\%}$	Melting enthalpy with 100% crystallinity ( $\text{J}\cdot\text{g}^{-1}$ )
$\chi_c$	Crystallinity (%)
$S_c$	Area of the crystalline phase
$S_a$	Area of the amorphous phase
$d$	Interplanar distance (nm)
$\lambda$	Wavelength of the incident beam (nm)
$\theta$	X-ray diffraction angle ( $^{\circ}$ )
$E$	Young's modulus (MPa)
$\sigma_b$	Stress at break (MPa)
$\varepsilon_b$	Strain at break (%)
$U$	Fracture energy ( $\text{kJ}\cdot\text{m}^{-3}$ )
$\gamma^t$	Total surface energy ( $\text{mN}\cdot\text{m}^{-1}$ )
$\gamma^d$	Dispersive part of surface energy ( $\text{mN}\cdot\text{m}^{-1}$ )
$\gamma^p$	Polar part of surface energy ( $\text{mN}\cdot\text{m}^{-1}$ )
$\theta_w$	Water contact angle ( $^{\circ}$ )
$M_t$	Water sorption or mass gain at $t$ time (%)
$M_{eq}$	Sorption of liquid water at equilibrium (%)
$m_t$	The film mass at $t$ time (g)
$m_d$	The dry film mass (g)
$m$	Reduced mass gain (g)
$a$	Activity
$a_w$	Water activity
$p$	Pressure
$p_{\text{sat}}$	Saturated vapor pressure (cmHg)
$A_L$	Langmuir's capacity constant

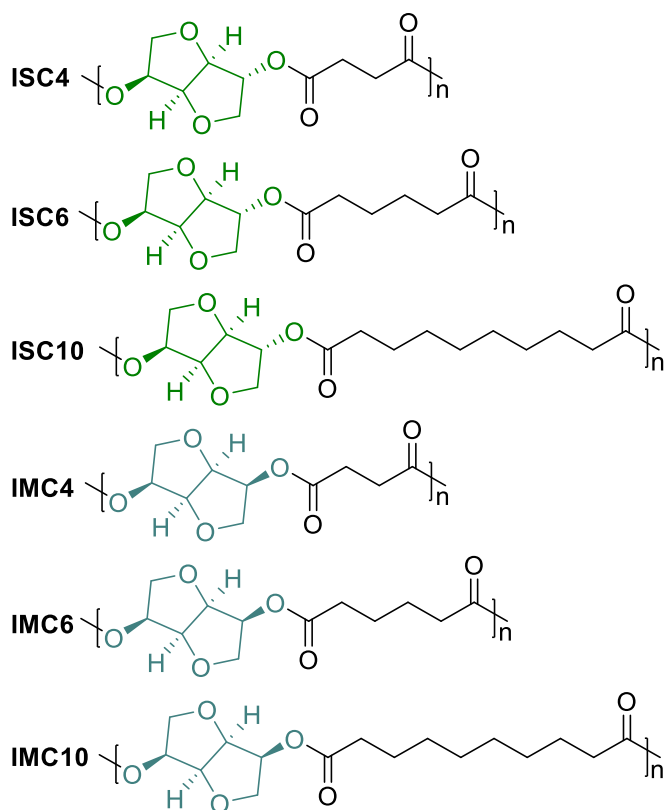
## Abbreviations

---

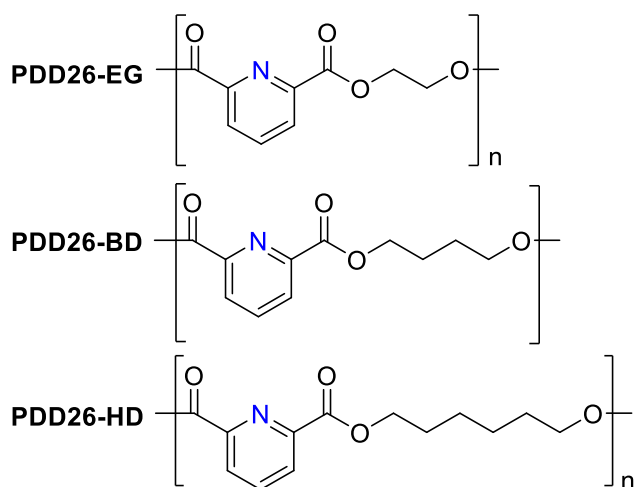
$b_L$	Langmuir's affinity constant
$k_H$	Henry's type solubility coefficient
$K_a$	The equilibrium constant for the clustering reaction
$n_a$	The average number of water molecules per cluster
$t$	Time
$t_{eq}$	Time at equilibrium of sorption (s)
$t_r$	Time to reach the equilibrium of sorption (s)
$t_s$	Time to reach the stationary state of permeation (s)
$t_l$	Time lag (s)
$\tau$	Dimensionless time
$t_i$	Isothermal crystallization time
$k_1$	The slope of the linear regression of curve $(M_t/M_{eq})^2 = f(t - t_r)$
$k_2$	The slope of the linear regression of curve $\ln(1 - M_t/M_{eq}) = f(t)$
$P$	Permeation coefficient (barrer)
$P_{H_2O}$	Water vapor permeation coefficient (barrer or $\text{g}\cdot\text{m}^{-1}\cdot\text{d}^{-1}$ )
$P_{CO_2}$	$\text{CO}_2$ permeation coefficient (barrer)
$P_{O_2}$	$\text{O}_2$ permeation coefficient (barrer)
$P_{N_2}$	$\text{N}_2$ permeation coefficient (barrer)
$P_t$	Total permeation coefficient of target film with PDMS membrane (barrer)
$P_{PDMS}$	Gas permeation coefficient of PDMS membrane (barrer)
$l_t$	Total thickness of target film and PDMS membrane (cm)
$l$	Thickness of target film (cm)
$l_{PDMS}$	Thickness of PDMS membrane (cm)
$L$	Polymer film thickness (cm)
$D$	Diffusion coefficient ( $\text{cm}^2\cdot\text{s}^{-1}$ )
$D_1$	First half diffusion coefficient ( $\text{cm}^2\cdot\text{s}^{-1}$ )
$D_2$	Second half diffusion coefficient ( $\text{cm}^2\cdot\text{s}^{-1}$ )
$D_0$	Diffusion coefficient when the penetrant concentration tends to 0 ( $\text{cm}^2\cdot\text{s}^{-1}$ )
$S$	Solubility coefficient ( $\text{cm}^3(\text{STP})\cdot\text{cm}^{-3}\cdot\text{cmHg}^{-1}$ )
$V_{\text{free}}$	Free volume ( $\text{cm}^3$ )
$\alpha_{A/B}$	Gas selectivity coefficient between gas A and B
$\alpha_{CO_2/O_2}$	$\text{CO}_2$ and $\text{O}_2$ selectivity coefficient
$Q_{\text{polar}}$	Polar groups in the amorphous domain in per kilo polymer ( $\text{mol}\cdot\text{kg}^{-1}$ )
$d_{N_2}$	Kinetic diameter of $\text{N}_2$ (nm)
$d_{O_2}$	Kinetic diameter of $\text{O}_2$ (nm)
$d_{N_2}$	Kinetic diameter of $\text{CO}_2$ (nm)
BIFp	Barrier Improvement Factor
$A_p$	Value of ability to decrease permeability
$p_1$	Gas permeation chamber upstream gas pressure (bar)
$p_2$	Gas permeation chamber downstream gas pressure (bar)
$A$	Film surface area exposed to diffusion or permeation ( $\text{cm}^2$ )
$J$	Diffusion flux ( $\text{cm}^3(\text{STP})\cdot\text{cm}^{-2}\cdot\text{s}^{-1}$ )
$J_{\text{st}}$	Steady state diffusion flux ( $\text{cm}^3(\text{STP})\cdot\text{cm}^{-2}\cdot\text{s}^{-1}$ )
$J_d$	Downstream permeation flux ( $\text{cm}^3(\text{STP})\cdot\text{cm}^{-2}\cdot\text{s}^{-1}$ )
$J(L,t)$	Permeation cell downstream flux ( $\text{cm}^3(\text{STP})\cdot\text{cm}^{-2}\cdot\text{s}^{-1}$ )
$C$	Penetrant concentration ( $\text{cm}^3(\text{STP})\cdot\text{cm}^{-3}$ )
$C_{eq}$	Equilibrium penetrant concentration ( $\text{cm}^3(\text{STP})\cdot\text{cm}^{-3}$ )
$C_0$	Permeation cell upstream water concentration ( $\text{cm}^3(\text{STP})\cdot\text{cm}^{-3}$ )
$Q(t)$	Penetrant quantity passed through film after $t$ time ( $\text{cm}^3(\text{STP})$ )

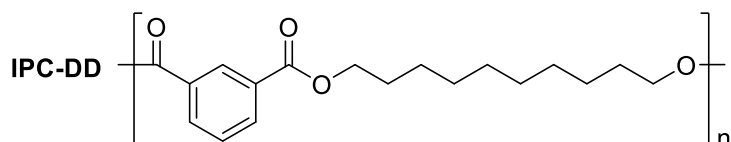
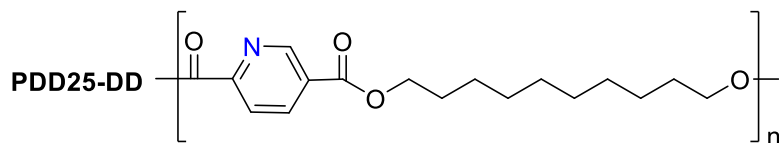
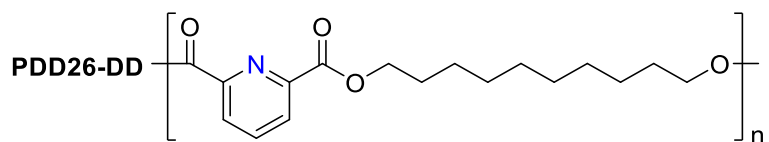
## Chemical structures of acronyms

### Chapter 2

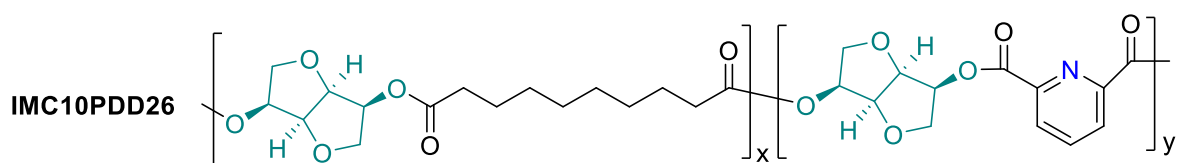
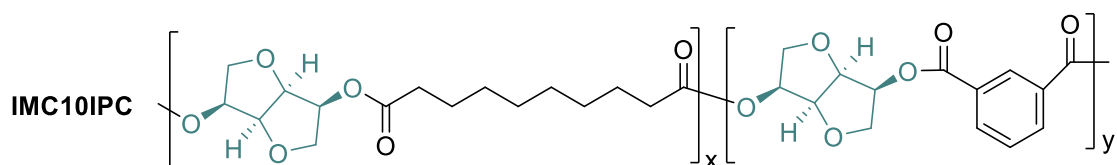
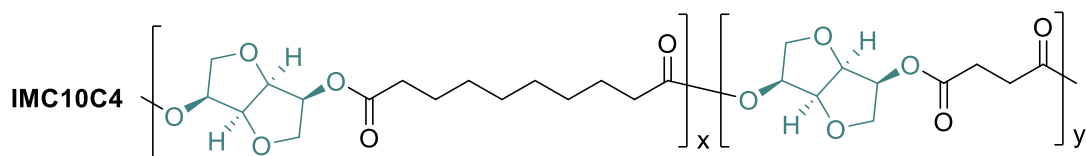
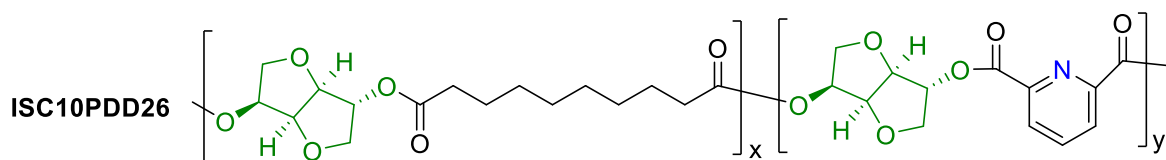
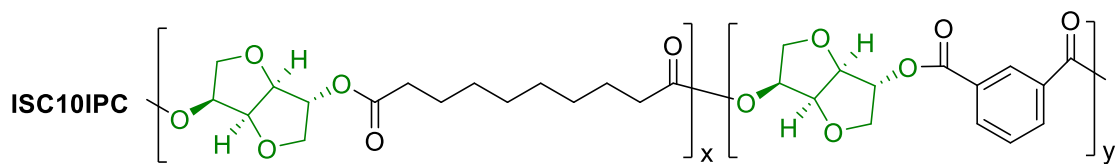
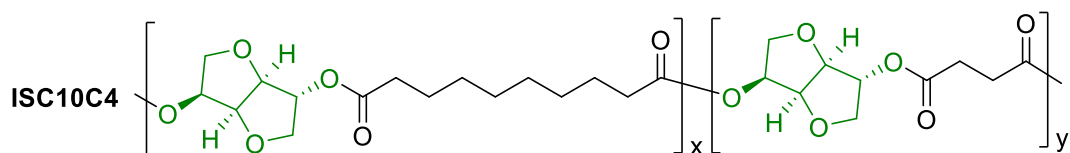


### Chapter 3





## Chapter 4



## List of Figures

Figure 1-1	Plastic food packaging classification .....	10
Figure 1-2	Third-generation bio-based packaging polymers. Adapted from [4] .....	12
Figure 1-3	Synthesis of starch blends [38].....	13
Figure 1-4	Mass transfer phenomena and their characteristic coefficients [214] .....	42
Figure 1-5	An activated diffusion process of permeants through a polymer film [216]. ....	43
Figure 2-1	Images of ISC10 polyester .....	65
Figure 2-2	Synthesis of aliphatic polyesters from IS and IM .....	66
Figure 2-3	FTIR spectra of the polyesters.....	67
Figure 2-4	<sup>1</sup> H NMR spectra of ISC10 and IMC10 polyesters.....	68
Figure 2-5	TGA curves of IS and IM polyesters.....	69
Figure 2-6	DSC thermograms of polyesters.....	70
Figure 2-7	IS and IM polyester films prepared by hot pressing.....	72
Figure 2-8	DSC first heating of ISC10, IMC10, and their films.....	72
Figure 2-9	XRD spectra of ISC10, IMC10, and their films .....	73
Figure 2-10	Microscopy images of ISC10 film (a) and IMC10 film (b) .....	74
Figure 2-11	Stress-strain curves of ISC10 and IMC10 films.....	75
Figure 2-12	Liquid water sorption of ISC10 and IMC10 films .....	77
Figure 2-13	Water vapor sorption isotherms of ISC10 and IMC10 films .....	78
Figure 2-14	Water vapor sorption of ISC10 and IMC10 films: (a) sorption kinetics (b) diffusion kinetics .....	79
Figure 2-15	Polymer chains (grey) and the corresponding space-filling models (black) predicted by Chemdraw® Software .....	83
Figure 3-1	FTIR spectra of PDD25 and PDA25 .....	90
Figure 3-2	<sup>1</sup> H NMR spectra of PDD25 and PDA25.....	91
Figure 3-3	Thermal stability of PDD26.....	93
Figure 3-4	Thermal stability of PDD25 .....	95
Figure 3-5	FTIR spectra of polyesters.....	96
Figure 3-6	<sup>1</sup> H NMR spectrum of PDD26-DD .....	97
Figure 3-7	<sup>1</sup> H NMR spectra of PDD26-EG and PDD26-BD .....	98

## List of Figures

Figure 3-8	TGA thermograms of polyesters .....	99
Figure 3-9	DSC thermograms of PDD26-DD and PDD25-DD .....	102
Figure 3-10	DSC thermograms of PDD26-DD heating (upper) after the melt polymer was cooled (lower) at different rates: (a) 1 °C·min <sup>-1</sup> (b) 5 °C·min <sup>-1</sup> (c) 10 °C·min <sup>-1</sup> (d) 20 °C·min <sup>-1</sup> (e) 30 °C·min <sup>-1</sup> .....	103
Figure 3-11	DSC thermograms of PDD26-DD: samples heated (10 °C·min <sup>-1</sup> ) directly after isothermal step for 120 min at 25 °C, or 30 min at 50, 60 and 75 °C .....	103
Figure 3-12	Films prepared by hot pressing.....	105
Figure 3-13	DSC thermograms (a) and XRD patterns (b) of films.....	106
Figure 3-14	POM images of PDD26-DD (a), PDD25-DD (b) and IPC-DD (c) films.....	108
Figure 3-15	Stress-strain curves of PDD25-DD, PDD26-DD and IPC-DD films .....	109
Figure 3-16	Liquid water sorption of PDD26-DD, PDD25-DD and IPC-DD .....	111
Figure 3-17	Water vapor sorption isotherms.....	112
Figure 3-18	Evolution of $D_1$ and $D_2$ as a function of $a_w$ .....	113
Figure 3-19	$\tan\delta$ versus temperature for PDD26-DD and PDD25-DD films .....	120
Figure 4-1	FTIR spectra of copolyesters .....	129
Figure 4-2	<sup>1</sup> H NMR spectra of ISC10C4 and IMC10C4.....	130
Figure 4-3	TGA thermograms of copolyesters .....	131
Figure 4-4	DSC thermograms of copolyesters .....	132
Figure 4-5	DSC thermograms of IMC10C4: isotherm at 55 °C for an indicated time ....	133
Figure 4-6	Copolyester films prepared by hot pressing .....	134
Figure 4-7	Stress-strain curves of copolyester films .....	134
Figure 4-8	Body external temperature triggered shape recovery of ISC10C4.....	136
Figure 4-9	Liquid water sorption of copolyester films .....	137
Figure 4-10	DSC thermograms of copolyester films before (solid line) and after (dashed line) liquid water sorption .....	138
Figure 4-11	Water vapor sorption isotherms of copolyester films.....	139
Figure 4-12	Evolution of $D_1$ and $D_2$ as a function of $a_w$ .....	141
Figure 4-13	<sup>1</sup> H NMR Spectra of PDD26-DD <sub>33</sub> -EG <sub>67</sub> and PDD26-DD <sub>x</sub> -IS <sub>y</sub> .....	149
Figure 4-14	FTIR spectra of PDD26-DD <sub>x</sub> -IS <sub>y</sub> and PDD26-DD <sub>33</sub> -EG <sub>67</sub> .....	150
Figure 4-15	TGA thermograms of PDD26-DD <sub>x</sub> -IS <sub>y</sub> and PDD26-DD <sub>33</sub> -EG <sub>67</sub> .....	151
Figure 4-16	DSC thermograms of PDD26-DD <sub>x</sub> -IS <sub>y</sub> and PDD26-DD <sub>33</sub> -EG <sub>67</sub> .....	152

Figure 4-17	Films prepared by hot pressing.....	153
Figure 4-18	DSC thermograms (a) and XRD patterns (b) of films.....	154
Figure 4-19	POM images of PDD26-DD <sub>92</sub> -IS <sub>8</sub> and PDD26-DD <sub>85</sub> -IS <sub>15</sub> films .....	155
Figure 4-20	Stress-strain curves of PDD26-DD <sub>92</sub> -IS <sub>8</sub> and PDD26-DD <sub>85</sub> -IS <sub>15</sub> .....	156
Figure 4-21	Liquid water sorption of PDD26-DD <sub>92</sub> -IS <sub>8</sub> and PDD26-DD <sub>85</sub> -IS <sub>15</sub> .....	157
Figure 4-22	Water vapor sorption isotherms.....	158
Figure 4-23	Evolution of $D_1$ and $D_2$ as a function of $a_w$ .....	159
Figure A2-1	Hot pressing procedure .....	182
Figure A3-1	Typical XRD spectra of polymers .....	185
Figure A3-2	1BB dumbbell-shaped specimens' dimensions .....	186
Figure A3-3	Profiles of liquids on different types of surface .....	186
Figure A3-4	Concentration profiles of sorption .....	189
Figure A3-5	Example of sorption kinetics at one given activity.....	190
Figure A3-6	Kinetics of sorption: (a) first half-sorption $m$ vs $\tau$ and (b) second half-sorption $\ln(1-m)$ vs $\tau$ .....	191
Figure A3-7	Classification of isotherms .....	192
Figure A3-8	Flow chart of liquid water sorption measurement .....	195
Figure A3-9	DVS device simplification.....	196
Figure A3-10	Plotting of water vapor sorption isotherms.....	197
Figure A3-11	Concentration profiles from $t = 0$ to $t = t_s$ (stationary state) with constant $D$ and reduced scales .....	197
Figure A3-12	Typical curves obtained from permeation: differential (1) and integral (2) .....	199
Figure A3-13	Experimental setup of water vapor permeation measurement (RH for relative humidity) .....	200
Figure A3-14	Gas permeation measurement setup .....	203





## List of Schemes

Scheme 1-1	Chemical structure of starch: amylose and amylopectin.....	12
Scheme 1-2	Chemical structure of cellulose .....	14
Scheme 1-3	Chitosan chemical structure: from chitin to chitosan.....	15
Scheme 1-4	Primary structure of a protein.....	15
Scheme 1-5	Routes to obtain bio-PE and bio-PP using bio-ethylene as a platform .....	16
Scheme 1-6	Ring-opening polymerization of PLA and the two isomers of lactic acid .....	17
Scheme 1-7	Synthetic routines of PHAs: microorganism (1) and ring-opening (2) [29] .....	18
Scheme 1-8	Chemical structure of PHBV.....	19
Scheme 1-9	Synthesis of PET via polycondensation .....	19
Scheme 1-10	Bio-origination of EG, TPA and IPA.....	21
Scheme 1-11	Synthesis of PEF by polycondensation reaction .....	22
Scheme 1-12	General scheme for the synthesis of isosorbide/isomannide from starch .....	25
Scheme 1-13	Scheme for the synthesis of aliphatic polyesters from 1,4:3,6-dianhydrohexitols.....	26
Scheme 1-14	General structure of semi-aromatic polyesters from 1,4:3,6- dianhydrohexitols.....	28
Scheme 1-15	Bio-routines to obtain pyridinedicarboxylic acids .....	31
Scheme 1-16	Schematic of step growth polymerization of polyesters .....	34
Scheme 2-1	Thermal stability (TGA and DSC) of isosorbide and isomannide.....	66
Scheme 3-1	Synthesis of PDD25 from PDA25 .....	90
Scheme 3-2	Synthesis of polyesters .....	92
Scheme 4-1	Synthesis of IS and IM copolyesters .....	128
Scheme 4-2	Synthesis of PDD26-DD copolyesters .....	147



## List of Tables

Table 1-1	PET and PET analogs investigated concerning food packaging applications .....	20
Table 1-2	PEF and PEF homologues investigated concerning food packaging .....	23
Table 1-3	Stereoisomers of 1,4:3,6-dianhydrohexitols .....	24
Table 1-4	1,4:3,6-dianhydrohexitol-based aliphatic polyesters .....	27
Table 1-5	Semi-aromatic (co)polyesters molar masses and thermal properties.....	29
Table 1-6	Chemical structures of 2,4-, 2,5- and 2,6-pyridinedicarboxylic acids .....	31
Table 1-7	Molar masses and thermal properties of pyridinedicarboxylate polyesters (catalyzed by enzyme ICalB at 85 °C and 20 mbar).....	33
Table 1-8	Thermal properties of food packaging polyesters.....	36
Table 1-9	Mechanical properties of food packaging polymers .....	37
Table 1-10	Protection requirements regarding H <sub>2</sub> O for foods and beverages (assuming 1-year shelf life at 25 °C) .....	38
Table 1-11	Protection requirements regarding O <sub>2</sub> for foods and beverages (assuming 1-year shelf life at 25 °C) .....	39
Table 1-12	Optimum atmosphere to preserve vegetables and fruits between 0 and 5 °C....	40
Table 1-13	Some parameters of N <sub>2</sub> , O <sub>2</sub> , CO <sub>2</sub> and H <sub>2</sub> O used in permeation experiments .....	41
Table 1-14	CO <sub>2</sub> and O <sub>2</sub> selectivity coefficient of polymers within the ideal range for fresh foods preserving .....	42
Table 1-15	Effects of functional groups on oxygen and water permeability coefficients ...	44
Table 1-16	Permeability data in terms of CO <sub>2</sub> , O <sub>2</sub> , N <sub>2</sub> and H <sub>2</sub> O of polymer films at 25 °C	45
Table 2-1	Molar masses and dispersities of polyesters and yields of synthesis.....	69
Table 2-2	Thermal degradation data recorded from TGA .....	70
Table 2-3	Information recorded from DSC thermograms.....	71
Table 2-4	Crystallinity ( $\chi_c$ ) and <i>d</i> -spacing information for ISC10 and IMC10 .....	74
Table 2-5	Mechanical properties of ISC10 and IMC10 polyester films .....	76
Table 2-6	Surface energies and contact angles of ISC10 and IMC10 films .....	76
Table 2-7	Sorption parameters of Park's model.....	78
Table 2-8	Water permeation coefficient ( $P_{H_2O}$ ) of ISC10 and IMC10 films at different water activities ( <i>a<sub>w</sub></i> ) .....	80
Table 2-9	Gas permeation ( <i>P</i> ) and diffusion ( <i>D</i> ) coefficients of N <sub>2</sub> , O <sub>2</sub> and CO <sub>2</sub> in ISC10 and IMC10 films .....	81

## List of Tables

Table 3-1	Chemical structure of PDD26, PDD25 and IPC .....	89
Table 3-2	Molar masses of polyesters and yields of bulk syntheses.....	94
Table 3-3	<sup>1</sup> H NMR chemical shifts of the prepared polyesters.....	96
Table 3-4	Thermal degradation data recorded from TGA .....	100
Table 3-5	Thermal information recorded from DSC .....	101
Table 3-6	XRD data of PDD25-DD, PDD26-DD and IPC-DD films .....	107
Table 3-7	Mechanical properties of PDD26-DD, PDD25-DD and IPC-DD films.....	110
Table 3-8	Surface energies and contact angles of polymer films .....	110
Table 3-9	Sorption parameters of Park's model.....	113
Table 3-10	Water vapor permeation coefficient ( $P_{H_2O}$ ) of PDD26-DD, PDD25-DD and IPC-DD films at different water activities ( $a_w$ ).....	115
Table 3-11	Quantity (mol) of polar groups in per kg polymer.....	116
Table 3-12	Gas permeation ( $P$ ) and diffusion ( $D$ ) coefficients of polyester films.....	117
Table 3-13	Comparison between different aromatic skeletons in permeability.....	119
Table 3-14	Information of PDD26-DD and PDD25-DD recorded from DMA.....	120
Table 4-1	Molar masses of polyesters and yields of syntheses.....	128
Table 4-2	Calculated monomer ratios in polymers .....	130
Table 4-3	Thermal degradation data recorded from TGA .....	131
Table 4-4	Thermal properties of copolyesters.....	133
Table 4-5	Tensile parameters of copolyester films .....	135
Table 4-6	Surface energies and water contact angles of copolyester films .....	136
Table 4-7	Sorption parameters of Park's model.....	140
Table 4-8	Water vapor permeation coefficient ( $P_{H_2O}$ ) of copolyester films at different water activities ( $a_w$ ).....	142
Table 4-9	Gas permeation coefficients ( $P$ ) of copolyester films .....	144
Table 4-10	Gas solubility and diffusion coefficients ( $S$ and $D$ ) of IS copolyester films and IMC10C4 film .....	145
Table 4-11	PDD26-DD <sub>x</sub> -X <sub>y</sub> copolyesters .....	149
Table 4-12	Molar masses of copolyesters and yields of syntheses .....	150
Table 4-13	Thermal properties of copolyesters.....	152
Table 4-14	Surface energies and water contact angle values of films .....	157

---

Table 4-15	Liquid water and water vapor sorption parameters of Park's model.....	159
Table 4-16	Water vapor permeation coefficients ( $P_{\text{H}_2\text{O}}$ ) of films .....	160
Table 4-17	Gas permeation ( $P$ ) coefficient of polyester films.....	161
Table 4-18	Gas diffusion ( $D$ ) and solubility ( $S$ ) coefficients of films .....	161
Table A2-1	Hot pressing temperatures.....	182
Table A3-1	Converting $P$ from different units to barrer .....	204
Table A9-1	Short name, chemical structure and CAS number of the reagents .....	226
Table A9-2	Physical information of the reagents.....	227
Table A9-3	Chemical safety information of the reagents .....	228



---

## ❧ Résumé de la Thèse en Français ❧

---





## Introduction générale

L'emballage alimentaire est essentiel dans notre vie quotidienne en raison des exigences requises pour protéger et préserver les aliments. Outre les métaux, le papier et le verre, les plastiques dominent le marché en raison de leur rapport coût/performance attractif : leur volume alloué aux emballages alimentaires est estimé à environ 40% de la consommation totale de plastiques. Traditionnellement, ce sont des polymères à base de pétrole. Toutefois, les ressources en pétrole sont limitées et les enjeux environnementaux prennent une importance croissante dans le monde entier. Ainsi, lors de la conférence de Paris sur le climat (COP21) en décembre 2015, 195 pays ont adopté le tout premier accord universel et juridiquement contraignant sur le climat mondial. Cet accord établit un plan d'action mondial pour limiter le réchauffement climatique avec la réorientation de l'économie mondiale vers un modèle à faibles émissions de carbone. Parmi les solutions proposées, l'accord suggère de préparer des matériaux naturels biodégradables fabriqués à partir de ressources renouvelables.

Les polymères biosourcés utilisés dans les emballages alimentaires peuvent être classés en trois catégories principales selon leur méthode de production, à savoir les polymères directement extraits de la biomasse, tels que l'amidon, la cellulose et la chitine, les polymères produits par synthèse chimique à partir de monomères issus de la biomasse, tels que le polyacide lactique (PLA), le bio-polyéthylène téréphtalate (bio-PET) et le bio-polyéthylène (bio-PE), et les polymères produits directement par des organismes naturels ou génétiquement modifiés, tels que les polyhydroxyalkanoates (PHAs).

Les polymères naturels extraits de la biomasse sont abondants et peu chers, mais présentent généralement une faible résistance à l'eau et sont difficiles à mettre en œuvre.

Le bio-PE est accessible, mais il n'existe actuellement aucun moyen bon marché pour le produire. De plus, ce biopolymère a les mêmes faibles propriétés barrières aux gaz que le PE et n'est pas plus biodégradable.

En revanche, les polyesters biosourcés sont attractifs en raison de leurs nombreux avantages, tels qu'un large éventail de monomères disponibles, des performances ajustables, une éventuelle biodégradation, de nombreuses voies de recyclage et de récupération, et des infrastructures industrielles bien établies en termes de réacteurs de polycondensation.

Bien que de nombreux efforts aient été faits pour développer le bio-PET qui est entièrement biosourcé, sa production est limitée du fait du coût élevé de l'acide téréphtalique

qui rend actuellement impossible l'augmentation de sa production. Les polyesters biosourcés réellement utilisés pour les applications d'emballage alimentaire sont donc limités aux PHAs et au PLA. Cependant, ces derniers possèdent des propriétés mécaniques et barrières souvent inférieures à celles des polymères à base de pétrole. La science des polymères, grâce aux progrès techniques réalisés ces dernières années, se doit d'améliorer les propriétés des PHAs et du PLA et de synthétiser de nouveaux polyesters biosourcés. Evidemment, leurs propriétés thermiques, mécaniques et de transport doivent être étudiées avant d'envisager le remplacement des polymères conventionnels.

Récemment, le polyéthylène furanoate (PEF), un polyester 100% renouvelable qui est destiné à remplacer dans le futur le PET pour l'emballage de l'eau et des sodas, a montré des propriétés barrières élevées à l'oxygène et au dioxyde de carbone. Ces excellentes propriétés ont été attribuées à la rigidité et à la polarité des groupements 2,5-furandicarboxylique. Ce résultat important nous a donc donné l'idée de travailler sur de nouvelles molécules bifonctionnelles non toxiques, rigides, et polaires, telles que les 1,4:3,6-dianhydrohexitols et les acides (2,4-, 2,5- et 2,6-)pyridinedicarboxyliques. De plus, ces molécules peuvent être extraites de la biomasse.

Ainsi, cette thèse vise à synthétiser des (co)polyesters 100% biosourcés à partir de 1,4:3,6-dianhydrohexitols et/ou d'acides pyridinedicarboxyliques, et à étudier leurs propriétés thermiques, mécaniques et surtout de transport.

Ce travail est organisé selon quatre chapitres. À la suite de cette Introduction générale, le Chapitre 1 donne un aperçu des principaux polymères biosourcés, de leurs limites les plus courantes et de leurs utilisations actuelles ou possibles dans le domaine des emballages alimentaires. L'accent est mis sur les polyesters biosourcés. Ensuite, une brève présentation des méthodes traditionnelles de synthèse des polyesters est donnée. Les propriétés thermiques, mécaniques et de perméation concernant les applications dans l'emballage alimentaire sont décrites. Les défis et les opportunités de ces polymères biosourcés sont ensuite rapidement présentés.

Le Chapitre 2 présente une série de polyesters aliphatiques à base d'isosorbide et d'isomannide. Ces polyesters ont déjà été synthétisés et étudiés en termes de biodégradabilité par Okada *et al.* L'originalité de notre travail est de s'intéresser à leurs propriétés de sorption/perméation aux gaz et à l'eau, qui sont cruciales pour les applications d'emballage

alimentaire. Des relations entre les microstructures et les propriétés de sorption/perméation sont établies.

Le Chapitre 3 ouvre sur une série de nouveaux polyesters semi-aromatiques à base de chlorure de 2,6-pyridinedicarbonyle (PDD26) et de diols aliphatiques linéaires (éthylène glycol EG, butanediol BD, hexanediol HD et décanediol DD). Leurs synthèses et leurs propriétés thermiques, mécaniques et de perméation sont discutées. Quelques comparaisons sont faites avec des polyesters préparés avec le chlorure de 2,5-pyridinedicarbonyle (PDD25) ou le chlorure d'isophtaloyle (IPC), quand cela est possible.

Le Chapitre 4, en combinant les résultats obtenus dans les Chapitres 2 et 3, développe une série de copolyesters basés sur l'isosorbide, l'isomannide et le chlorure de 2,6-pyridinedicarbonyle. Leurs synthèses et leurs propriétés thermiques, mécaniques et de transport sont systématiquement étudiées et discutées.

Enfin, une conclusion générale et des perspectives sont présentées avant les Annexes.

## **Chapitre 1 : Etat de l'art**

En raison du nombre de pages limité consacré à ce résumé de la thèse en français et afin de se consacrer davantage aux résultats expérimentaux, l'aperçu général concernant les matériaux traditionnellement utilisés dans l'emballage alimentaire et certains polyesters biosourcés comme le PLA, les PHAs, le bio-PET et le PEF, ne sont pas présentés ici. Seuls quelques nouveaux monomères biosourcés et les polyesters correspondants, prometteurs pour ce secteur, seront développés, ainsi que leurs propriétés de perméation.

### **Nouveaux polyesters biosourcés pour les applications d'emballage alimentaire**

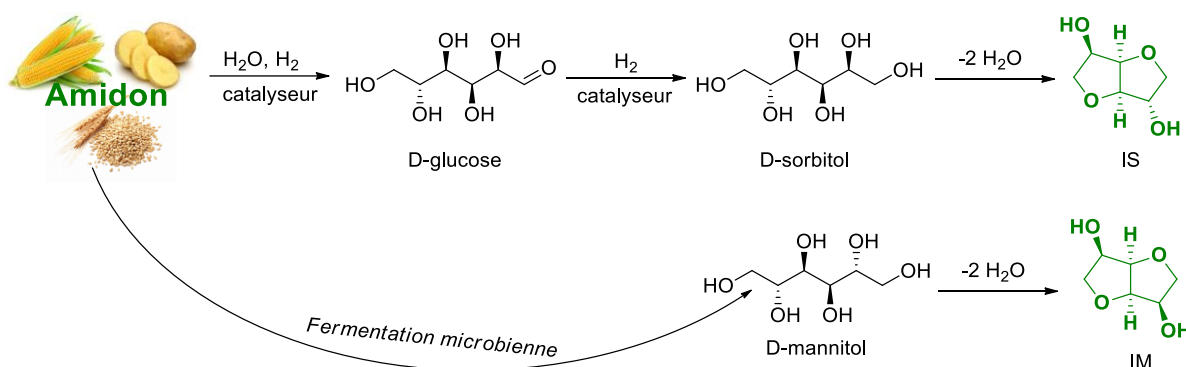
#### **Les 1,4:3,6-dianhydrohexitols comme plates-formes**

Les 1,4:3,6-dianhydrohexitols (DAHs) sont attractifs en raison de leurs propriétés uniques, telles que la non-toxicité, la chiralité et la rigidité. Ces propriétés les rendent intéressants à utiliser comme plates-formes biosourcées pour préparer des polyesters à température de transition vitreuse élevée et ayant des propriétés optiques particulières. De plus, les DAHs ont

des prix attractifs en raison d'une production industrielle importante, en particulier l'isosorbide, ce qui ouvre des possibilités pour les applications d'emballage alimentaire.

Les 1,4:3,6-dianhydrohexitols (DAHs) sont connus sous le nom d'isosorbide (IS), d'isomannide (IM) et d'isoidide (II). Leur structure renferme un cycle en forme de V avec un angle de  $120^\circ$ , qui conditionne des différences exo-endo entre les monomères. En général, la fonction alcool exo est plus accessible que l'endo, donc plus réactive. L'isosorbide a une fonction alcool endo et une fonction alcool exo, tandis que l'isomannide possède deux groupements endo et que l'isoidide a deux fonctions exo. Des mesures RMN ont montré que la fonction endo forme une liaison hydrogène avec l'oxygène du cycle tétrahydrofurane, ce qui diminue par conséquent la réactivité des monomères [1]. Ainsi, l'isoidide possède logiquement la réactivité la plus élevée, et l'isomannide la plus faible. Cependant, l'isoidide n'est pas disponible commercialement.

La synthèse générale de l'isosorbide et de l'isomannide est présentée sur le Schéma R-1.



**Schéma R-1** Synthèse de l'isosorbide et de l'isomannide à partir de l'amidon

De nombreux polyesters, aliphatiques et semi-aromatiques, à base d'isosorbide et d'isomannide ont été synthétisés et étudiés en termes de biodégradabilité [2,3], biocompatibilité [4] et cristallinité [5]. Les données correspondantes concernant les masses molaires et les principales propriétés thermiques sont rassemblées dans le Tableau R-1 pour les aliphatiques et dans le Tableau R-2 pour les aromatiques.

**Tableau R-1** Polyesters aliphatiques à base de 1,4:3,6-dianhydrohexitols

Diol	Diacide carboxylique ou dérivé <sup>a</sup>	$\overline{M}_n$ (g·mol <sup>-1</sup> )	$\overline{M}_w$ (g·mol <sup>-1</sup> )	$T_g$ (°C)	$T_f$ (°C)	Réf
IS	Cl—C4—Cl	7 500	10 800	65	-	[6]
		8 000	14 400	36	-	[2,3]
		8 600	16 300	78	-	[5]
	HO—C4—OH	2 900	3 700	73	145	[4]
	Cl—C5—Cl	16 000	27 200	28	-	[2,3]
		13 000	37 700	43	-	[5]
	Cl—C6—Cl	26 000	39 000	21	-	[7]
		13 000	25 000	25	-	[6]
		7 300	13 900	19	-	[5]
	HO—C6—OH	8 800	15 800	34	84	[4]
	Cl—C7—Cl	22 000	30 800	11	-	[7]
	Cl—C8—Cl	20 000	49 000	11	-	[6]
		9 400	16 000	11	-	[5]
	Cl—C9—Cl	18 000	30 600	-1	54	[7]
	Cl—C10—Cl	20 000	28 000	-10	61	[7]
		23 000	60 000	0	-	[6]
		8 500	11 900	-7	59	[5]
	HO—C10—OH	19 200	45 300	6	50	[4]
	Cl—C12—Cl	17 000	28 900	-8	70	[7]
		15 000	28 000	-2	-	[6]
		13 000	24 700	-10	65	[5]
	Cl—C14—Cl	14 700	31 300	-4	53/67/79	[6]
	Cl—C16—Cl	11 400	26 000	-4	81/88	[6]
IM	Cl—C4—Cl	nd	nd	60	-	[6]
		10 000	17 000	75	175	[2,3]
		9 400	19 700	82	185	[5]
		19 000	60 900	80	185	[8]
	Cl—C5—Cl	11 000	17 600	37	-	[2]
		7 400	14 000	43	-	[5]
	Cl—C6—Cl	16 000	27 200	28	-	[2,3]
		8 800	15 000	30	-	[6]
		16 000	41 600	36	-	[5]
	Cl—C8—Cl	7 600	16 000	9	-	[5]
	Cl—C10—Cl	18 000	25 200	-8	-	[2,3]
		13 700	26 000	0	-	[6]
		9 300	13 000	-10	43	[5]
	Cl—C12—Cl	13 000	23 400	-10	65	[5]

<sup>a</sup> Exprimé par le nombre de carbones du squelette acide carboxylique ou chlorure d'acyle. $\overline{M}_n$ ,  $\overline{M}_w$  : mesurées par SEC étalonnage PS ; nd : non déterminé. $T_g$ ,  $T_f$  : mesurées par DSC sous N<sub>2</sub> à 10°C·min<sup>-1</sup>.

**Tableau R-2** Polyesters semi-aromatiques à base de 1,4:3,6-dianhydrohexitols

Diol		Diacide carboxylique ou dérivé	$\overline{M}_n$ (g·mol <sup>-1</sup> )	$T_g$ (°C)	$T_f$ (°C)	Réf
IS		TPC	3 000 <sup>a</sup>	155	194	[9]
			25 600 <sup>b</sup>	205	-	[10]
			23 200 <sup>b</sup>	204	-	
			21 300 <sup>b</sup>	203	-	
			14 200 <sup>b</sup>	197	-	
			7 900 <sup>b</sup>	187	-	
			6 400 <sup>b</sup>	180	-	
			3 200 <sup>a</sup>	158	-	
		IPC	3 600	138	-	[6]
		PC	2 200	118	-	[6]
		2,5-FDCC	25 000 <sup>b</sup>	194	-	[11]
22 500 <sup>b</sup>	190		-			
9 000 <sup>b</sup>	173		-			
IM		TPC	ins.	nd	nd	[9,10]
		IPC	3 000	149	-	[6]
		PC	ins.	109	-	[6]
		2,5-FDCC	20 400 <sup>b</sup>	191	-	[11]
EG	1.4% molaire d'IS 3.4% molaire d'IS 6.3% molaire d'IS 10.1% molaire d'IS	TPA	nd	82	251	[1]
			nd	83	243	
			nd	86	235	
			nd	90	221	
BD	6% molaire d'IS 18% molaire d'IS 24% molaire d'IS 42% molaire d'IS	DMT	nd	55	208	[12]
			nd	58	191	
			nd	84	162	
			nd	92	-	

TPC : chlorure de téréphtaloyle ; IPC : chlorure d'isophtaloyle ; PC : chlorure de phtaloyle ; 2,5-FDCC : dichlorure de 2,5-furandicarbone ; TPA : acide téréphtalique ; DMT : téréphtalate de diméthyle ; EG : éthylène glycol ; BD : 1,4-butanediol.

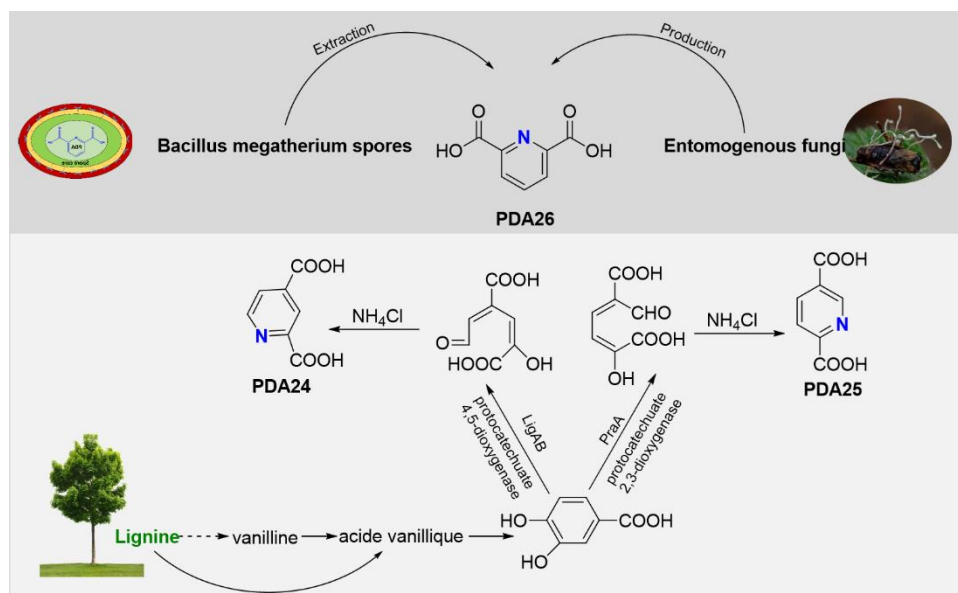
$\overline{M}_n$  : mesurée par SEC étalonnage PS, sauf <sup>a</sup>par osmométrie de pression de vapeur dans 1,1,2,2-tétrachloroéthane à 30°C, <sup>b</sup>par osmométrie membranaire dans 1,1,2,2-tétrachloroéthane à 30°C, ins. : insoluble, nd : non déterminé.

$T_g$ ,  $T_f$  : mesurées par DSC sous N<sub>2</sub> à 10°C·min<sup>-1</sup>.

## Les acides pyridinedicarboxyliques comme plates-formes

Les acides pyridinedicarboxyliques, à savoir l'acide 2,4-pyridinedicarboxylique (PDA24), l'acide 2,5-pyridinedicarboxylique (PDA25) et l'acide 2,6-pyridinedicarboxylique (PDA26), peuvent être obtenus à partir de la biomasse [13,14], et présentent des similitudes avec l'acide 2,5-furandicarboxylique (2,5-FDCA), comme la polarité et la rigidité de la structure.

Ils peuvent être divisés en deux catégories : les PDA24 et PDA25 dérivés de la lignine par conversion biocatalytique [13], et le PDA26 isolé des spores de *Bacillus megatherium* [14] ou produit par des champignons entomogènes [15] (Schéma R-2).



**Schéma R-2** Biosynthèse des acides pyridinedicarboxyliques

Quelques polyesters contenant des groupes 2,5 et 2,6-pyridinedicarbonyle ont été rapportés dans plusieurs articles. Selon Isfahani *et al.*, la présence de 2,5-pyridyle dans la chaîne principale augmente la solubilité dans les solvants organiques des polyesters qui contiennent beaucoup de structures aromatiques [16]. En outre, ces polyesters ont montré une bonne résistance thermique avec des résidus à 600°C allant jusqu'à 42%, ce qui pourrait en faire des matériaux utiles dans la protection incendie. Saleh *et al.* ont préparé une série de polyesters réticulés par des métaux, contenant le groupement 2,6-pyridyl et des diols aliphatiques, avec l'intention d'obtenir des films résistants à l'adhésion bactérienne [17]. Très récemment, une série de polyesters à partir des esters (2,4-, 2,5-, 2,6-)pyridinedicarboxylate de diéthyle



(DEPD24, DEPD25, DEPD26) et de diols aliphatiques (possédant de 4 à 8 carbones) ont été synthétisés par catalyse enzymatique en masse ou en solution dans le diphényléther [18]. Les masses molaires et les propriétés thermiques de ces polyesters sont résumées dans le Tableau R-3. Les masses molaires les plus élevées concernent les polyesters contenant des motifs 2,4-pyridinedicarboxyle tandis que des polyesters semi-cristallins ont été obtenus avec les 2,5- et 2,6-pyridinedicarboxylate de diéthyle.

**Tableau R-3** Polyesters obtenus à partir des pyridinedicarboxylates de diéthyle (catalysés par l'enzyme ICalB à 85°C et 20 mbar)

Méthode	Diester	Diol	$\overline{M}_n$ (g·mol <sup>-1</sup> )	$\overline{M}_w$ (g·mol <sup>-1</sup> )	$T_g^a$ (°C)	$T_f^b$ (°C)	$T_f^a$ (°C)
Masse	DEPD24	BD	800	1 400	-10	-	-
		HD	1 300	2 900	-20	-	-
		OD	1 800	4 200	-22	-	-
	DEPD25	BD	600	800	-	-	105
		HD	900	1 300	-	91	100
		OD	1 000	1 800	-	85	95
	DEPD26	BD	600	700	-	-	133
		HD	800	1 100	-	87	100
		OD	1 300	2 200	-	-	88
Solution (diphényléther)	DEPD24	BD	2 100	4 400	31	-	-
		HD	5 900	17 600	11	-	-
		OD	14 300	32 100	-1	-	-
	DEPD25	BD	1 200	1 900	-	-	157
		HD	4 800	10 800	-	122	131
		OD	8 100	12 100	-	120	128
	DEPD26	BD	600	700	-	-	165
		HD	2 200	4 300	-	111	128
		OD	3 200	7 000	-	86	102

DEPD : pyridinedicarboxylate de diéthyle ; BD : 1,4-butanediol ; HD : 1,6-hexanediol ; OD : 1,8-octanediol.

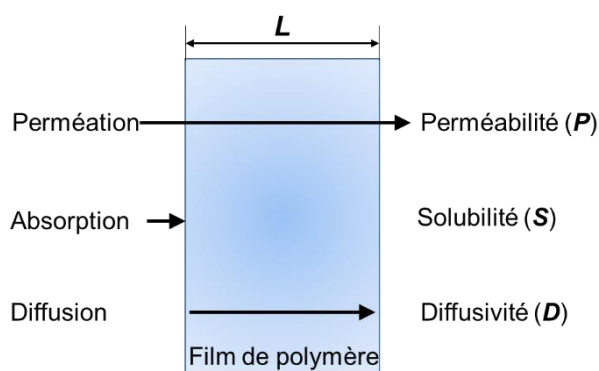
$\overline{M}_n$  : mesurées par SEC étalonnage PS.

<sup>a,b</sup> mesurées par DSC sous N<sub>2</sub> à 5°C·min<sup>-1</sup>; <sup>a</sup> deuxième chauffage ; <sup>b</sup> premier chauffage.

## Propriétés de perméation

### Paramètres utilisés pour caractériser les propriétés de perméation

Le transfert de masse à travers un film polymère par processus de perméation implique un phénomène d'absorption (dissolution) et de diffusion. Les paramètres caractéristiques sont le coefficient de perméabilité ( $P$ ), le coefficient de solubilité ( $S$ ) et le coefficient de diffusion ( $D$ ) (Figure R-1).



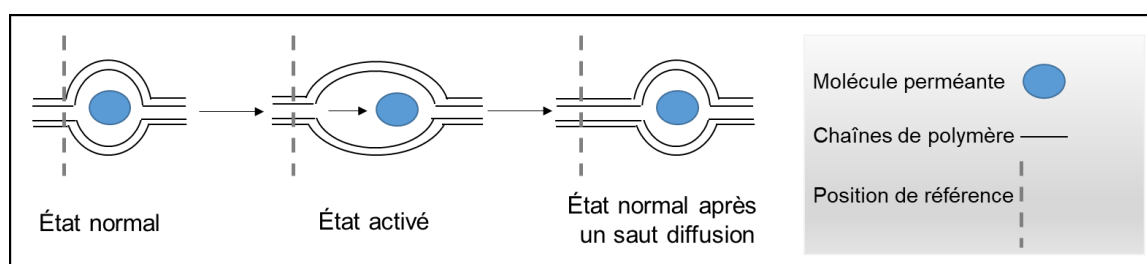
**Figure R-1** Phénomènes de transfert de masse et leurs coefficients caractéristiques [19]

Nous savons que la perméabilité d'un film polymère est le résultat d'un processus de dissolution-diffusion des pénétrants, où la dissolution (solubilité) décrit le processus thermodynamique et la diffusion reflète le processus cinétique [20]. Ainsi, le coefficient de perméabilité  $P$  est le résultat combiné du coefficient de solubilité  $S$  et du coefficient de diffusion  $D$  ( $P = D \times S$ ). Plus la valeur  $P$  est faible, plus le matériau est barrière.

### Facteurs influençant les propriétés de perméation

Comme  $P$  est le résultat combiné de  $D$  et de  $S$ , tous les facteurs qui peuvent affecter  $D$  et  $S$  peuvent par conséquent influencer  $P$ . En règle générale, le coefficient de perméabilité  $P$  est régi par les structures chimiques des polymères (comme la polarité, la linéarité des chaînes ou la présence de ramifications), et par les structures physiques (comme la densité, la cristallinité et l'orientation). D'autres facteurs environnementaux, tels que la pression, la température et l'humidité, peuvent également influencer  $P$ .

Un processus de diffusion activé, représenté sur la Figure R-2, peut être utilisé pour expliquer l'influence de la structure du polymère sur le transport des perméants. La diffusion activée, avec le déplacement du perméant d'un espace vide à l'autre, ne peut se produire que lorsqu'il y a une mobilité des segments de chaîne (relaxation ou déplacement) [20]. Par conséquent, tous les facteurs qui affectent la mobilité des segments de chaîne peuvent influencer les propriétés de transfert de masse du film polymère [20].



**Figure R-2** Processus de diffusion activé des perméants à travers un film polymère [21]

Pour être barrières, les polymères doivent posséder les caractéristiques suivantes [20,22] :

- (1) Un certain degré de polarité. Les polymères très polaires peuvent être fortement barrière aux gaz, mais faiblement barrière à l'eau vapeur, tandis qu'un polymère non polaire peut présenter un comportement inverse. En effet, un certain degré de polarité permet des interactions polymère-polymère au détriment des interactions polymère-pénétrant, ce qui diminue donc la diffusivité et par conséquent la perméabilité.
- (2) Une rigidité élevée des chaînes. La rigidité de la chaîne est généralement liée à la faible mobilité des segments de chaîne, ce qui entraîne une faible perméabilité.
- (3) Une inertie aux perméants. Les polymères, en particulier les polaires, lorsqu'ils absorbent des vapeurs vont se plastifier, induisant un gonflement et donc une diminution des propriétés barrières.
- (4) Un empilement compact des chaînes. Cette compacité induit de petites quantités de volume libre, de sorte que la diffusion du pénétrant est limitée. Elle est favorisée par la symétrie, l'ordre, la cristallinité et l'orientation de la structure.

- (5) Des liaisons ou des interactions entre les chaînes. Les réticulations et les attractions entre chaînes réduisent les mouvements moléculaires et entraînent donc une diffusion limitée des pénétrants.
- (6) Une  $T_g$  élevée. On sait que les polymères à l'état vitreux montreront peu de mobilité, ce qui offre un volume libre limité pour la diffusion des pénétrants, et diminue donc la perméabilité. Pour les applications d'emballage alimentaire, il est préférable d'utiliser un film polymère en dessous de sa  $T_g$  pour garder les propriétés barrières.

Parmi les caractéristiques mentionnées ci-dessus, certaines sont à double tranchant. Un film en polymère polaire peut fournir un certain degré de polarité et d'interactions entre chaînes, mais perdre en inertie vis-à-vis de certains pénétrants. Un groupe latéral encombrant peut, d'une part, réduire la mobilité des chaînes et ainsi diminuer la perméabilité, mais d'autre part, augmenter la distance entre les chaînes et favoriser la perméabilité.

Les données sur la perméabilité des polymères utilisés traditionnellement et potentiellement dans les emballages alimentaires sont résumées dans le Tableau R-4.

**Tableau R-4** Perméabilités à CO<sub>2</sub>, O<sub>2</sub>, N<sub>2</sub> et H<sub>2</sub>O à 25°C des polymères

Polymère	<i>P</i> (Barrer)				Réf
	N <sub>2</sub>	O <sub>2</sub>	CO <sub>2</sub>	H <sub>2</sub> O (90% RH)	
LLDPE	1,5	1,3-3,0	13	-	[22]
LDPE	0,6-1,9	3,0-6,7	13-28	80	[22]
HDPE	0,14-0,33	0,6-1,1	1,7-4,5	13	[22]
EVA (12% VA)	-	3,0-4,2	13,1-17,3	29	[22]
PP	0,44	0,9-2,3	9,2	57	[22]
PVC	0,04	0,005-0,12	0,03-1,0	156-275	[22]
PVdC	0,0009	0,0006	0,0022-0,0036	1,4-4,5	[22]
PS (orienté)	0,29-0,78	1,1-2,7	8,8-10,5	900-1 800	[22,23]
PAN	-	0,00024	0,006	2,2	[22]
PA6 (0% RH)	0,01	0,012-0,038	0,04-0,16	700	[22]
Nylon-MXD6	-	0,001-0,003	0,0093	-	[22]
PC	-	1,5	6,4	-	[22]
EVOH (32% C <sub>2</sub> H <sub>4</sub> )	0,000012	0,00012	0,00036	-	[22]
EVOH (44% C <sub>2</sub> H <sub>4</sub> )	0,00005	0,00048	0,0014	-	[22]
PCTF	0,01-0,13	0,03-0,50	0,05-1,25	0,3-36	[22]
CA	0,2-0,5	0,4-0,8	2,4-18	1 500-10 600	[22]
Cellophane	0,0032	0,0021	0,0047	1 900	[22]
PLA (98% L)	4,99	0,11-0,56	1,88	3 000	[22]
PLA (96% L)	1,3	3,3	10,2		[24]
PLA ( $\chi_c$ = 1.2%, 38°C)	-	0,59-0,64	-	216-223	[25]

Polymère	<i>P</i> (Barrer)				Réf
	N <sub>2</sub>	O <sub>2</sub>	CO <sub>2</sub>	H <sub>2</sub> O (90% RH)	
PEN	-	0,0075	0,022	-	[22]
PET ( $\chi_c$ = 40%)	0,006	0,01-0,030	0,12-0,16	130-183	[22]
PET (amorphe)	0,005	0,055-0,075	0,21-0,30	-	[22]
PET (amorphe, 30-35°C)	-	0,114	0,32-0,57	-	[26–30]
PEI (amorphe, 30°C)	-	0,015	0,038-0,045	-	[26,27,29]
PETI (T50/I50, 30°C)	-	0,025	-	-	[23]
PTT ( $\Delta H_f$ =55.5 J/g)	-	0,022-0,024	0,179-0,217	-	[31]
PBT	-	0,114	-	-	[32]
PEF (amorphe, 35°C)	-	0,011	0,026	-	[29,30]
PEF ( $\chi_c$ = 6-25%, 35°C)	-	0,0038-0,0058	0,012-0,017	-	[33]
PEF (amorphe)	-	-	1,14	-	[34]
PPF (amorphe)	-	-	-	19 (100% RH)	[35]
PPF ( $\Delta H_f$ =7.1 J/g)	0,0023	0,0038	0,0046	-	[36]
PNF	-	0,0049	0,00339	-	[37]

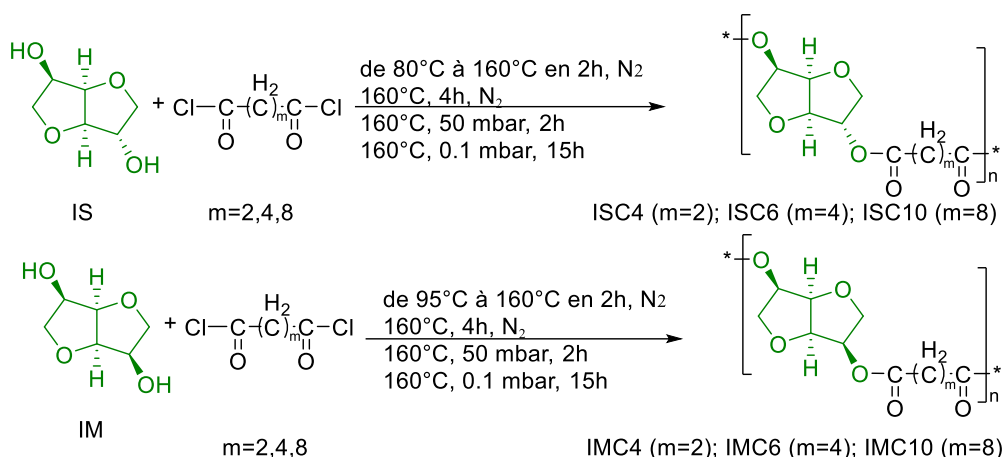
RH : humidité relative ; 1 barrer =  $10^{-10}$  cm<sup>3</sup> STP·cm·cm<sup>-2</sup>·s<sup>-1</sup>·cmHg<sup>-1</sup>.

## Chapitre 2 : Polyesters aliphatiques à base de 1,4:3,6-dianhydrohexitols

Ce Chapitre présente une série de polyesters aliphatiques à base d'isosorbide et d'isomannide. Ces polyesters ont déjà fait l'objet d'études en termes de propriétés thermiques et de biodégradabilité [2–7]. L'originalité de ce travail est d'étudier leurs propriétés de sorption/perméation aux gaz et à l'eau, qui sont cruciales pour les applications d'emballage alimentaire.

### Synthèse

Ces polyesters ont été synthétisés selon la méthode utilisée par Okada *et al* (Schéma R-3).



**Schéma R-3** Synthèse des polyesters aliphatiques à partir d'IS, d'IM

## Caractérisation des polyesters

Les principales caractéristiques des polyesters synthétisés sont résumées dans le Tableau R-5. Ces résultats sont cohérents avec ceux rapportés par Marubayashi *et al.* et Park *et al.* [4,5]. Les masses molaires et les températures de dégradation thermique augmentent avec le nombre de carbones aliphatiques, tandis que la  $T_g$  varie en sens inverse : la  $T_g$  la plus élevée ( $65^\circ\text{C}$ ) a été observée pour IMC4 et la plus basse ( $0^\circ\text{C}$ ) pour IMC10. Seuls ISC10, IMC4 et IMC10 sont semi-cristallins. Pour une chaîne aliphatique donnée, l'utilisation d'IS ou d'IM a peu d'influence sur  $T_g$ , mais modifie davantage la cristallisation : il semble que les différences stéréoscopiques exo-endo et endo-endo affectent la cristallisation plutôt que la relaxation des chaînes.

**Tableau R-5** Polyesters à base d'IS, d'IM et de chlorures d'acyle aliphatiques

Polyester	$\overline{M}_n$ ( $\text{g}\cdot\text{mol}^{-1}$ )	$\overline{D}$	Rendement (%)	$T_{5\%}$ ( $^\circ\text{C}$ )	$T_{\text{max}}$ ( $^\circ\text{C}$ )	$T_g^a$ ( $^\circ\text{C}$ )	$T_f^b$ ( $^\circ\text{C}$ )	$\Delta H_f^b$ ( $\text{J}\cdot\text{g}^{-1}$ )
ISC4	10 800	2,1	80	334	403	56	-	-
ISC6	10 600	1,7	88	372	419	28	-	-
ISC10	18 500	2,1	90	377	427	2	46/62*	18,7
IMC4	4 300	1,8	62	328	406	65	173	34,8
IMC6	10 500	2,5	85	358	417	26	-	-
IMC10	19 000	2,0	89	400	448	0	45/53*	15,9

$T_{5\%}$ , température de perte de masse de 5% ;  $T_{\text{max}}$ , température de vitesse de dégradation maximale ; mesurées par TGA sous  $\text{N}_2$  à  $10^\circ\text{C}\cdot\text{min}^{-1}$ .

$\overline{M}_n$  : mesurée par SEC étalonnage PMMA.

<sup>a</sup>DSC deuxième chauffage ; <sup>b</sup>DSC premier chauffage ; \*pics de fusion multiples ; mesurées sous  $\text{N}_2$  à  $10^\circ\text{C}\cdot\text{min}^{-1}$ .

## **Caractérisation des films**

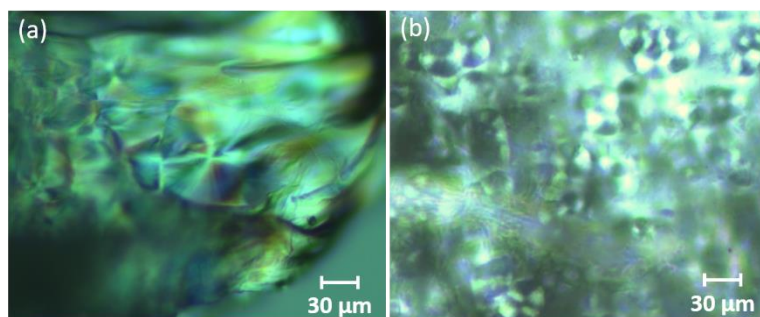
Seuls ISC10 et IMC10 ont pu être préparés avec succès sous forme de films utilisables. Leurs propriétés mécaniques et de perméation ainsi que leur cristallinité et énergie de surface ont été caractérisées. Les principaux résultats sont donnés dans le Tableau R-6.

**Tableau R-6** Films ISC10 et IMC10

Film	$\chi_c$ (%)	$E$ (MPa)	$\sigma_b$ (MPa)	$\varepsilon_b$ (%)	$\theta_w$ (°)	$P_{N_2}$ (barrer)	$P_{O_2}$ (barrer)	$P_{CO_2}$ (barrer)
ISC10	36,3	127±20	4,2±0,8	19±5	85±1,0	0,09±0,006	0,26±0,02	1,32±0,09
IMC10	25,9	125±10	1,0±0,2	16±3	83±0,5	0,18±0,01	0,46±0,03	2,04±0,14

$\chi_c$ , taux de cristallinité déterminé par DRX ;  $E$ , module d'Young ;  $\sigma_b$ , contrainte à la rupture ;  $\varepsilon_b$ , elongation à la rupture ;  $\theta_w$ , angle de contact à l'eau ;  $P_{N_2}$ ,  $P_{O_2}$  and  $P_{CO_2}$ , coefficients de perméabilité à  $N_2$ ,  $O_2$  et  $CO_2$  ; 1 barrer =  $10^{-10} \text{ cm}^3 \text{ STP} \cdot \text{cm} \cdot \text{cm}^{-2} \cdot \text{s}^{-1} \cdot \text{cmHg}^{-1}$ .

Les films ISC10 et IMC10 possèdent des valeurs élevées de  $\theta_w$ , témoin de leur hydrophobicité. Le film ISC10 est plus cristallin avec des cristaux plus gros que le film IMC10 (Figure R-3). Ces caractéristiques expliquent les meilleures propriétés mécaniques et barrières obtenues pour le film ISC10.

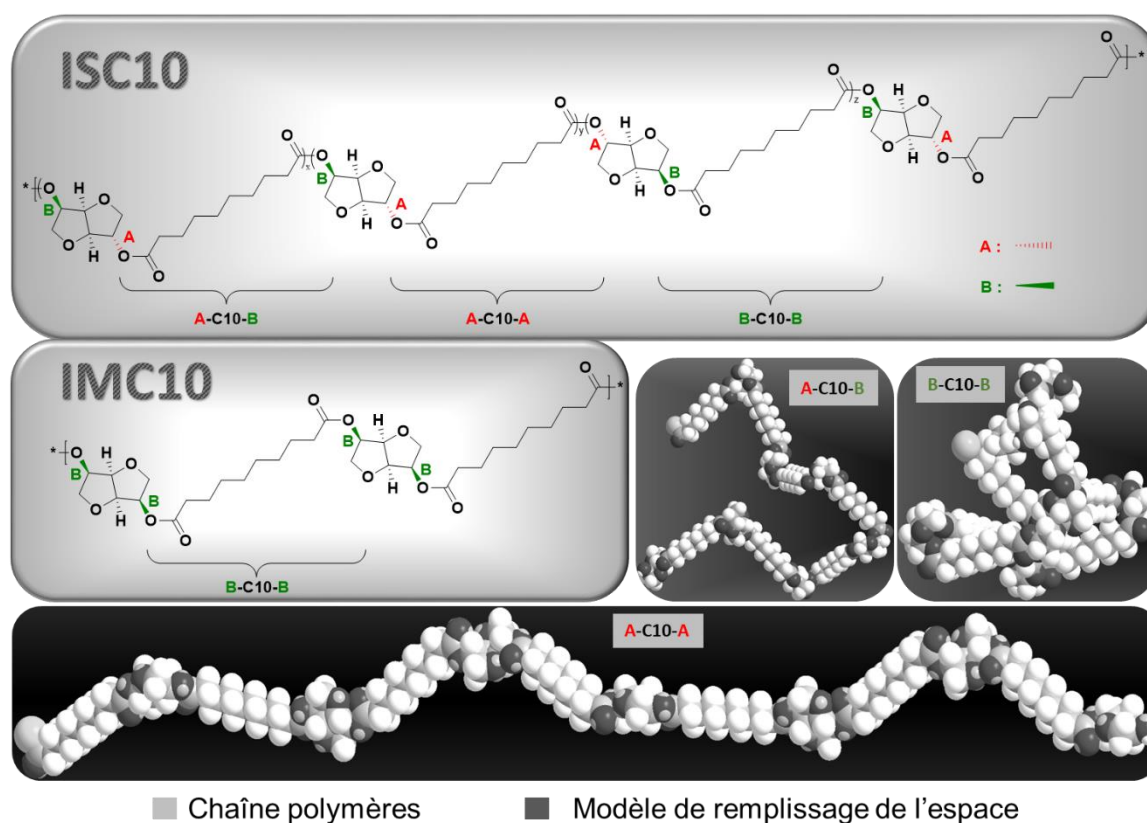


**Figure R-3** Microscopie optique polarisée des films ISC10 (a) et IMC10 (b)

## **Relations entre microstructure et propriétés**

La différente capacité de cristallisation entre ISC10 et IMC10 peut être attribuée à l'orientation de leurs chaînes comme le montre la Figure R-4, où A fait référence aux enchaînements exo et B aux endo. Ainsi, le motif ISC10 présente trois types d'enchaînements : exo-endo (A-C10-B), exo-exo (A-C10-A) et endo-endo (B-C10-B), tandis que le motif IMC10 ne contient que des liens endo-endo (B-C10-B). Il en résulte que IMC10 semble plus régulier si on considère peu de motif de répétition, et est donc plus propice à cristalliser. Mais à plus

grande échelle, les chaînes sont très incurvées, ce qui rend leur cristallisation par empilement plus difficile. A l'inverse, les enchaînements exo de l'ISC10 entraînent une chaîne plus linéaire sur de longues distances, qui peut donc facilement cristalliser et donner une microstructure plus dense [38,39] : plus les maillons exo-exo se répètent dans la chaîne, plus les chaînes vont pouvoir s'empiler. Cette différence dans l'orientation de la chaîne pourrait expliquer pourquoi ISC10 montre de plus gros cristaux avec une cristallinité plus élevée, d'où de meilleures propriétés mécaniques et barrières que IMC10.



**Figure R-4** Chaînes polymères (grises) et modèles correspondants dans l'espace (noir) prédits par le logiciel Chemdraw®

### Chapitre 3 : Polyesters à base de 2,6-pyridinedicarbone

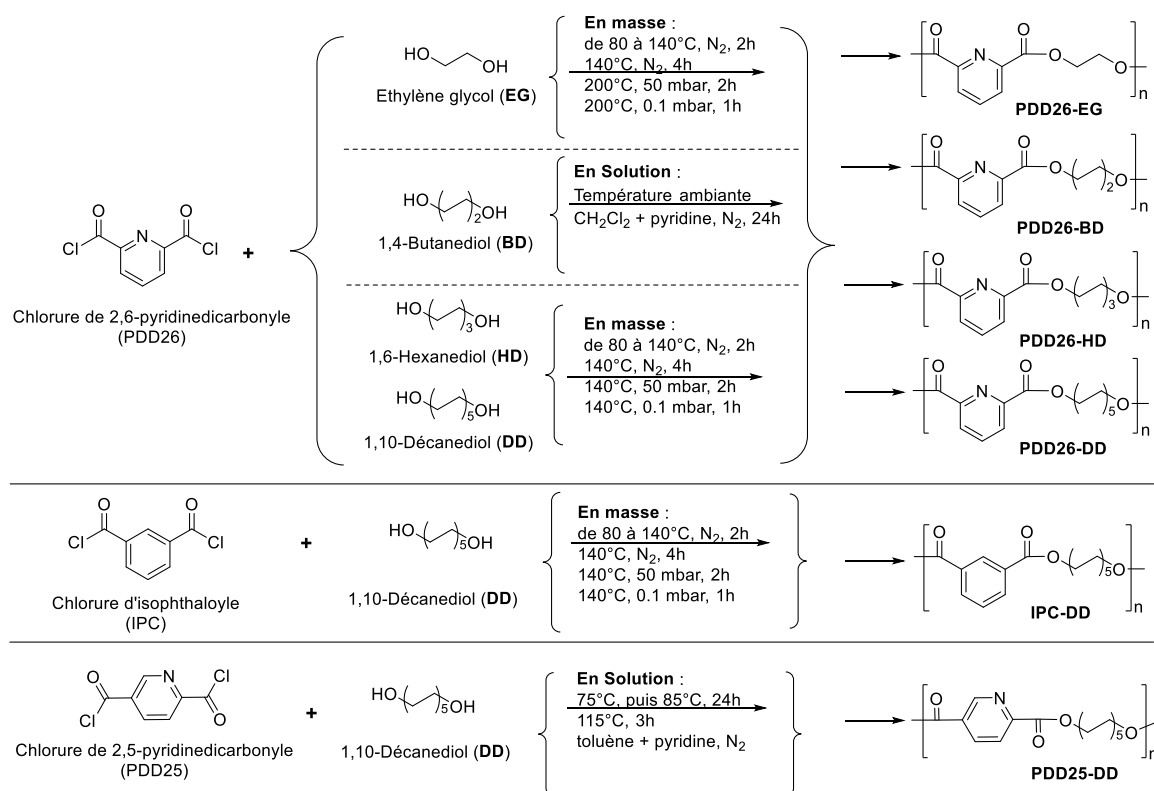
Ce Chapitre décrit une série de polyesters semi-aromatiques à base de chlorure de 2,6-pyridinedicarbone (PDD26) et de diols aliphatiques linéaires (éthylène glycol EG, butanediol BD, hexanediol HD et décanediol DD). Leurs synthèses et leurs propriétés thermiques sont discutées. Une étude plus approfondie des propriétés mécaniques et de perméation est réalisée sur le PDD26-DD qui est le seul à permettre l'obtention de film. Deux



analogues du PDD26-DD, nommés PDD25-DD et IPC-DD et synthétisés respectivement à partir du chlorure de 2,5-pyridinedicarbonyl (PDD25) et du chlorure d'isophthalyle (IPC), sont également étudiés à titre de comparaison.

## Synthèse

Les PDD26-BD et PDD26-HD ont déjà été synthétisés par d'autres auteurs en utilisant d'autres techniques [17,18], mais les masses molaires obtenues étaient faibles. Ainsi, en nous inspirant de différentes sources [3-5], plusieurs voies de synthèse ont été explorées (Schéma R-4).



**Schéma R-4** Synthèse des polyesters semi-aromatiques

## Caractérisation des polyesters

Les principales grandeurs caractéristiques de ces polyesters sont résumées dans le Tableau R-7. Tous les polyesters obtenus sont semi-cristallins. Les masses molaires et les rendements les plus élevés sont obtenus avec les polyesters contenant du DD, quel que soit le

noyau aromatique utilisé, confirmant que la nature du diol influence grandement la synthèse [17]. La stabilité thermique des polyesters à base de PDD26 augmente avec la masse molaire : PDD26-EG < PDD26-BD < PDD26-HD < PDD26-DD, tendance qui a déjà été observée pour PDD26-BD et PDD26-HD par Pellis *et al* [18]. La  $T_g$  diminue naturellement avec l'augmentation de la longueur du diol, mais la  $T_f$  semble suivre la tendance inverse. D'autre part, considérant que les polyesters comprenant une partie DD ont des masses molaires similaires, la structure PDD26 apporte moins de volume libre ( $T_g$  plus élevée) que les structures PDD25 et IPC, tandis que PDD25 permet d'atteindre la cristallinité la plus élevée.

**Tableau R-7** Polyesters semi-aromatiques

Polyester	$\overline{M}_n$ (g.mol <sup>-1</sup> )	$\bar{D}$	Rendement (%)	$T_{5\%}$ (°C)	$T_{max}$ (°C)	$T_g$ (°C)	$T_f$ (°C)	$\Delta H_f$ (J.g <sup>-1</sup> )
PDD26-EG	2 400/300 <sup>@</sup>	1,5/ 1,0 <sup>@</sup>	38	269	330	80	187 <sup>a</sup> /- <sup>b</sup>	32,4 <sup>a</sup> /- <sup>b</sup>
PDD26-BD	2 800/390 <sup>@</sup>	1,8/1,0 <sup>@</sup>	61	275	372	65*	189 <sup>a</sup> /183 <sup>b</sup>	68,2 <sup>a</sup> /49,4 <sup>b</sup>
PDD26-HD	5 100	1,9	73	329	385	14	123 <sup>a</sup> /128 <sup>b</sup>	42,1 <sup>a</sup> /38,1 <sup>b</sup>
PDD26-DD	24 500	2,1	92	341	384	0	110 <sup>a</sup> /111 <sup>b</sup>	29,5 <sup>a</sup> /31,2 <sup>b</sup>
PDD25-DD	25 700	2,0	90	304	365	-6*	124 <sup>a</sup> /124 <sup>b</sup>	61,3 <sup>a</sup> /52,5 <sup>b</sup>
IPC-DD	25 900	2,2	93	371	405	-14	45 <sup>a</sup> /- <sup>b</sup>	3,5 <sup>a</sup> /- <sup>b</sup>

<sup>@</sup>Deux populations observées par SEC (étalonnage PMMA).

$T_{5\%}$ , température de perte de masse de 5% ;  $T_{max}$ , température de vitesse de dégradation maximale ; mesurées par TGA sous N<sub>2</sub> à 10°C.min<sup>-1</sup>.

<sup>a</sup>DSC premier chauffage ; <sup>b</sup>DSC deuxième chauffage ; mesurées sous N<sub>2</sub> à 10°C.min<sup>-1</sup>.

\*mesurée par DMA sur la poudre ; \*mesurée par DMA sur le film en traction ; DMA à 3°C.min<sup>-1</sup>.

## Caractérisation des films

Les résultats correspondant aux PDD26-DD, PDD25-DD et IPC-DD, seuls polymères ayant permis l'obtention de films utilisables, sont rassemblés dans le Tableau R-8.

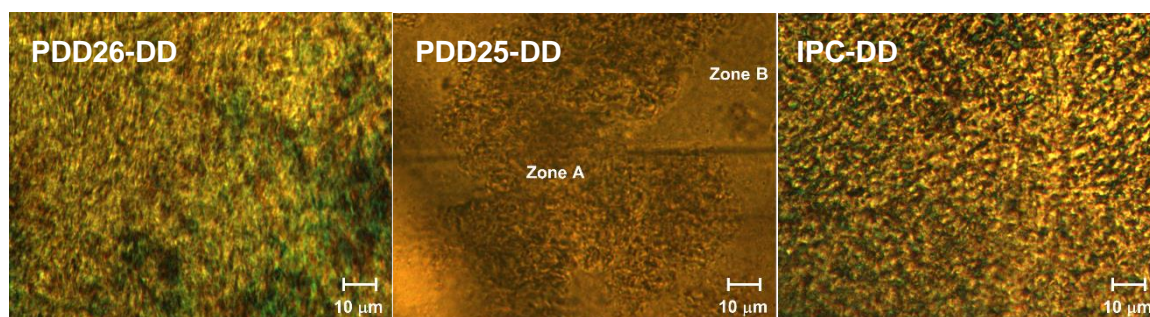
**Tableau R-8** Films de polyesters semi-aromatiques

Film	$\chi_c$ (%)	$E$ (MPa)	$\sigma_b$ (MPa)	$\varepsilon_b$ (%)	$\theta_w$ (°)	$P_{N_2}$ (barrer)	$P_{O_2}$ (barrer)	$P_{CO_2}$ (barrer)
PDD26-DD	36,0	770±25	12,5±4,8	25,0±6,0	90,0±0,4	0,030±0,003	0,070±0,005	0,30±0,02
PDD25-DD	50,4	880±20	21,0±2,0	3,4 ± 0,6	92,0±1,0	0,18±0,01	0,40±0,03	1,4±0,1
IPC-DD	20,5	140±15	5,5±1,2	420 ± 140	94,0±2,0	0,22±0,02	0,90±0,07	5,4±0,4

$\chi_c$ , taux de cristallinité déterminé par DRX ;  $E$ , module d'Young ;  $\sigma_b$ , contrainte à la rupture ;  $\varepsilon_b$ , elongation à la rupture ;  $\theta_w$ , angle de contact à l'eau ;  $P_{N_2}$ ,  $P_{O_2}$  and  $P_{CO_2}$ , coefficients de perméabilité à N<sub>2</sub>, O<sub>2</sub> et CO<sub>2</sub> ; 1 barrer = 10<sup>-10</sup> cm<sup>3</sup> STP.cm.cm<sup>-2</sup>.s<sup>-1</sup>.cmHg<sup>-1</sup>.

Tous les films sont hydrophobes ( $\theta_w \geq 90^\circ$ ). Ceux contenant la structure pyridine sont plus rigides que celui contenant le noyau benzénique. La cristallinité la plus élevée de PDD25-DD lui apporte une rigidité ( $E$ ) et une résistance ( $\sigma_b$ ) élevées, en contrepartie d'une

plasticité plus faible ( $\varepsilon_b$ ). Considérant qu'un allongement à la rupture trop long ou trop court peut être problématique lors de la mise en œuvre industrielle du film pour une application dans l'emballage, PDD26-DD semble être le meilleur candidat en termes de propriétés mécaniques. De plus, il possède la plus grande imperméabilité aux gaz, mais est peu performant vis-à-vis de l'eau. Ceci pourrait s'expliquer par le fait que l'eau, de nature plus condensable que les gaz, se condense davantage à cause de la polarité du motif, alors que les gaz sont freinés par la cristallinité. Cependant, PDD25-DD est moins barrière aux gaz que PDD26-DD bien que plus cristallin : ceci est probablement dû à une répartition cristalline beaucoup moins homogène pour PDD25-DD qui permet aux gaz de diffuser à travers les larges domaines amorphes (Figure R-5).



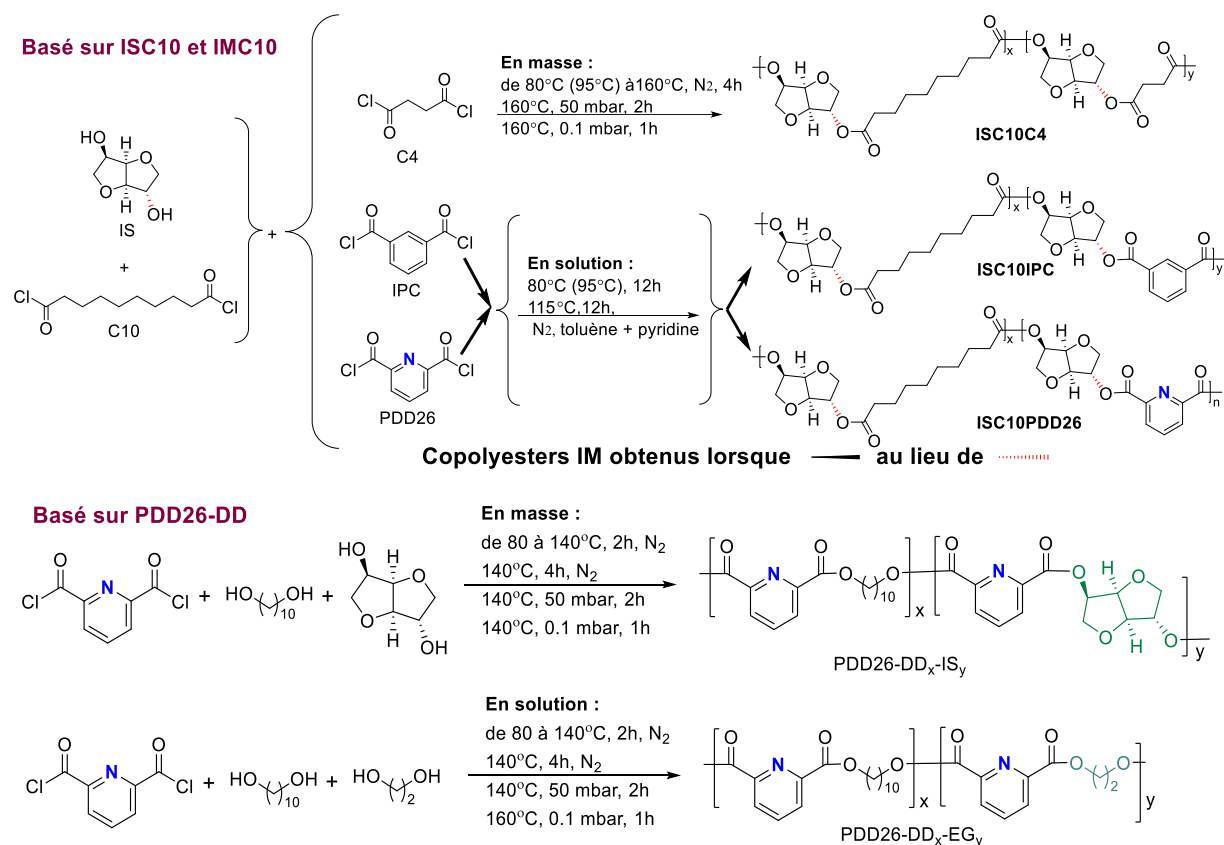
**Figure R-5** Microscopie optique polarisée des films

## Chapitre 4 : Copolyesters à base de 1,4:3,6-dianhydrohexitols ou de 2,6-pyridinedicarbonyle

Etant donné les résultats positifs obtenus précédemment avec les polyesters issus de 1,4:3,6-dianhydrohexitols d'une part, et de chlorure de 2,6-pyridinedicarbonyle d'autre part, ce Chapitre décrit une série de copolyesters les plus prometteurs à base d'isosorbide (IS), d'isomannide (IM) et de chlorure de 2,6-pyridinedicarbonyle (PDD26). Plus précisément, les polymères à base d'ISC10, IMC10 et PDD26-DD sont étudiés. L'objectif est d'augmenter la  $T_g$  de ces polymères afin d'améliorer leurs propriétés barrières, en incorporant un comonomère C4, IPC ou PDD26 sur les ISC10 et IMC10, ou bien une partie IS ou EG sur le PDD26-DD.

## Synthèse

Selon les monomères utilisés, différentes synthèses ont été mises en œuvre, comme le montre le Schéma R-5.



**Schéma R-5 Synthèse des copolyesters**

## Caractérisation des polyesters

Les principaux résultats obtenus pour les copolyesters sont donnés dans le Tableau R-9.

Concernant les copolyesters basés sur ISC10 et IMC10, l'utilisation de comonomères aromatiques (PDD26 et IPC) donnent systématiquement des masses molaires inférieures. Tous les copolyesters montrent une augmentation de  $T_g$  par rapport à ISC10 et IMC10, qui devient supérieure à la température ambiante. En outre, les noyaux aromatiques sont plus efficaces pour augmenter  $T_g$  qu'une courte chaîne aliphatique en C4. Entre les aromatiques, la structure 2,6-pyridine est la plus efficace. En revanche, tous les copolyesters sont amorphes à l'exception d'IMC10C4.

Pour les copolyesters basés sur PDD26-DD, l'introduction d'éthylène glycol dans PDD26-DD<sub>33</sub>-EG<sub>67</sub> entraîne, comme avec PDD26-EG, une chute de la masse molaire, accompagnée de la présence de deux populations, signe que la synthèse ne se déroule pas simplement. Néanmoins, PDD26-DD<sub>33</sub>-EG<sub>67</sub> donne une  $T_g$  relativement élevée, certainement en raison de la grande quantité d'EG dans le copolymère. L'introduction d'IS, quant à elle, entraîne une diminution générale des masses molaires à mesure que la proportion d'IS augmente. La  $T_g$  la plus élevée de la gamme PDD26-DD<sub>x</sub>-IS<sub>y</sub> n'est que de 12°C.

**Tableau R-9** Principaux résultats des copolyesters

Copolyester	$\overline{M}_n$ (g·mol <sup>-1</sup> )	$\overline{D}$	Rendement (%)	$T_{5\%}$ (°C)	$T_{max}$ (°C)	$T_g^1$ (°C)	$T_f^{2,*}$ (°C)	$\Delta H_f^2$ (J·g <sup>-1</sup> )
Basé sur ISC10 et IMC10								
ISC10C4	18 000	1,87	91	370	428	30	-	-
ISC10IPC	15 300	3,12	90	369	427	61	-	-
ISC10PDD26	11 500	2,34	85	328	398	40	-	-
IMC10C4	13 000	1,90	89	354	422	30	84 <sup>a</sup>	12
IMC10IPC	11 000	2,68	89	361	424	55	-	-
IMC10PDD26	10 600	2,28	86	338	400	64	-	-
Basé sur PDD26-DD								
PDD26-DD <sub>92</sub> -IS <sub>8</sub> <sup>#</sup>	17 100	1,98	90	350	392	6	110 <sup>b</sup>	32,3
PDD26-DD <sub>85</sub> -IS <sub>15</sub> <sup>#</sup>	11 100	2,19	83	343	391	12	109 <sup>c</sup>	32,1
PDD26-DD <sub>76</sub> -IS <sub>24</sub> <sup>#</sup>	4 000	2,00	76	336	388	8	103 <sup>d</sup>	28,2
PDD26-DD <sub>33</sub> -EG <sub>67</sub> <sup>#</sup>	2 700/320	1,51/1,00	66	256	346	35	75-146 <sup>e</sup>	30,5

<sup>#</sup>le nombre en indice correspond au rapport molaire des motifs de répétition dans le copolymère.

$T_{5\%}$ , température de perte de masse de 5% ;  $T_{max}$ , température de vitesse de dégradation maximale ; mesurées par TGA sous N<sub>2</sub> à 10°C·min<sup>-1</sup>.

$\overline{M}_n$  : mesurée par SEC étalonnage PMMA.

<sup>1</sup>DSC deuxième chauffage ; <sup>2</sup>DSC premier chauffage ; \*pics de fusion multiples : <sup>a</sup>74/84/96°C, <sup>b</sup>92/110°C, <sup>c</sup>94/109°C, <sup>d</sup>79/88/103°C ; <sup>e</sup>gamme de fusion large ; mesurées sous N<sub>2</sub> à 10°C·min<sup>-1</sup>.

## **Caractérisation des films**

Tous les copolyesters basés sur ISC10 et IMC10, mais seuls PDD26-DD<sub>92</sub>-IS<sub>8</sub> et PDD26-DD<sub>85</sub>-IS<sub>15</sub>, ont permis d'élaborer des films par compression. Les propriétés correspondantes des films sont résumées dans le Tableau R-10.

**Tableau R-10** Principaux résultats des films de copolyester

Film	$\chi_c$ (%)	$E$ (MPa)	$\sigma_b$ (MPa)	$\varepsilon_b$ (%)	$\theta_w$ (°)	$P_{N_2}$ (barrer)	$P_{O_2}$ (barrer)	$P_{CO_2}$ (barrer)
Basés sur ISC10 et IMC10								
ISC10C4	-	770±90	11,8±1,1	220±16	86,0±1,7	0,085±0,006	0,161±0,011	0,63±0,04
ISC10IPC	-	2100±50	59,0±1,7	3,6±0,4	87,0±1,2	0,045±0,003	0,079±0,005	0,40±0,03
ISC10PDD26	-	850±80	8,0±2,6	6,0±1,5	84,0±1,5	0,043±0,003	0,077±0,005	0,37±0,02
IMC10C4	11,7	1180±80	21,0±2,7	12,0±1,0	86,0±0,8	0,019±0,001	0,042±0,003	0,26±0,02
IMC10IPC	-	1820±30	50,0±1,7	3,0±0,3	87,0±1,0	0,051±0,003	0,096±0,007	0,59±0,04
IMC10PDD26	-	1900±40	50,0±1,2	3,0±0,4	83,0±1,3	0,014±0,001	0,025±0,002	0,12±0,01
Basés sur PDD26-DD								
PDD26-DD <sub>92</sub> -IS <sub>8</sub> <sup>#</sup>	29,9	1390±170	31,6±2,7	9,6±1,6	88,0±0,8	0,027±0,002	0,08±0,005	0,36±0,02
PDD26-DD <sub>85</sub> -IS <sub>15</sub> <sup>#</sup>	32,8	1095±110	21,0±1,0	2,5±0,2	86,0±1,2	0,037±0,002	0,11±0,007	0,45±0,03

$\chi_c$ , taux de cristallinité déterminé par DRX ;  $E$ , module d'Young ;  $\sigma_b$ , contrainte à la rupture ;  $\varepsilon_b$ , élongation à la rupture ;  $\theta_w$ , angle de contact à l'eau ;  $P_{N_2}$ ,  $P_{O_2}$  and  $P_{CO_2}$ , coefficients de perméabilité à  $N_2$ ,  $O_2$  et  $CO_2$  ; 1 barrer =  $10^{-10}$  cm<sup>3</sup> STP·cm·cm<sup>-2</sup>·s<sup>-1</sup>·cmHg<sup>-1</sup>.

Les films basés sur ISC10 et IMC10 montre tous une rigidité ( $E$ ) et une résistance ( $\sigma_b$ ) accrues par rapport aux films ISC10 ( $E = 127 \pm 20$  MPa,  $\sigma_b = 4,2 \pm 0,8$  MPa,  $\varepsilon_b = 19 \pm 5$  %) et IMC10 ( $E = 125 \pm 10$  MPa,  $\sigma_b = 1,0 \pm 0,2$  MPa,  $\varepsilon_b = 16 \pm 3$  %), avec une diminution de l'allongement à la rupture. Le cas particulier de ISC10C4, dont l'allongement à la rupture est élevé, pourrait s'expliquer par sa masse molaire élevée combinée à une  $T_g$  proche de la température ambiante, de sorte qu'un léger échauffement localisé dû à la traction pourrait favoriser le désenchevêtrement des chaînes [41,42]. Globalement, les noyaux aromatiques apportent davantage de rigidité, de résistance et de comportement fragile. Tous les copolyesters ont un caractère barrière à l'eau et aux gaz nettement amélioré par rapport aux films initiaux ISC10 et IMC10. Ceci est certainement dû à l'augmentation de la  $T_g$ , conséquence de la diminution de volume libre apportée par ces motifs moins mobiles. De plus, la structure 2,6-pyridine permet d'obtenir les meilleures propriétés barrières aux gaz.

De même, les films PDD26-DD<sub>92</sub>-IS<sub>8</sub> et PDD26-DD<sub>85</sub>-IS<sub>15</sub> montrent les mêmes améliorations en termes de comportement mécanique par rapport au PDD26-DD. Cependant, les propriétés barrières sont légèrement moins bonnes : même si la  $T_g$  augmente, elle reste en-dessous de la température ambiante, ce qui ne parvient pas à compenser, en termes de propriétés barrières, la légère baisse de cristallinité.

## Conclusion Générale

Au cours de cette thèse, plusieurs nouveaux polyesters entièrement biosourcés et destinés à des applications d'emballage alimentaire ont été synthétisés. Ils ont été étudiés en termes de propriétés thermiques, mécaniques et en particulier de transport à l'eau et aux gaz ( $N_2$ ,  $O_2$  et  $CO_2$ ). Des relations entre la microstructure, la morphologie, les propriétés physicochimiques et fonctionnelles ont également été établies.

Tout d'abord, six polyesters biosourcés aliphatiques ont été obtenus par polycondensation en masse entre l'isosorbide (IS) ou l'isomannide (IM) et les chlorures de succinyle (C4), d'adipoyle (C6) et de sébacoylole (C10). Des masses molaires variant de 4 300 à 19 000  $g \cdot mol^{-1}$ , des stabilités thermiques supérieures à 325°C, des  $T_g$  allant de 0°C à 65°C ont été obtenues, avec parfois de la cristallinité. Il a été établi que la stéréoisomérisation de IS et de IM influence principalement les propriétés de cristallisation, tandis que la longueur des unités dichlorure influence la dégradation thermique, la température de transition vitreuse ainsi que la cristallisation. Des films flexibles n'ont pu être obtenus qu'avec ISC10 et IMC10. Le remarquable ISC10 possède des cristaux plus grands et une cristallinité plus élevée, contribuant à une contrainte à la rupture en traction plus élevée ( $\sigma_b$ ) et à de meilleures propriétés barrières à l'eau et aux gaz, ces dernières étant par ailleurs similaires à celles du PLA. Même si les propriétés barrières d'ISC10 sont inférieures à celles du PET et du PEF, les sélectivités au  $CO_2$  et à  $O_2$  sont cependant au moins aussi bonnes que celles du PET et du PEF, ce qui est très favorable à la conservation des fruits et légumes.

Deuxièmement, quatre polyesters biosourcés semi-aromatiques contenant le chlorure de 2,6-pyridinedicarbonylole (PDD26) et des diols aliphatiques (éthylène glycol, EG ; 1,4-butanediol, BD ; 1,6-hexanediol, HD ; 1,10-décantediol, DD) ont été synthétisés par polycondensation. Seul PDD26-DD a montré des masses molaires élevées, de sorte que deux analogues, nommés PDD25-DD et IPC-DD, ont été synthétisés, avec des masses molaires tout aussi satisfaisantes (environ 25 000  $g \cdot mol^{-1}$ ), et ont été comparés au PDD26-DD. Les polyesters contenant des cycles pyridine (PDD26-DD et PDD25-DD) ont montré des températures de dégradation thermique plus faibles (341 et 304°C) par rapport à celui contenant des noyaux phényle (IPC-DD, 371°C). Cependant, les  $T_g$ , toujours en dessous de la température ambiante, les  $T_f$  et les taux de cristallinité se sont avérés plus élevés. Parmi tous, PDD26-DD a montré des propriétés mécaniques préférables avec les propriétés barrières aux gaz les plus élevées, meilleures que le PLA et comparables au PET amorphe. En un mot, PDD26-DD a un grand

potentiel dans le domaine de l'emballage alimentaire, en particulier lorsque des propriétés barrières élevées au CO<sub>2</sub> et à O<sub>2</sub> sont nécessaires.

Enfin, les travaux ont porté sur l'amélioration des propriétés barrières des ISC10, IMC10 et PDD26-DD en augmentant leur  $T_g$ . L'idée générale était d'incorporer un troisième monomère rigide ou à chaîne courte par copolycondensation. Deux scénarios ont été envisagés : l'un sur des copolyesters basés sur ISC10 et IMC10, et l'autre sur des copolyesters basés sur le PDD26-DD. Dans la première partie, six copolyesters, impliquant ISC10 ou IMC10 et un deuxième dichlorure d'acyle (aliphatique (C4) ou aromatique (IPC et PDD26)), ont été synthétisés. Les copolyesters ont été obtenus avec des  $\overline{M}_n$  entre 10 600 et 18 000 g·mol<sup>-1</sup>, des stabilités thermiques ( $T_{5\%}$ ) supérieures à 328°C et des  $T_g$  entre 10 et 64°C. Le dichlorure d'acyle a donc considérablement augmenté la  $T_g$  d'ISC10 et d'IMC10, et plus généralement le squelette aromatique, en particulier le cycle pyridine, s'est montré le plus efficace. Tous les copolyesters ont montré des propriétés barrières améliorées (à la fois à l'eau et aux gaz) par rapport à ISC10 et IMC10. D'un point de vue propriétés barrières aux gaz, IMC10PDD26 est le meilleur, ce qui est lié à sa  $T_g$  élevée ( $T_g = 64^\circ\text{C}$ ) et à sa structure pyridine. Ses propriétés hautement barrières sont bien meilleures que celles des matériaux couramment utilisés dans l'emballage alimentaire, tels que les PE, PP, PS, et PLA, et même comparable au très largement utilisé PET semi-cristallin. Dans la deuxième partie, des copolyesters impliquant PDD26-DD et un deuxième diol linéaire bicyclique ou à chaîne courte (IS ou EG) ont été synthétisés. Cependant, des difficultés ont été rencontrées pour incorporer le deuxième diol rigide et une diminution générale des masses molaires a été observée. Pour cette raison, PDD26-DD<sub>33</sub>-EG<sub>67</sub>, malgré sa  $T_g$  satisfaisante à 35°C, ne nous a pas permis d'obtenir un film utilisable. Même si la  $T_g$  de PDD26-DD<sub>x</sub>-IS<sub>y</sub> n'a pu être augmentée au-delà de 12°C, l'obtention de films contenant 8% molaire (PDD26-DD<sub>92</sub>-IS<sub>8</sub>) et 15% molaire (PDD26-DD<sub>85</sub>-IS<sub>15</sub>) d'IS a été encourageante pour mener une étude plus approfondie. Même si l'incorporation d'IS a généralement diminué la cristallinité des films et légèrement diminué les propriétés barrières à l'eau et aux gaz par rapport à PDD26-DD, les propriétés mécaniques en termes de  $E$  et  $\sigma_b$  ont été fortement améliorées. PDD26-DD<sub>92</sub>-IS<sub>8</sub> fournit ainsi des propriétés supplémentaires, notamment mécaniques, à PDD26-DD pour une application dans l'emballage alimentaire.

En résumé, une série de polyesters et copolyesters biosourcés basés sur les 1,4:3,6-dianhydrohexitols et/ou le chlorure de 2,6-pyridinedicarbonyl ont été synthétisés par des réactions de polycondensation. Des caractéristiques importantes, telles que les propriétés



thermiques, mécaniques et de transport à l'eau et aux gaz, pour des applications dans le domaine de l'emballage alimentaire, ont été étudiées. Ces polyesters présentent une grande variété de propriétés thermiques et mécaniques et de bonnes à excellentes propriétés barrières à l'eau et aux gaz ( $N_2$ ,  $O_2$ ,  $CO_2$ ). Celles-ci sont parfois au niveau de celles du PET, suggérant ainsi un large éventail d'applications dans l'emballage alimentaire.

## **Perspectives**

Afin d'étendre ces travaux et de continuer à recueillir des informations sur ces polymères prometteurs, plusieurs perspectives peuvent être envisagées.

Considérant que l'augmentation de  $T_g$  par copolymérisation améliore les propriétés mécaniques et barrières à l'eau et aux gaz, il semble intéressant d'utiliser ISC4 et IMC4, qui ont déjà une  $T_g$  élevée, pour développer des matériaux hautement barrières. Cependant, nous avons montré que ces polyesters n'étaient pas filmogènes. Il serait donc intéressant d'améliorer les conditions de synthèse pour obtenir des polyesters de masses molaires plus élevées, et donc plus aptes à former des films.

La présence de cycles 2,6-pyridine dans la structure des chaînes polyesters a montré son efficacité pour augmenter la  $T_g$  et la cristallinité, et apporter de bonnes propriétés mécaniques et d'excellentes propriétés barrières aux gaz. Ainsi, les monomères à cycle 2,6-pyridine pourraient devenir une sorte de plateforme pour développer de nouveaux et prometteurs polyesters biosourcés destinés à l'emballage alimentaire. En particulier, le PDD26-EG pourrait posséder de meilleures propriétés barrières aux gaz que l'inégalé PEF. En outre, les polymères contenant des cycles pyridine dans leur structure peuvent également montrer un intérêt en tant que matériaux antibactériens. Ainsi, l'étude des propriétés antibactériennes des polyesters à base de 2,6-pyridine et de 2,5-pyridine pourrait apporter une valeur supplémentaire à ces polymères et élargir leurs applications dans les emballages alimentaires.

Il convient de souligner que dans ce travail, nous n'avons pas maîtrisé la cristallisation lors de la préparation des films. Des études approfondies de cristallisation et de recuit, ainsi que leurs conséquences sur la cristallinité, le polymorphisme et les propriétés mécaniques et de transport, pourraient être très pertinentes sur ces structures particulières basées sur les 2,6 et 2,5-pyridine, telles que les PDD26-EG, PDD26-BD, PDD26-DD et PDD25-DD.

Il serait également intéressant d'étudier les propriétés barrières aux gaz des films sous différentes teneurs en humidité. En effet, l'hydrophilie apportée par les groupes polaires des polyesters pourrait modifier leurs propriétés de perméation lorsqu'ils seront utilisés dans un environnement humide.

Enfin, en prenant en compte la chimie verte et les questions environnementales, il reste plusieurs travaux à réaliser : optimiser les conditions de synthèse en partant de diacides ou de diesters au lieu de dichlorures d'acyle ; étudier la biodégradabilité des polyesters obtenus ; évaluer la recyclabilité chimique et mécanique de ces polyesters.

## Références

- [1] F. Fenouillot, A. Rousseau, G. Colomines, R. Saint-Loup, J.P. Pascault, Polymers from renewable 1,4:3,6-dianhydrohexitols (isosorbide, isomannide and isoidide): A review, *Prog. Polym. Sci.* 35 (2010) 578–622.
- [2] M. Okada, Y. Okada, A. Tao, K. Aoi, Biodegradable polymers based on renewable resources: Polyesters composed of 1,4 : 3,6-dianhydrohexitol and aliphatic dicarboxylic acid units, *J. Appl. Polym. Sci.* 62 (1996) 2257–2265.
- [3] M. Okada, Y. Okada, K. Aoi, Dianhydrohexitols and aliphatic dicarboxylic acids, *J. Polym. Sci. Part A Polym. Chem.* 33 (1995) 2813–2820.
- [4] H.S. Park, M.S. Gong, J.C. Knowles, Synthesis and biocompatibility properties of polyester containing various diacid based on isosorbide, *J. Biomater. Appl.* 27 (2012) 99–109.
- [5] H. Marubayashi, T. Ushio, S. Nojima, Crystallization of polyesters composed of isohexides and aliphatic dicarboxylic acids: effects of isohexide stereoisomerism and dicarboxylic acid chain length, *Polym. Degrad. Stab.* 146 (2017) 174–183.
- [6] D. Braun, M. Bergmann, 1,4:3,6 - Dianhydrohexite als bausteine für polymere, *J. Für Prakt. Chemie/Chemiker-Zeitung.* 334 (1992) 298–310.
- [7] M. Okada, K. Tsunoda, K. Tachikawa, K. Aoi, Biodegradable polymers based on renewable resources. IV. Enzymatic degradation of polyesters composed of 1,4:3,6-dianhydro-D-glucitol and aliphatic dicarboxylic acid moieties, *J. Appl. Polym. Sci.* 77 (2000) 338–346.
- [8] H. Marubayashi, T. Ushio, S. Nojima, Crystal polymorphism of biobased polyester composed of isomannide and succinic acid, *Macromolecules.* 52 (2019) 4624–4633.
- [9] J. Thiem, H. Lüders, Synthesis of polyterephthalates derived from dianhydrohexitols, *Polym. Bull.* 11 (1984) 365–369.
- [10] R. Storbeck, M. Rehahn, M. Ballauff, Synthesis and properties of high-molecular-weight polyesters based on 1,4 : 3,6-dianhydrohexitols and terephthalic acid, 64 (1993) 53–64.
- [11] R. Storbeck, M. Ballauff, Synthesis and properties of polyesters based on 2,5-furandicarboxylic acid and 1,4:3,6-dianhydrohexitols, *Polymer.* 34 (1993) 5003–5006.

- [12] H.R. Kricheldorf, G. Behnken, M. Sell, Influence of isosorbide on glass-transition temperature and crystallinity of poly(butylene terephthalate), *J. Macromol. Sci. Part A Pure Appl. Chem.* 44 (2007) 679–684.
- [13] Z. Mycroft, M. Gomis, P. Mines, P. Law, T.D.H. Bugg, Biocatalytic conversion of lignin to aromatic dicarboxylic acids in *rhodococcus jostii* RHA1 by re-routing aromatic degradation pathways, *Green Chem.* 17 (2015) 4974–4979.
- [14] J.F. Powell, Isolation of dipicolinic acid (pyridine-2:6-dicarboxylic acid) from spores of *Bacillus megatherium.*, *Biochem. J.* 54 (1953) 210–211.
- [15] N. Watanabe, M. Hattori, E. Yokoyama, S. Isomura, M. Ujita, A. Hara, Entomogenous fungi that produce 2,6-pyridine dicarboxylic acid (dipicolinic acid), *J. Biosci. Bioeng.* 102 (2006) 365–368.
- [16] H.N. Isfahani, K. Faghihi, New thermally stable polyesters based on 2,5-pyridinedicarbonyl dichloride and aromatic diols: Synthesis and characterization, *Chinese Chem. Lett.* 20 (2009) 885–888.
- [17] S. Saleh, B. Sweileh, S.O. Taha, R. Mahmoud, M.O. Taha, Preparation of polyester-based metal-cross linked polymeric composites as novel materials resistant to bacterial adhesion and biofilm formation, *Molecules.* 16 (2011) 933–950.
- [18] A. Pellis, J.W. Comerford, S. Weinberger, G.M. Guebitz, J.H. Clark, T.J. Farmer, Enzymatic synthesis of lignin derivable pyridine based polyesters for the substitution of petroleum derived plastics, *Nat. Commun.* 10 (2019).
- [19] J.H. Han, M.G. Scanlon, Mass transfer of gas and solute through packaging materials, in: *Innov. Food Packag.*, 2nd ed, Elsevier Ltd, 2013: pp. 37–49.
- [20] K.S. Miller, J.M. Krochta, Oxygen and aroma barrier properties of edible films: a review, *Trends Food Sci. Technol.* 8 (1997) 228–237.
- [21] A.T. DiBenedetto, Molecular properties of amorphous high polymers. II. An interpretation of gaseous diffusion through polymers, *J. Polym. Sci. Part A Gen. Pap.* 1 (1963) 3477–3487.
- [22] Robertson, G. L, *Food packaging-Principles and practice*, 3rd ed., Taylor & Francis, 2013.
- [23] J. Brandrup, E.H. Immergut, E.A. Grulke, *Polymer handbook*, 4th ed, 1999.
- [24] H.J. Lehermeier, J.R. Dorgan, J. Douglas Way, Gas permeation properties of poly(lactic acid), *J. Memb. Sci.* 190 (2001) 243–251.
- [25] G. Flodberg, I. Helland, L. Thomsson, S. Bodil Fredriksen, Barrier properties of polypropylene carbonate and poly(lactic acid) cast films, *Eur. Polym. J.* 63 (2015) 217–226.
- [26] R.R. Light, R.W. Seymour, Effect of sub - Tg relaxations on the gas transport properties of polyesters, *Polym. Eng. Sci.* 22 (1982) 857–864.
- [27] R. Kotek, K. Pang, B. Schmidt, A. Tonelli, Synthesis and gas barrier characterization of poly(ethylene isophthalate), *J. Polym. Sci. Part B Polym. Phys.* 42 (2004) 4247–4254.
- [28] W.I.M. Brolly J B, Bower D I, Diffusion and sorption of CO<sub>2</sub> in poly (ethylene terephthalate) and poly (ethylene naphthalate), *J. Polym. Sci. Part B Polym. Phys.* 34 (1996) 769–780.

- 
- [29] S.K. Burgess, O. Karvan, J.R. Johnson, R.M. Kriegel, W.J. Koros, Oxygen sorption and transport in amorphous poly(ethylene furanoate), *Polymer*. 55 (2014) 4748–4756.
  - [30] S.K. Burgess, R.M. Kriegel, W.J. Koros, Carbon dioxide sorption and transport in amorphous poly(ethylene furanoate), *Macromolecules*. 48 (2015) 2184–2193.
  - [31] J. Diani, K. Gall, Finite strain 3D thermoviscoelastic constitutive model for shape memory polymers, *Polym. Eng. Sci.* 46 (2006) 486–492.
  - [32] R.R. Smith, J.R. Wilson, Polyester melt blends having high gas barrier properties, 1982.
  - [33] S.K. Burgess, G.B. Wenz, R.M. Kriegel, W.J. Koros, Penetrant transport in semicrystalline poly(ethylene furanoate), *Polymer*. 98 (2016) 305–310.
  - [34] L. Sun, J. Wang, S. Mahmud, Y. Jiang, J. Zhu, X. Liu, New insight into the mechanism for the excellent gas properties of poly(ethylene 2,5-furandicarboxylate) (PEF): role of furan ring's polarity, *Eur. Polym. J.* 118 (2019) 642–650.
  - [35] M. Vannini, P. Marchese, A. Celli, C. Lorenzetti, Fully biobased poly(propylene 2,5-furandicarboxylate) for packaging applications: excellent barrier properties as a function of crystallinity, *Green Chem.* 17 (2015) 4162–4166.
  - [36] G. Guidotti, L. Genovese, M. Soccio, M. Gigli, A. Munari, V. Siracusa, N. Lotti, Block copolyesters containing 2,5-furan and trans-1,4-cyclohexane subunits with outstanding gas barrier properties, *Int. J. Mol. Sci.* 20 (2019) 2187.
  - [37] L. Genovese, N. Lotti, V. Siracusa, A. Munari, Poly(neopentyl glycol furanoate): a member of the furan-based polyester family with smart barrier performances for sustainable food packaging applications, *Materials (Basel)*. 10 (2017) 1028.
  - [38] V. Morillon, F. Debeaufort, G. Blond, M. Capelle, A. Voilley, Factors affecting the moisture permeability of lipid-based edible films: A review, *Crit. Rev. Food Sci. Nutr.* 42 (2002) 67–89.
  - [39] Q. Liu, X. Sun, H. Li, S. Yan, Orientation-induced crystallization of isotactic polypropylene, *Polymer*. 54 (2013) 4404–4421.
  - [40] M. Garaleh, T. Yashiro, H.R. Kricheldorf, P. Simon, T. Yashiro, P. Simon, ( Co- ) Polyesters derived from isosorbide and 1,4-Cyclohexane dicarboxylic acid and succinic acid, 211 (2010) 1206–1214.
  - [41] H.G.. Van Melick, L.E. Govaert, H.E.H. Meijer, On the origin of strain hardening in glassy polymers, *Polymer*. 44 (2003) 2493–2502.
  - [42] D.C. Prevorsek, B.T. De Bona, On chain entanglement in high-Tg amorphous polymers, *J. Polym. Sci. Part B Polym. Phys.* 19 (1981) 605–622.



---

## ∞ General Introduction ∞

---



Food packaging is essential in our daily life due to the mandatory requirements to protect and preserve foods. Besides metals, paper and glass, plastics dominate the market due to their attractive cost/performance ratio: their volume allocated to food packaging is estimated around 40% of the whole plastics consumption. Traditionally, they are petroleum-based polymers. However, the limited crude oil and the increasing environmental issues are arising awareness worldwide. Hence, at the Paris climate conference (COP21) in December 2015, 195 countries adopted the first-ever universal, legally binding global climate deal. This agreement sets out a global action plan to limit global warming with the reorientation of the world economy towards a low carbon model. Among the proposed solutions, one would be to prepare natural, biodegradable materials made from renewable resources.

The bio-based polymers used in food packaging can be classified into three main categories according to their method of production, namely, polymers directly extracted from biomass, such as starch, cellulose and chitin, polymers produced by chemical synthesis from biomass monomers, such as polylactic acid (PLA), bio-polyethylene terephthalate (bio-PET) and bio-polyethylene (bio-PE), and polymers produced directly by natural or genetically modified organisms, such as polyhydroxyalkanoates (PHAs).

Natural polymers extracted from biomass are abundant and cost-effective but usually show poor water resistance and are difficult to process.

Even if bio-PE is accessible, there is currently no low-cost way to produce bioethylene, and moreover, the biopolymer has the same poor gas barrier properties as PE and is not biodegradable either.

In contrast, bio-based polyesters are attractive for their comprehensive advantages, such as a wide range of available monomers, tunable performances, possible biodegradability, numerous recycling and recovery options, and well-established industrial polycondensation reactor infrastructures.

Although many efforts have been made to develop full bio-PET, the limited production associated with the high cost of terephthalic acid make it currently impossible to scale-up. The bio-based polyesters used for food packaging applications are therefore limited to polyhydroxyalkanoates (PHAs) and polylactic acid (PLA). However, they show mechanical and barrier properties often lower than petroleum-based polymers. In addition to improving the properties of PHA and PLA, the progress in polymer science encourages to synthesize new bio-



based polyesters. Of course, their thermal, mechanical, and transport properties must be studied before considering the replacement of conventional polymers.

Recently, polyethylene furanoate (PEF), a 100% renewable polyester that is intended to replace in the future PET for water and soda packaging, has been confirmed with high oxygen and carbon dioxide barrier properties. Such excellent properties were attributed to the rigidity and polarity of the 2,5-furandicarboxylic moiety. This inspires us to work on some new nontoxic bifunctional molecules, such as 1,4:3,6-dianhydrohexitols and (2,4-, 2,5- and 2,6-) pyridinedicarboxylic acids, which also show rigidity and polarity and can be extracted from biomass.

Thus, this thesis is directed to preparing 100% bio-based (co)polyesters from 1,4:3,6-dianhydrohexitols and/or pyridinedicarboxylic acids. Their thermal, mechanical and especially, transport properties are investigated.

Four chapters are orderly organized. Following this general Introduction, Chapter 1 gives an overview of the main bio-based polymers, their most common limitations and the current or possible use in food packaging. The emphasis is put on bio-based polyesters. Then, a brief introduction of the traditional methods to synthesize polyesters is provided. General properties, regarding thermal, mechanical and permeation properties for food packaging applications are made in the context. Challenges and opportunities that remain for bio-based food packaging polymers are shortly reviewed.

Chapter 2 presents a series of aliphatic polyesters based on isosorbide and isomannide. These polyesters have already been synthesized and investigated in terms of biodegradability by Okada *et al.* The originality of our work is to study their gas and water sorption/permeation properties, which are crucial for food packaging applications. Relationships between microstructures and sorption/permeation properties are established.

Chapter 3 opens up a series of new semi-aromatic polyesters based on 2,6-pyridinedicarbonyl dichloride (PDD26) and linear aliphatic diols (ethylene glycol EG, butanediol BD, hexanediol HD and decanediol DD). Their synthesis and thermal, mechanical and permeation properties are discussed. Some comparisons are made with 2,5-pyridinedicarbonyl dichloride (PDD25) and isophthaloyl dichloride (IPC) when possible.

Chapter 4, taking the advantages of the results obtained in Chapters 2 and 3, develops a series of copolyesters based on isosorbide, isomannide and 2,6-pyridinedicarbonyl dichloride. Their synthesis, thermal, mechanical and transport properties are systematically investigated and discussed.

Finally, a general conclusion and perspectives are presented prior to the Annexes.



---

# Chapter 1

## ☞ Overview of bio-based food packaging polymers ☞

---



## **1.1 Definition of food packaging**

Food packaging is defined as a way to protect food and gives food information to customers [1]. Robertson described packaging as “a socioscientific discipline that operates in society to ensure delivery of goods to the ultimate consumer of those goods in the best condition intended for their use” [2]. Bio-based food packaging can be defined the same as food packaging but with renewable raw materials [3] or precisely, with raw materials that can be regenerated on a relevant time scale [4,5].

## **1.2 Function of food packaging**

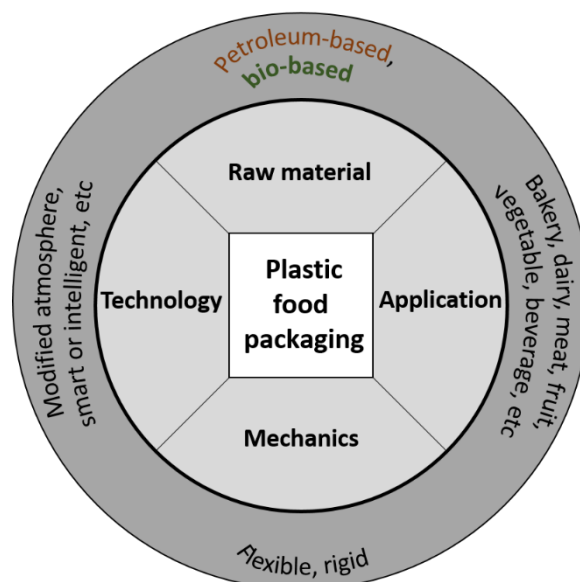
Packaging serves throughout the food supply chain. The most important function of packaging is to maintain the quality of food until its final consumption [2]. During this process, packaging plays container and protector roles, while delivering the food information and making the food distribution more convenient [6,7]. Besides, packaging provides uniform information of food content [8,9], allowing brands to be differentiated and to promote their product [10]. Good packaging not only prolongs the shelf-life of food but also contributes to the business profit [11].

## **1.3 Classification of food packaging materials**

The use of food packaging can trace back to the beginning of the 18<sup>th</sup> century [12]. There are usually three levels of food packaging, namely, primary, secondary and tertiary packaging. Primary packaging is the only one that is directly in contact with food, secondary and tertiary packaging are usually used to contain or assemble the primary packaging [13,14]. Primary packaging can be further divided into metals, papers and paper-based, glass and plastics [7,15]. Among them, plastics are superior to others due to the versatility of their processing methods (essentially extrusion, injection, and compression moulding) and their attractive cost/performance ratio [4]. There are advantages to use plastics instead of metal and glass packaging materials for their lightweight and facility for handling [16,17].

## 1.4 Plastic food packaging materials

Plastic packaging materials can be classified by their mechanical properties, food categories, technologies, and raw materials as shown in Figure 1-1. In terms of mechanical properties, they can be divided into flexible films and rigid containers [16]. According to the applications, there are packaging for bakery, confectionery, dairy, meat, fruits, vegetables, and beverages, etc [18]. Regarding the technology, there are modified atmosphere packaging (passive and active packaging) and smart (or intelligent) packaging, etc [19–23]. Concerning the raw materials, it can be separated as petroleum-based and bio-based [14,24].



**Figure 1-1** Plastic food packaging classification

Plastics as food packaging materials have an increasing demand [25]. The most commonly used polymers for food packaging applications are high/low-density polyethylene (HDPE, LDPE), polypropylene (PP), and poly(ethylene terephthalate) (PET). Other prominent materials include poly(vinyl chloride) (PVC), poly(vinylidene chloride) (PVdC), polystyrene (PS), polycarbonate (PC), polycaprolactone (PCL), and poly(ethylene-vinyl alcohol) (EVOH) [14,26]. Traditionally, these polymers are synthesized by chemicals from crude oil, and so named petroleum-based plastics.

Although petroleum plastics as food packaging materials have many performance advantages, their drawbacks are increasingly exposed due to crude oil depletion and

environmental problems [14,27]. Other concerns are the uncertainty of their availability and cost, which are influenced by the fluctuating oil price [14]. The possibility of petroleum monomer residues and additives migration to food has already caused consumer fears, which will also challenge the application of petroleum-based polymers in the food packaging industry [14].

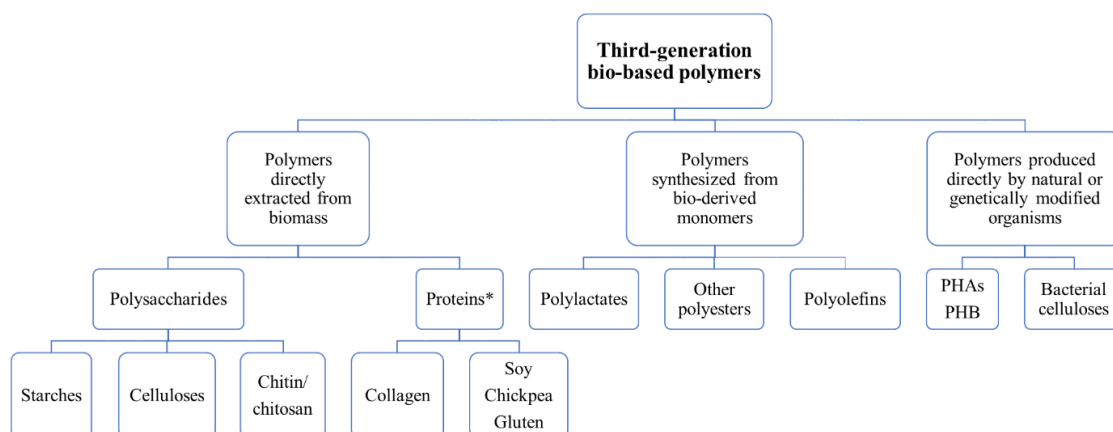
## **1.5 Bio-based food packaging plastics**

To reduce the influence of food packaging materials on the environment and decrease the dependence of packaging materials on crude oil, sustainable packaging has been developed [14]. Generally, sustainable packaging can be achieved at three levels [28]: raw materials, production process, and waste management. From the level of raw materials, renewable resources can be developed [29]. In this aspect, bio-based packaging is a good alternative to petroleum-based packaging [30]. The clear environmental benefits of bio-based polymers and their possible biodegradability gained worldwide attention, especially in Europe [14]. As stated in “Innovations in Food Packaging” by Han, natural and environmentally friendly packaging will not only contribute to our living environment but also be attractive to consumers [11].

Bio-based food packaging plastics means plastic materials directly obtained from natural polymers or indirectly from natural monomers. Based on their historical development, there are three generations of bio-based packaging plastics. The first generation contains synthetic polymers (such as LDPE) mixed with starch fillers (5-15%) and pro-oxidative additives. The second generation contains mixtures of gelatinized starch (40–75%), LDPE, and hydrophilic copolymers, where the hydrophilic copolymers, such as poly(ethylene-co-acrylic acid) (PEAA), poly(vinyl alcohol) (PVOH), and poly(vinyl acetate) (PVAc), act as the compatibility agent [4]. The third generation is bio-based polymers. The main members are depicted in Figure 1-2.

As seen in Figure 1-2, the third generation of bio-based food packaging materials covers a wide range, from natural polymers directly extracted from biomass (including proteins which are macromolecules) or directly produced by natural or genetically modified organisms, to polymers synthesized from bio-derived monomers. In this section, their application in food packaging will be briefly introduced.





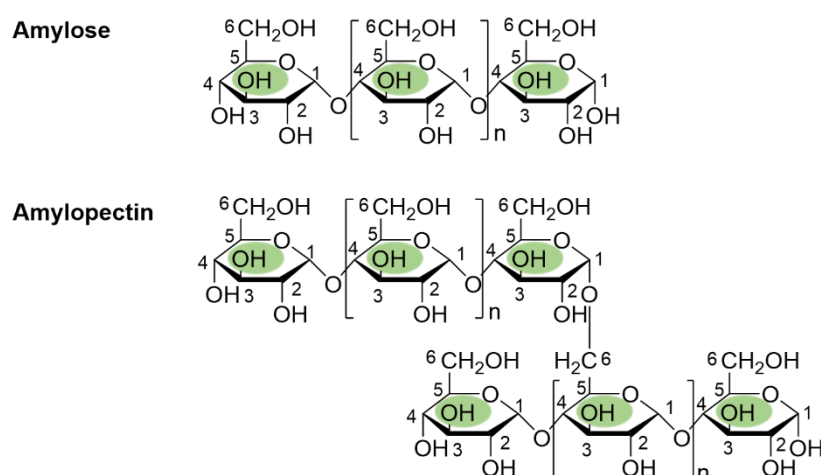
\*Proteins here are not exactly polymers but macromolecules.

**Figure 1-2** Third-generation bio-based packaging polymers. Adapted from [4]

## 1.5.1 Polysaccharides

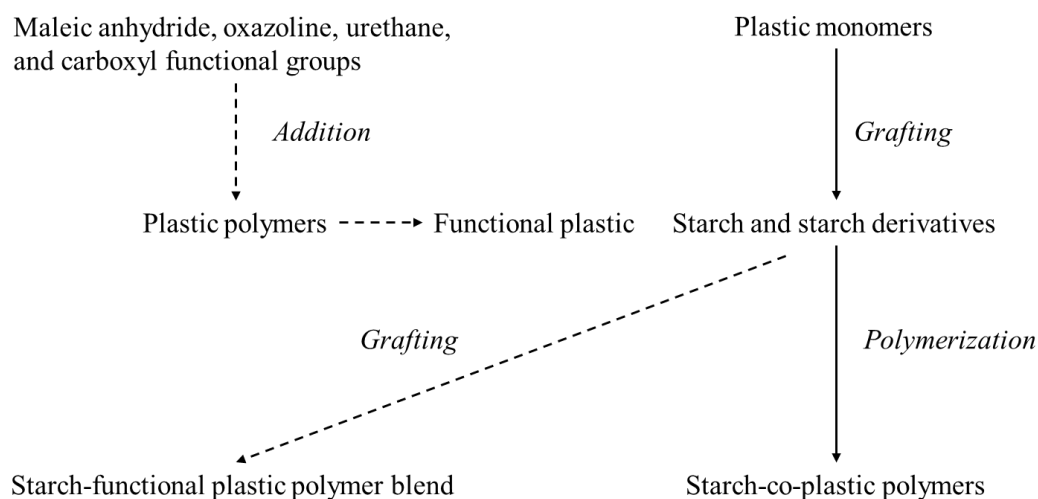
### 1.5.1.1 Starch-based plastics

Starch is a widely available polysaccharide with good biodegradability. Generally, it is made up of thousands of alpha-D-glucose repeating units. Due to the difference in glucose link, it can be divided into amylose (via  $\alpha$  1-4 glycosidic bonds) and amylopectin (via  $\alpha$  1-4 and 1-6 glycosidic bonds) as shown in Scheme 1-1.



**Scheme 1-1** Chemical structure of starch: amylose and amylopectin

To produce starch-based films, plasticizers (glycerol, sorbitol) are usually needed [31]. These plasticized materials are called thermoplastic starch (TPS), which can be an alternative for polystyrene in food packaging. Starch-based thermoplastic materials (blends of TPS with synthetic/biodegradable polymer components, like PCL, EVOH or PVOH) have been successfully applied on an industrial level for foaming, injection moulding, blow moulding, and extrusion applications [32–34]. However, their poor mechanical properties and high hydrophilicity make them unusable in food packaging [35,36]. Thus, they are often used as biodegradable additives for synthetic polymers, and are divided into starch-filled (<15 wt%) and starch-based (>40 wt%) materials depending on their loading quantity [37]. A simple schematic explanation of the starch blends synthesis ways is depicted in Figure 1-3.

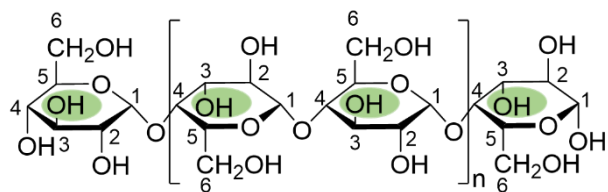


**Figure 1-3** Synthesis of starch blends [38]

The application of starch-based blends is now limited to niche applications because significant hurdles exist in using high amounts of starch (>25–30 wt%). Future researches need to focus on reactive starch blends containing significant amounts of starch or modified starches to enrich their applications in food packaging [38].

### 1.5.1.2 Cellulose

Cellulose is the most abundant polysaccharide with linear D-glucose containing  $\beta$  1-4 linkages as shown in Scheme 1-2.

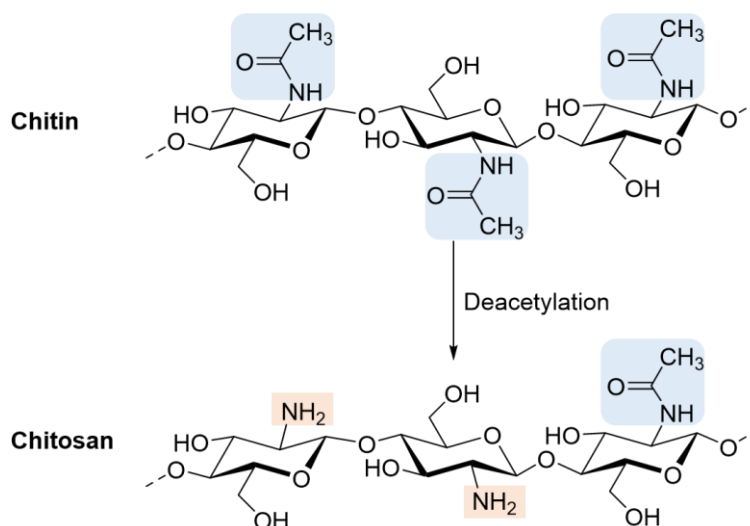


**Scheme 1-2** Chemical structure of cellulose

Cellulose is a biopolymer with biodegradability and low-cost production, furthermore, it does not compete with food, which makes it interesting for many researches. However, it is infusible and insoluble, which makes the process complicate [39]. Even if it can be prepared into cellophane, it is rarely used in food packaging because the process involves hazardous materials (such as carbon disulfide) [29]. Another drawback of using cellulose in food packaging is its high hydrophilicity, which will lead to the loss of mechanical strength and barrier properties when exposed to moisture. To minimize these problems, two main strategies have been developed. First, preparing cellulose composites [40–47]: the nanostructured cellulose crystals and fibers make them interesting to use as a reinforcement phase in nanocomposites [48]. Bio-nanocomposites can be also prepared by producing bacterial cellulose in a medium containing other biopolymers [49]. Second, preparing cellulosic materials by chemical modification: the hydroxyl groups (-OH) of cellulose can be partially or fully reacted with various reagents to afford derivatives with useful properties. The common cellulose derivatives are methylcellulose, hydroxyethyl cellulose, cellulose acetate, cellulose butyrate, and cellulose acetate-butyrate [50,51].

### 1.5.1.3 Chitosan

Chitosan is one of the most abundant polysaccharides just next to cellulose. It is the deacetylation product of chitin [52] as shown in Scheme 1-3.

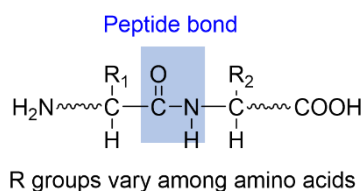


**Scheme 1-3** Chitosan chemical structure: from chitin to chitosan

Chitosan shows non-toxicity, biodegradability, biofunctionality, biocompatibility, and antimicrobial properties. The presence of amino groups in the chain makes it soluble in dilute acid solutions ( $pH < 6$ ). Thereby, it can be prepared into films but with high rigidity. For this reason, chitosan is often blended with other food packaging components, most often starch, to prepare active packaging films or coatings [53].

### 1.5.2 Proteins

Proteins are biomacromolecules that are made up of amino acids linked by peptide bonds. Their primary structure can be referred to Scheme 1-4.



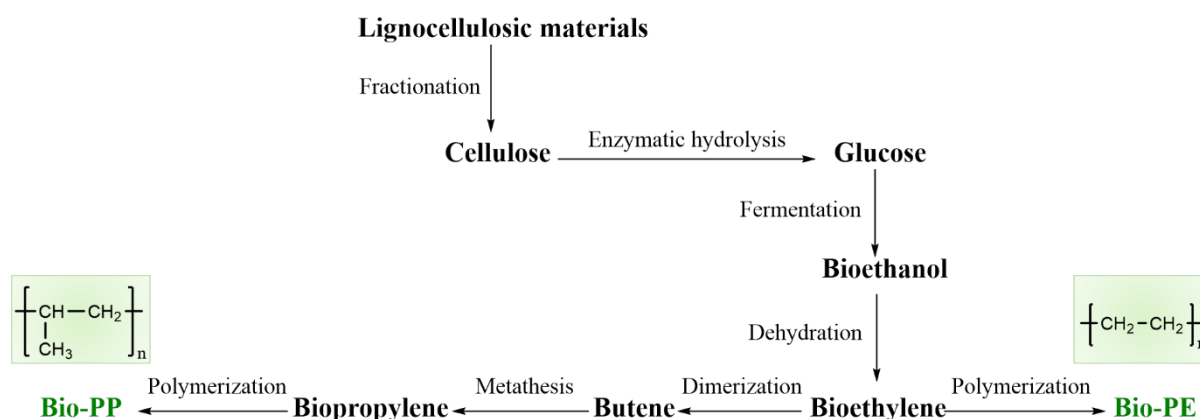
**Scheme 1-4** Primary structure of a protein

Due to the existence of 22 different amino acids, proteins have more structure diversity and more functionality compared to biopolymers [54]. However, their intrinsic hydrophilicity

and poor mechanical properties limit them to be used directly in food packaging [54]. The applications of proteins in food packaging are usually structure-modified films [55–57], composite films or coatings [58–60], and packaging sensors [54]. The proteins used in composite films or coatings are mainly soy and whey proteins, which function as plasticizers [58], oxygen barrier [59], and biodegradable components [60]. Silk fibers can be used as sensors for smart packaging [54]. Currently, radio frequency identification (RFID)-like silk sensors have been developed to indicate the status of fruit maturing. Fibroin-based packaging sensors have been also developed to detect the spoilage of milk and milk products [54]. Nevertheless, no information was found about the use of proteins as an independent matrix in food packaging.

### 1.5.3 Bio-based polyolefins

Bio-based polyolefins (bio-POs) refer to bio-based polyethylene (bio-PE) and polypropylene (bio-PP). Their bio-origination is presented in Scheme 1-5. Bio-PE and bio-PP have no characteristic difference compared to their petroleum counterparts, thus they can be used in the same applications [7]. The main advantage of bio-PE and bio-PP over their petroleum counterparts is their origin from renewable resources, namely bioethylene and biopropylene. Bioethylene can be produced by catalytic dehydration of bioethanol [61]. However, due to the removal of water, the theoretical yield is only 50% [7]. Biopropylene can be synthesized via transalkylation reactions between bioethylene and its butane biodimer [61].

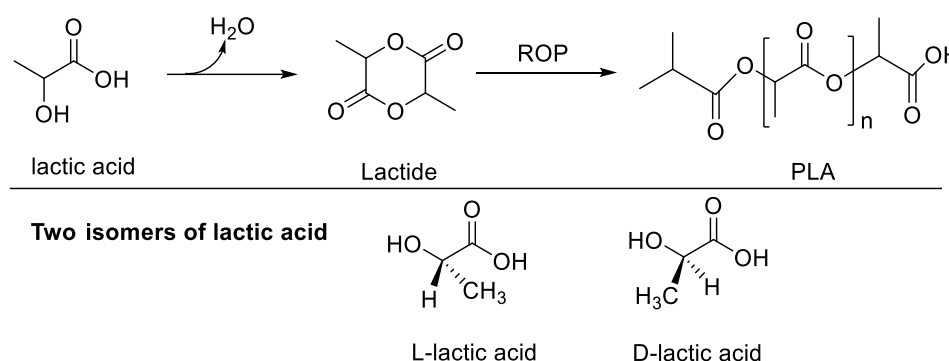


**Scheme 1-5** Routes to obtain bio-PE and bio-PP using bio-ethylene as a platform

## 1.5.4 Bio-based polyesters

### 1.5.4.1 Poly(lactic acid) (PLA)

Poly(lactic acid) (PLA) is a bio-originated polyester with a long period of investigation history. During the last decade, it gained a fast growth in the biodegradable plastic market compared to starch-based plastics. Due to its good biocompatibility and biodegradability, many research works and review articles have been reported broaching its synthesis, shaping processes, structure, and properties [62–65]. PLA can be synthesized by the polycondensation reaction between lactic acids (normally a mixture of L- and D-lactic acids), but commercial PLAs are usually synthesized via ring-opening polymerization (ROP) of lactides, which are the dehydration condensate of lactic acids as shown in Scheme 1-6.



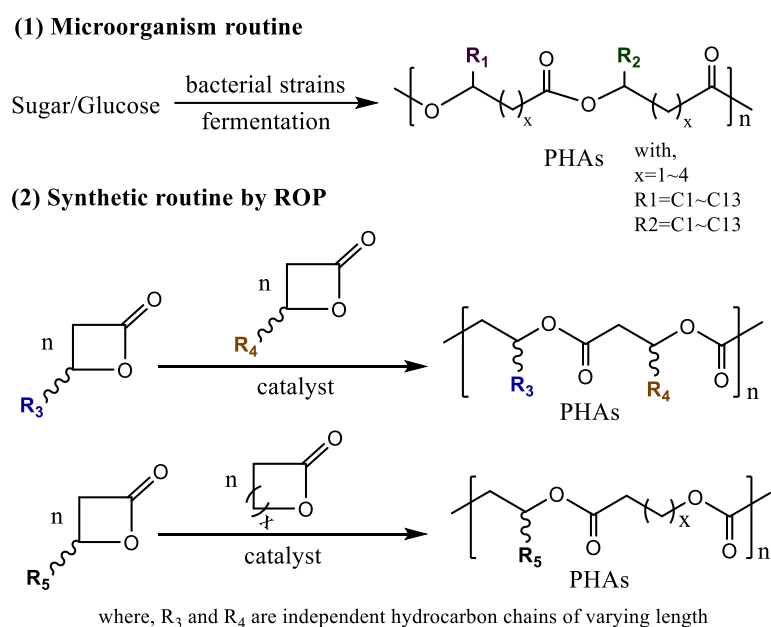
**Scheme 1-6** Ring-opening polymerization of PLA and the two isomers of lactic acid

The bulky properties of the PLAs synthesized via ROP can be tuned by the proportion of L- and D-lactide in their backbones, which largely influences their molar mass, chain architecture, and crystallinity [66]. The ROP of PLA has been reported as early as 1932 by the American chemist Wallace Carothers from DuPont [7]. However, it became a hot topic until the 1960s due to its high biodegradability for medical applications [7]. In food packaging applications, PLA has been reviewed by Ahmed *et al.* and Auras *et al.* [66,67]. It has been commercially produced on a large scale and proved with food contact safety by FDA [68,69]. Two commercialized PLAs, Ingeo® (Trademark of NatureWorks LLC) and LACEA (Mitsui Chemicals), are accessible on the market [66]. Even if PLA is highly qualified for food

packaging applications, the current problems of its brittleness, thermal instability, low melt strength, and difficult heat seal ability must be solved.

#### 1.5.4.2 Poly(hydroxyalkanoates) (PHAs)

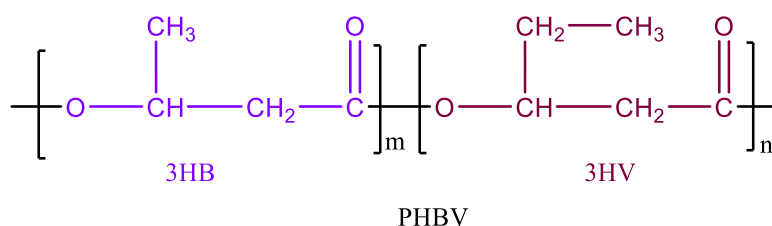
PHAs are known as a family of linear aliphatic biodegradable biopolyesters consisting of homo- or co-polymers of  $\beta$ -hydroxyalkanoic acids. They are commercially synthesized by microorganisms [70,71] (Scheme 1-7(1)). A few research works also reported syntheses via ring-opening polymerization [72,73] (Scheme 1-7(2)).



**Scheme 1-7** Synthetic routines of PHAs: microorganism (1) and ring-opening (2) [29]

As seen in Scheme 1-7, the variety of R groups in PHAs leads to various structures, which enable tunable properties. Among PHAs, poly(hydroxybutyrate) (PHB) is the most common one and is classified as a short-chain PHA with four carbon atoms in its monomers. It was first discovered in bacteria by Lemoigne (Pasteur Institute) in 1925 [74]. In the late 1980s, it was commercialized by Imperial Chemical Industries (ICI) under the trade name of Biopol® [7]. Thereafter, PHB was produced and registered under the trade name Biomer in 1994 [75]. During the development of PHB, studies found that poly(hydroxybutyrate-co-hydroxyvalerate) (PHBV)

can be obtained by changing the growth medium of the bacteria (propanoic acid and glucose) [76]. PHBV is a random copolymer composed of 3-hydroxybutyrate (HB) and 3-hydroxyvalerate (HV) (Scheme 1-8). The properties of PHBV can be tuned by changing the ratio of HB and HV. For example, PHBV can perform either as PP (low HV) or as LDPE (high HV) in terms of flexibility, tensile strength, and melting point [7]. The world-leading producer of PHBV is Ningbo Tianan Biologic Material Co. Ltd that was established in China in 2000. Further historical information of PHAs can be referred to the book of Gordon (third edition) [7] and the review article published by Chen [77].

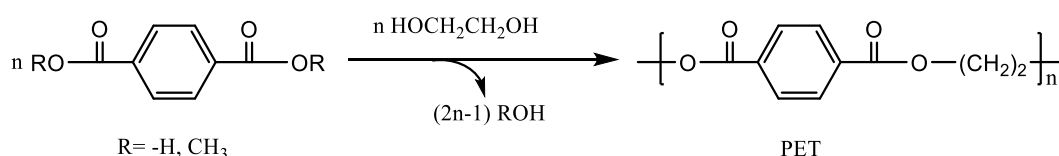


**Scheme 1-8** Chemical structure of PHBV

PHAs have many advantages for food packaging applications, such as fully bio-based and biodegradable, good chemical and moisture resistance, good O<sub>2</sub> and aroma barrier properties. They can be used as food packaging materials covering all short-time-life products. However, they are more used in biomedical applications (mainly as suture thread) than in food packaging for their quite high production cost, despite many years of efforts towards commercialization in this field [29,78–80].

#### 1.5.4.3 Polyethylene terephthalate (PET)

PET is a semi-aromatic polyester widely used in food packaging, especially for the beverage. It is usually synthesized by polycondensation reaction between ethylene glycol (EG) and terephthalic acid (TPA) or dimethyl terephthalate (DMT) (Scheme 1-9).



**Scheme 1-9** Synthesis of PET via polycondensation



The low cost and high performance of PET make it a widely used food packaging material, especially for soda bottles and plastic bags. A large number of PET analogs, such as poly(trimethylene terephthalate) (PTT), poly(butylene terephthalate) (PBT), poly(butylene adipate-co-terephthalate) (PBAT) and poly(ethylene isophthalate) (PEI) have also attracted attention (Table 1-1 ).

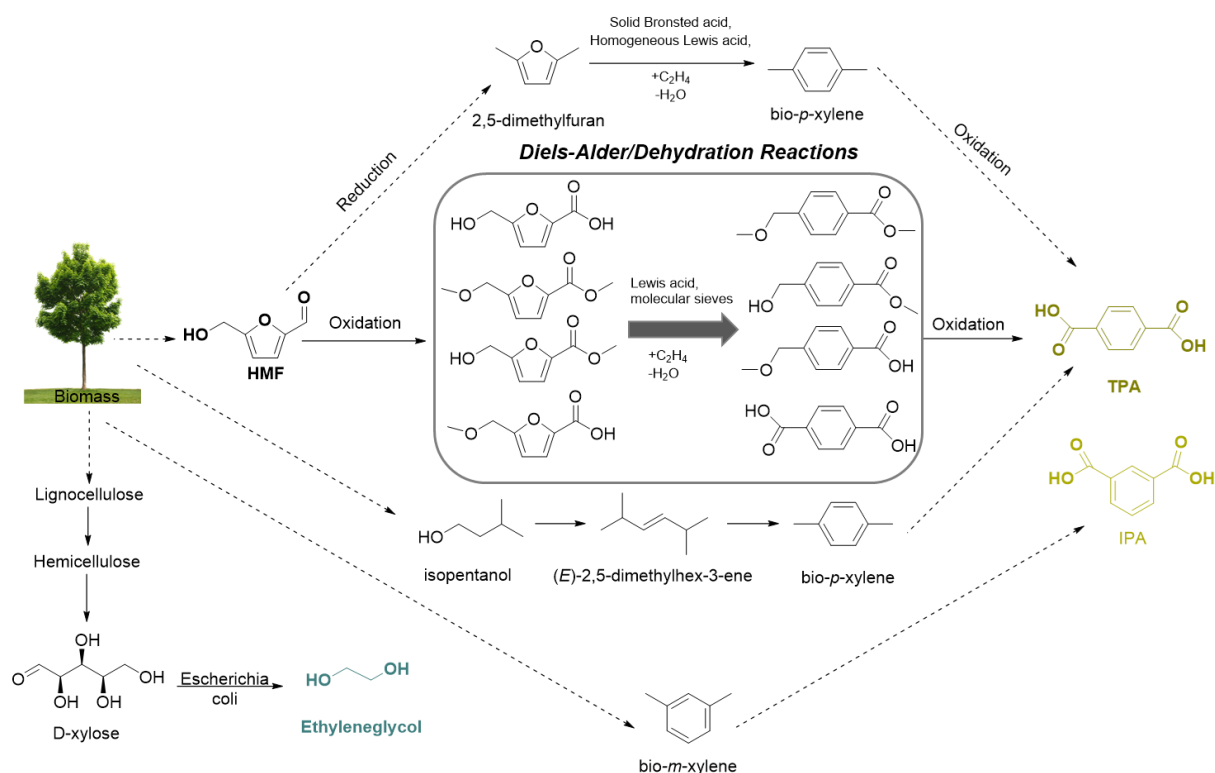
**Table 1-1** PET and PET analogs investigated concerning food packaging applications

Polymer	Chemical structure	Monomers	Permeation investigations	Commercial products	Ref
PEI		EG	O <sub>2</sub> , CO <sub>2</sub>	/	[91,92]
		IPA/DEI			
PET		EG	H <sub>2</sub> O, O <sub>2</sub> , CO <sub>2</sub> , N <sub>2</sub>	Dupont™ Biomax®, BioBTX B.V.	[91]
		TPA/DET			
PTT		PD	O <sub>2</sub> , CO <sub>2</sub>	Dupont™ Sorona®	[93,94]
		TPA/DET			
PBT		BD	O <sub>2</sub>	Crastin®-DuPont, Pocan®-Lanxess	[95]
		TPA/DET			
PBAT		BD	H <sub>2</sub> O, O <sub>2</sub> , CO <sub>2</sub>	Ecoflex®-BASF	[7,96,97]
		AA			
		TPA/DET			

PEI: poly(ethylene isophthalate); PET: poly(ethylene terephthalate); PTT: poly(trimethylene terephthalate); PBT: poly(butylene terephthalate); PBAT: poly(butylene adipate-co-terephthalate); EG: ethylene glycol; IPA: isophthalic acid ; DEI: diethyl isophthalate; TPA: terephthalic acid; DET: diethyl terephthalate; PD: 1,3-propanediol; BD: 1,4-butanediol; AA: adipic acid.

As PET and its analogs are petroleum-based polyesters, their extensive use consumes large amounts of crude oil and leads to environmental problems. With the development of bioengineering and chemical engineering, bio-PET can be now prepared from renewable ethylene glycol (EG) and bio-based terephthalic acid (TPA) (Scheme 1-10) [81–85]. In 2009, Coca-Cola Company launched bio-based PET with renewable EG for PlantBottle™ production [7,86]. In 2011, PepsiCo used C5 and/or C6 sugars as raw materials for its bio-terephthalic acid to produce 100% bio-based PET bottles [7,29,87–89]. Bio-PET has been vigorously promoted in both research and industrial areas under the decision made by the two largest PET bottle

users. However, the real commercialization is far from satisfaction due to the high cost of bio-TPA compared to the petroleum one [29,90].

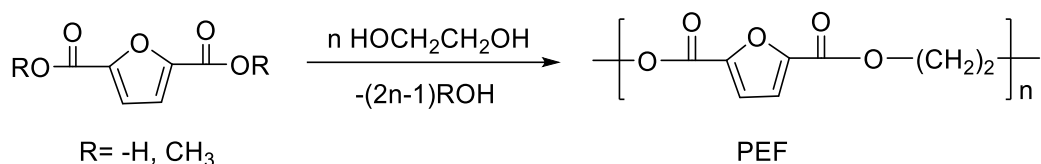


**Scheme 1-10** Bio-origination of EG, TPA and IPA

An alternative way to minimize the PET dependence on crude oil and the influence on the environment is to recycle PET, which involves PET reuse and PET depolymerization. The reused PET can make numerous products for various applications, especially in the fiber area [98]. The depolymerization of PET can be performed to obtain monomers or oligomers [99], which can be then re-polymerized [100]. Besides, the depolymerized PET waste could be used to improve the quality of polyurethane dispersions [101]. However, only 30% of the PET chains can be recycled [7]. Very recently, a collaborative research project between the University of Toulouse, INSA Toulouse, and Carbios Company reported that an enzyme can degrade 200 g of PET within 10 h with an efficiency of up to 90%. They emphasize that the enzymatically depolymerized PET waste can be used to produce bio-recyclable PET with the same properties as petrochemical PET, thereby realizing the concept of circular PET economy [102]. From another point, if the raw materials can be bio-based, it will be a real sustainable and green packaging.

#### 1.5.4.4 Poly(ethylene furanoate) (PEF)

PEF is recognized as a semi-aromatic polyester that can be 100% bio-based by using renewable 2,5-furandicarboxylic acid (2,5-FDCA) and ethylene glycol (EG) as seen in Scheme 1-11.



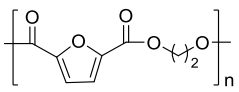
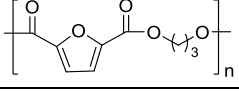
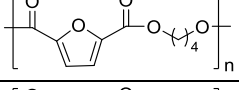
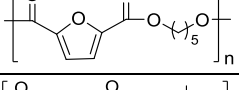
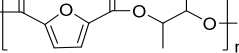
**Scheme 1-11** Synthesis of PEF by polycondensation reaction

PEF has been developed to replace PET with more than 70 years of history [103]. In 2019, Avantium (Netherlands) announced to create new avenues for commercializing their YXY® (plants-to-plastics) technology, especially focusing on the production of scaled-up PEF [104]. Before that time, there were already numerous research studies published on PEF. However, limited by the access of high purity FDCA, they only focused on the small-scale synthesis, discussing precursors (di-acid or di-ester), monomers stoichiometry, temperatures, pressures, and catalysts. With the Avantium's up-scaling production of FDCA, a comprehensive investigation of PEF was achieved by Jong *et al* [105]. They made a full evaluation of PEF compared with PET. Their results showed that PEF can compete with PET concerning mechanical property and price but with significantly better gas barrier property and environmental footprint. Even if Jong *et al.* mentioned the better gas barrier property for PEF, they didn't explain why. Burgess *et al.* conducted a more detailed investigation at the molecular level to explain the permeation performance of PEF films highlighting the furan-ring influence [106–110]. With the development of more economical synthetic routines and new performance information, PEF will have a great potential for using in food packaging [111].

Although PEF has many advantages for food packaging applications, there still exists problems to be overcome, like the high rigidity and relatively low water barrier properties. Hence, many PEF homologues, such as poly(propylene 2,5-furanoate) (PPF), poly(butylene

2,5-furanoate) (PBF), poly(pentamethylene furanoate) (PPeF), poly(neopentyl glycol 2,5-furanoate) (PNF) have been developed, as summarized in Table 1-2 .

**Table 1-2** PEF and PEF homologues investigated concerning food packaging

Polymer	Molecular structure	Monomers	Permeation investigations	Company, brand or trademark	Ref
PEF		EG	H <sub>2</sub> O, O <sub>2</sub> , CO <sub>2</sub> ,	Actinium, Coca-Cola®, Danone, Avantium	[107–110,112–114]
		FDCA/DMFD			
PPF		PD	O <sub>2</sub> , CO <sub>2</sub> , N <sub>2</sub>	/	[115–117]
		FDCA/ DMFD			
PBF		BD	H <sub>2</sub> O, O <sub>2</sub> , CO <sub>2</sub> ,	/	[118–121]
		FDCA/ DMFD			
PPeF		PeD	O <sub>2</sub>	/	[122]
		FDCA			
PNF		NPG	O <sub>2</sub> , CO <sub>2</sub>	/	[123]
		FDCA			

PEF: poly(ethylene 2,5-furanoate); PPF: poly(propylene 2,5-furanoate); PBF: poly(butylene 2,5-furanoate); PPeF: poly(pentylene 2,5-furanoate); PNF: poly(neopentyl glycol 2,5-furanoate). EG: ethylene glycol; FDCA: 2,5-furandicarboxylic acid; DMFD: dimethyl furan 2,5-dicarboxylate; PD: 1,3-propanediol; BD: 1,4-butanediol; PeD: 1,5-pentanediol; NPG: neopentyl glycol.

## 1.6 New trends in bio-based polyesters for food packaging

As previously mentioned, natural polymers are abundant and cost-effective but show poor water resistance and are difficult to process [124–127]. Even if bio-based polyolefins (bio-PE and bio-PP) are accessible due to the bio-occurring of ethylene and propylene, there is currently no low-cost way to produce bioethylene and biopropylene. Besides, bio-POs are poor in terms of gas barrier properties and biodegradability. The limited monomers also make them less attracting compared to bio-based polyesters. Polyesters are thermoplastic and water resistant. Like natural polymers, they are typically biodegradable except for those containing extensive aromatic backbones [128]. In addition, the polyesters produced with renewable diols and diacids are attractive for industries because they use well-established polycondensation reactions with existing reactor infrastructures. More importantly, the wide availability of renewable monomers provides more performance possibilities [129,130]. These unique properties of polyesters motivated the scientific community to develop new bio-based polyesters for food packaging applications.

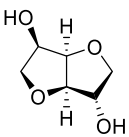
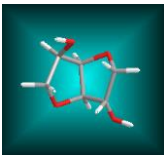
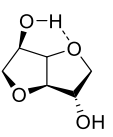
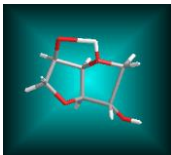
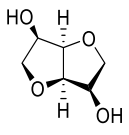
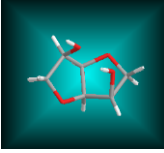
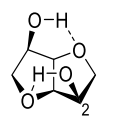
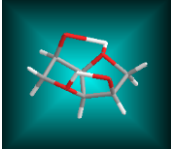
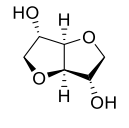
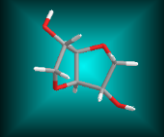
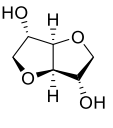
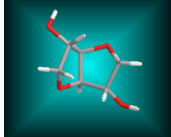
### 1.6.1 1,4:3,6-dianhydrohexitols as platforms for bio-based polyesters

1,4:3,6-dianhydrohexitols (DAHs) derive from starch and can be used to synthesize polyesters with good biodegradability and high thermal stability, thus, showing attractive prospects for many applications, including food packaging.

#### 1.6.1.1 1,4:3,6-dianhydrohexitols

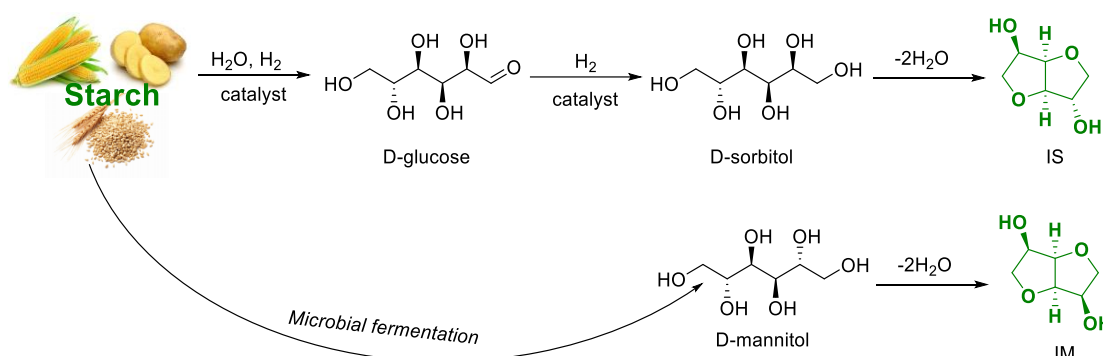
1,4:3,6-dianhydrohexitols (DAHs) are known as isosorbide (IS), isomannide (IM) and isoidide (II). Their structure shows a V-shaped ring with an angle of  $120^\circ$ , which determine exo-endo differences between monomers. Generally, the exo hydroxyl group is more accessible than the endo one, thus more active during chemical reactions. Isosorbide has one endo hydroxyl group and one exo hydroxyl group, whereas isomannide has two endo hydroxyl groups, and isoidide has two exo hydroxyl groups. As determined by NMR measurements, the endo hydroxyl group forms a hydrogen bond with the oxygen in the tetrahydrofuran ring, which decreases the reactivity of the monomers [131]. Thus, isoidide possesses normally the highest reactivity, while isomannide the lowest. The chemical structures of isosorbide, isomannide and isoidide with and without intramolecular hydrogen bonds are given in Table 1-3.

**Table 1-3** Stereoisomers of 1,4:3,6-dianhydrohexitols

Name	Chemical structure without hydrogen bond		Chemical structure with hydrogen bond	
	2D	3D	2D	3D
Isosorbide				
Isomannide				
Isoidide				

The unique properties of DAHs, such as non-toxicity, chirality and rigidity, make them interesting for preparing polyesters with high glass transition temperature and special optical properties. As bio-based platforms, DAHs have attractive prices due to the upscale industrial production, especially isosorbide, which opens possibilities for food packaging applications. Due to the lack of commercial availability, isoidide will not be discussed further.

The general routine to prepare isosorbide and isomannide is presented in Scheme 1-12.



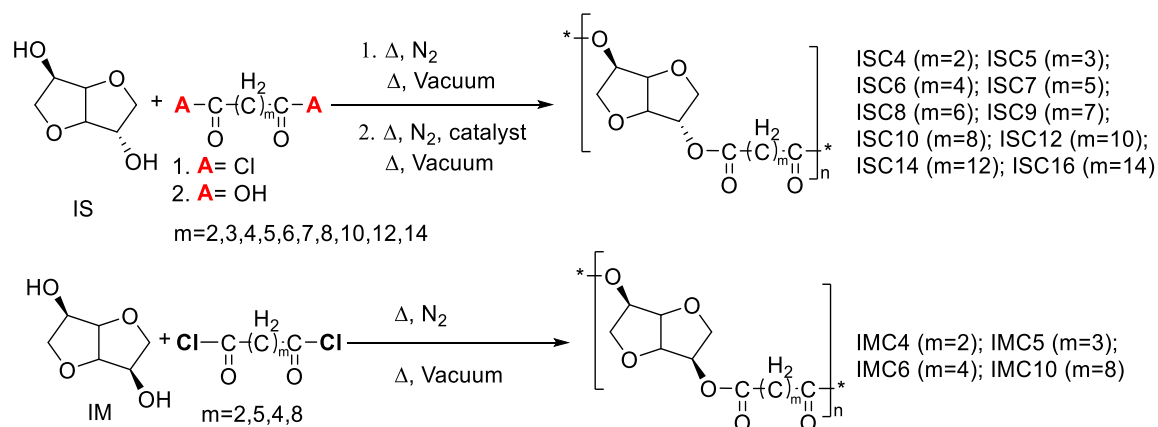
**Scheme 1-12** General scheme for the synthesis of isosorbide/isomannide from starch

Since 1984, 1,4:3,6-dianhydrohexitols have been used to synthesize polyesters but only IS and IM were widely studied due to their commercial availability [132]. Numerous patents and a large amount of research articles, based on these platforms, especially isosorbide, have been published. Within the recent ten years, four review articles have covered all aspects of isosorbide chemistry [131,133–135]. In polymer chemistry, the sustainable, high-temperature resistant and biodegradable polymers based on 1,4:3,6-dianhydrohexitols are ongoing hot topics. The combination of isosorbide with other renewable chemicals, such as aliphatic diacids and 2,5-furandicarboxylic acid to prepare thermosets have been reported as well [136–139]. The commercial polycarbonates and polyesters based on isosorbide, such as Polysorb® PSA, LP and PA, have been produced by Roquette [140]. However, the low reactivity of the secondary alcohols of IS and IM make it hard to obtain high molar mass polyesters. Chemical modifications to increase the reactivity of IS were tried but with complicated and costly steps [141]. General ways to obtain aliphatic polyesters by reacting a wide range of dicarboxylic acids, from 2 to 36 carbons, with IS or IM were presented [142,143]. These polyesters were proved to be biodegradable [144,145] and compatible for use in implant biomedical materials [146].

Furthermore, the tetrahydropyran rings were found to increase the rigidity of the chains and then the  $T_g$  [147]. Multiple isosorbide-derived monomers for the synthesis of high thermal performance polyesters which could be used for hot-fill containers were also overviewed [148]. More recently, the effects of stereoisomerism of IS or IM and chain length of dicarboxylic acid units on the crystallization of the polyesters were investigated [149,150]. In the following two sections, aliphatic and aromatic polyesters based on 1,4:3,6-dianhydrohexitols are introduced.

### 1.6.1.2 1,4:3,6-dianhydrohexitol-based polyesters

Aliphatic polyesters based on 1,4:3,6-dianhydrohexitols are usually synthesized by bulk polycondensation of isosorbide (IS) or isomannide (IM) with aliphatic carboxylic diacids or acid dichlorides [144,145,151] (Scheme 1-13).



**Scheme 1-13** Scheme for the synthesis of aliphatic polyesters from 1,4:3,6-dianhydrohexitols

Braun *et al.* [142] were the first to prepare aliphatic polyesters based on 1,4:3,6-dianhydrohexitols, and thereafter, numerous research works focused on these polyesters. Okada *et al.* studied the biodegradability of these polyesters [144,145,151]. Park *et al.* further examined the biocompatibility [146] and Marubayashi *et al.* did a systematic investigation of the crystallization behavior of these polyesters [149,150]. The monomers used, the molar masses and the main thermal properties of the obtained polyesters are recorded in Table 1-4.

**Table 1-4** 1,4:3,6-dianhydrohexitol-based aliphatic polyesters

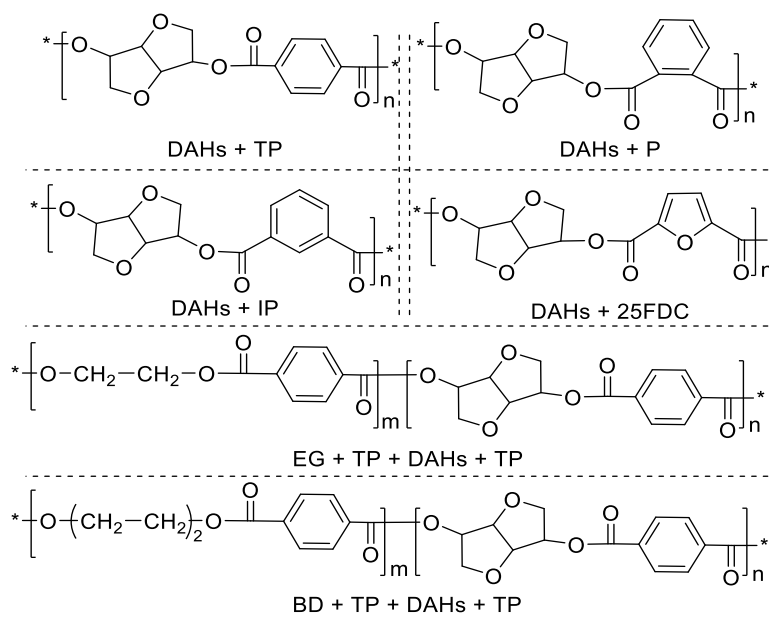
Polyester	Diacid or dichloride unit <sup>a</sup>	$\overline{M}_n^b$ (g/mol)	$\overline{M}_w^b$ (g/mol)	$T_g^c$ (°C)	$T_m^c$ (°C)	Ref
ISC4	Cl—C4—Cl	7 500	10 800	65	-	[142]
		8 000	14 400	36	-	[145,151]
		8 600	16 300	78	-	[149]
	HO—C4—OH	2 900	3 700	73	145	[146]
ISC5	Cl—C5—Cl	16 000	27 200	28	-	[145,151]
		13 000	37 700	43	-	[149]
ISC6	Cl—C6—Cl	26 000	39 000	21	-	[144]
		13 000	25 000	25	-	[142]
		7 300	13 900	19	-	[149]
	HO—C6—OH	8 800	15 800	34	84	[146]
ISC7	Cl—C7—Cl	22 000	30 800	11	-	[144]
ISC8	Cl—C8—Cl	20 000	49 000	11	-	[142]
		9 400	16 000	11	-	[149]
ISC9	Cl—C9—Cl	18 000	30 600	-1	54	[144]
ISC10	Cl—C10—Cl	20 000	28 000	-10	61	[144]
		23 000	60 000	0	-	[142]
		8 500	11 900	-7	59	[149]
	HO—C10—OH	19 200	45 300	6	50	[146]
ISC12	Cl—C12—Cl	17 000	28 900	-8	70	[144]
		15 000	28 000	-2	-	[142]
		13 000	24 700	-10	65	[149]
ISC14	Cl—C14—Cl	14 700	31 300	-4	53/67/79	[142]
ISC16	Cl—C16—Cl	11 400	26 000	-4	81/88	[142]
IMC4	Cl—C4—Cl	-	6 000 <sup>d</sup>	60	-	[142]
		10 000	17 000	75	175	[145,151]
		9 400	19 700	82	185	[149]
		19 000	60 900	80	185	[150]
IMC5	Cl—C5—Cl	11 000	17 600	37	-	[145]
		7 400	14 000	43	-	[149]
IMC6	Cl—C6—Cl	16 000	27 200	28	-	[145,151]
		8 800	15 000	30	-	[142]
		16 000	41 600	36	-	[149]
IMC8	Cl—C8—Cl	7 600	16 000	9	-	[149]
IMC10	Cl—C10—Cl	18 000	25 200	-8	-	[145,151]
		13 700	26 000	0	-	[142]
		9 300	13 000	-10	43	[149]
IMC12	Cl—C12—Cl	13 000	23 400	-10	65	[149]

<sup>a</sup> Expressed by their carbon number and functional groups. <sup>b</sup> Average molar masses determined by SEC (PS standards). <sup>c</sup> Determined by DSC (heating rate 10 °C/min). <sup>d</sup> From light scattering experiments.



### 1.6.1.3 1,4:3,6-dianhydrohexitol-based semi-aromatic (co)polyesters

Semi-aromatic polyesters based on 1,4:3,6-dianhydrohexiols (DAHs) were investigated and their general formula are shown in Scheme 1-14.



**Scheme 1-14** General structure of semi-aromatic polyesters from 1,4:3,6-dianhydrohexitols

Thiem and Liiders reported the first the synthesis of semi-aromatic polyesters with DAHs and terephthalic acid or terephthaloyl chloride [131,152]. These polyesters always showed high glass transition temperature due to the high rigidity of both 1,4:3,6-dianhydrohexiols and the aromatic diacid moieties, which is interesting for hot-fill containers applications. However, contrary to aliphatic polyesters that can be easily obtained by melt polycondensation, aromatic ones usually give oligomers [142,152] or crosslinked products [132,153] by this path. Besides, the low solubility of semi-aromatic polyesters makes it difficult to measure molar masses and get structure analyses [152]. Thus, one efficient way to obtain semi-aromatic polyesters is conducting the reaction in solution, as detailed below.

Storbeck *et al.* reported the first polycondensation of DAHs and aromatic acid dichlorides in solution. In 1992, they stated that high molar masses were obtained by polycondensing DAHs with terephthaloyl chloride (TPC) or 2,5-diethoxyterephthaloyl dichloride (2,5-DETD) in boiling toluene with the presence of pyridine. [152]. Then, in the same year, they reported

another series of fully renewable semi-aromatic polyesters with high molar masses, prepared by the polycondensation of DAHs with 2,5-furandicarbonyl dichloride (2,5-FDCD) in 1,1,2,2-tetrachloroethane with the presence of pyridine at room temperature [154]. The  $T_g$  of the resulted polyesters was between 173 °C and 196 °C. Later, they extended this solution method to copolymerization by incorporating isosorbide to PET [155]. As expected, their results showed the  $T_g$  increased. In 2007, Kricheldorf *et al.* [156] conducted the copolymerization of terephthaloyl chloride (TPC) with isosorbide and 1,4-butanediol, in toluene at 100 °C, or in dry  $\text{CH}_2\text{Cl}_2$  at 40 °C, with pyridine as HCl acceptor. They found these reactions in solutions offered higher molar masses than that in bulk by polycondensing dimethyl terephthalate (DMT) with isosorbide and 1,4-butanediol at 250 °C with  $\text{Ti}(\text{OBu})_4$  as the catalyst. However, the copolyesters prepared by incorporating isosorbide, such as poly(ethylene-co-isosorbide terephthalate) (PEIT), poly(trimethylene-co-isosorbide terephthalate) (PTIT) and poly(butylene-co-isosorbide terephthalate) (PBIT), showed the isosorbide ratio was always lower than its feeding ratio, which indicated a loss of isosorbide under these experimental conditions [131]. Despite the low incorporation ratio, the benefits of the increased  $T_g$  and decreased melting temperature ( $T_m$ ) of the obtained polyesters have already been commercially applied in the production of PEIT by Roquette [131,157].

The molar masses and main thermal properties of the above-mentioned semi-aromatic (co)polyesters are summarized in Table 1-5.

**Table 1-5** Semi-aromatic (co)polyesters molar masses and thermal properties

Diol	Diacid or dichloride unit	Method	$\overline{M}_n$ (g/mol)	$T_g$ (°C)	$T_m$ (°C)	Ref
IS	TPC	Bulk <sup>1</sup>	3 000 <sup>a</sup>	155	194	[153]
		Solution <sup>2</sup>	25 600 <sup>b</sup>	205	-	[152]
			23 200 <sup>b</sup>	204	-	
			21 300 <sup>b</sup>	203	-	
			14 200 <sup>a</sup>	197	-	
			7 900 <sup>b</sup>	187	-	
			6 400 <sup>b</sup>	180	-	
			3 200 <sup>a</sup>	158	-	
	IPC	Bulk <sup>3</sup>	3 600 <sup>c</sup>	138	-	[142]
	PC	Bulk <sup>3</sup>	2 200 <sup>c</sup>	118	-	[142]
IM	2,5-FDCD	Solution <sup>4</sup>	25 000 <sup>b</sup>	194	-	[154]
			22 500 <sup>b</sup>	190	-	
			9 000 <sup>b</sup>	173	-	
	TPC	Bulk <sup>1</sup> or solution <sup>5</sup>	nd	-	-	[152,153]
	IPC	Bulk <sup>3</sup>	3 000 <sup>c</sup>	149	-	[142]
	PC	Bulk <sup>3</sup>	nd	109	-	[142]
	2,5-FDCD	Solution <sup>4</sup>	20 400 <sup>b</sup>	191	-	[154]

Diol		Diacid or dichloride unit	Method	$\overline{M}_n$ (g/mol)	$T_g$ (°C)	$T_m$ (°C)	Ref
EG	1.4 mol % IS	TPA	Bulk <sup>6</sup>	nd	82	251	[131]
	3.4 mol % IS			nd	83	243	
	6.3 mol % IS			nd	86	235	
	10.1 mol % IS			nd	90	221	
BD	6.0 mol % IS	DMT	Solution <sup>7</sup>	nd	55	208	[156]
	18 mol % IS			nd	58	191	
	24 mol % IS			nd	84	162	
	42 mol % IS			nd	92	-	

TPC: terephthaloyl chloride; IPC: isophthaloyl chloride; PC: phthaloyl chloride; 2,5-FDCD: 2,5-furandicarbonyl dichloride; TPA: terephthalic acid; DMT: dimethyl terephthalate; <sup>1</sup>conducted at 180 °C under vacuum; <sup>2</sup>toluene as solvent and pyridine as HCl acceptor; <sup>3</sup>conducted at 120 °C under vacuum; <sup>4</sup>using 1,1,2,2-tetrachloroethane as solvent and pyridine as HCl acceptor; <sup>5</sup>sulfolane as solvent and pyridine as HCl acceptor at room temperature; <sup>6</sup>Sb<sub>2</sub>O<sub>3</sub> as catalyst, 260-285 °C under vacuum; <sup>7</sup>CH<sub>2</sub>Cl<sub>2</sub> as solvent and pyridine as HCl acceptor at 40 °C; <sup>a</sup>determined by vapour pressure osmometry in 1,1,2,2-tetrachloroethane at 30 °C; <sup>b</sup>determined by membrane osmometry in 1,1,2,2-tetrachloroethane at 30 °C; <sup>c</sup>SEC measurement with PS standard; nd: not determined.

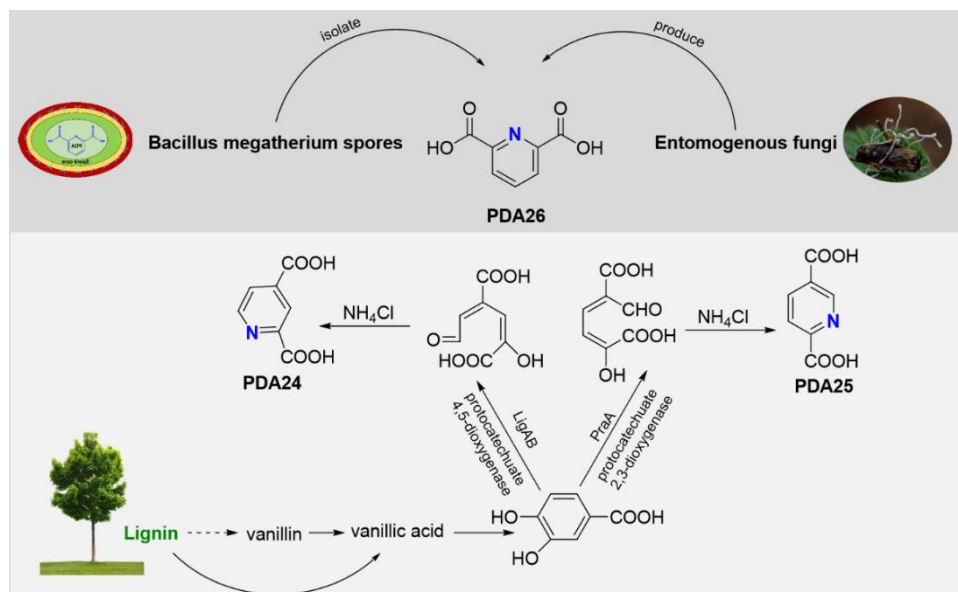
To recap, aliphatic polyesters containing DAHs can be easily prepared by melt polycondensation with acid dichlorides, but the preparation of DAHs-based semi-aromatic polyesters or copolyesters involving esterification or transesterification in bulk is difficult to perform. Thus, in most cases acid dichlorides are preferred [131,132,153], especially in solution [152,155,156]. All these polymers show a wide range of transition temperatures ( $T_g$  and  $T_m$ ), which is interesting for further food packaging applications.

### 1.6.2 Pyridinedicarboxylic acids as platforms for bio-based polyesters

Recently, a new aromatic dicarboxylic family with a pyridine ring, comprising 2,4-pyridinedicarboxylic acid (PDA24), 2,5-pyridinedicarboxylic acid (PDA25) and 2,6-pyridinedicarboxylic acid (PDA26), which can be obtained from biomass, has been reported [158,159]. As mentioned before, PET occupies a large market share in food packaging materials and its analogue PEF has shown increased gas barrier properties [109]. Hence, the aromatic moieties of pyridinedicarboxylic acids (PDAs) might offer rigidity when being incorporated into a polymer, yet retaining the potentially interesting polar pyridine ring, which may affect the stacking/crystallization behavior of the final product and similarly to the furan ring, be promising to prepare highly gas barrier polyesters.

### 1.6.2.1 Pyridinedicarboxylic acids

The three pyridinedicarboxylic acids, whose chemical structures are given in Table 1-6, can be divided into two categories: PDA24 and PDA25 are derived from lignin by biocatalytic conversion [158], whereas PDA26 is isolated from *Bacillus megatherium* spores [159] or produced by entomogenous fungi [160], as depicted in Scheme 1-15.



**Scheme 1-15** Bio-routines to obtain pyridinedicarboxylic acids

**Table 1-6** Chemical structures of 2,4-, 2,5- and 2,6-pyridinedicarboxylic acids

Name	2D structure	3D structure model	
		Stick	Space filling
2,4-pyridinedicarboxylic acid (PDA24)			
2,5-pyridinedicarboxylic acid (PDA25)			
2,6-pyridinedicarboxylic acid (PDA26)			

### 1.6.2.2 Pyridinedicarboxylic acid-based polyesters

Polyesters containing 2,5- and 2,6-pyridinedicarbonyl moieties were reported in several articles. According to Isfahani *et al.*, the presence of the 2,5-pyridyl moiety in the main chain could increase the solubility in organic solvents of polyesters that contain numerous aromatic structures [161]. Besides, these polyesters showed good thermal resistance with residual chars up to 42% at 600 °C, which could be considered using as fire safety materials. Saleh *et al.* prepared a series of metal-crosslinked polyesters, containing the 2,6-pyridyl moiety and aliphatic diols, intended for films with resistance to bacterial adhesion [162]. Very recently, a series of polyesters containing (2,4-, 2,5-, 2,6-) diethyl pyridinedicarboxylate (DEPD24, DEP25, DEP26) and aliphatic diols (with a carbon number ranging from 4 to 8) were synthesized by an enzymatic catalytic method in bulk or in diphenyl ether [163]. The molar masses and thermal properties of these polyesters are summarized in Table 1-7. The highest molar masses were found for 2,4-pyridinedicarboxylic-based polyesters while semi-crystalline polyesters were obtained with 2,5- and 2,6- pyridinedicarboxylic-based polyesters. Pyridinedicarboxylic acid-based water-soluble polyesters, which were intended for metals or some hard surface coating application, were also reported [164]. These polyesters were prepared by glycols or ether glycols (with carbon numbers ranging from 2 to 10) and PDA25 via a conventional polyesterification process. Another work reported the synthesis of polyesters based on PDA25 and various diols, containing but not limited to the linear diols. The optimal reaction conditions for the direct polymerization of PDA25 with various diols was in pyridine with the presence of picryl chloride [165]. Other syntheses and characterizations concerning polyesters based on PDA25 and PDA26 could be found in the literature [161,162,166].

**Table 1-7** Molar masses and thermal properties of pyridinedicarboxylate polyesters  
(catalyzed by enzyme ICalB at 85 °C and 20 mbar)

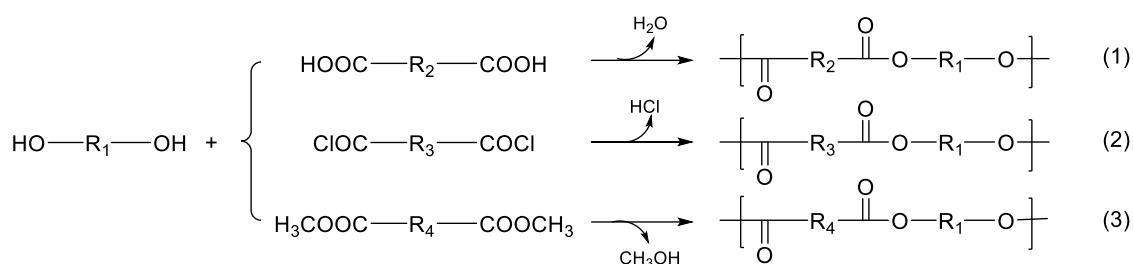
Method	Diester	Diol	$\overline{M}_n^a$ (g·mol <sup>-1</sup> )	$\overline{M}_w^a$ (g·mol <sup>-1</sup> )	$T_g^b$ (°C)	$T_m^c$ (°C)	$T_m^d$ (°C)
Bulk	DEPD24	BD	800	1 400	-10	-	-
		HD	1 300	2 900	-20	-	-
		OD	1 800	4 200	-22	-	-
	DEPD25	BD	600	800	-	-	105
		HD	900	1 300	-	91	100
		OD	1 000	1 800	-	85	95
	DEPD26	BD	600	700	-	-	133
		HD	800	1 100	-	87	100
		OD	1 300	2 200	-	-	88
Solution (diphenyl ether)	DEPD24	BD	2 100	4 400	31	-	-
		HD	5 900	17 600	11	-	-
		OD	14 300	32 100	-1	-	-
	DEPD25	BD	1 200	1 900	-	-	157
		HD	4 800	10 800	-	122	131
		OD	8 100	12 100	-	120	128
	DEPD26	BD	600	700	-	-	165
		HD	2 200	4 300	-	111	128
		OD	3 200	7 000	-	86	102

DEPD: diethyl pyridinedicarboxylate; BD: 1,4-butanediol; HD: 1,6-hexanediol; OD: 1,8-octanediol; <sup>a</sup> SEC with PS standards; <sup>b,c,d</sup> DSC under N<sub>2</sub> atmosphere at 5 °C·min<sup>-1</sup>; <sup>b,d</sup> second heating; <sup>c</sup> first heating.

## 1.7 Polymerization methods

Polyesters can be prepared by step-growth polymerization (esterification or transesterification) and chain-growth polymerization (ring-opening polymerization) [167].

The step-growth polymerization usually happens between diol and dicarboxyl functional groups, *e.g.* (1) diacids, (2) acid dichlorides or (3) dimethyl esters as shown in Scheme 1-16. Normally, these reactions are equilibrium reactions. The small by-products molecules (H<sub>2</sub>O, HCl and CH<sub>3</sub>OH) must be continuously removed to obtain high molar masses, which means high temperature and vacuum conditions are required.



**Scheme 1-16** Schematic of step growth polymerization of polyesters

Generally, reaction (1) results in low molar mass or crosslinked polyesters. It needs a catalyst to accelerate the reaction and high temperature to eliminate water molecules [167,168]. Both reactions (2) and (3) can be used to obtain high molar mass polyesters. Compared to reaction (3), reaction (2) is more reactive, therefore catalyst can be avoided but hydrogen chloride (HCl) by-product is very corrosive.

Another way to synthesize polyesters is chain-growth polymerization. The most common one is ring-opening polymerization (ROP) of cyclic monomers to poly(lactones) by using catalysts (organocatalysts, metal alkoxides, and various metal complexes) [169–171]. This strategy has many advantages, such as well-controlled molar masses, low molar mass dispersities, high molar masses at low monomer conversion, no by-products, but it still has limitations, such as the availability of cyclic monomers [172].

Bulk (or mass) polymerization is a favorable way for step-growth polymerization in terms of environmental issues. But high temperatures are always needed and side reactions are involved during these procedures [173]. Thus, many polymerizations in solution were conducted when the bulk polymerization cannot give the desired product [167].

For food packaging applications, polyesters are usually expected to possess thermal stability, mechanical strength, and barrier properties. Homopolyesters can be good for one aspect, but bad for another, thus, incorporating other monomers in copolyesters can make up for the shortcomings if necessary [174]. Taking PET and its analogues as examples, by incorporating succinic acid into PET, a more flexible copolyester PEST was obtained. To improve the mechanical strength of poly(butylene succinate) (PBS), terephthalic acid was introduced to provide the tougher PBST copolyester. These copolyesters gained currently industrial scale production under the trade name Biomax (PEST / PBST) [175]. Another famous

copolyester commercialized by DuPont is Ecoflex (PBAT) [7]. Overall, copolymerization is a widely used method to modify or improve the properties of current polymers.

## **1.8 General properties required for food packaging polyesters**

Considering the wide range of monomers, bio-based polyesters offer great potential for food packaging applications [30], and some of them, such as PLA, PHAs, and PEF, have already been commercialized. However, it is important to do a thorough evaluation of their properties before considering their use in food packaging. Many factors need to be taken into consideration, such as optical, thermal, and mechanical properties, processability, migration, food contact safety, chemical resistance, and permeation properties towards water and gases [176]. Among them, thermal, mechanical and permeation properties are essential requirements.

### **1.8.1 Thermal properties**

The knowledge of the thermal performance of a polymer is necessary for its processing and applications. Upon elevated heating, their chains will break into small gaseous molecules, and polymers will undergo a weight loss and lose their performance. Two important temperatures were introduced to determine the thermal degradation: the temperature with 5% weight loss ( $T_{5\%}$ ), which indicates the onset of the thermal degradation, and the temperature which highlights the fastest thermal degradation rate ( $T_{\max}$ ).

The melting temperature ( $T_m$ ) for semicrystalline polyesters and the glass transition temperature ( $T_g$ ) for amorphous ones are also important, not only because they are the guidance temperature for thermal processing but also because they indicate the upper and lower application temperature in food packaging [7]. Normally, amorphous polymers should be used below  $T_g$  and semi-crystalline ones should be used below  $T_m$ . Besides,  $T_g$  will influence the mechanical and barrier properties of a polymer, which will be discussed in the following sections.

The thermal properties of polyesters that have been used or are intended for food packaging applications are summarized in Table 1-8.



**Table 1-8** Thermal properties of food packaging polyesters

Polymer	$T_{5\%}$ (°C)	$T_{\max}$ (°C)	$T_g$ (°C)	$T_m$ (°C)	Ref
LDPE	408	460	-	105-125	[177,178]
HDPE	410	478	-127 to -118 <sup>e</sup>	118-146	[178]
PP	418	482	-12 to -8 <sup>e</sup>	43-186	[178]
PPC	233-278	-	25-45	-	[179]
PS	300	364	100	240	[178]
PET	413	426/524 <sup>a</sup>	69	255-267	[7,180,181]
PTT	377 <sup>b</sup>	399 <sup>c</sup>	45-55	228	[7,182]
PBT	366	405	20-40	221	[7,183]
PBAT	350	400	-30	115-120	[7] [184]
PBS	300	384	-32	115	[7,185]
PCL	340	450	-61	65	[7,186]
PGA	-	350	35	224-227	[7,187]
PHA	210-260	-	-30 to 10	70-170	[7]
PHB	~270	-	4	178	[7,188]
PHBV	~260	-	-1 to -5	145-153	[7,188]
PLA	334 <sup>c</sup>	368 <sup>c</sup>	58	152	[120]
PEF	376	416	89	211	[122]
PPF	360	387	50	168 <sup>f</sup>	[117,123]
PBF	316-376 <sup>d</sup>	388-407 <sup>d</sup>	35-38	164-169	[118-120]
PPeF	342	366	24	-	[122]
PNF	364	395	70	197	[123]

$T_g$  and  $T_m$  recorded from DSC second heating under N<sub>2</sub> atmosphere, 10 °C/min;  $T_{5\%}$  and  $T_{\max}$  obtained by TGA under N<sub>2</sub> atmosphere with 10 °C/min heating rate; <sup>a</sup>two degradation stages; <sup>b</sup> $T_{10\%}$ , <sup>c</sup> $T_{50\%}$ ; <sup>d</sup>TGA 20 °C/min; <sup>e</sup>DMA 0.1-1.0 Hz; <sup>f</sup>DSC first heating; PPC: poly(propylene carbonate); PGA: poly(glycolic acid).

### 1.8.2 Mechanical properties

Generally, the mechanical properties of polymers are associated with their molar mass, chemical composition, chain architecture, crystallinity, load speed, and environmental temperature [7,189]. Polymers can behave as glassy solids, elastic rubbers or viscous liquids depending on the applied temperature and load. Thus, it is important to precise the environmental conditions. The mechanical data of some polymers used or for use in food packaging are given in Table 1-9.

**Table 1-9** Mechanical properties of food packaging polymers

Polymer	$E$ (MPa)	$\sigma_b$ (MPa)	$\varepsilon_b$ (%)	Ref
Starch <sup>a</sup>	100-400	24-30	200-1000	[7]
Starch <sup>b</sup>	200-2000	20-30	20-500	[7]
Starch	600-850	35-80	580-820	[7]
LDPE	300-500	8-20	500-1000	[7]
HDPE	400-800	10-60	400-1800	[178]
PP	1000-2000	30-40	400-900	[7]
PPC	200-1400	7-33	600-1200	[7,179]
PS	3000-3500	34-50	3-5	[7]
PET	2800-4100	48-72	30-300	[7]
PTT	1830	180	28-33	[7]
PBT	2400	45-55	24-29	[7,190]
PBAT	80	17-23	470-700	[7]
PBS	645	35	170-560	[7]
PCL	190	14	500	[7]
PGA	7000	-	600	[7]
PHA	0.7-1.8	18-24	3-25	[7]
PHB	1000-2000	25-40	5-8	[7]
PHBV (7 mol% HV)	900	-	15	[7]
PHBV (20 mol% HV)	800	20	50	[7]
PLA	2050	40-63	9	[7]
PEF	2070	66.7	4.2	[103]
PPF	1550	68.2	46	[103]
PBF	1110	19.8	2.8	[103]
PNF	1650	45	4	[191]

$E$ , Young's modulus;  $\sigma_b$ , strength at break;  $\varepsilon_b$ , elongation at break. <sup>a</sup> film grade; <sup>b</sup> injection moulding grade.

### 1.8.3 Permeation properties

Foods are complex biologically and chemically active systems that require strict control of their manufacturing, distribution, and storage conditions to maintain their safety and nutritional values. The primary function of food packaging, in addition to serving as a containment, is to store food in a controlled microenvironment [192]. Thus, the knowledge of the permeation properties of the packaging materials is crucial for predicting or estimating the shelf-life of the packaged food. A high barrier is usually needed to maintain the in-package atmosphere, and preserve the food or extend its shelf-life. The global market of high barrier films for packaging is booming and many multinational companies are involved [193].

### 1.8.3.1 Common investigated permeants

Polymers are usually known to have relative permeability to small molecules, such as gases (oxygen, carbon dioxide, and nitrogen), vapors (water and organic vapors), and liquids. Among them, due to the interactions with food, water (H<sub>2</sub>O), oxygen (O<sub>2</sub>) and carbon dioxide (CO<sub>2</sub>) are the most investigated. Nitrogen (N<sub>2</sub>) is usually studied as a reference molecule and molecular probe, besides, it is rich in the air, thus of importance to be investigated.

#### Water (H<sub>2</sub>O)

H<sub>2</sub>O is one of the most studied molecules, because its transport from the external to the internal of the packaging wall, or in reverse, will change the food quality [7]. The packaging must play a buffer role between the environment whose humidity varies constantly and the product which needs a stable water activity. Indeed, the gain or loss of water from the food is very costly for the industrial, and only good knowledge of the moisture transfer in the food and its packaging can allow control [194]. For example, H<sub>2</sub>O mass gain should not exceed 10 % to preserve salads and not exceed 1% for condiments and dry foods, as seen in Table 1-10.

**Table 1-10** Protection requirements regarding H<sub>2</sub>O for foods and beverages (assuming 1-year shelf life at 25 °C)

Food/Beverage	Maximum H <sub>2</sub> O gain or loss	Food/Beverage	Maximum H <sub>2</sub> O gain or loss
Dried foods	1% Gain	Baby foods	3% Loss
Instant coffee	2% Gain	Canned milk and flesh foods	3% Loss
Nuts, snacks	5% Gain	Beers and wine	3% Loss
Condiments	1% Gain	Canned soups, vegetables and sauces	3% Loss
Peanut butter	10% Gain	Canned fruits	3% Loss
Oils and shortenings	10% Gain	Fruit juices and drinks	3% Loss
Salad dressings	10% Gain	Carbonated soft drinks	3% Loss
Jams, jellies, syrups, pickles, olives, vinegars	10% Gain	Liquors	3% Loss

Data taken from [7].

Polymeric materials will necessarily encounter humid environments during their usable lifetime [108,194]. The sorption and transport of H<sub>2</sub>O through polymer films can induce undesirable plasticization or swelling, causing reduction of thermal, mechanical, and barrier properties [195–200]. Understanding the sorption and transport behavior of H<sub>2</sub>O in polymeric materials is of importance for their applications when they are in contact with liquid water and high activity water vapor [108,113].

### **Oxygen (O<sub>2</sub>)**

O<sub>2</sub> has a major importance for in-packaged food because it promotes several deteriorative reactions in foods and it stimulates the growth of bacteria and fungi. Thus, many studies concerning O<sub>2</sub> transport properties have been performed [107,201,202]. Generally, O<sub>2</sub> should be excluded except when it is needed for the respiration of fruits and vegetables or to preserve the color of the red meat [203].

Depending on foods, different degrees of protection regarding O<sub>2</sub> are required (Table 1-11 ). For example, a maximum O<sub>2</sub> amount between 50 and 200 ppm should be maintained to preserve salads, oils and jams during one year, whereas a maximum between 1 and 5 ppm O<sub>2</sub> is needed for flesh food and sauces.

**Table 1-11** Protection requirements regarding O<sub>2</sub> for foods and beverages (assuming 1-year shelf life at 25 °C)

Food/Beverage	Maximum amount of O <sub>2</sub> gain (ppm)	Food/Beverage	Maximum amount of O <sub>2</sub> gain (ppm)
Dried foods	5-15	Baby foods	1-5
Instant coffee	1-5	Canned milk and flesh foods	1-5
Nuts, snacks	5-15	Beers and wine	1-5
Condiments	50-200	Canned soups, vegetables and sauces	1-5
Peanut butter	50-200	Canned fruits	5-15
Oils and shortenings	50-200	Fruit juices and drinks	10-40
Salad dressings	50-200	Carbonated soft drinks	10-40
Jams, jellies, syrups, pickles, olives, vinegars	50-200	Liquors	50-200

Data taken from [7].

### **Carbon dioxide (CO<sub>2</sub>)**

CO<sub>2</sub> permeability is known as an important parameter for carbonated beverages. Furthermore, with the development of packaging technology, fresh food can be stored under a modified atmosphere (MA) [174,175]. CO<sub>2</sub> is the most important gas component for modified atmosphere packaging (MAP), because it can not only inhibit food respiration but also restrict the growth of bacteria and fungi [7]. MAP can be achieved either passively or actively. It involves the modification of the inside atmosphere of the package to provide an optimum environment, thus to maintain the food quality and increase the food shelf-life. In the case of fresh products, respiration is a parameter that should be considered. For example, to maintain a good taste in fresh food, food respiration should be slowed down, thus it is necessary to limit the O<sub>2</sub> content while increasing the concentration of CO<sub>2</sub>. However, the packaging must maintain a certain permeability to O<sub>2</sub> because the continuous breath of a fresh product will consume O<sub>2</sub> and produce more CO<sub>2</sub>, and a too low oxygen concentration can trigger an anaerobic breathing process which induces bad taste and bad odors to the food products, and then decrease their shelf-life [206].

Different food shows different sensibility to O<sub>2</sub> and CO<sub>2</sub>. As mentioned before, the fresh products are usually stored in a modified atmosphere, where CO<sub>2</sub> and O<sub>2</sub> concentrations should be maintained at a proper level. Examples of the optimum atmosphere to preserve the vegetables and fruits are given in Table 1-12.

**Table 1-12** Optimum atmosphere to preserve vegetables and fruits between 0 and 5 °C

Vegetables and fruits	% O <sub>2</sub>	% CO <sub>2</sub>
Sliced apple	< 1	-
Iceberg lettuce	0.5-3	10-15
Butter lettuce	1	5-10
Strawberry	1-2	5-10
Kiwi	1-2	3-5
Broccoli	2-3	6-7
Grape	2-5	1-3
Cabbage	5-7	15
Citrus	5-10	0-10
Fig	5-10	15-20
Sliced orange	14-21	7-10

Data recorded from [207].

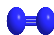
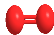


**Nitrogen (N<sub>2</sub>)**

Even if CO<sub>2</sub> is the most important MAP gas component, its intrinsic solubility in the aqueous phase will induce the collapse of the package when dissolving in the food [7]. In this case, N<sub>2</sub> can be added to the packaging as a gas filler because it is an inert gas with low water and food solubilities, and a lower density than air [7].

**Permeants influence on permeation properties)**

Considering the nature of the permeants can influence their transport within the polymer matrix, some important parameters, such as molecular size and shape, and critical temperature are given in Table 1-13. The relative dimensionless transport performance parameters depending on the molecule's nature are also given as a general reference.

**Table 1-13** Some parameters of N<sub>2</sub>, O<sub>2</sub>, CO<sub>2</sub> and H<sub>2</sub>O used in permeation experiments

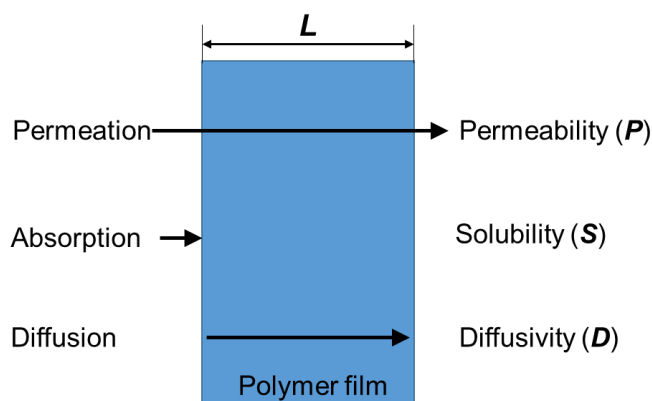
Properties	N <sub>2</sub>	O <sub>2</sub>	CO <sub>2</sub>	H <sub>2</sub> O
Molecular shape				
Kinetic diameter (Å)	3.64	3.46	3.30	2.65
Critical temperature (K)	126.2	154.6	304.2	647
Relative dimensionless permeation coefficient <i>P</i>	1	3.8	24	550
Relative dimensionless diffusion coefficient <i>D</i>	1	1.7	1	5
Relative dimensionless dissolution coefficient <i>S</i>	1	2.3	24	110

Data taken from [7,208,209].

The molecular kinetic diameter was used to correlate the diffusivity and molecule size [210]. A decrease in diffusivity with an increase in the permeant size has been reported for many polymers [211–213]. Water is a special case for its strong polarity, which will induce interactions with the polymer matrix. The permeant shape influence on the permeation property can be explained by the case that the flattened or elongated molecules have higher diffusion coefficients than spherical molecules of equal molecular volume [213]. Generally, the influence of permeant size and shape on permeation properties are much more marked in glassy than in rubbery polymers [213]. The solubility of gases or vapors strongly depends on their condensability and molecule interactions, which are positively in line with their critical temperature and Lennard–Jones force constant, respectively [109,210]. Usually, higher solubility in a polymer is obtained for gases or vapors with greater condensability (e.g. CO<sub>2</sub> or H<sub>2</sub>O) and stronger interactions [210].

### 1.8.3.2 Parameters for permeation properties

The mass transfer through a polymer film by a permeation process involves absorption (dissolution) and diffusion. Thus, the corresponding parameters are the permeability coefficient ( $P$ ), the solubility coefficient ( $S$ ) and the diffusion coefficient ( $D$ ), as shown in Figure 1-4.



**Figure 1-4** Mass transfer phenomena and their characteristic coefficients [214]

It is known that the permeability of a polymer film is a result of the penetrants dissolution-diffusion process, where dissolution (solubility) describes the thermodynamic process and diffusion reflects the kinetic process [201]. Thus, the permeability coefficient  $P$  is a combined product of the solubility coefficient  $S$  and diffusion coefficient  $D$  ( $P = D \times S$ ). The lower the  $P$  value, the higher the barrier of the material. Due to the continuous respiration of the fresh food product, the outlet and inlet of  $\text{CO}_2$  and  $\text{O}_2$  should be “controlled”. A polymer film with a selectivity coefficient  $\alpha_{\text{CO}_2/\text{O}_2}$  ranging from 3 to 5, depending on the desired atmosphere, is considered as a good choice for preserving fresh food. The selectivity coefficient of some polymers that match this criterion are gathered in Table 1-14.

**Table 1-14**  $\text{CO}_2$  and  $\text{O}_2$  selectivity coefficient of polymers within the ideal range for fresh foods preserving

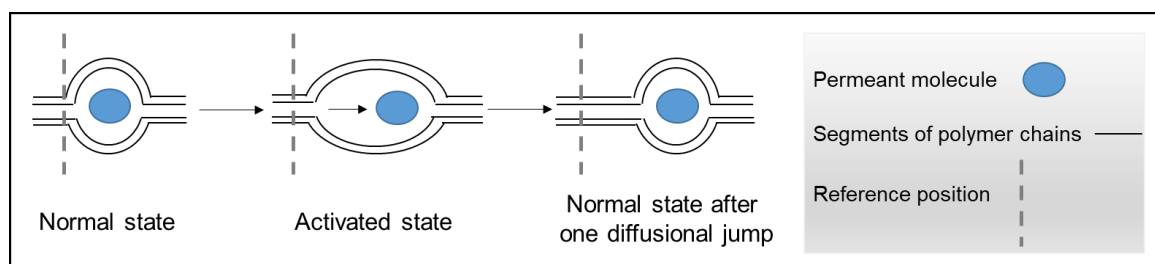
Polymer films	$\alpha_{\text{CO}_2/\text{O}_2}$		Polymer films	$\alpha_{\text{CO}_2/\text{O}_2}$
LDPE	2.0-5.9		PS	3.4-3.8
PVC	3.6-6.9		Saran™	5.8-6.5
PP	3.3-5.9		Polyester	3.0-3.5

Adapted from [215]. Saran™ from Dow Chemical: trade name of poly(vinylidene chloride) (PVdC).

### 1.8.3.3 Polymers influence on permeation properties

As defined before,  $P$  is a combined result of  $D$  and  $S$ , any factor that can affect  $D$  and  $S$  can consequently influence  $P$ . It can be said in general that the permeability coefficient  $P$  of molecules is governed by the polymer chemical structure, like polar or non-polar, linear or branching, and the physical structure, such as density, crystallinity, and orientation. Other environmental factors, such as pressure, temperature and humidity, can also influence  $P$ .

An activated diffusion process depicted in Figure 1-5 can be used to explain the polymer structure influence on the permeants transport. The activation diffusion, with the permeant move from one void space to another, can happen only when there is polymer chain segment mobility (the chain relax or shift its structure) [201]. Therefore, the factors, including polymer structures, which affect the chain segment mobility can finally influence the mass transfer properties of the polymer film [201].



**Figure 1-5** An activated diffusion process of permeants through a polymer film [216].

To be barrier materials, polymers should possess the following characteristics [7,201]:

- (1) Some degree of polarity. Highly polar polymers may provide a strong barrier to gases but low barrier to water (vapor), while a non-polar polymer may have an excellent water (vapor) barrier but poor gas barrier. Some degree of polarity allows chain-chain attraction and chain-penetrant interaction, thus decreases diffusivity, then permeability. The effects of chemical functional groups on oxygen and water permeability coefficients are shown in Table 1-15. Take EVOH and PE as examples. EVOH is a highly polar polymer and its hydroxyl groups offer an excellent barrier to gases ( $P_{O_2} = 0.00002$  barrer) but a poor barrier to water (water soluble). In contrast, PE is a non-polar polymer that shows outstanding water barrier properties ( $P_{H_2O} =$



1539 barrer) but low gas barrier ( $P_{O_2} = 2.89$  barrer) properties. For polar polymers, humidity will decrease their gas barrier properties, because the absorption of water molecules will plasticize the polymer or induce its swelling.

**Table 1-15** Effects of functional groups on oxygen and water permeability coefficients

Nature of R in ( $-\text{CH}_2-\text{CHR}$ ) <sub>n</sub>	P (barrer) <sup>a</sup>		Nature of R in ( $-\text{CH}_2-\text{CHR}$ ) <sub>n</sub>	P (barrer) <sup>a</sup>	
	O <sub>2</sub>	H <sub>2</sub> O		O <sub>2</sub>	H <sub>2</sub> O
—OH	0.00002	— <sup>b</sup>	—COOCH <sub>3</sub>	0.35	130844
—CN	0.0006	4618	—CH <sub>3</sub>	0.90 <sup>c</sup>	— <sup>d</sup>
—Cl	0.055	3848	—C <sub>6</sub> H <sub>5</sub>	2.58	16932
—F	0.09 <sup>c</sup>	— <sup>d</sup>	—H	2.89	1539

Data from [201]. <sup>a</sup>Permeability coefficient at 25 °C. <sup>b</sup>Water soluble. <sup>c</sup>Data from [7]. <sup>d</sup>Not accessible.

- (2) High chain stiffness. The chain stiffness is usually related to the low mobility of chain segments, and then to low permeability.
- (3) Inertness to the permeants. Polymers (especially the polar ones mentioned in (1) but not limited to) will absorb vapors which will plasticize the polymer or induce its swelling, then decreasing the barrier properties.
- (4) Close chain-to-chain packing. A tight chain-chain packing induces small amounts of free volume, thus the penetrants diffusion is limited. Molecular symmetry or order, crystallinity or orientation are favored for a close chain-chain packing.
- (5) Bonding or attraction between chains. Crosslinking and chain-chain attractions induce restricted chain movements, and thus limit penetrants diffusion.
- (6) High  $T_g$ . It is known that polymers in the glassy state (below  $T_g$ ) will show little mobility, which offers limited free volume for penetrants diffusion and then decreases the permeability. For food packaging applications, it is better to use a polymer film below its  $T_g$  to keep the barrier property.

Among the above-mentioned characteristics, some are double-edged. A polar polymer film can provide some degree of polarity and chain-chain attractions, but loses penetrants inertness. A bulky side group can on one hand reduce the mobility of the molecular chains and so decrease the penetrant permeability, but on the other hand increase the distance between chains thus increasing the permeability.

### 1.8.3.4 Permeability of polymers

Different applications of polymers have different requirements on their barrier properties. Before considering the use of bio-based polyesters for food packaging, their permeability properties should be investigated and compared to the traditional packaging materials, and then decide how they can replace some of the existing petroleum-based food packaging materials. A summary of the carbon dioxide, oxygen, nitrogen and water (CO<sub>2</sub>, O<sub>2</sub>, N<sub>2</sub> and H<sub>2</sub>O) permeation data of traditional food packaging polymers and some bio-based polyesters are gathered in Table 1-16. The polymers were chosen for their universal importance for food packaging applications as mentioned before.

**Table 1-16** Permeability data in terms of CO<sub>2</sub>, O<sub>2</sub>, N<sub>2</sub> and H<sub>2</sub>O of polymer films at 25 °C

Polymer	<i>P</i> (Barrer)				Ref
	N <sub>2</sub>	O <sub>2</sub>	CO <sub>2</sub>	H <sub>2</sub> O #	
LLDPE	1.5	1.3-3.0	13	-	[7]
LDPE	0.6-1.9	3.0-6.7	13-28	80	[7]
HDPE	0.14-0.33	0.6-1.1	1.7-4.5	13	[7]
EVA (12% VA)	-	3.0-4.2	13.1-17.3	29	[7]
PP	0.44	0.9-2.3	9.2	57	[7]
PVC	0.04	0.005-0.12	0.03-1.0	156-275	[7]
PVdC	0.0009	0.0006	0.0022-0.0036	1.4-4.5	[7]
PS (oriented)	0.29-0.78	1.1-2.7	8.8-10.5	900-1800	[7,217]
PAN	-	0.00024	0.006	2.2	[7]
PA6	0.01	0.012-0.038	0.04-0.16	700	[7]
Nylon-MXD6	-	0.001-0.003	0.0093	-	[7]
PC	-	1.5	6.4	-	[7]
EVOH (32% C <sub>2</sub> H <sub>4</sub> )	0.000012	0.00012	0.00036	-	[7]
EVOH (44% C <sub>2</sub> H <sub>4</sub> )	0.00005	0.00048	0.0014	-	[7]
PCTF	0.01-0.13	0.03-0.50	0.05-1.25	0.3-36	[7]
CA	0.2-0.5	0.4-0.8	2.4-18	1500-10600	[7]
Cellophane	0.0032	0.0021	0.0047	1900	[7]
PLA (98% L)	4.99	0.11-0.56	1.88	3000	[7]
PLA (96% L)	1.3	3.3	10.2	-	[218]
PLA ( $\chi_c$ = 1.2%, 38 °C)	-	0.59-0.64	-	216-223	[219]
PEN	-	0.0075	0.022	-	[7]
PET ( $\chi_c$ = 40%)	0.006	0.018-0.030	0.12-0.16	130-183	[7]
PET (amor)	0.005	0.055-0.075	0.21-0.30	-	[7]
PET (amor, 30-35 °C)	-	0.114	0.32-0.57	-	[91,92,107,109,220]
PEI (amor, 30 °C)	-	0.015	0.038-0.045	-	[91,92,107]
PETI (T50/I50, 30 °C)	-	0.025	-	-	[217]
PTT ( $\Delta H_m$ =55.5 J/g)	-	0.022-0.024	0.179-0.217	-	[93]
PBT	-	0.114	-	-	[95]
PEF (amor, 35 °C)	-	0.011	0.026	-	[107,109]
PEF ( $\chi_c$ = 6-25%, 35 °C)	-	0.0038-0.0058	0.012-0.017	-	[114]
PEF (amor)	-	-	1.14	-	[112]
PPF (amor)	-	-	-	19*	[115]
PPF ( $\Delta H_m$ =7.1 J/g)	0.0023	0.0038	0.0046	-	[117]
PNF	-	0.0049	0.00339	-	[123]

RH refers to relative humidity; # 90% RH; \*100% RH; amor: amorphous.

## **1.9 Bio-based polyesters for food packaging: opportunities and challenges**

### **1.9.1 Challenges**

Currently, bio-based polyesters share only a small part of the food packaging market. Challenges mainly exist in the limitations in terms of economics and performances [176,221]. The associated higher cost compared to petroleum materials is mainly due to the low accessibility of a large quantity of highly pure bio-based monomers. Their low thermal resistance and inferior mechanical properties also limit their entering into the food packaging market. Thus, more research efforts are required to improve their performances and competitiveness [14,222]. Another point cannot be ignored: the development of bio-based materials should not conflict with the food supply. Thus, the raw materials are expected to derive from non-food crops or food processing waste [223,224].

### **1.9.2 Opportunities**

Renewable food packaging materials would lead to a better future for the environment [225]. Even if large-scale markets of bio-based packaging are not available now, it still progresses in terms of technology and price. The legislation and policy encouragements from the governments, the environmental awareness and purchase willingness of consumers have already initiated commercial interests and stimulated the development of bio-based food packaging [176]. With wider monomer accessibility than bio-based polyolefins and larger performance advantage than starch-based materials, bio-based polyesters will have undoubtedly a place in future food packaging as long as environmental issues have not been resolved [225].

## References

- [1] Food packaging-new world encyclopedia, (2017). [https://www.newworldencyclopedia.org/entry/Food\\_packaging](https://www.newworldencyclopedia.org/entry/Food_packaging).
- [2] G.L. Robertson, Food packaging principle and practice, 2nd ed, CRC Press, Taylor & Francis Group, 2006.
- [3] R. Tuil, P. Fowler, M. Lawther, C.J. Weber, Properties of biobased packaging materials, in: C.J. Weber (Ed.), Prod. Biobased Packag. Mater. Food Ind., Center for Skov, Landskab og Planlægning/Københavns Universitet, 2000: pp. 13–39.
- [4] E. Chiellini, ed., Environmentally compatible food packaging, CRC Press, Cambridge England, 2008.
- [5] J.L. Scott, A. Buchard, Polymers from plants: biomass fixed carbon dioxide as a resource, in: L. Trevor M (ed.), Manag. Glob. Warm. An Interface Technol. Hum. Issues, Elsevier, 2019: pp. 503–525.
- [6] Z. Henk, K. Matthias, R. Alberto, H. Sunderesh, Operations, logistics and supply chain management, 1st ed., Springer International Publishing, 2019.
- [7] Robertson, G. L, Food packaging-principles and practice, 3rd ed., Taylor & Francis, 2013.
- [8] T. Hine, The total package: the evolution and secret meanings of boxes, bottles, cans, and tubes, NY: Little, Brown, New York, 1995.
- [9] S.D.F. Mihindukulasuriya, L.T. Lim, Nanotechnology development in food packaging: A review, Trends Food Sci. Technol. 40 (2014) 149–167.
- [10] A. Regattieri, G. Santarelli, The important role of packaging in operations management, in: Oper. Manag., InTech, 2013
- [11] J.H. Han, New technologies in food packaging. Overview, Innov. Food Packag. (2005) 3–11.
- [12] R.K. Gupta, P. Dudeja, Chapter 46 Food packaging. In: Food safety in the 21st century., 2017.
- [13] M. Saghir, The concept of packaging logistics, in: Proc. Fifteenth Annu. POMS, Cancun, 2004.
- [14] V. Katiyar, Bio-based plastics for food packaging applications., Smithers Rapra Technology, 2017.
- [15] K. Marsh, B. Bugusu, Food packaging-roles, materials, and environmental issues, J. Food Sci. 72 (2007) 39–55.
- [16] B.J. Lange, Y. Wyser, Recent innovations in barrier technologies for plastic packaging-a review, Packag. Technol. Sci. 16 (2003) 149–158.
- [17] Plastic packaging market growth, trends, and forecast (2020-2025), (2019). <https://www.mordorintelligence.com/industry-reports/plastic-packaging-market>.
- [18] Food packaging market research report forecast to 2023, (2017).

- <https://www.marketresearchfuture.com/reports/food-packaging-market-2086>.
- [19] S. Yildirim, B. Röcker, M.K. Pettersen, J. Nilsen-Nygaard, Z. Ayhan, R. Rutkaite, T. Radusin, P. Suminska, B. Marcos, V. Coma, Active packaging applications for food, *Compr. Rev. Food Sci. Food Saf.* 17 (2018) 165–199.
- [20] M. Ozdemir, J.D. Floros, Active food packaging technologies, *Crit. Rev. Food Sci. Nutr.* 44 (2004) 185–193.
- [21] R. Ahvenainen, E. Hurme, Active and smart packaging for meeting consumer demands for quality and safety, *Food Addit. Contam.* 14 (1997) 753–763.
- [22] B. Kuswandi, Y. Wicaksono, Jayus, A. Abdullah, L.Y. Heng, M. Ahmad, Smart packaging: sensors for monitoring of food quality and safety, *Sens. Instrum. Food Qual. Saf.* 5 (2011) 137–146.
- [23] K.B. Biji, C.N. Ravishankar, C.O. Mohan, T.K. Srinivasa Gopal, Smart packaging systems for food applications: a review, *J. Food Sci. Technol.* 52 (2015) 6125–6135.
- [24] M. Joo, N. Lewandowski, R. Auras, J. Harte, E. Almenar, Comparative shelf life study of blackberry fruit in bio-based and petroleum-based containers under retail storage conditions, *Food Chem.* 126 (2011) 1734–1740.
- [25] Increasing demand from food packaging, medical and pharmaceutical products to drive growth of thermoformed plastics market, (2016). <http://www.plastemart.com/plastic-technical-articles/substitution-of-traditional-materials-for-medical-devices-and-implants-to-propel-global-medical-polymers-market-to-2022/2360>.
- [26] Types of packaging material used in food - BTSA, (2020). <https://www.btsa.com/en/packaging-material-food/>.
- [27] J.W. Han, L. Ruiz-Garcia, J.P. Qian, X.T. Yang, Food packaging: a comprehensive review and future trends, *Compr. Rev. Food Sci. Food Saf.* 17 (2018) 860–877.
- [28] E. Cavagnaro, H. George, The three levels of sustainability, Greenleaf, 2012.
- [29] M. Rabnawaz, I. Wyman, R. Auras, S. Cheng, A roadmap towards green packaging: the current status and future outlook for polyesters in the packaging industry, *Green Chem.* 19 (2017) 4737–4753.
- [30] N. Peelman, P. Ragaert, B. De Meulenaer, D. Adons, R. Peeters, L. Cardon, F. Van Impe, F. Devlieghere, Application of bioplastics for food packaging, *Trends Food Sci. Technol.* 32 (2013) 128–141.
- [31] L. Jiang, J. Zhang, Biodegradable polymers and polymer blends, in: *Handb. Biopolym. Biodegrad. Plast. Prop. Process. Appl.*, Elsevier, 2012: pp. 109–128.
- [32] E. Bastioli, Catia, Handbook of biodegradable polymers, 2nd ed, 2016.
- [33] F. Chivrac, E. Pollet, L. Avérous, Progress in nano-biocomposites based on polysaccharides and nanoclays, *Mater. Sci. Eng. R Reports.* 67 (2009) 1–17.
- [34] G. Mensitieri, E. Di Maio, G.G. Buonocore, I. Nedi, M. Oliviero, L. Sansone, S. Iannace, Processing and shelf life issues of selected food packaging materials and structures from renewable resources, *Trends Food Sci. Technol.* 22 (2011) 72–80.

- 
- [35] M. Avella, J.J. De Vlieger, M.E. Errico, S. Fischer, P. Vacca, M.G. Volpe, Biodegradable starch/clay nanocomposite films for food packaging applications, *Food Chem.* 93 (2005) 467–474.
- [36] S. Mali, M.V.E. Grossmann, M.A. García, M.N. Martino, N.E. Zaritzky, Effects of controlled storage on thermal, mechanical and barrier properties of plasticized films from different starch sources, *J. Food Eng.* 75 (2006) 453–460.
- [37] Y. Pan, M. Farmahini-Farahani, P. O’Hearn, H. Xiao, H. Ocampo, An overview of bio-based polymers for packaging materials, *J. Bioresour. Bioprod.* 1 (2016) 106–113.
- [38] S. Kalambur, S.S.H. Rizvi, An overview of starch-based plastic blends from reactive extrusion, *J. Plast. Film Sheeting.* 22 (2006) 39–58.
- [39] B. Tajeddin, Cellulose-based polymers for packaging applications, *Lignocellul. Polym. Compos.* (2014) 477–498.
- [40] I. Gan, W.S. Chow, Antimicrobial poly(lactic acid)/cellulose bionanocomposite for food packaging application: a review, *Food Packag. Shelf Life.* 17 (2018) 150–161.
- [41] S.M. Noorbakhsh-Soltani, M.M. Zerafat, S. Sabbaghi, A comparative study of gelatin and starch-based nano-composite films modified by nano-cellulose and chitosan for food packaging applications, *Carbohydr. Polym.* 189 (2018) 48–55.
- [42] F.J. Rodríguez, A. Torres, Á. Peñaloza, H. Sepúlveda, M.J. Galotto, A. Guarda, J. Bruna, Development of an antimicrobial material based on a nanocomposite cellulose acetate film for active food packaging, *Food Addit. Contam. - Part A Chem. Anal. Control. Expo. Risk Assess.* 31 (2014) 342–353.
- [43] A. Ach, Biodegradable plastics based on cellulose acetate, *J. Macromol. Sci. Part A.* 30 (1993) 733–740.
- [44] X. Niu, Y. Liu, Y. Song, J. Han, H. Pan, Rosin modified cellulose nanofiber as a reinforcing and co-antimicrobial agents in polylactic acid /chitosan composite film for food packaging, *Carbohydr. Polym.* 183 (2018) 102–109.
- [45] F. Li, P. Biagioni, M. Bollani, A. Maccagnan, L. Piergiovanni, Multi-functional coating of cellulose nanocrystals for flexible packaging applications, *Cellulose.* 20 (2013) 2491–2504.
- [46] K.L. Spence, R.A. Venditti, O.J. Rojas, Y. Habibi, J.J. Pawlak, The effect of chemical composition on microfibrillar cellulose films from wood pulps: water interactions and physical properties for packaging applications, *Cellulose.* 17 (2010) 835–848.
- [47] Y. Makino, T. Hirata, Modified atmosphere packaging of fresh produce with a biodegradable laminate of chitosan-cellulose and polycaprolactone, *Postharvest Biol. Technol.* 10 (1997) 247–254.
- [48] H.M.C. Azeredo, M.F. Rosa, L.H.C. Mattoso, Nanocellulose in bio-based food packaging applications, *Ind. Crops Prod.* 97 (2017) 664–671.
- [49] K. Oksman, Y. Aitomäki, A.P. Mathew, G. Siqueira, Q. Zhou, S. Butylina, S. Tanpichai, X. Zhou, S. Hooshmand, Review of the recent developments in cellulose nanocomposite processing, *Compos. Part A Appl. Sci. Manuf.* 83 (2016) 2–18.

- [50] C. Harper, *Modern plastics handbook*, McGraw Hill Professional, New York, 2000.
- [51] A. Albertsson, S. Karlsson, T. Royal, Biodegradable polymers, in: *Degrad. Aliphatic Polyesters*, Springer, 2002: pp. 285–297.
- [52] M. Rinaudo, Chitin and chitosan: properties and applications, *Prog. Polym. Sci.* 31 (2006) 603–632.:
- [53] P.K. Dutta, S. Tripathi, G.K. Mehrotra, J. Dutta, Perspectives for chitosan based antimicrobial films in food applications, *Food Chem.* 114 (2009) 1173–1182.:
- [54] T. Bourtoom, Edible protein films: properties enhancement, *Int. Food Res. J.* 16 (2009) 1–9.
- [55] C. Vachon, H.L. Yu, R. Yefsah, R. Alain, D. St-Gelais, M. Lacroix, Mechanical and structural properties of milk protein edible films cross-linked by heating and  $\gamma$ -irradiation, *J. Agric. Food Chem.* 48 (2000) 3202–3209.
- [56] J.W. Rhim, A. Gennadios, D. Fu, C.L. Weller, M.A. Hanna, Properties of ultraviolet irradiated protein films, *LWT - Food Sci. Technol.* 32 (1999) 129–133.
- [57] A.H. Brandenburg, C.L. Weller, R.F. Testin, Edible films and coatings from soy protein, *J. Food Sci.* 58 (1993) 1086–1089.
- [58] J.W. Lee, S.M. Son, S.I. Hong, Characterization of protein-coated polypropylene films as a novel composite structure for active food packaging application, *J. Food Eng.* 86 (2008) 484–493.
- [59] M. Schmid, K. Dallmann, E. Bugnicourt, D. Cordoni, F. Wild, A. Lazzeri, K. Noller, Properties of whey-protein-coated films and laminates as novel recyclable food packaging materials with excellent barrier properties, *Int. J. Polym. Sci.* 2012 (2012).
- [60] A. González, C.I. Alvarez Igarzabal, Soy protein - Poly (lactic acid) bilayer films as biodegradable material for active food packaging, *Food Hydrocoll.* 33 (2013) 289–296.:
- [61] C.M. Mendieta, M.E. Vallejos, F.E. Felissia, G. Chinga-Carrasco, M.C. Area, Review: bio-polyethylene from wood wastes, *J. Polym. Environ.* 28 (2020).
- [62] R. Mehta, V. Kumar, H. Bhunia, S.N. Upadhyay, Synthesis of poly(lactic acid): a review, *J. Macromol. Sci. - Polym. Rev.* 45 (2005) 325–349.
- [63] R. Datta, M. Henry, Lactic acid: recent advances in products, processes and technologies : a review, *J. Chem. Technol. Biotechnol.* 81 (2006) 1119–1129.
- [64] S. Saeidlou, M.A. Huneault, H. Li, C.B. Park, Poly(lactic acid) crystallization, *Prog. Polym. Sci.* 37 (2012) 1657–1677.
- [65] A. Södergård, M. Stolt, Industrial production of high molecular weight poly(lactic acid), in: R. Auras, L. Tak Lim, S. E.M.Selke, H. Tsuji (Eds.), *Poly (Lactic Acid) Synth. Struct. Prop. Process. Appl.*, John Wiley & Sons, Inc., Hoboken, NJ, USA, 2010: pp. 27–41.
- [66] R. Auras, B. Harte, S. Selke, An overview of polylactides as packaging materials, *Macromol. Biosci.* 4 (2004) 835–864.
- [67] J. Ahmed, S.K. Varshney, Polylactides-chemistry, properties and green packaging technology: a review, *Int. J. Food Prop.* 14 (2011) 37–58.

- 
- [68] T. Jin, H. Zhang, Biodegradable polylactic acid polymer with nisin for use in antimicrobial food packaging, *J. Food Sci.* 73 (2008) 127–134.
  - [69] PLA packaging-Bio4Pack, (n.d.). <https://www.bio4pack.com/embalaje-de-pla/>.
  - [70] E. Bugnicourt, P. Cinelli, A. Lazzeri, V. Alvarez, Polyhydroxyalkanoate (PHA): review of synthesis, characteristics, processing and potential applications in packaging, *Express Polym. Lett.* 8 (2014) 791–808.
  - [71] T. Keshavarz, I. Roy, Polyhydroxyalkanoates: bioplastics with a green agenda, *Curr. Opin. Microbiol.* 13 (2010) 321–326.
  - [72] T. Ebrahimi, D.C. Aluthge, S.G. Hatzikiriakos, P. Mehrkhodavandi, Highly active chiral zinc catalysts for immortal polymerization of  $\beta$ -butyrolactone from melt processable syndio-rich poly(hydroxybutyrate), *Macromolecules.* 49 (2016) 8812–8824.
  - [73] Y. Hori, M. Suzuki, A. Yamaguchi, T. Nishishita, Ring-opening polymerization of optically active  $\beta$ -butyrolactone using distannoxane catalysts: synthesis of high molecular weight poly(3-hydroxybutyrate), *Macromolecules.* 26 (1993) 5533–5534.
  - [74] J. Liggat, ICI's BIOPOL Cautionary Tales, 2019. <https://www.scotchem.ac.uk/wp-content/uploads/2019/02/Biopol-IBioIC-compressed.pdf>.
  - [75] Biomer Biopolyesters. <http://www.biomer.de/>.
  - [76] J. Lu, R.C. Tappel, C.T. Nomura, Mini-review: biosynthesis of poly(hydroxyalkanoates), *Polym. Rev.* 49 (2009) 226–248.
  - [77] G.Q. Chen, A microbial polyhydroxyalkanoates (PHA) based bio- and materials industry, *Chem. Soc. Rev.* 38 (2009) 2434–2446.
  - [78] A. Steinbüchel, T. Lütke-Eversloh, Metabolic engineering and pathway construction for biotechnological production of relevant polyhydroxyalkanoates in microorganisms, *Biochem. Eng. J.* 16 (2003) 81–96.
  - [79] F. Masood, T. Yasin, A. Hameed, Polyhydroxyalkanoates-what are the uses? current challenges and perspectives, *Crit. Rev. Biotechnol.* 35 (2015) 514–521.
  - [80] S.F. Williams, D.P. Martin, D.M. Horowitz, O.P. Peoples, PHA applications: addressing the price performance issue I. tissue engineering, in: *Int. J. Biol. Macromol.*, 1999: pp. 111–121.
  - [81] J. Zakzeski, P.C.A. Bruijninx, A.L. Jongerius, B.M. Weckhuysen, The catalytic valorization of lignin for the production of renewable chemicals, *Chem. Rev.* 110 (2010) 3552–3599.
  - [82] P. Matthew W, Renewable xylenes produced from biological C4 and C5 molecules, US20120171741A1, 2012.
  - [83] M. Shiramizu, F.D. Toste, On the diels-alder approach to solely biomass-derived polyethylene terephthalate (PET): conversion of 2,5-dimethylfuran and acrolein into p-xylene, *Chem. - A Eur. J.* 17 (2011) 12452–12457.
  - [84] J.J. Pacheco, M.E. Davis, Synthesis of terephthalic acid via Diels-Alder reactions with ethylene and oxidized variants of 5-hydroxymethylfurfural, *Proc. Natl. Acad. Sci. U. S.*



- A. 111 (2014) 8363–8367.
- [85] Y. Byun, Y.T. Kim, Bioplastics for food packaging: chemistry and physics, in: *Innov. Food Packag.*, 2nd ED, Elsevier Ltd., 2013: pp. 353–368.
- [86] H. Ren, F. Qiao, Y. Shi, M.W. Knutzen, Z. Wang, H. Du, H. Zhang, PlantBottle™ Packaging program is continuing its journey to pursue bio-mono-ethylene glycol using agricultural waste, *J. Renew. Sustain. Energy*. 7 (2015) 041510.
- [87] PepsiCo develops world's first 100 percent plant-based, renewably sourced PET bottle, (2011). <https://www.gillettepepsicola.com/about-us/news/pepsico-develops-worlds-first-100-percent-plant-based%2C-renewably-sourced-pet-bottle/>.
- [88] A.F. Sousa, M. Matos, C.S.R. Freire, A.J.D. Silvestre, J.F.J. Coelho, New copolyesters derived from terephthalic and 2,5-furandicarboxylic acids: a step forward in the development of biobased polyesters, *Polymer*. 54 (2013) 513–519.
- [89] R.A. Sheldon, Green and sustainable manufacture of chemicals from biomass: State of the art, *Green Chem.* 16 (2014) 950–963.
- [90] D.I. Collias, A.M. Harris, V. Nagpal, I.W. Cottrell, M.W. Schultheis, Biobased terephthalic acid technologies: A literature review, *Ind. Biotechnol.* 10 (2014) 91–105.
- [91] R.R. Light, R.W. Seymour, Effect of sub-T<sub>g</sub> relaxations on the gas transport properties of polyesters, *Polym. Eng. Sci.* 22 (1982) 857–864.
- [92] R. Kotek, K. Pang, B. Schmidt, A. Tonelli, Synthesis and gas barrier characterization of poly(ethylene isophthalate), *J. Polym. Sci. Part B Polym. Phys.* 42 (2004) 4247–4254.
- [93] J. Diani, K. Gall, Finite strain 3D thermoviscoelastic constitutive model, *Society*. (2006).
- [94] DuPont performance polymers Sorona® 3301V NC010 polytrimethylene terephthalate (PTT), <http://www.matweb.com/search/datasheettext.aspx?matguid=e9dee43ad01c4095b791b04558f37378>.
- [95] R.R. Smith, J.R. Wilson, Polyester melt blends having high gas barrier properties, 1982.
- [96] S. Charlon, N. Follain, J. Soulestin, M. Sclavons, S. Marais, Water transport properties of poly(butylene succinate) and poly[(butylene succinate)-co-(butylene adipate)] nanocomposite films: influence of the water-assisted extrusion process, *J. Phys. Chem. C*. 121 (2017) 918–930.
- [97] P.G. Ren, X.H. Liu, F. Ren, G.J. Zhong, X. Ji, L. Xu, Biodegradable graphene oxide nanosheets/poly-(butylene adipate-co-terephthalate) nanocomposite film with enhanced gas and water vapor barrier properties, *Polym. Test*. 58 (2017) 173–180.
- [98] N. Malik, P. Kumar, S. Shrivastava, S.B. Ghosh, An overview on PET waste recycling for application in packaging, *Int. J. Plast. Technol.* 21 (2017).
- [99] A.M. Al-Sabagh, F.Z. Yehia, G. Eshaq, A.M. Rabie, A.E. ElMetwally, Greener routes for recycling of polyethylene terephthalate, *Egypt. J. Pet.* 25 (2016) 53–64.
- [100] D.E. Nikles, M.S. Farahat, New motivation for the depolymerization products derived from poly(ethylene terephthalate) (PET) waste: A review, *Macromol. Mater. Eng.* 290 (2005) 13–30.

- 
- [101] M.R. Patel, A.J. V Patel, A.D. Mishra, A.V.K. Sinha, Synthesis and characterization of low volatile content polyurethane dispersion from depolymerised polyethylene terephthalate, *J. Polym. Environ.* 15 (2007) 97–105.
- [102] V. Tournier, C.M. Topham, A. Gilles, B. David, C. Folgoas, E. Moya-Leclair, E. Kamionka, M.-L. Desrousseaux, H. Texier, S. Gavalda, M. Cot, E. Guémard, M. Dalibey, J. Nomme, G. Cioci, S. Barbe, M. Chateau, I. André, S. Duquesne, A. Marty, An engineered PET depolymerase to break down and recycle plastic bottles, *Nature*. 580 (2020) 216–219.
- [103] G.Z. Papageorgiou, D.G. Papageorgiou, Z. Terzopoulou, D.N. Bikiaris, Production of bio-based 2,5-furan dicarboxylate polyesters: recent progress and critical aspects in their synthesis and thermal properties, *Eur. Polym. J.* 83 (2016) 202–229.
- [104] YXY - Avantium. <https://www.avantium.com/technologies/yxy/>.
- [105] E. De Jong, M.A. Dam, L. Sipos, Furandicarboxylic acid ( FDCA ), a versatile building block for a very interesting class of polyesters, in: *Biobased Monomers*, Polym. Mater., 2012: pp. 1–13.
- [106] S.K. Burgess, J.E. Leisen, B.E. Kraftschik, C.R. Mubarak, R.M. Kriegel, W.J. Koros, Chain mobility, thermal, and mechanical properties of poly(ethylene furanoate) compared to poly(ethylene terephthalate), *Macromolecules*. 47 (2014) 1383–1391.
- [107] S.K. Burgess, O. Karvan, J.R. Johnson, R.M. Kriegel, W.J. Koros, Oxygen sorption and transport in amorphous poly(ethylene furanoate), *Polymer*. 55 (2014) 4748–4756.
- [108] S.K. Burgess, D.S. Mikkilineni, D.B. Yu, D.J. Kim, C.R. Mubarak, R.M. Kriegel, W.J. Koros, Water sorption in poly(ethylene furanoate) compared to poly(ethylene terephthalate). Part 2: Kinetic sorption, *Polymer*. 55 (2014) 6870–6882.
- [109] S.K. Burgess, R.M. Kriegel, W.J. Koros, Carbon dioxide sorption and transport in amorphous poly(ethylene furanoate), *Macromolecules*. 48 (2015) 2184–2193.
- [110] S.K. Burgess, Fundamentals of transport in poly ( ethylene terephthalate ) and poly ( ethylene furanoate ) barrier materials fundamentals of Transport in Poly ( Ethylene Terephthalate ) and Poly ( ethylene furanoate ) barrier materials, 2015.
- [111] A. Banerjee, G.R. Dick, T. Yoshino, M.W. Kanan, Carbon dioxide utilization via carbonate-promoted C-H carboxylation, *Nature*. 531 (2016) 215–219.
- [112] L. Sun, J. Wang, S. Mahmud, Y. Jiang, J. Zhu, X. Liu, New insight into the mechanism for the excellent gas properties of poly(ethylene 2,5-furandicarboxylate) (PEF): role of furan ring's polarity, *Eur. Polym. J.* 118 (2019) 642–650.
- [113] S.K. Burgess, D.S. Mikkilineni, D.B. Yu, D.J. Kim, C.R. Mubarak, R.M. Kriegel, W.J. Koros, Water sorption in poly(ethylene furanoate) compared to poly(ethylene terephthalate). part 1: equilibrium sorption, *Polymer*. 55 (2014) 6861–6869.
- [114] S.K. Burgess, G.B. Wenz, R.M. Kriegel, W.J. Koros, Penetrant transport in semicrystalline poly(ethylene furanoate), *Polymer*. 98 (2016) 305–310.
- [115] M. Vannini, P. Marchese, A. Celli, C. Lorenzetti, Fully biobased poly(propylene 2,5-furandicarboxylate) for packaging applications: excellent barrier properties as a function

- of crystallinity, *Green Chem.* 17 (2015) 4162–4166.
- [116] G. Guidotti, M. Soccio, N. Lotti, M. Gazzano, V. Siracusa, A. Munari, Poly(propylene 2,5-thiophenedicarboxylate) vs. poly(propylene 2,5-furandicarboxylate): two examples of high gas barrier bio-based polyesters, *Polymers (Basel)*. 10 (2018).
- [117] G. Guidotti, L. Genovese, M. Soccio, M. Gigli, A. Munari, V. Siracusa, N. Lotti, Block copolyesters containing 2,5-furan and trans-1,4-cyclohexane subunits with outstanding gas barrier properties, *Int. J. Mol. Sci.* 20 (2019) 2187.
- [118] M. Soccio, M. Costa, N. Lotti, M. Gazzano, V. Siracusa, E. Salatelli, P. Manaresi, A. Munari, Novel fully biobased poly(butylene 2,5-furanoate/diglycolate) copolymers containing ether linkages: structure-property relationships, *Eur. Polym. J.* 81 (2016) 397–412.
- [119] Y. Long, R. Zhang, J. Huang, J. Wang, Y. Jiang, G.H. Hu, J. Yang, J. Zhu, Tensile property balanced and gas barrier improved poly(lactic acid) by blending with biobased poly(butylene 2,5-furan dicarboxylate), *ACS Sustain. Chem. Eng.* 5 (2017) 9244–9253.
- [120] H. Hu, R. Zhang, L. Shi, W. Bin Ying, J. Wang, J. Zhu, Modification of poly(butylene 2,5-furandicarboxylate) with lactic acid for biodegradable copolyesters with good mechanical and barrier properties, *Ind. Eng. Chem. Res.* 57 (2018) 11020–11030.
- [121] H. Hu, R. Zhang, J. Wang, W. Bin Ying, J. Zhu, Synthesis and structure-property relationship of biobased biodegradable poly(butylene carbonate- co-furandicarboxylate), *ACS Sustain. Chem. Eng.* 6 (2018) 7488–7498.
- [122] H. Xie, L. Wu, B.G. Li, P. Dubois, Modification of poly(ethylene 2,5-furandicarboxylate) with biobased 1,5-pentanediol: significantly toughened copolyesters retaining high tensile strength and O<sub>2</sub> barrier property, *Biomacromolecules*. 20 (2019) 353–364.
- [123] L. Genovese, N. Lotti, V. Siracusa, A. Munari, Poly(neopentyl glycol furanoate): a member of the furan-based polyester family with smart barrier performances for sustainable food packaging applications, *Materials (Basel)*. 10 (2017).
- [124] S.A. Attaran, A. Hassan, M.U. Wahit, Materials for food packaging applications based on bio-based polymer nanocomposites, *J. Thermoplast. Compos. Mater.* 30 (2017) 143–173.
- [125] F. Xie, L. Yu, H. Liu, L. Chen, Starch modification using reactive extrusion, *Starch - Stärke*. 58 (2006) 131–139.
- [126] M. Gáspár, Z. Benko, G. Dogossy, K. Réczey, T. Czigány, Reducing water absorption in compostable starch-based plastics, *Polym. Degrad. Stab.* 90 (2005) 563–569.
- [127] V.P. Cyras, C.M. Soledad, V. Analía, Biocomposites based on renewable resource: Acetylated and non acetylated cellulose cardboard coated with polyhydroxybutyrate, *Polymer*. 50 (2009) 6274–6280.
- [128] Y. Tokiwa, B.P. Calabia, Biodegradability and biodegradation of polyesters, *J. Polym. Environ.* 15 (2007) 259–267.
- [129] F. Carolyn, Demand for biodegradable plastics expected to surge, (2018). <https://cleantechnica.com/demand-for-biodegradable-plastics-expected-to-surge/ics->

expected-to-surge/.

- [130] C. Vilela, A.F. Sousa, A.C. Fonseca, A.C. Serra, J.F.J. Coelho, C.S.R. Freire, A.J.D. Silvestre, The quest for sustainable polyesters-insights into the future, *Polym. Chem.* 5 (2014) 3119–3141.
- [131] F. Fenouillot, A. Rousseau, G. Colomines, R. Saint-Loup, J.P. Pascault, Polymers from renewable 1,4:3,6-dianhydrohexitols (isosorbide, isomannide and isoidide): a review, *Prog. Polym. Sci.* 35 (2010) 578–622.
- [132] J. Thiem, H. Lüders, Darstellung und gezielte polykondensation von anhydroalditolbausteinen aus stärke, *Starch - Stärke.* 36 (1984) 170–176.
- [133] M. Rose, R. Palkovits, Isosorbide as a renewable platform chemical for versatile applications-quo vadis?, *ChemSusChem.* 5 (2012) 167–176.
- [134] D.J. Saxon, A.M. Luke, H. Sajjad, W.B. Tolman, T.M. Reineke, Next-generation polymers: isosorbide as a renewable alternative, *Prog. Polym. Sci.* 101 (2020) 101196.
- [135] F. Aricò, P. Tundo, Isosorbide and dimethyl carbonate: a green match, *Beilstein J. Org. Chem.* 12 (2016) 2256–2266.
- [136] A.F. Sousa, A.C. Fonseca, A.C. Serra, C.S.R. Freire, A.J.D. Silvestre, J.F.J. Coelho, New unsaturated copolyesters based on 2,5-furandicarboxylic acid and their crosslinked derivatives, *Polym. Chem.* 7 (2016) 1049–1058.
- [137] J. Dai, S. Ma, N. Teng, X. Dai, X. Shen, S. Wang, X. Liu, J. Zhu, 2,5-Furandicarboxylic acid- and itaconic acid-derived fully biobased unsaturated polyesters and their cross-linked networks, *Ind. Eng. Chem. Res.* 56 (2017) 2650–2657.
- [138] Y. Xu, G. Hua, M. Hakkarainen, K. Odelius, Isosorbide as core component for tailoring biobased unsaturated polyester thermosets for a wide structure-property window, *Biomacromolecules.* 19 (2018) 3077–3085.
- [139] S. Ma, D.C. Webster, F. Jabeen, Hard and flexible, degradable thermosets from renewable bioresources with the assistance of water and ethanol, *Macromolecules.* 49 (2016) 3780–3788.
- [140] Isosorbide polycarbonate: POLYSORB® bisphenol an alternative, isosorbide based polycarbonate. <https://www.roquette.com/industries/performance-materials/polycarbonates>.
- [141] R. Tamion, F. Marsais, P. Ribereau, G. Queguiner, D. Abenhaim, A. Loupy, L. Munnier, Synthesis of new chiral auxiliaries derived from isosorbide, *Tetrahedron: Asymmetry.* 4 (1993) 1879–1890.
- [142] D. Braun, M. Bergmann, 1,4:3,6-Dianhydrohexite als bausteine für polymere, *J. Für Prakt. Chemie/Chemiker-Zeitung.* 334 (1992) 298–310.
- [143] C.J. Brandenburg, Process to produce polyesters which incorporate isosorbide, US 6818730B2, 2004.
- [144] M. Okada, K. Tsunoda, K. Tachikawa, K. Aoi, Biodegradable polymers based on renewable resources. IV. enzymatic degradation of polyesters composed of 1,4:3.6-

- dianhydro-D-glucitol and aliphatic dicarboxylic acid moieties, *J. Appl. Polym. Sci.* 77 (2000) 338–346.
- [145] M. Okada, Y. Okada, A. Tao, K. Aoi, Biodegradable polymers based on renewable resources: polyesters composed of 1,4 : 3,6-dianhydrohexitol and aliphatic dicarboxylic acid units, *J. Appl. Polym. Sci.* 62 (1996) 2257–2265.
- [146] H.S. Park, M.S. Gong, J.C. Knowles, Synthesis and biocompatibility properties of polyester containing various diacid based on isosorbide, *J. Biomater. Appl.* 27 (2012) 99–109.
- [147] C. Lavilla, A. Alla, A. Martínez de Ilarduya, S. Muñoz-Guerra, High Tg bio-based aliphatic polyesters from bicyclic mannitol, *Biomacromolecules*. 14 (2013) 781–793.
- [148] X. Feng, A.J. East, W.B. Hammond, Y. Zhang, M. Jaffe, Overview of advances in sugar-based polymers, *Polym. Adv. Technol.* 22 (2011) 139–150.
- [149] H. Marubayashi, T. Ushio, S. Nojima, Crystallization of polyesters composed of isohexides and aliphatic dicarboxylic acids: effects of isohexide stereoisomerism and dicarboxylic acid chain length, *Polym. Degrad. Stab.* 146 (2017) 174–183.
- [150] H. Marubayashi, T. Ushio, S. Nojima, Crystal polymorphism of biobased polyester composed of isomannide and succinic acid, *Macromolecules*. 52 (2019) 4624–4633.
- [151] M. Okada, Y. Okada, K. Aoi, Synthesis and degradabilities of polyesters from 1,4:3,6-dianhydrohexitols and aliphatic dicarboxylic acids, *J. Polym. Sci. Part A Polym. Chem.* 33 (1995) 2813–2820.
- [152] R. Storbeck, M. Rehahn, M. Ballauff, Synthesis and properties of high-molecular-weight polyesters based on 1,4 : 3,6-dianhydrohexitols and terephthalic acid, 64 (1993) 53–64.
- [153] J. Thiem, H. Lüders, Synthesis of polyterephthalates derived from dianhydrohexitols, *Polym. Bull.* 11 (1984) 365–369.
- [154] R. Storbeck, M. Ballauff, Synthesis and properties of polyesters based on 2,5-furandicarboxylic acid and 1,4:3,6-dianhydrohexitols, *Polymer*. 34 (1993) 5003–5006.
- [155] R. Storbeck M. Ballauff, Synthesis and thermal analysis of copolyesters deriving from 1,4:3,6- dianhydrosorbitol, ethylene glycol, and terephthalic acid, *J. Appl. Polym. Sci.* 59 (1996) 1199–1202.
- [156] H.R. Kricheldorf, G. Behnken, M. Sell, Influence of isosorbide on glass-transition temperature and crystallinity of poly(butylene terephthalate), *J. Macromol. Sci. Part A Pure Appl. Chem.* 44 (2007) 679–684.
- [157] Polyester resin: plant-based POLYSORB® isosorbide for polyester resin, (n.d.). <https://www.roquette.com/industries/performance-materials/polyesters>.
- [158] Z. Mycroft, M. Gomis, P. Mines, P. Law, T.D.H. Bugg, Biocatalytic conversion of lignin to aromatic dicarboxylic acids in *rhodococcus jostii* RHA1 by re-routing aromatic degradation pathways, *Green Chem.* 17 (2015) 4974–4979.
- [159] J.F. Powell, Isolation of dipicolinic acid (pyridine-2:6-dicarboxylic acid) from spores of *Bacillus megatherium*., *Biochem. J.* 54 (1953) 210–211.

- [160] N. Watanabe, M. Hattori, E. Yokoyama, S. Isomura, M. Ujita, A. Hara, Entomogenous fungi that produce 2,6-pyridine dicarboxylic acid (dipicolinic acid), *J. Biosci. Bioeng.* 102 (2006) 365–368.
- [161] H.N. Isfahani, K. Faghihi, New thermally stable polyesters based on 2,5-pyridinedicarbonyl dichloride and aromatic diols: synthesis and characterization, *Chinese Chem. Lett.* 20 (2009) 885–888.
- [162] S. Saleh, B. Sweileh, S.O. Taha, R. Mahmoud, M.O. Taha, Preparation of polyester-based metal-cross linked polymeric composites as novel materials resistant to bacterial adhesion and biofilm formation, *Molecules.* 16 (2011) 933–950.
- [163] A. Pellis, J.W. Comerford, S. Weinberger, G.M. Guebitz, J.H. Clark, T.J. Farmer, Enzymatic synthesis of lignin derivable pyridine based polyesters for the substitution of petroleum derived plastics, *Nat. Commun.* 10 (2019).
- [164] R.L. Broadhead, P. Forest, E.K. Fields, Polyester resin containing pyridine dicarboxylic acid, US3035025, 1962.
- [165] H. Tanaka, Y. Iwanaga, G.C. Wu, K. Sanui, N. Ogata, Synthesis of polyesters by direct polycondensation with picryl chloride, *Polym. J.* 14 (1982) 643–648.
- [166] C.P. Roupakias, G.Z. Papageorgiou, G.P. Karayannidis, Synthesis and thermal behavior of polyesters derived from 1,3-propanediol and various aromatic dicarboxylic acids, *J. Macromol. Sci. - Pure Appl. Chem.* 40 A (2003) 791–805.
- [167] G. Odian, *Principles of polymerization*, 4th ed., 2004.
- [168] R. Boca, ed., *Poly(ethylene terephthalate) (chemistry and preparation) in polymeric materials encyclopedia*, J. C. Sala, CRC Press, 1996.
- [169] S. Paul, Y. Zhu, C. Romain, R. Brooks, P.K. Saini, C.K. Williams, Ring-opening copolymerization (ROCOP): synthesis and properties of polyesters and polycarbonates, *Chem. Commun.* 51 (2015) 6459–6479.
- [170] P. Lecomte, C. Jérôme, Recent developments in ring-opening polymerization of lactones, *Adv. Polym. Sci.* 245 (2012) 173–218.
- [171] A.C. Albertsson, I.K. Varma, Recent developments in ring opening polymerization of lactones for biomedical applications, *Biomacromolecules.* 4 (2003) 1466–1486.
- [172] J.M. Longo, M.J. Sanford, G.W. Coates, Ring-opening copolymerization of epoxides and cyclic anhydrides with discrete metal complexes: structure-property relationships, *Chem. Rev.* 116 (2016) 15167–15197.
- [173] K. Pang, R. Kotek, A. Tonelli, Review of conventional and novel polymerization processes for polyesters, *Prog. Polym. Sci.* 31 (2006) 1009–1037.
- [174] M. Ajioka, H. Suizu, C. Higuchi, T. Kashima, Aliphatic polyesters and their copolymers synthesized through direct condensation polymerization, *Polym. Degrad. Stab.* 59 (1998) 137–143.
- [175] N. Jacquel, R. Saint-Loup, J.P. Pascault, A. Rousseau, F. Fenouillot, Bio-based alternatives in the synthesis of aliphatic-aromatic polyesters dedicated to biodegradable

- film applications, *Polymer*. 59 (2015) 234–242.
- [176] K. Petersen, P. Væggemose Nielsen, G. Bertelsen, M. Lawther, M.B. Olsen, N.H. Nilsson, G. Mortensen, Potential of biobased materials for food packaging, *Trends Food Sci. Technol.* 10 (1999) 52–68.
- [177] S.M. Lomakin, S.Z. Rogovina, A. V. Grachev, E. V. Prut, C. V. Alexanyan, Thermal degradation of biodegradable blends of polyethylene with cellulose and ethylcellulose, *Thermochim. Acta*. 521 (2011) 66–73.
- [178] S. Contents, P. Class, *Polymer data handbook*, Oxford University Press, 1999.
- [179] G.A. Luinstra, Poly(propylene carbonate), old copolymers of propylene oxide and carbon dioxide with new interests: Catalysis and material properties, *Polym. Rev.* 48 (2008) 192–219.
- [180] H. Liu, R. Wang, X. Xu, Thermal stability and flame retardancy of PET/magnesium salt composites, *Polym. Degrad. Stab.* 95 (2010) 1466–1470.
- [181] F. Awaja, D. Pavel, Recycling of PET, *Eur. Polym. J.* 41 (2005) 1453–1477.
- [182] P. Krutphun, P. Supaphol, Thermal and crystallization characteristics of poly(trimethylene terephthalate)/poly(ethylene naphthalate) blends, *Eur. Polym. J.* 41 (2005) 1561–1568.
- [183] D. Bakirtzis, A. Ramani, M.A. Delichatsios, J. Zhang, Structure of the condensed phase and char of fire-retarded PBT nanocomposites by TGA/ATR in N<sub>2</sub>, *Fire Saf. J.* 44 (2009) 1023–1029.
- [184] G. Guo, C. Zhang, Z. Du, W. Zou, H. Tian, A. Xiang, H. Li, Structure and property of biodegradable soy protein isolate/PBAT blends, *Ind. Crops Prod.* 74 (2015) 731–736.
- [185] S.M. Lee, D. Cho, W.H. Park, S.G. Lee, S.O. Han, L.T. Drzal, Novel silk/poly(butylene succinate) biocomposites: the effect of short fibre content on their mechanical and thermal properties, *Compos. Sci. Technol.* 65 (2005) 647–657.
- [186] C. Vogel, H.W. Siesler, Thermal degradation of poly( $\epsilon$ -caprolactone), poly(L-lactic acid) and their blends with poly(3-hydroxy-butyrate) studied by TGA/FT-IR spectroscopy, in: *Macromol. Symp.*, 2008: pp. 183–194.
- [187] K.D. Murugan, S. Radhika, I. Baskaran, R. Anbarasan, Clay catalyzed synthesis of biodegradable poly(glycolic acid), *Chinese J. Polym. Sci.* 26 (2008) 393–398.
- [188] M. Venkateswar Reddy, Y. Mawatari, R. Onodera, Y. Nakamura, Y. Yajima, Y.C. Chang, Polyhydroxyalkanoates (PHA) production from synthetic waste using *Pseudomonas pseudoflava*: PHA synthase enzyme activity analysis from *P. pseudoflava* and *P. palleronii*, *Bioresour. Technol.* 234 (2017) 99–105.
- [189] I.M. Ward, J. Sweeney, *Mechanical properties of solid polymers*, 3rd ed., Wiley, West Sussex, 2013.
- [190] S. Hashemi, Temperature dependence of work of fracture parameters in polybutylene terephthalate (PBT), *Polym. Eng. Sci.* 40 (2000) 1435–1446.
- [191] L. Genovese, N. Lotti, V. Siracusa, A. Munari, Poly(neopentyl glycol furanoate): A

- member of the furan-based polyester family with smart barrier performances for sustainable food packaging applications, *Materials* (Basel). 10 (2017).
- [192] P.S. Taoukis, A. El Mesquine, T.P. Labuza, Moisture transfer and shelf life of packaged foods, in: 1988: pp. 243–261.
- [193] High barrier packaging films market global analysis, challenges, opportunities, trends, market segments by 2023, (2019). <https://bestmarketherald.com/2019/11/26/high-barrier-packaging-films-market-global-analysis-challenges-opportunities-trends-market-segments-by-2023/>.
- [194] S. Desobry, Maîtrise des transferts d'eau grâce aux emballages hydrosensibles: application à la conservation des fromages, in: N. Gontard (ed.), *Les Emballages Act.*, TEC & DOC, Paris, 2000: p. 139.
- [195] R.M. Hodge, T.J. Bastow, G.H. Edward, G.P. Simon, A.J. Hill, Free volume and the mechanism of plasticization in water-swollen poly(vinyl alcohol), *Macromolecules*. 29 (1996) 8137–8143.
- [196] C. Bastioli, I. Guanella, G. Romano, Effects of water sorption on the physical properties of PET, PBT, and their long fibers composites, *Polym. Compos*. 11 (1990) 1–9.
- [197] S. Mali, L.S. Sakanaka, F. Yamashita, M.V.E. Grossmann, Water sorption and mechanical properties of cassava starch films and their relation to plasticizing effect, *Carbohydr. Polym*. 60 (2005) 283–289.
- [198] S.A. Jabarin, E.A. Lofgren, Effects of water absorption on physical properties and degree of molecular orientation of poly (ethylene terephthalate), *Polym. Eng. Sci*. 26 (1986) 620–625.
- [199] D. Langevin, J. Grenet, J.M. Saiter, Moisture sorption in pet influence on the thermokinetic parameters, *Eur. Polym. J*. 30 (1994) 339–345.
- [200] L. Sanna, S.Kirsi, F. Laura, Changes in water absorption and modulus of elasticity of flexible printed circuit board materials in high humidity testing, 18th Eur. Microelectron. Packag. Conf. (2011) 1–6.
- [201] K.S. Miller, J.M. Krochta, Oxygen and aroma barrier properties of edible films: a review, *Trends Food Sci. Technol*. 8 (1997) 228–237.
- [202] M. Schmid, W. Zillinger, K. Müller, S. Sänglerlaub, Permeation of water vapour, nitrogen, oxygen and carbon dioxide through whey protein isolate based films and coatings-Permeability and activation energy, *Food Packag. Shelf Life*. 6 (2015) 21–29.
- [203] K.W. McMillin, Where is MAP Going? A review and future potential of modified atmosphere packaging for meat, *Meat Sci*. 80 (2008) 43–65.
- [204] A.R. Mackintosh, J.J. Ligat, Dynamic mechanical analysis of poly(trimethylene terephthalate)-a comparison with poly(ethylene terephthalate) and poly(ethylene naphthalate), *J. Appl. Polym. Sci*. 92 (2004) 2791–2796.
- [205] A.A. Kader, D. Zagory, E.L. Kerbel, Modified atmosphere packaging of fruits and vegetables, *Crit. Rev. Food Sci. Nutr*. 28 (1989) 1–30.



- [206] H.P.S. Abdul Khalil, C.K. Saurabh, M.I. Syakir, M.R. Nurul Fazita, A. Bhat, A. Banerjee, H.M. Fizree, S. Rizal, P.M. Tahir, Barrier properties of biocomposites/hybrid films, in: *Mech. Phys. Test. Biocomposites, Fibre-Reinforced Compos. Hybrid Compos.*, Woodhead P, Elsevier, 2019: pp. 241–258.
- [207] V. Patrick, Les films à perméabilité aux gaz ajustable: application aux fruits et légumes, in: N. Gontard (ed.), *Les Emballages Actifs*, TEC&DOC, Paris, 2000: p. 95.
- [208] V. Siracusa, Food packaging permeability behaviour: A report, *Int. J. Polym. Sci.* 2012 (2012).
- [209] B. Freeman, Y. Yampolskii, I. Pinnau, *Materials science of membranes for gas and vapor separation*, John Wiley & Sons, Ltd, Chichester, 2006.
- [210] H. Lin, B.D. Freeman, Gas solubility, diffusivity and permeability in poly(ethylene oxide), *J. Memb. Sci.* 239 (2004) 105–117.
- [211] H. Fujita, A. Kishimoto, K. Matsumoto, Concentration and temperature dependence of diffusion coefficients for systems polymethyl acrylate and n-alkyl acetates, *Trans. Faraday Soc.* 56 (1960) 424–437.
- [212] S. Prager, E. Bagley, F.A. Long Vol, B.S. Prager, F.A. Long, *Equilibrium Sorption data for polyisobutylene-hydrocarbon systems*, UTC, 1953.
- [213] S.C. George, S. Thomas, Transport phenomena through polymeric systems, *Prog. Polym. Sci.* 26 (2001) 985–1017.
- [214] J.H. Han, M.G. Scanlon, Mass transfer of gas and solute through packaging materials, in: *Innov. Food Packag.*, 2nd ed, Elsevier Ltd, 2013: pp. 37–49.
- [215] K.L. Bajaj, G. Kaur, Spectrophotometric determination of l-ascorbic acid in vegetables and fruits, *Food Technol.* 42 (1981) 70–77.
- [216] A.T. DiBenedetto, Molecular properties of amorphous high polymers. II. An interpretation of gaseous diffusion through polymers, *J. Polym. Sci. Part A Gen. Pap.* 1 (1963) 3477–3487.
- [217] J. Brandrup, E.H. Immergut, E.A. Grulke, *Polymer handbook*, 4th ed, 1999.
- [218] H.J. Lehermeier, J.R. Dorgan, J. Douglas Way, Gas permeation properties of poly(lactic acid), *J. Memb. Sci.* 190 (2001) 243–251.
- [219] G. Flodberg, I. Helland, L. Thomsson, S. Bodil Fredriksen, Barrier properties of polypropylene carbonate and poly(lactic acid) cast films, *Eur. Polym. J.* 63 (2015) 217–226.
- [220] W.I.M. Brolly J B, Bower D I, Diffusion and sorption of CO<sub>2</sub> in poly (ethylene terephthalate) and poly (ethylene naphthalate), *J. Polym. Sci. Part B Polym. Phys.* 34 (1996) 769–780.
- [221] A.K. Mohanty, M. Misra, L.T. Drzal, Sustainable bio-composites from renewable resources in green materials world, *J. Polym. Environ.* 10 (2002) 19–26.
- [222] S. Bonhomme, A. Cuer, A.M. Delort, J. Lemaire, M. Sancelme, G. Scott, Environmental biodegradation of polyethylene, *Polym. Degrad. Stab.* 81 (2003) 441–452.

- [223] D. Briassoulis, C. Dejean, P. Picuno, Critical review of norms and standards for biodegradable agricultural plastics Part II: composting, *J. Polym. Environ.* 18 (2010) 364–383.
- [224] T. Leejarkpai, U. Suwanmanee, Y. Rudeekit, T. Mungcharoen, Biodegradable kinetics of plastics under controlled composting conditions, *Waste Manag.* 31 (2011) 1153–1161.
- [225] S. Tariq, Success factors for the adoption of bio-based packaging, 2013.



---

## Chapter 2

∞ 1,4:3,6-dianhydrohexitols based aliphatic polyesters: synthesis, thermal, mechanical and permeation properties ∞

---



In this Chapter, bio-based polyesters were prepared by reacting isosorbide (IS) or isomannide (IM) with aliphatic acid dichlorides (succinyl, adipoyl and sebacoyl chlorides, named C4, C6 and C10, respectively) according to the melt polycondensation reactions previously published by Okada *et al.* [1]. The obtained polyesters were identified as follows: the first two letters corresponded to the dianhydrohexitol (IS or IM), followed by the acid dichloride (C4, C6, C10). As stated in Chapter 1, all these already-known polyesters were proved to be biodegradable [1,2]. The originality of this work was to prepare films and investigate their gas and water sorption/permeation properties, which are crucial for food packaging applications. Relationships between microstructures and sorption/permeation properties were established.

## 2.1 Synthesis

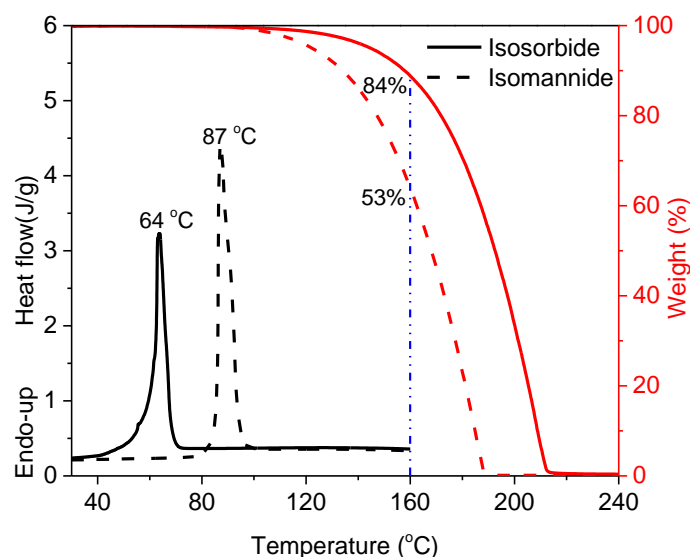
The first synthesis involved isosorbide (IS) and sebacoyl chloride (C10) since high molar masses have already been obtained in the literature [1]. The initial synthesis scheme described in Annex 1.1.1 was inspired by Okada *et al.* [1]. However, a dark brown and insoluble (maybe crosslinked) ISC10\* was obtained (Figure 2-1).



**Figure 2-1** Images of ISC10 polyester

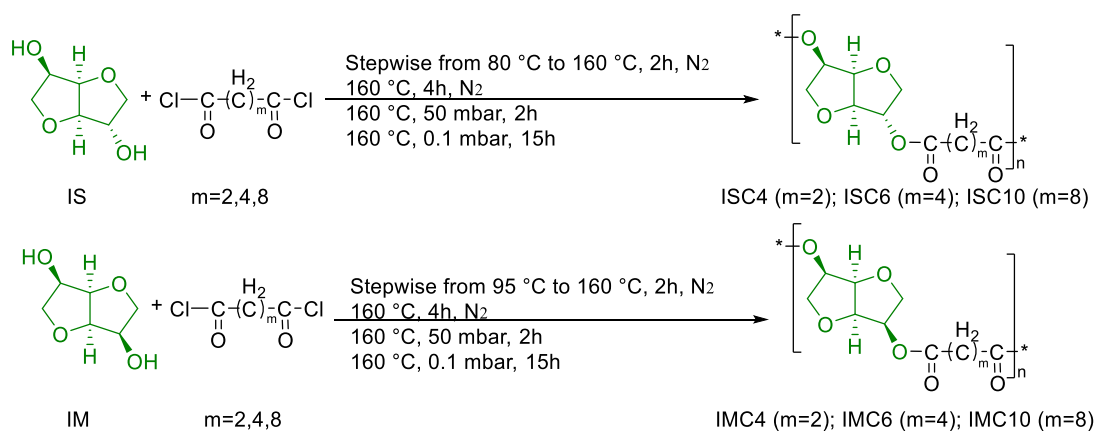
Considering the isosorbide moiety has an intrinsic sensitivity to thermal oxidation at high temperature, the coloration and crosslinking were probably due to the inlet of atmospheric oxygen [3]. Changing the order of introduction of the chemicals and adding a nitrogen flow during the first 6 hours was then experienced (Operation 2 detailed in Annex 1.1.2). A soluble light brown powder was obtained ISC10\*\* (Figure 2-1), but with low molar mass ( $\overline{M}_n = 8\,000\text{ g}\cdot\text{mol}^{-1}$ ) (Annex 4). For both operations, crystals deposited on the reaction flask walls were observed. This phenomenon, which can change the stoichiometry and hence strongly limit the molar masses, was supposed to result from the evaporation/condensation of isosorbide, which

was investigated by TGA and DSC as shown in Figure 2-2 (isomannide was also investigated and shown for later reference). From the TGA curves, we can see that both reagents have a great weight loss at 160 °C (the applied temperature for polymerization) under N<sub>2</sub> atmosphere, 16 and 47% for IS and IM, respectively. However, there is no visible decomposition on DSC, only the melting peaks were noticed. Thus, the crystals deposited on the flask walls were linked to the evaporation of isosorbide, which was also confirmed by <sup>1</sup>H NMR analysis.



**Figure 2-2** Thermal stability (TGA and DSC) of isosorbide and isomannide

According to the above investigations, improved conditions (Operation 3 described in Annex 1.1.3) were used for the synthesis of the target polyesters (ISC10 was recognized as white flakes in Figure 2-1) by decreasing the starting temperature (Scheme 2-1).

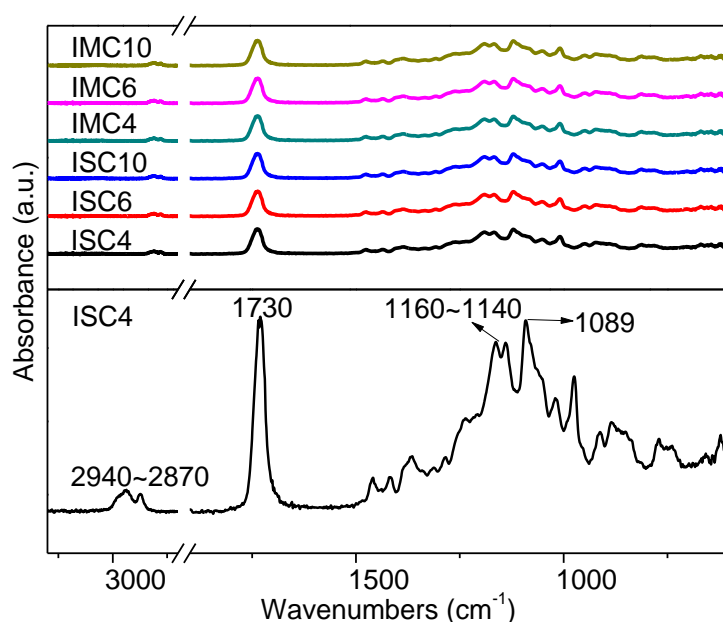


**Scheme 2-1** Synthesis of aliphatic polyesters from IS and IM

## 2.2 Characterization of polyesters

### 2.2.1 Structures

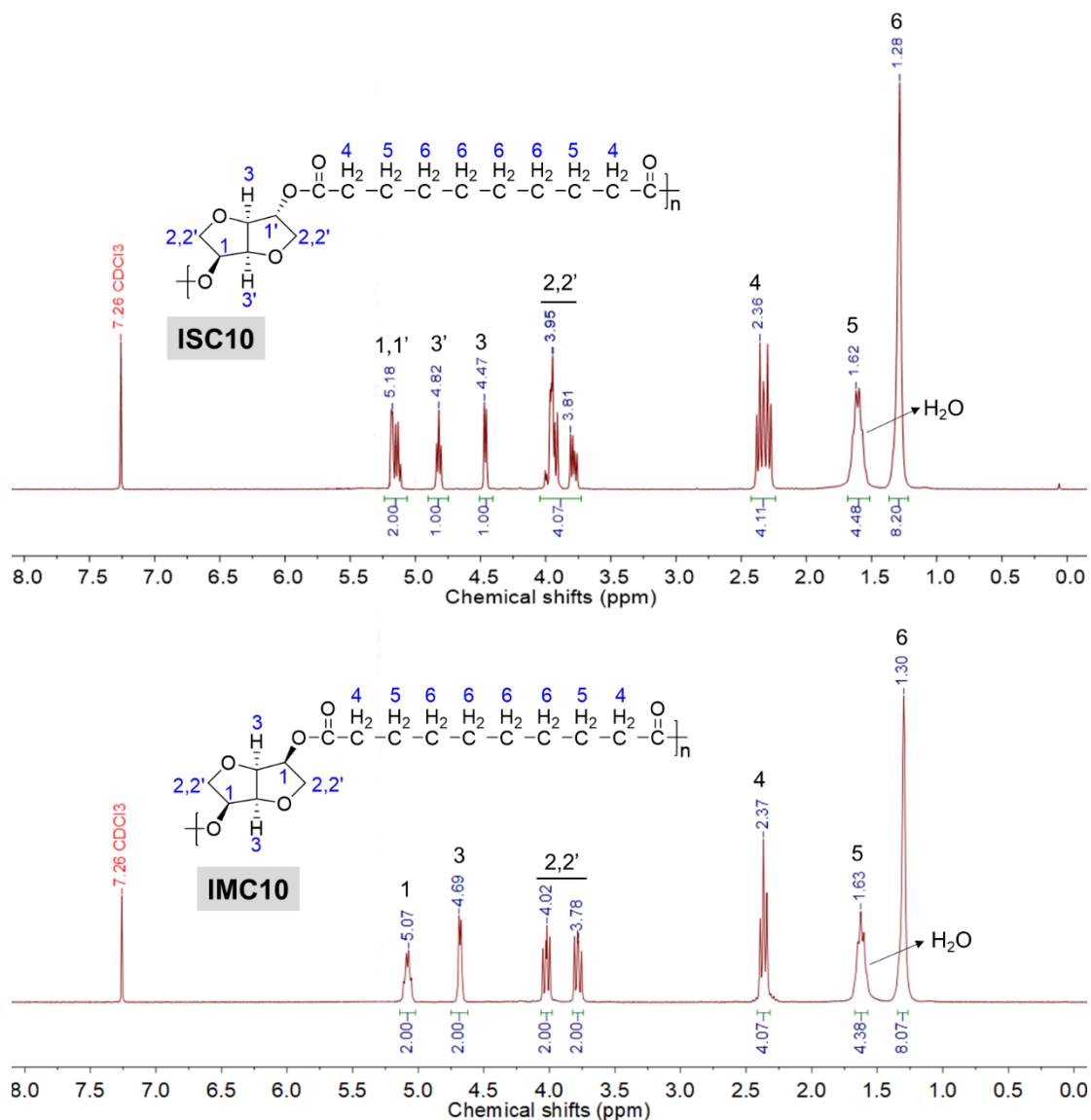
FT-IR spectra of the synthesized polyesters were given in Figure 2-3. Due to their similar chemical structures, all polyesters showed almost identical spectra. Taking ISC4 as an example (bottom of Figure 2-4), the double CH<sub>2</sub> stretching signals of the aliphatic chain appeared in the range from 2940 to 2870 cm<sup>-1</sup> and the signal of ether cyclic bond in IS was at 1089 cm<sup>-1</sup>. The presence of the ester group was proved by the pronounced C=O peak at 1730 cm<sup>-1</sup> and the C-O double peaks at 1160 and 1140 cm<sup>-1</sup>, which confirmed the successful synthesis.



**Figure 2-3** FTIR spectra of the polyesters

The chemical structures of the polyesters were characterized by <sup>1</sup>H NMR and shown in Annex 5. Taking ISC10 and IMC10 as examples (Figure 2-4), all proton signals from the repeating units were found at the expected chemical shifts with matching multiplicities. For ISC10, the signals with a total integration close to 8 protons (8H) in the range from 3.68 to 5.22 ppm corresponded to isosorbide unit and the signals at 2.33, 1.61 and 1.29 ppm agreed with the 16H of sebacoyl unit. Similarly for IMC10, the signals in the range from 3.67 to 5.19 ppm (around 8H) were ascribed to isomannide unit and the signals at 2.37, 1.63 and 1.30 ppm (approximately 16H) belonged to sebacoyl unit. The exo-endo hydroxyl groups of the isosorbide ring induced an irregular structure in ISC10, which resulted in stereo differences between ISC10 and IMC10 and could explain why the peaks split more in ISC10 spectrum [4].





**Figure 2-4**  $^1\text{H}$  NMR spectra of ISC10 and IMC10 polyesters

## 2.2.2 Molar masses and yields

The yields in polymer (after precipitation) were measured and the corresponding molar masses were determined by Steric Exclusion Chromatography (SEC) (Table 2-1, corresponding chromatograms were given in Annex 4). Except for IMC4, high yields were obtained and the number average molar masses ( $\overline{M}_n$ ) of polyesters exceeded  $10\,000\text{ g}\cdot\text{mol}^{-1}$ . The case of IMC4 can be ascribed to its high melting temperature around  $173\text{ }^\circ\text{C}$  (see section 2.2.4), higher than the reaction temperature ( $160\text{ }^\circ\text{C}$ ), which limited the polycondensation reaction [4].

Concerning all other samples, there is a general tendency that the molar mass increased with the length of the acid dichloride, probably due to the higher flexibility brought by the methylene units which would favor the motion of the growing chains in a very viscous bulk medium.

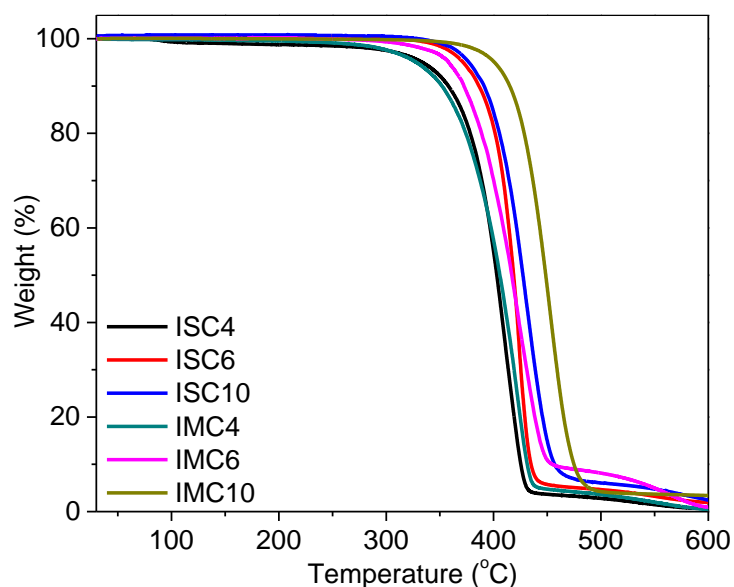
**Table 2-1** Molar masses and dispersities of polyesters and yields of synthesis

Polyester	$M$ of repeat unit ( $\text{g}\cdot\text{mol}^{-1}$ )	$\overline{DP}_n$	$\overline{M}_n^{1)}$ ( $\text{g}\cdot\text{mol}^{-1}$ )	$\overline{M}_w^{1)}$ ( $\text{g}\cdot\text{mol}^{-1}$ )	$\overline{D}^{2)}$	Yield <sup>3)</sup> (%)
ISC4	228	94	10 800	22 700	2.1	80
ISC6	256	82	10 600	18 000	1.7	88
ISC10	312	118	18 500	38 900	2.1	90
IMC4	228	38	4 300	7 700	1.8	62
IMC6	256	82	10 500	18 800	2.5	85
IMC10	312	122	19 000	38 000	2.0	89

$\overline{DP}_n$ , degree of polymerization calculated from  $\overline{M}_n$ ; <sup>1)</sup> SEC conducted in  $\text{CH}_2\text{Cl}_2$  with PMMA standards; <sup>2)</sup> Dispersity; <sup>3)</sup> In precipitated polymer.

### 2.2.3 Thermal degradation

The thermal degradation of polyesters was investigated by thermal gravimetric analysis, as shown in Figure 2-5.



**Figure 2-5** TGA curves of IS and IM polyesters

The degradation data were recorded in Table 2-2. All polyesters showed thermal stability greater than 325 °C with a rapid decomposition around 400-450 °C. The degradation seemed to begin at higher temperatures when the length of the aliphatic diacid chain increased, with 5% weight loss temperature ( $T_{5\%}$ ) values  $T_{5\%}$  (ISC4) <  $T_{5\%}$  (ISC6) <  $T_{5\%}$  (ISC10) and  $T_{5\%}$  (IMC4) <  $T_{5\%}$  (IMC6) <  $T_{5\%}$  (IMC10). Even if IMC10 showed the highest thermal stability, we cannot generally conclude that IM polyesters were more stable than IS homologs. It means that the diacid chain length has more influence on thermal degradation than stereoisomerism. These results were consistent with literature values [4,5].

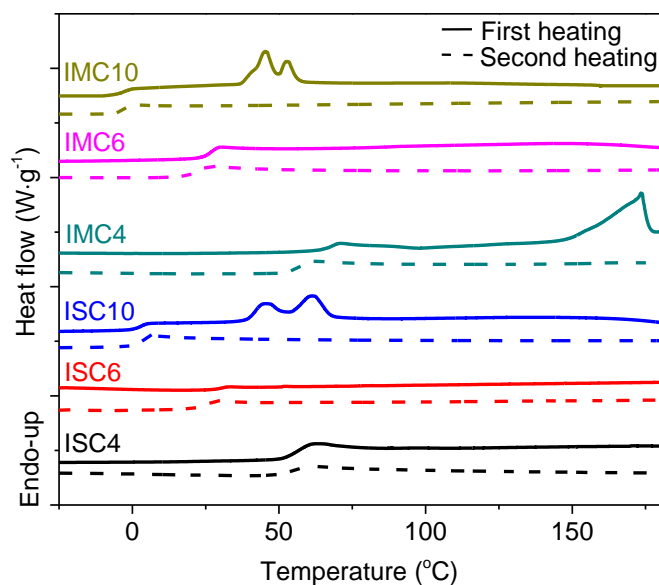
**Table 2-2** Thermal degradation data recorded from TGA

Polyester	$T_{5\%}$ (°C)	$T_{\max}$ (°C)	Polyester	$T_{5\%}$ (°C)	$T_{\max}$ (°C)
ISC4	334	403	IMC4	328	406
ISC6	372	419	IMC6	358	417
ISC10	377	427	IMC10	400	448

$T_{5\%}$ , 5% weight loss temperature;  $T_{\max}$ , maximum degradation rate temperature.

## 2.2.4 Differential scanning calorimetry (DSC)

DSC measurements were carried out to determine the glass transition temperature ( $T_g$ ) and the crystallization behavior of the polyesters. The heating thermograms were presented in Figure 2-6.



**Figure 2-6** DSC thermograms of polyesters

The thermograms showed that only ISC10, IMC4 and IMC10 were semi-crystalline due to the presence of melting peaks at 46/62, 173 and 45/53 °C (detailed in Table 2-3), respectively. These melting peaks were complex, and could reveal not only melting / crystallization phenomena but more certainly crystalline polymorphism (as evidenced later from XRD patterns in Figure 2-10), as already observed in such polymers before [4]. However, the crystals cannot be obtained back upon cooling, even at very low cooling speed, probably due to the very slow crystallization rate. These results are in good agreement with those obtained by Marubayashi et al. [4], except for IMC4, probably due to the low molar mass in our case. The  $T_g$  values decreased with the increase of the aliphatic carbon number, which is quite logical since more  $\text{CH}_2$  in the chain induced more flexibility and free volume. The highest  $T_g$  (65 °C) was observed for IMC4 and the lowest (0 °C) for IMC10. For a given aliphatic chain, considering almost the same molar masses of ISC10 and IMC10, it seemed that IM and IS polyesters showed only a slight difference in  $T_g$  value, but larger differences in crystallinity. It means that the exo-endo and endo-endo stereoscopic differences affected the crystallization rather than the chain relaxation [4].

**Table 2-3** Information recorded from DSC thermograms

Polyester	$T_g^a$ (°C)	$T_m^b$ (°C)	$\Delta H_m^b$ (J·g <sup>-1</sup> )	Polyester	$T_g^a$ (°C)	$T_m^b$ (°C)	$\Delta H_m^b$ (J·g <sup>-1</sup> )
ISC4	56	-	-	IMC4	65	173	34.8
ISC6	28	-	-	IMC6	26	-	-
ISC10	2	46/62*	18.7	IMC10	0	45/53*	15.9

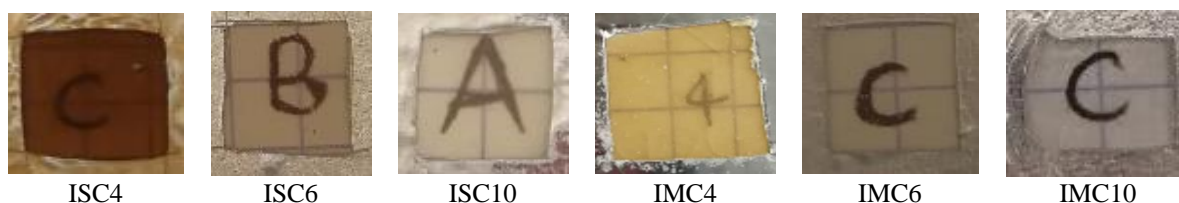
<sup>a</sup> DSC second heating; <sup>b</sup> DSC first heating; \* shoulder peaks.

## 2.3 Characterization of films

### 2.3.1 Preparation of films

The polymer films shown in Figure 2-7 were prepared by hot pressing under different temperatures depending on their thermal properties established by DSC, and then stored at room temperature in dry atmosphere (with  $\text{P}_2\text{O}_5$  protection). The yellow to brown color of some films shown in Figure 2-8 came from polymerization but deepened after hot pressing, which was probably due to thermal oxidation. Since the obtained polymers could not recrystallize upon cooling, and the crystalline phase is well known to bring barrier properties, the films were sometimes prepared with partial melting. Unfortunately, ISC4, ISC6, IMC4 and IMC6 films

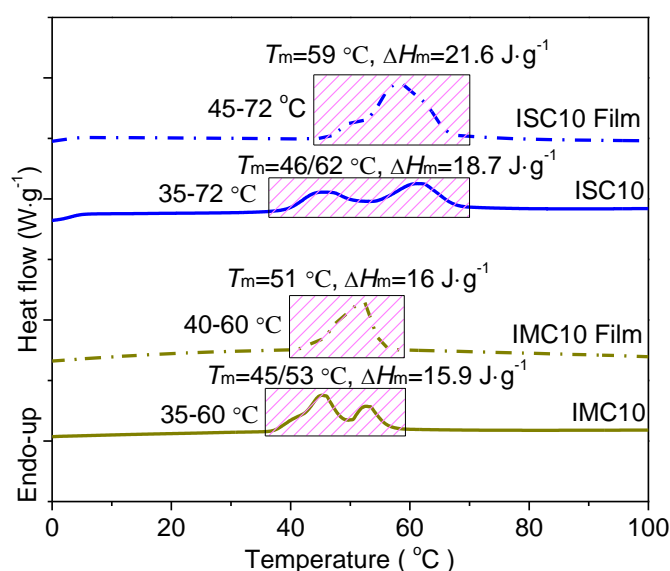
appeared too brittle, which was probably due to their short methylene units and low molar masses. Only ISC10 and IMC10 films with the highest molar masses and longer methylene units were flexible enough for further experiments. IMC10 film was prepared at 45 °C (melting range: 35 - 60 °C) and ISC10 film was prepared at 50 °C (melting range: 35 - 72 °C).



**Figure 2-7** IS and IM polyester films prepared by hot pressing

### 2.3.2 Crystallinity of films

Since the crystals of ISC10 and IMC10 are known to change during time in the temperature range of 20-40 °C [4], the crystal structures of the polyester films must be checked before investigating their mechanical and barrier properties. Therefore, the melting behaviors of the polyesters were studied by DSC before and after the preparation of films by hot pressing in Figure 2-8.

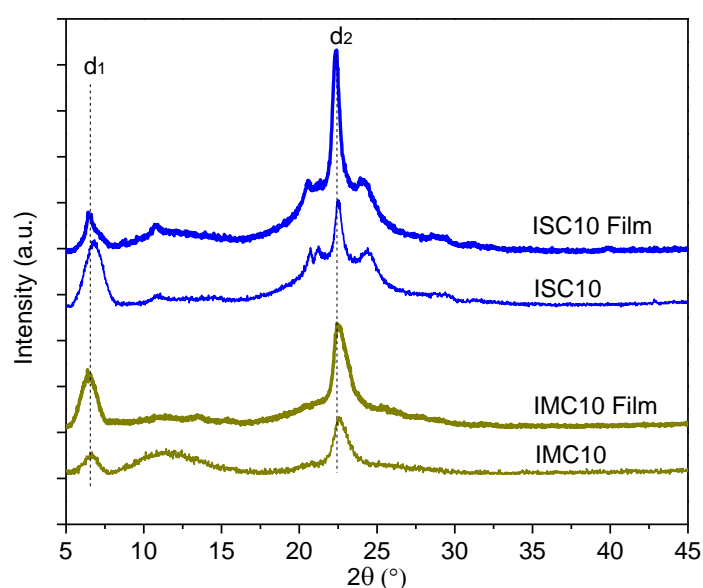


**Figure 2-8** DSC first heating of ISC10, IMC10, and their films

Both ISC10 and IMC10 films showed broad but less complex melting peaks compared to the corresponding polyesters. Furthermore, it seemed the initial melting temperature increased. The melting enthalpy ( $\Delta H_m$ ) of ISC10 film was  $26.1 \text{ J}\cdot\text{g}^{-1}$ , which is higher than that of ISC10 ( $\Delta H_m = 18.7 \text{ J}\cdot\text{g}^{-1}$ ), but the  $\Delta H_m$  of IMC10 ( $\Delta H_m = 15.9 \text{ J}\cdot\text{g}^{-1}$ ) and IMC10 film ( $\Delta H_m = 16.0 \text{ J}\cdot\text{g}^{-1}$ ) were almost the same. ISC10 film was more crystalline with a higher melting temperature than IMC10 film. Despite the partial melting during film making and the fact that no crystallization was observed during cooling in DSC for both polyesters, the recrystallization could effectively happen due to the annealing process during the hot pressing and the 60 days of storage under room temperature.

### 2.3.3 XRD of films

Figure 2-9 exhibited the XRD diffractograms of ISC10, IMC10 and their films.



**Figure 2-9** XRD spectra of ISC10, IMC10, and their films

The crystallinity ( $\chi_c$ ) and  $d$ -spacing were recorded in Table 2-4. Two obvious diffraction peaks located at  $2\theta \sim 6.5^\circ$  and  $2\theta \sim 22.5^\circ$  corresponded to  $d_1 = 1.60 \text{ nm}$  and  $d_2 = 0.46 \text{ nm}$  respectively for both polyesters and films. This result was consistent with Marubayashi *et al.* [4]. The  $d$ -spacing  $d_1$  corresponded to the spacing parallel to the chain direction and  $d_2$  was that perpendicular to the chain direction (chain-chain packing). The crystallinity for both polyesters

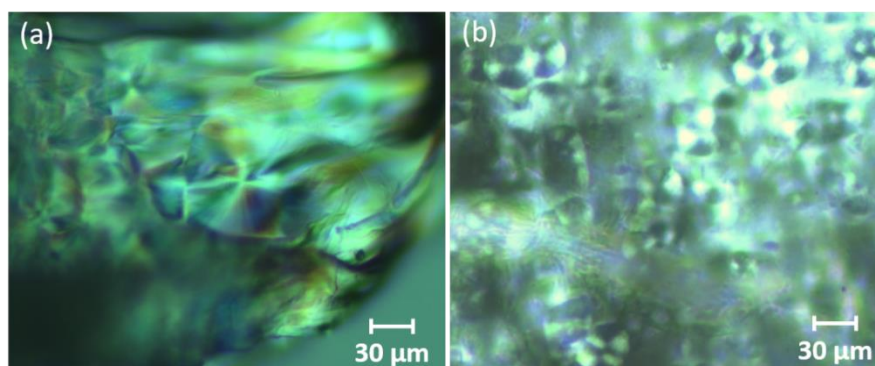
is less than the corresponding films which was consistent with the DSC results. The crystallinity of ISC10 film ( $\chi_c = 36.3\%$ ) was higher than IMC10 film ( $\chi_c = 25.9\%$ ). Considering the stronger intensity at  $d_2$  than  $d_1$  for ISC10, while almost the same for IMC10, it seemed that ISC10 is more crystallized by chain-chain packing than IMC10. Besides, the diffractometric patterns showed scattering peaks at very low  $2\theta$  values ( $5\text{--}10^\circ$ ) which can be related to liquid crystal regions as reported by Ding *et al.* [6].

**Table 2-4** Crystallinity ( $\chi_c$ ) and  $d$ -spacing information for ISC10 and IMC10

Sample	$\chi_c$ (%)	$d_1$ (nm)	$d_2$ (nm)
ISC10	31.1	1.60	0.46
ISC10 film	36.3	1.60	0.46
IMC10	23.6	1.60	0.46
IMC10 film	25.9	1.60	0.46

### 2.3.4 Microscopy of films

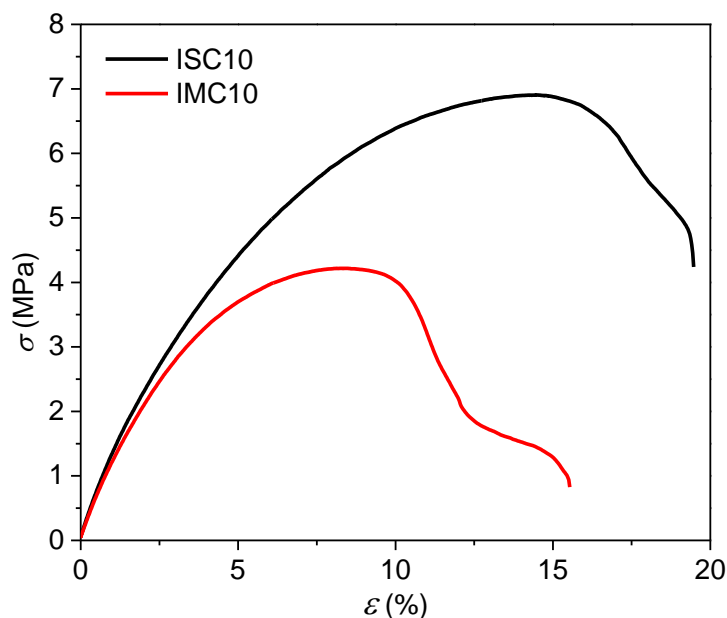
The polarized microscopy images of polyester films were shown in Figure 2-10. It proved that ISC10 film contained larger but less homogeneous crystals than IMC10, which well corresponded to a broader and higher melting temperature of ISC10 observed by DSC, compared to IMC10. It evidenced that the endo-exo stereoscopic configuration in IS polymer chains were more inclined to crystallize in larger size than the endo-endo stereoscopic configuration in IM polymer chains: the IS chains are more readily to crystallize by chain-chain interactions (chain-chain packing) [4]. Moreover, the textures evidenced on POM images are typical of liquid crystal phases [6–8].



**Figure 2-10** Microscopy images of ISC10 film (a) and IMC10 film (b)

### 2.3.5 Mechanical properties

The representative stress-strain curves of ISC10 and IMC10 films were given in Figure 2-11 and the corresponding data were gathered in Table 2-5.



**Figure 2-11** Stress-strain curves of ISC10 and IMC10 films

ISC10 had a better resistance to stretch than IMC10. The Young's modulus values of ISC10 and IMC10 were similar ( $127 \pm 20$  MPa and  $125 \pm 10$  MPa, respectively). Comparing the tensile stress and elongation at break, ISC10 ( $\sigma_b = 4.2 \pm 0.8$  MPa,  $\epsilon_b = 19 \pm 5$  %) seemed tougher than IMC10 ( $\sigma_b = 1.0 \pm 0.2$  MPa,  $\epsilon_b = 16 \pm 3$  %). Since their molar masses and  $T_g$  were very similar, it seemed that the higher crystallinity and larger crystal size of ISC10 brought more resistance at break. Both ISC10 and IMC10 had more toughness than those well-known bio-based polyesters, such as PLA, PHB and PEF (elongation at break less than 10%, 8% and 5%, respectively) [9]. However, our ISC10 films were more rigid and more brittle than those prepared by Park *et al.* ( $E = 53$  MPa and  $\sigma_b = 10.5$  MPa) [5]. The differences may be due to the solvent casting technique used by Park *et al.* to prepare their films. With this technique, solvent molecules can be retained and plasticize the film.



**Table 2-5** Mechanical properties of ISC10 and IMC10 polyester films

Polyester film	$E$ (MPa)	$\sigma_b$ (MPa)	$\varepsilon_b$ (%)
ISC10	$127 \pm 20$	$4.2 \pm 0.8$	$19 \pm 5$
IMC10	$125 \pm 10$	$1.0 \pm 0.2$	$16 \pm 3$

$E$ , Young's modulus;  $\sigma_b$ , stress at break;  $\varepsilon_b$ , strain at break.

### 2.3.6 Contact angle measurements

The surface energy (with dispersity and polar parts) and water contact angle values of polyester films were presented in Table 2-6.

**Table 2-6** Surface energies and contact angles of ISC10 and IMC10 films

Polyester film	$\gamma^t$ (mN·m <sup>-1</sup> )	$\gamma^d$ (mN·m <sup>-1</sup> )	$\gamma^p$ (mN·m <sup>-1</sup> )	$\theta_w$ (°)
ISC10	31.0	26.1	4.9	$85 \pm 1.0$
IMC10	29.6	24.1	5.4	$83 \pm 0.5$

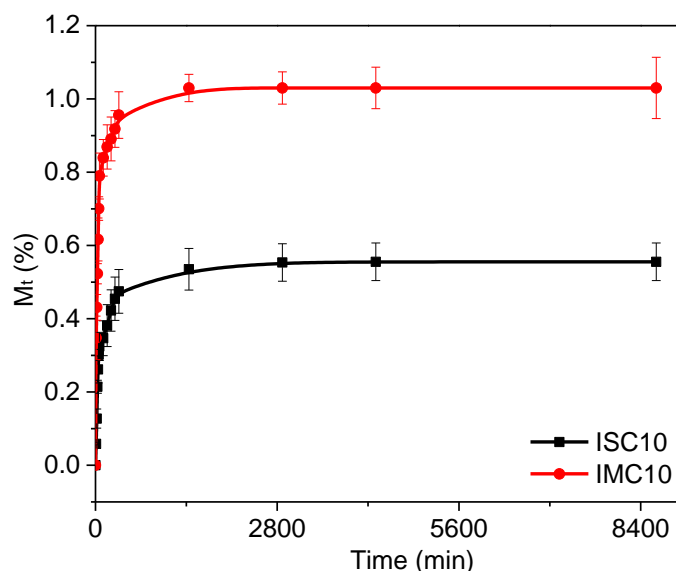
$\gamma^t$ , total surface energy with the dispersive ( $\gamma^d$ ) and polar ( $\gamma^p$ ) parts;  $\theta_w$ , water contact angle.

The surface energy values for ISC10 (31.0 mN·m<sup>-1</sup>) and IMC10 (29.6 mN·m<sup>-1</sup>) were similar. The water contact angle values,  $85 \pm 1.0^\circ$  for ISC10 and  $83 \pm 0.5^\circ$  for IMC10, highlighted the hydrophobicity of the films. These results showed almost no difference between ISC10 and IMC10, indicating that the surface properties of the films were not influenced by the stereoisomerism of IS and IM. The water contact angles of ISC10 and IMC10 were lower than the common used packaging materials PE ( $120 \pm 0.1^\circ$ ) [10] and PP ( $97 \pm 0.4^\circ$ ) [11], but comparable to semi-crystalline polyesters like PET ( $83.8 \pm 1.0^\circ$ ) [12] and PLA ( $80.0 \pm 0.1^\circ$  and  $73.0 \pm 2.0^\circ$ ) [9,14].

### 2.3.7 Liquid water sorption and water vapor sorption

Figure 2-12 showed that the sorption of liquid water (gain of mass  $M_t$ ) at equilibrium ( $M_{eq}$ ) is low whatever the sample (ISC10,  $M_{eq} = 0.55 \pm 0.05$  %, and IMC10,  $M_{eq} = 1.03 \pm 0.09$  %). This behavior can be explained by the hydrophobic properties and the semi-crystalline microstructures of the polyester films. The equilibrium was reached earlier for IMC10 (before 2800 min) than for ISC10 (after 2800 min), which meant IMC10 proceeded a quicker dissolution-

diffusion process than ISC10. This is due to the bigger crystals and the higher crystallinity of ISC10, which bring a more compact structure favorable for water barrier properties [14].

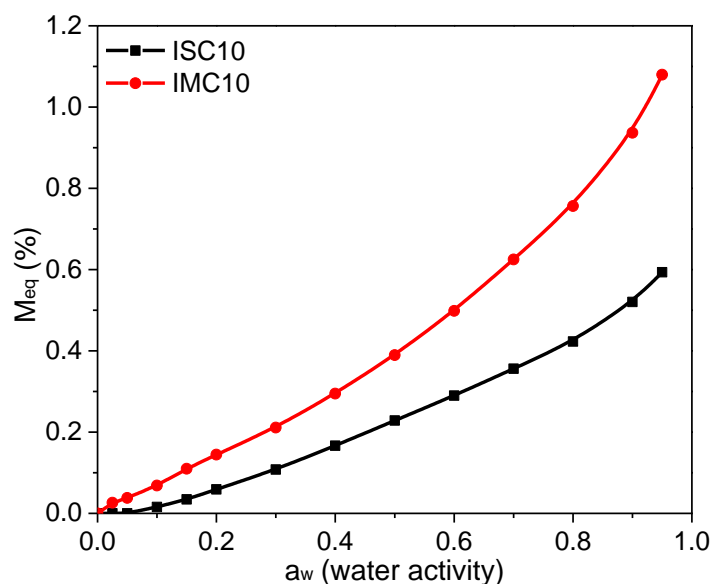


**Figure 2-12** Liquid water sorption of ISC10 and IMC10 films

As observed before for liquid water sorption, water vapor sorption was less for ISC10 than for IMC10 (*e.g.*  $M_{eq} = 0.58\%$  and  $M_{eq} = 1.08\%$  at water activity  $a_w = 0.95$ , respectively) (Figure 2-14). Both ISC10 and IMC10 showed a constant sorption of water vapor at the lowest  $a_w$  then a larger increase. Considering the “sigmoid” shape of the isotherms, Park’s model is convenient to interpret the sorption behavior: Langmuir-type sorption followed by Henry-type sorption and finally water clustering (see Annex 3) [15–19]. The Park’s model parameters ( $A_L$ ,  $b_L$ ,  $k_H$ ,  $K_a$  and  $n_a$ ) were obtained by fitting the sorption isotherms with Table curve2D® software and the corresponding values were given in Table 2-7. The isotherms were divided into three parts. The first concave part of the curve ( $a_w < 0.1$ ) follows a Langmuir-type adsorption behavior corresponding to the presence of a first monolayer of water molecules on the surface of the film. This behavior results from a combination of two processes: adsorption at the surface of micro-cavities (free volume, micropores, etc.) and adsorption due to the presence of hydrophilic groups. The corresponding parameters  $A_L$  and  $b_L$  were larger for IMC10 than for ISC10 probably due to their difference in crystallinity. The following linear part of the isotherm corresponds to a Henry’s type process, which involves random absorption (dissolution) and diffusion of water molecules inside the film. This part corresponds to the adsorption of water molecules in the amorphous domains of the film. The slope of the straight line corresponds to

the solubility coefficient  $S$  (similar to  $k_H$ ) of water vapor in the film. ISC10 showed a constant sorption until  $a_w = 0.8$  ( $S = 5.3 \times 10^{-3} \text{ g}_{\text{H}_2\text{O}}/\text{g}_{\text{pol}}$ ) and IMC10 until  $a_w = 0.5$  ( $S = 8.0 \times 10^{-3} \text{ g}_{\text{H}_2\text{O}}/\text{g}_{\text{pol}}$ ). The convex part of the curve ( $a_w > 0.8$ ) corresponds to adsorption of water molecules with formation of aggregates, which induce a larger swelling of the film. This accumulation of water molecules took place at the surface of film and in the free volume of the amorphous phase. The more convex curve and the larger  $K_a$  and  $n_a$  values for IMC10 means a quicker formation of larger water molecules aggregates in the film. This is due to the presence of more free volume in IMC10.

The generally lower Park's parameters for ISC10 compared to IMC10 evidenced the globally lower water vapor sorption, which is consistent with the higher crystallinity and larger crystal size for ISC10.



**Figure 2-13** Water vapor sorption isotherms of ISC10 and IMC10 films

**Table 2-7** Sorption parameters of Park's model

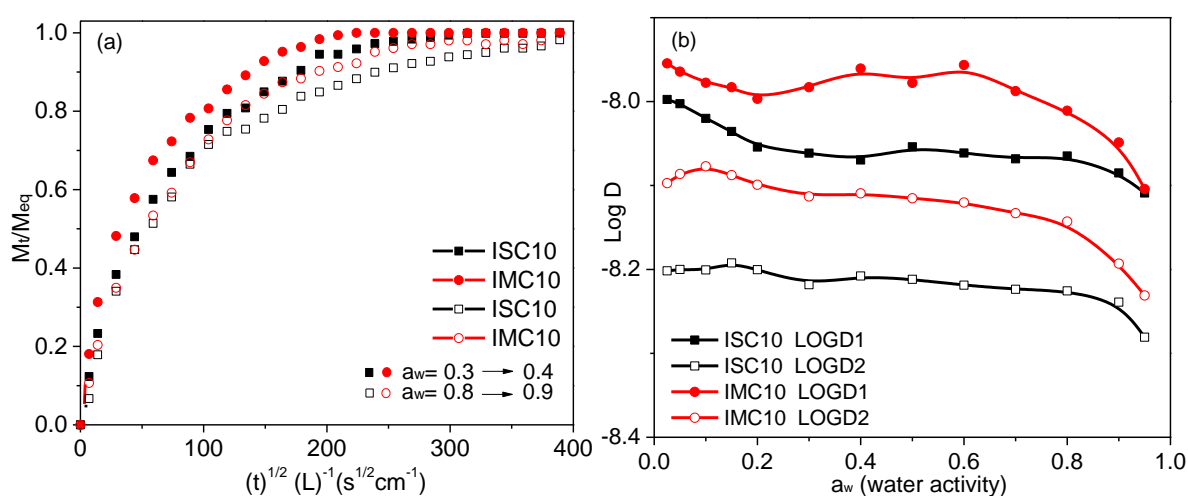
Polyester film	$A_L \times 10^3 \text{ (g/g)}$	$b_L$	$k_H \times 10^3 \text{ (g/g)}$	$K_a \times 10^3 \text{ (g/g)}$	$n_a$
ISC10	$0.10 \pm 0.01$	$0.30 \pm 0.04$	$5.0 \pm 0.1$	$0.40 \pm 0.01$	$2.0 \pm 0.4$
IMC10	$0.60 \pm 0.02$	$0.40 \pm 0.01$	$10.0 \pm 0.3$	$0.50 \pm 0.02$	$4.0 \pm 0.3$

$A_L$ , Langmuir's capacity constant;  $b_L$ , Langmuir's affinity constant;  $k_H$ , Henry's type solubility coefficient;  $K_a$ , equilibrium constant for clustering reaction;  $n_a$ , average number of water molecules per cluster.

The kinetics of water sorption were presented by the normalized gain of mass ( $M_t/M_{eq}$ ) vs reduced time ( $t^{1/2} L^{-1}$ ) for different vapor activities (Figure 2-14(a)). It is obvious that IMC10

showed a quicker dissolution-diffusion process of water vapor than ISC10, which agreed with the liquid water sorption. A slowing-down process was observed at high  $a_w$ . The detailed sorption kinetics data were interpreted in terms of the rate of diffusion of water molecules by considering  $t_r$  time to reach the equilibrium of sorption. For a short time (when  $M_t/M_{eq} < 0.2$ ), the slope ( $k_1$ ) of the linear regression of the curves  $(M_t/M_{eq})^2 = f(t - t_r)$  allowed the calculation of water diffusion coefficient  $D_1$ :  $D_1 = k_1 \pi L^2 / 16$ . For a longer time ( $M_t/M_{eq} > 0.7$ ), the slope  $k_2$  of the linear regression of the curve  $(\ln(1 - M_t/M_{eq})) = f(t)$  allowed the determination of the water diffusion coefficient  $D_2$ :  $D_2 = k_2 L^2 / \alpha_1$  ( $\alpha_1 = 2.40483$ ) [22]. The changes of  $D_1$  and  $D_2$  for IMC10 and ISC10 as a function of  $a_w$  were given in Figure 2-14(b). The variation of  $D_1$  and  $D_2$  values agrees with the isotherm. The  $D_1$  values appeared higher than  $D_2$  probably due to the aggregation of water molecules during the sorption, which makes them less mobile. It could be also the result of a structuring effect of water in the films during the water sorption, improving the cohesion between the chains by hydrogen bonds [21].

The  $D$  values were constant on large water activity range. This constant diffusion of water molecules inside the film was in accordance with the Henry's behavior previously observed on the isotherms. The decrease of  $D_1$  and  $D_2$  coefficients at high  $a_w$  ( $> 0.8$ ) could be explained by the largest aggregation of water molecules.  $D_1$  and  $D_2$  values were higher for IMC10 than for ISC10, which is consistent with the kinetics. The larger size of crystals and the higher crystallinity previously observed in ISC10 can explain this result. The low permeable crystal structures that stand in the way of water molecules increased the tortuosity of the diffusion path and consequently decreased  $D$  [14].



**Figure 2-14** Water vapor sorption of ISC10 and IMC10 films: (a) sorption kinetics (b) diffusion kinetics

### 2.3.8 Water vapor permeation

Water vapor permeation coefficients ( $P_{H_2O}$ ) of ISC10 and IMC10 for different water activities were given in Table 2-8. ISC10 film showed the lowest  $P_{H_2O}$  values whatever  $a_w$  (e.g.  $P_{H_2O} = 1.55 \text{ g}\cdot\text{m}^{-1}\cdot\text{d}^{-1}$  and  $P_{H_2O} = 2.81 \text{ g}\cdot\text{m}^{-1}\cdot\text{d}^{-1}$  at  $a_w \cong 0.5$  for ISC10 and IMC10, respectively). These results are in accordance with those previously obtained by sorption measurements. The lowest  $P_{H_2O}$  values obtained for ISC10 could be related to the lowest solubility coefficients  $S$  and diffusion coefficients  $D$  ( $P = D \times S$ ). Considering the same elemental composition of ISC10 and IMC10, it could be concluded that the better barrier for water molecules of ISC10 is due to its microstructure. ISC10 showed a comparable water vapor barrier referred to PLA (25 °C,  $a_w=0.5$ ,  $P_{H_2O} = 1.39\text{-}1.63 \text{ g}\cdot\text{m}^{-1}\cdot\text{d}^{-1}$ ) [22]. However, ISC10 was less barrier than PET (21 °C,  $a_w=0.4$ ,  $P_{H_2O} = 0.47 \text{ g}\cdot\text{m}^{-1}\cdot\text{d}^{-1}$ ) [23], which is probably due to its low glass transition temperature and the presence of polar “oxygen” atoms in the IS ring.

**Table 2-8** Water permeation coefficient ( $P_{H_2O}$ ) of ISC10 and IMC10 films at different water activities ( $a_w$ )

Polyester film	$a_w$	$P_{H_2O} (\text{g}\cdot\text{m}^{-1}\cdot\text{d}^{-1})$	$P_{H_2O} (\text{barrer})$
ISC10	0.25	$0.040 \pm 0.003$	$26\,000 \pm 400$
	0.48	$1.55 \pm 0.12$	$937\,000 \pm 800$
	0.55	$3.78 \pm 0.28$	$2\,300\,000 \pm 300$
	0.65	$5.10 \pm 0.41$	$3\,100\,000 \pm 700$
IMC10	0.19	$0.33 \pm 0.03$	$199\,700 \pm 100$
	0.49	$2.81 \pm 0.22$	$1\,690\,000 \pm 800$
	0.55	$5.61 \pm 0.45$	$3\,400\,000 \pm 100$
	0.60	$5.95 \pm 0.48$	$3\,600\,000 \pm 500$

1 barrer =  $10^{-10} \text{ cm}^3 \text{ STP}\cdot\text{cm}\cdot\text{cm}^{-2}\cdot\text{s}^{-1}\cdot\text{cmHg}^{-1}$ .

### 2.3.9 Gas permeation measurements

Table 2-9 presented the values of permeation ( $P$ ) and diffusion ( $D$ ) coefficients of  $\text{N}_2$ ,  $\text{O}_2$  and  $\text{CO}_2$  in ISC10 and IMC10 films.

**Table 2-9** Gas permeation ( $P$ ) and diffusion ( $D$ ) coefficients of  $N_2$ ,  $O_2$  and  $CO_2$  in ISC10 and IMC10 films

Polyester film	$N_2$		$O_2$		$CO_2$	
	$P$	$D \times 10^6$	$P$	$D \times 10^7$	$P$	$D \times 10^8$
ISC10	$0.09 \pm 0.006$	$1.26 \pm 0.09$	$0.26 \pm 0.02$	$2.78 \pm 0.19$	$1.32 \pm 0.09$	$1.98 \pm 0.14$
IMC10	$0.18 \pm 0.01$	$2.50 \pm 0.17$	$0.46 \pm 0.03$	$3.86 \pm 0.27$	$2.04 \pm 0.14$	$2.54 \pm 0.18$

$P$  expressed in barrer ( $1 \text{ barrer} = 10^{-10} \text{ cm}^3 \text{ STP} \cdot \text{cm} \cdot \text{cm}^{-2} \cdot \text{s}^{-1} \cdot \text{cmHg}^{-1}$ ),  $D$  expressed in  $\text{cm}^2 \cdot \text{s}^{-1}$ .

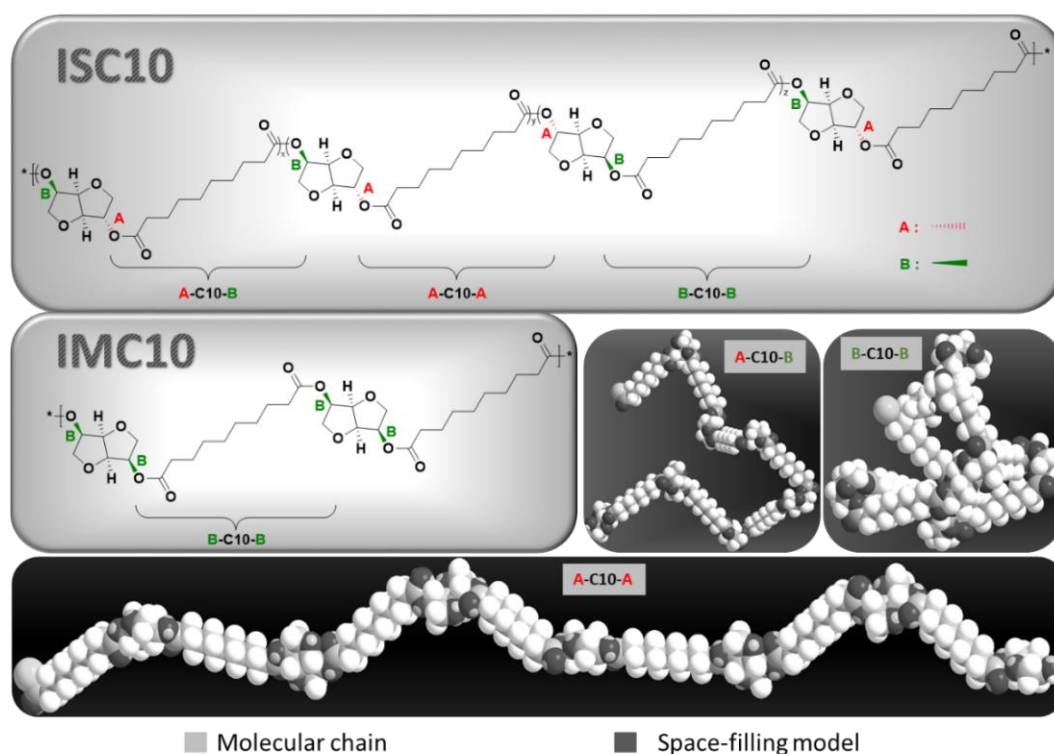
It could be easily observed that both ISC10 and IMC10 showed low gas permeability, which is probably due to the presence of crystals and liquid crystal regions, which are strongly barrier to gases [24–26]. ISC10 showed higher barrier properties than IMC10 due to its higher crystallinity, as previously explained for water. The permeability coefficients  $P$  of ISC10 for  $N_2$ ,  $O_2$  and  $CO_2$  were 0.09, 0.26 and 1.32 barrer, respectively, which is similar to PLA ( $P_{O_2}$ = 0.16 barrer,  $P_{CO_2}$ = 1.27 barrer) [27]. ISC10 and IMC10 appeared both more barrier to gases than the commonly used food packaging material PE ( $P_{O_2}$ =3.2 barrer,  $P_{CO_2}$ =11.7 barrer) [28] but less barrier than PET ( $P_{N_2}$  = 0.008 barrer,  $P_{O_2}$ = 0.03 barrer,  $P_{CO_2}$ = 0.15 barrer) [29] and PEF ( $P_{O_2}$ = 0.004~0.006 barrer,  $P_{CO_2}$ = 0.01~0.02 barrer) [30].

To optimize a packaging, the selectivity between  $CO_2$  and  $O_2$  ( $\alpha_{CO_2/O_2}$ ) should be controlled because the respiration rate of fruits and vegetables should be slowed down [31]. Thus, it is necessary to limit the oxygen content while increasing the concentration of carbon dioxide to keep the vegetables fresh as long as possible [32]. However, the packaging must be a little permeable to oxygen because a too low concentration of oxygen triggers an anaerobic breathing process which induces bad taste and bad odors to vegetables, and then decreases their shelf-life. The selectivity coefficient  $\alpha_{CO_2/O_2}$  for ISC10 ( $\alpha_{CO_2/O_2}$ = 5.1) was comparable to petroleum-based common food packaging polyester PET ( $\alpha_{CO_2/O_2}$ = 5.0) [29], but higher than for IMC10 ( $\alpha_{CO_2/O_2}$ = 4.4), bio-based potential food packaging polyester PLA ( $\alpha_{CO_2/O_2}$ = 1.0~2.0) [33] and PEF ( $\alpha_{CO_2/O_2}$   $\approx$  3) [30], which indicated that ISC10 is more favorable for the fruits and vegetables preservation.

The diffusion coefficient  $D$  was lower for ISC10 than for IMC10 whatever the gas (Table 2-9). These results were consistent with those obtained with water: the higher crystallinity and bigger crystals in ISC10 increased the tortuosity of the diffusion pathway, and also meant less free volume and less exposure of oxygen atoms in the ISC10 film, which could explain the lowest solubility to  $O_2$  and  $CO_2$  gases ( $S=P/D$ ).

### **2.3.10 Relationship between microstructure and permeation properties**

As discussed before, the barrier properties of ISC10 and IMC10 may result not only from their semi-crystalline nature but also from the presence of liquid crystal regions, since these polymers contain rigid moieties (IS and IM) alternating with flexible PE-like sequences, which have a deep impact on barrier properties. The difference in mechanical and barrier properties for ISC10 and IMC10 films mainly depends on their crystal structures and crystallinity. The difference of crystallization ability between ISC10 and IMC10 can be attributed to the chain orientation degree as shown in Figure 2-15, where A refers to exo-links and B refers to endo-links. It is obvious that ISC10 repetition unit contains three kinds of links: exo-endo (A-C10-B), exo-exo (A-C10-A) and endo-endo (B-C10-B), while IMC10 repetition unit contains only endo-endo (B-C10-B) links. As predicted by Chemdraw<sup>®</sup> Software, IMC10 has more regular bond connections in a short range that can crystallize, but the highly curved chains make it hard to crystallize by chain-chain packing. On the contrary, the exo-links in ISC10 induces a more oriented chain which can readily crystallize and give a more dense microstructure [34,35]: the more the exo-exo links are repeated in the chain the easier the chains crystallize by chain-chain packing. This difference in chain orientation could explain why ISC10 showed better barrier properties than IMC10.



**Figure 2-15** Polymer chains (grey) and the corresponding space-filling models (black) predicted by Chemdraw® Software

## 2.4 Conclusion

Six aliphatic bio-based polyesters including isosorbide and isomannide were synthesized by bulk polycondensation method. The chain length of the diacid units influenced the thermal degradation and glass transition temperature as well as the crystallization. Only polyesters containing the most CH<sub>2</sub> units (ISC10 and IMC10) afforded flexible films. Crystalline structures, with the presence of liquid crystal phase, were evidenced in both ISC10 and IMC10. The endo/exo stereoisomerism of isohexide units (IS or IM) slightly influenced the thermal degradation and glass transition temperature, but influenced the crystallization properties. The exo-exo stereoscopic configurations in polyesters were more inclined to crystallize than the endo-endo configurations. Thus, polyesters prepared from isosorbide showed better tensile stress and better barrier properties to water and gases than isomannide polyesters. Furthermore, ISC10 polyester showed more toughness and similar barrier properties for both water and gases compared to PLA, and was even more barrier to gases than the common food packaging material PE. Even if the barrier properties of ISC10 were lower than PET and PEF, the selectivity to CO<sub>2</sub> and O<sub>2</sub> was more favorable for fruits and vegetables preservation.



## References

- [1] M. Okada, Y. Okada, A. Tao, K. Aoi, Biodegradable polymers based on renewable resources: polyesters composed of 1,4 : 3,6-dianhydrohexitol and aliphatic dicarboxylic acid units, *J. Appl. Polym. Sci.* 62 (1996) 2257–2265.
- [2] M. Okada, K. Tsunoda, K. Tachikawa, K. Aoi, Biodegradable polymers based on renewable resources. IV. enzymatic degradation of polyesters composed of 1,4:3.6-dianhydro-D-glucitol and aliphatic dicarboxylic acid moieties, *J. Appl. Polym. Sci.* 77 (2000) 338–346.
- [3] F. Fenouillot, A. Rousseau, G. Colomines, R. Saint-Loup, J.P. Pascault, Polymers from renewable 1,4:3,6-dianhydrohexitols (isosorbide, isomannide and isoidide): a review, *Prog. Polym. Sci.* 35 (2010) 578–622.
- [4] H. Marubayashi, T. Ushio, S. Nojima, Crystallization of polyesters composed of isohexides and aliphatic dicarboxylic acids: effects of isohexide stereoisomerism and dicarboxylic acid chain length, *Polym. Degrad. Stab.* 146 (2017) 174–183.
- [5] H.S. Park, M.S. Gong, J.C. Knowles, Synthesis and biocompatibility properties of polyester containing various diacid based on isosorbide, *J. Biomater. Appl.* 27 (2012) 99–109.
- [6] Q. Ding, D. Jehnichen, M. Göbel, M. Soccio, N. Lotti, D. Cavallo, R. Androsch, Smectic liquid crystal Schlieren texture in rapidly cooled poly(butylene naphthalate), *Eur. Polym. J.* 101 (2018) 90–95.
- [7] J. Maiz, G. Liu, F. Ruipérez, N. Delbosc, O. Coulembier, D. Wang, A.J. Müller, How cyclic chain topology can reduce the crystallization rate of poly(3-hexylthiophene) and promote the formation of liquid crystalline phases in comparison with linear analogue chains, *J. Mater. Chem. C.* 7 (2019) 6548–6558.
- [8] Q. Ding, M. Soccio, N. Lotti, N. Mahmood, D. Cavallo, R. Androsch, Crystallization of poly(butylene 2,6-naphthalate) containing diethylene 2,6-naphthalate constitutional defects, *Polym. Cryst.* 2 (2019).
- [9] S. Farah, D.G. Anderson, R. Langer, Physical and mechanical properties of PLA, and their functions in widespread applications - a comprehensive review, *Adv. Drug Deliv. Rev.* 107 (2016) 367–392.
- [10] J.Y. Kim, Y. Lee, D.Y. Lim, Plasma-modified polyethylene membrane as a separator for lithium-ion polymer battery, *Electrochim. Acta.* 54 (2009) 3714–3719.
- [11] S. Thanakkasaranee, D. Kim, J. Seo, Preparation and characterization of polypropylene/sodium propionate (PP/SP) composite films for bread packaging application, *Packag. Technol. Sci.* 31 (2018) 221–231.
- [12] K. Gotoh, A. Yasukawa, Y. Kobayashi, Wettability characteristics of poly(ethylene terephthalate) films treated by atmospheric pressure plasma and ultraviolet excimer light, *Polym. J.* 43 (2011) 545–551.
- [13] E. Fortunati, F. Luzi, D. Puglia, F. Dominici, C. Santulli, J.M. Kenny, L. Torre, Investigation of thermo-mechanical, chemical and degradative properties of PLA-

- limonene films reinforced with cellulose nanocrystals extracted from *Phormium tenax* leaves, *Eur. Polym. J.* 56 (2014) 77–91.
- [14] J. Trifol, D. Plackett, P. Szabo, A.E. Dugaard, M. Giacinti Baschetti, Effect of crystallinity on water vapor sorption, diffusion, and permeation of PLA-based nanocomposites, *ACS Omega*. 5 (2020) 15362–15369.
- [15] N. Follain, S. Belbekhouche, J. Bras, G. Siqueira, S. Marais, A. Dufresne, Water transport properties of bio-nanocomposites reinforced by *Luffa cylindrica* cellulose nanocrystals, *J. Memb. Sci.* 427 (2013) 218–229.
- [16] N. Follain, S. Roualdes, S. Marais, J. Frugier, M. Reinholdt, J. Durand, Water transport properties of plasma-modified commercial anion-exchange membrane for solid alkaline fuel cells, *J. Phys. Chem. C*. 116 (2012) 8510–8522.
- [17] V. Detallante, D. Langevin, C. Chappey, M. Métayer, R. Mercier, M. Pinéri, Water vapor sorption in naphthalenic sulfonated polyimide membranes, *J. Memb. Sci.* 190 (2001) 227–241.
- [18] S. Marais, Q.T. Nguyen, D. Langevin, M. Métayer, Transport of water and gases through EVA copolymer films, EVA 70/PVC, and EVA70/PVC/gluten blends, *Macromol. Symp.* 175 (2001) 329–348.
- [19] S. Alix, E. Philippe, A. Bessadok, L. Lebrun, C. Morvan, S. Marais, Effect of chemical treatments on water sorption and mechanical properties of flax fibres, *Bioresour. Technol.* 100 (2009) 4742–4749.
- [20] S. Alix, S. Marais, C. Morvan, L. Lebrun, Biocomposite materials from flax plants: Preparation and properties, *Compos. Part A Appl. Sci. Manuf.* 39 (2008) 1793–1801.
- [21] S. Belbekhouche, J. Bras, G. Siqueira, C. Chappey, L. Lebrun, B. Khelifi, S. Marais, A. Dufresne, Water sorption behavior and gas barrier properties of cellulose whiskers and microfibrils films, *Carbohydr. Polym.* 83 (2011) 1740–1748.
- [22] R.A. Auras, B. Harte, S. Selke, R. Hernandez, Mechanical, physical, and barrier properties of poly(lactide) films, *J. Plast. Film Sheeting*. 19 (2003) 123–135.
- [23] D. Cava, E. Giménez, R. Gavara, J.M. Lagaron, Comparative performance and barrier properties of biodegradable thermoplastics and nanobiocomposites versus PET for food packaging applications, *J. Plast. Film Sheeting*. 22 (2006) 265–274.
- [24] D.H. Weinkauff, D.R. Paul, Gas transport properties of thermotropic liquid-crystalline copolyesters. II. The effects of copolymer composition, *J. Polym. Sci. Part B Polym. Phys.* 30 (1992) 837–849.
- [25] T. Kajiyama, Y. NAagata, E. Maemura, M. Takayanag, Motowo TAKAYANAG, Molecular motion-permeability relationships in polycarbonate/liquid crystal (EBBA) composites membrane, *Chem. Lett.* (1979) 679–682.
- [26] J. Hoshikawa, E. Seiko, K. Kabushiki, Liquid crystal display with barrier layer to reduce permeability, US4709991A, 1986.
- [27] M.A. Ortenzi, L. Basilissi, H. Farina, G. Di Silvestro, L. Piergiovanni, E. Mascheroni, Evaluation of crystallinity and gas barrier properties of films obtained from PLA

- nanocomposites synthesized via “in situ” polymerization of L-lactide with silane-modified nanosilica and montmorillonite, *Eur. Polym. J.* 66 (2015) 478–491.
- [28] M. Gholizadeh, J. Razavi, S.A. Mousavi, Gas permeability measurement in polyethylene and its copolymer films, *Mater. Des.* 28 (2007) 2528–2532.
- [29] N. Gontard, *Les emballages actifs*, Tec et Doc, Paris, 2000: pp.72.
- [30] S.K. Burgess, G.B. Wenz, R.M. Kriegel, W.J. Koros, Penetrant transport in semicrystalline poly(ethylene furanoate), *Polymer*. 98 (2016) 305–310.
- [31] P.M. Budd, N.B. McKeown, Highly permeable polymers for gas separation membranes, *Polym. Chem.* 1 (2010) 63–68.
- [32] B. Bideau, J. Bras, N. Adoui, E. Loranger, C. Daneault, Polypyrrole/nanocellulose composite for food preservation: barrier and antioxidant characterization, *Food Packag. Shelf Life*. 12 (2017) 1–8.
- [33] L. Genovese, M. Soccio, N. Lotti, M. Gazzano, V. Siracusa, E. Salatelli, F. Balestra, A. Munari, Design of biobased PLLA triblock copolymers for sustainable food packaging: Thermo-mechanical properties, gas barrier ability and compostability, *Eur. Polym. J.* 95 (2017) 289–303.
- [34] V. Morillon, F. Debeaufort, G. Blond, M. Capelle, A. Voilley, Factors affecting the moisture permeability of lipid-based edible films: A review, *Crit. Rev. Food Sci. Nutr.* 42 (2002) 67–89.
- [35] Q. Liu, X. Sun, H. Li, S. Yan, Orientation-induced crystallization of isotactic polypropylene, *Polymer*. 54 (2013) 4404–4421.

---

## Chapter 3

∞ 2,6-Pyridinedicarbonyl based polyesters: synthesis, thermal, mechanical and permeation properties ∞

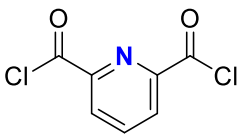
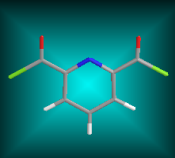

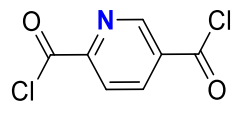
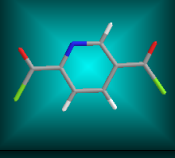
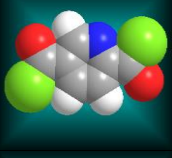
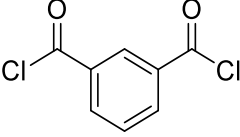
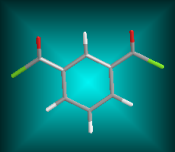

---



As stated in Chapter 1, 2,4-, 2,5- and 2,6-pyridinedicarboxylic acids (PDA24, PDA25, PDA26) are derived from biomass and present aromatic rigid structures as terephthalic acid (TPA), isophthalic acid (IPA) and 2,5-furandicarboxylic acid (2,5-FDCA), thus of interest for preparing bio-based polyesters. Pellis *et al.* [1] synthesized a series of polyesters based on these pyridinedicarboxylic monomers and interestingly found that the ones based on PDA25 and PDA26 were semi-crystalline. We insight that these polyesters could be useful for food packaging applications, however, no literature was referenced. Thus, it is attracting to investigate their thermal, mechanical and permeation properties, which are crucial for food packaging applications. Considering the melting and thermal decomposition of the acid monomers proceed simultaneously (242-250 °C) and the molar masses obtained by transesterification reaction using the corresponding diesters in the presence of a catalyst (Pellis method) are too low, we decided to use acid dichlorides (2,5-pyridinedicarbonyl dichloride (PDD25) and 2,6-pyridinedicarbonyl dichloride (PDD26)) for our syntheses.

In this Chapter, due to the extremely high commercial price of PDD25 (up to 500 €/g, or 80 times higher than PDD26), a series of polyesters based on PDD26 and linear aliphatic diols were first synthesized. The as mentioned diols are ethylene glycol (EG), butanediol (BD), hexanediol (HD) and decanediol (DD), and the corresponding polyesters are named PDD26-EG, PDD26-BD, PDD26-HD, and PDD26-DD. Then, the best results were compared, in terms of thermal, mechanical and permeation properties, with the polymers synthesized from PDD25 (obtained from PDA25) or isophthaloyl chloride (IPC), which have similar molecular structures (Table 3-1).

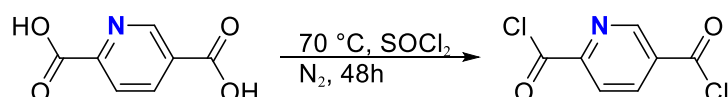
**Table 3-1** Chemical structure of PDD26, PDD25 and IPC

Name	2D structure	3D structure model	
		Stick	Space filling
PDD26			
PDD25			
IPC			

### 3.1 Synthesis

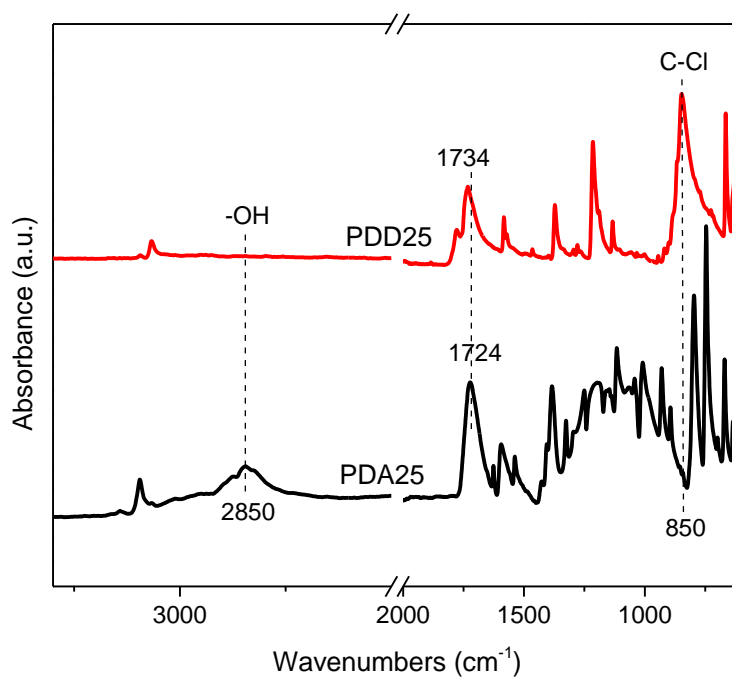
#### 3.1.1 Synthesis of monomer

The high commercial price of PDD25 made us decide to synthesize it from the much cheaper acid analog PDA25 (Scheme 3-1). Details were described in Annex 1.4.1.



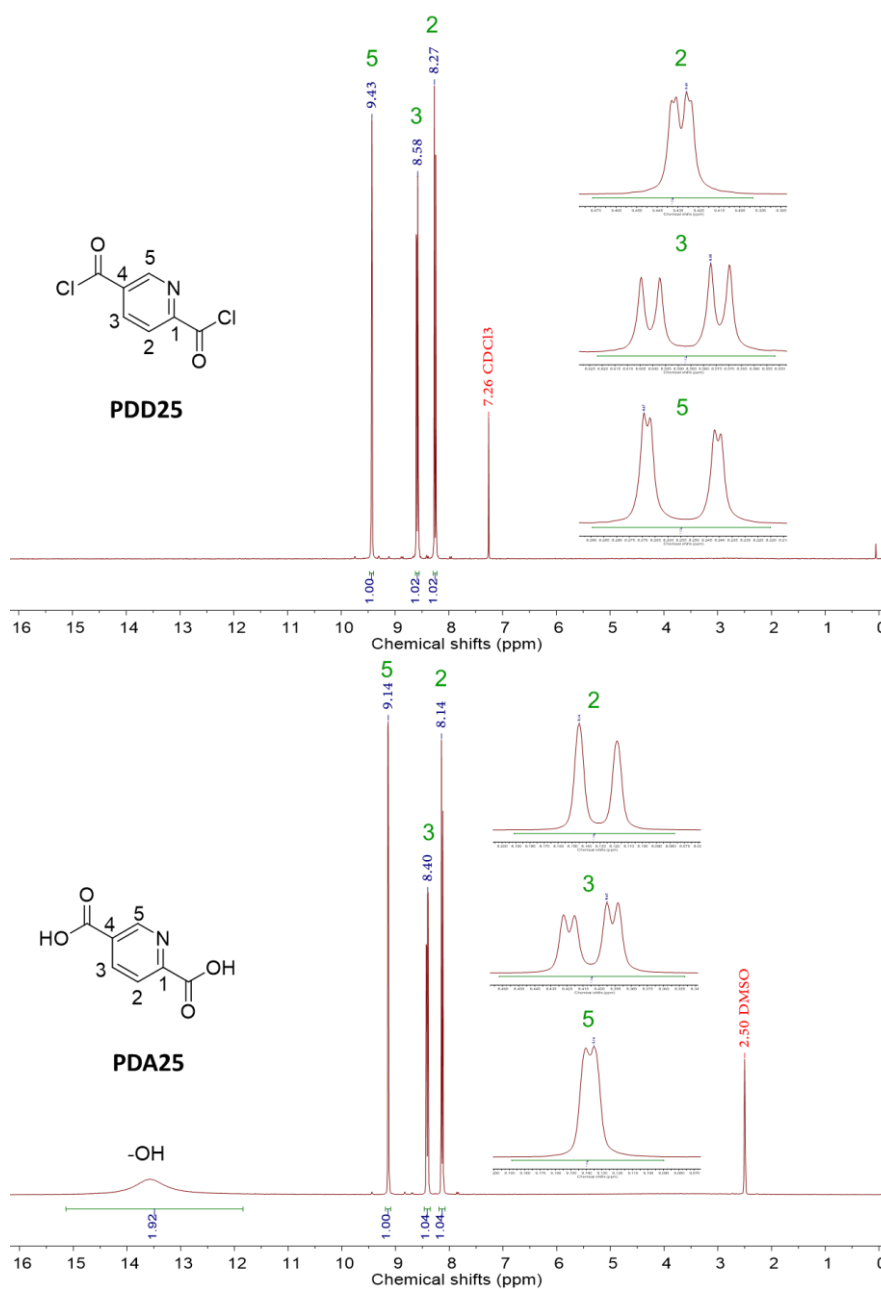
**Scheme 3-1** Synthesis of PDD25 from PDA25

The successful synthesis of PDD25 was confirmed first by FTIR as shown in Figure 3-1. On the one hand, compared to PDA25, the OH signal at  $2850\text{ cm}^{-1}$  disappeared while the Cl signal at  $850\text{ cm}^{-1}$  appeared on PDD25 spectrum. On the other hand, the electron-withdrawing characteristic of the Cl group resulted in a carbonyl peak shifting to a higher wavenumber ( $1734\text{ cm}^{-1}$ ) for acid dichloride compared to diacid ( $1724\text{ cm}^{-1}$ ), which has already been observed by Isfahani *et al.* [2].



**Figure 3-1** FTIR spectra of PDD25 and PDA25

The chemical structure of PDD25 was further determined by  $^1\text{H}$  MNR as presented in Figure 3-3. The proton signals on the pyridine ring at position C2, C3 and C5 for PDD25 appeared at 8.2-8.3 (1H), 8.5-8.6 (1H) and 9.4-9.5 (1H) ppm, respectively, which matched the three proton signals on PDA25 at 8.1-8.2 (1H), 8.3-8.5 (1H) and 9.1-9.2 (1H) ppm, correspondingly. The OH signal observed with PDA25 disappeared on PDD25. This information is consistent with the FTIR results and further confirmed the successful synthesis of PDD25. However, some additional signals on PDD25 spectrum seemed to correspond to the impurities present in commercial PDA25.

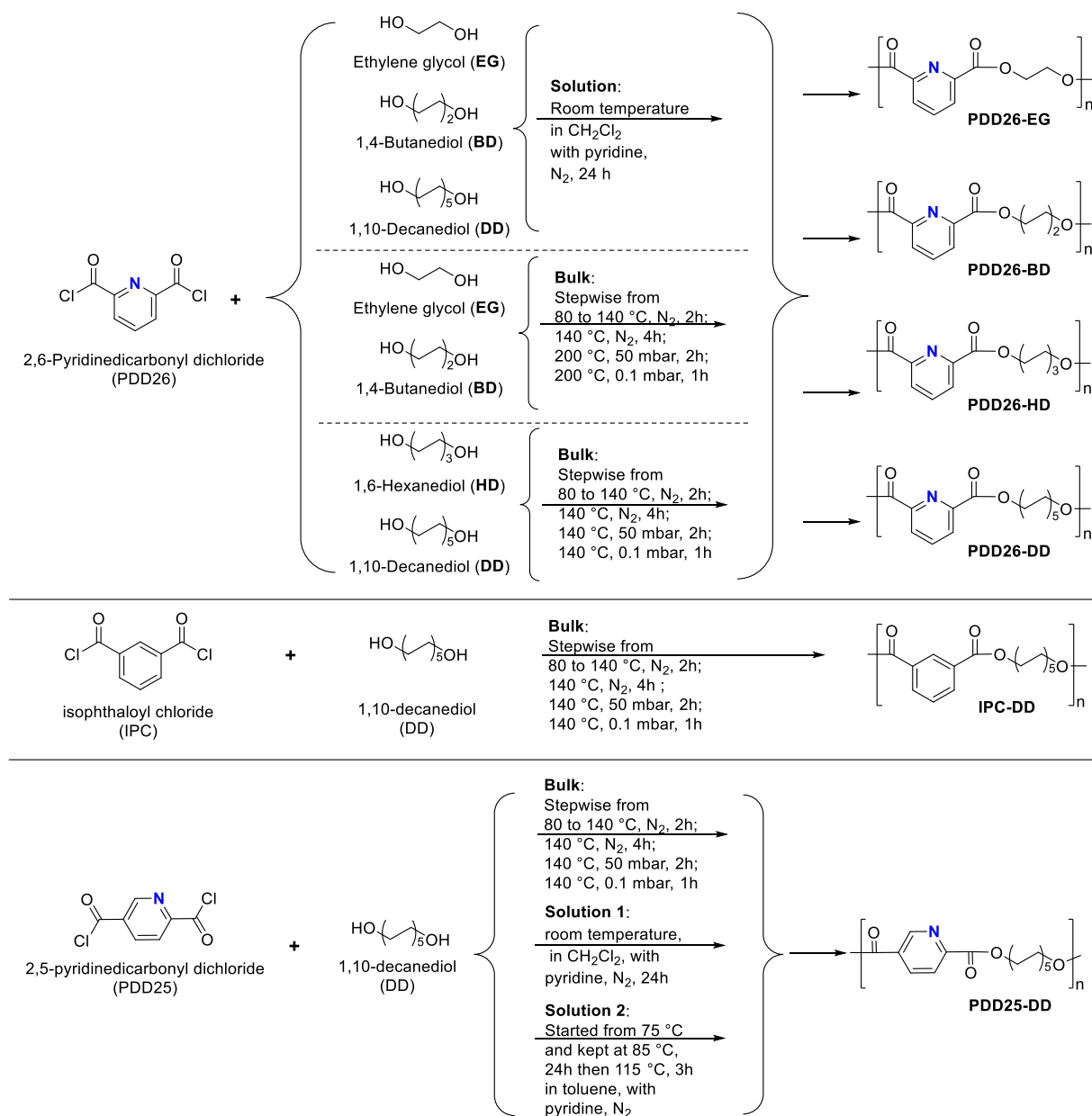


**Figure 3-2**  $^1\text{H}$  NMR spectra of PDD25 and PDA25



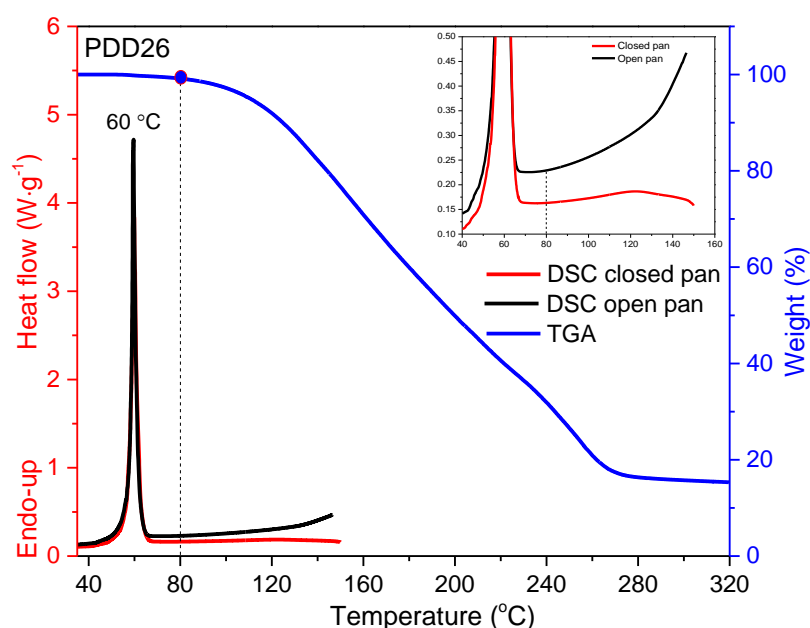
## 3.1.2 Synthesis of polyesters

All polyesters have been synthesized as shown in Scheme 3-2 and detailed procedures, inspired by the literature [3–5], can be referred to Annex 1.2, 1.3, and 1.4.



Scheme 3-2 Synthesis of polyesters

Considering the poor thermal stability of PDD26 (Figure 3-5), reactions in  $\text{CH}_2\text{Cl}_2$  solution with pyridine (as HCl capture) under room temperature were first tried for PDD26-EG, PDD26-BD and PDD26-DD. However, only low molar masses were obtained ( $\overline{M}_n = 1\,900$ ,  $2\,800$  and  $7\,500\text{ g}\cdot\text{mol}^{-1}$  for PDD26-EG, PDD26-BD and PDD26-DD, respectively), their corresponding SEC chromatograms were given in Annex 4.



**Figure 3-3** Thermal stability of PDD26

Then non-solvent (bulk) method was tried according to the established conditions in Chapter 2 (Okada method), but starting at  $80\text{ }^{\circ}\text{C}$  (above which continuous evaporation of PDD26 was observed by DSC and TGA in Figure 3-3) and ending at a high enough temperature to melt the targeted polymers. The bulk method involved not only the above three polyesters but also PDD26-HD, and the best results obtained were gathered in Table 3-2 (corresponding chromatograms in Annex 4). Nevertheless, except for PDD26-DD which gave a satisfying high molar mass ( $\overline{M}_n = 24\,500\text{ g}\cdot\text{mol}^{-1}$ ), no better results were obtained:

- PDD26-EG and PDD26-HD afforded low molar masses ( $\overline{M}_n = 2\,400$  and  $5\,100\text{ g}\cdot\text{mol}^{-1}$ , respectively),
- PDD26-BD was insoluble in  $\text{CH}_2\text{Cl}_2$ , the mobile phase of SEC, thus no molar mass could be obtained, so the value obtained by the solution method in  $\text{CH}_2\text{Cl}_2$  was indicated.

Furthermore, PDD26-EG (solution and bulk methods) and PDD26-BD exhibited complex chromatograms by SEC (Annex 4), with two distinct populations: these syntheses gave several different chains, possibly linear together with cyclic structures [1,6].

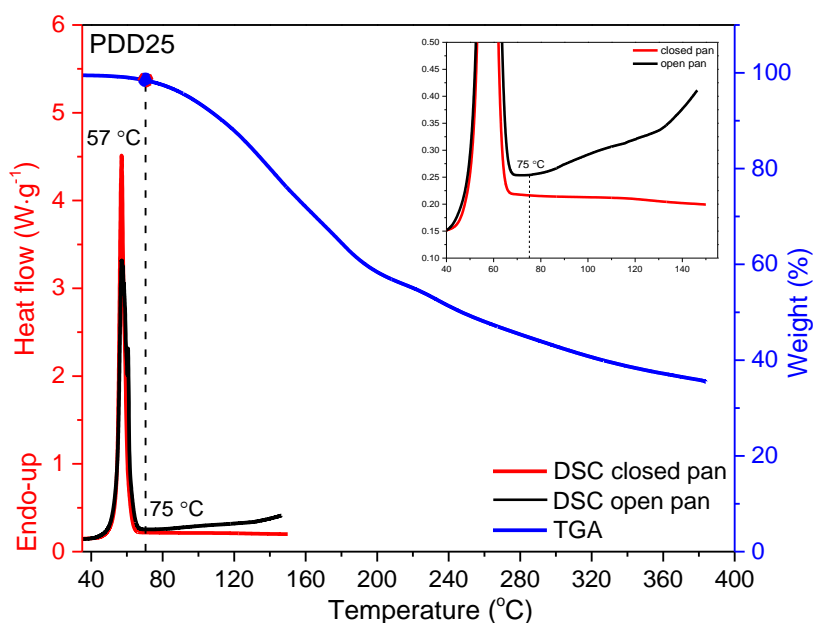
Finally, the yields of PDD26-EG, PDD26-BD and PDD26-HD were lower the shorter the diol, perhaps due to the low molar masses of polymers coupled with the higher polarity of the shorter diols, which could result in a higher solubility in methanol during precipitation and thus decreased the yield in precipitated polymer [1].

**Table 3-2** Molar masses of polyesters and yields of bulk syntheses

Polyester	$M$ of repeating unit ( $\text{g}\cdot\text{mol}^{-1}$ )	$\overline{DP}_n$	$\overline{M}_n^{(1)}$ ( $\text{g}\cdot\text{mol}^{-1}$ )	$\overline{M}_w^{(1)}$ ( $\text{g}\cdot\text{mol}^{-1}$ )	$\overline{D}^{(2)}$	Yield <sup>(3)</sup> (%)
PDD26-EG	193.16	24	2 400	3 600	1.50	38
		4	300	310	1.02	
PDD26-BD*	221.21	26	2 800	4 900	1.76	61
		4	390	390	1.00	
PDD26-HD	249.26	40	5 100	9 700	1.90	73
PDD26-DD	305.37	160	24 500	51 600	2.11	92
PDD25-DD <sup>+</sup>	305.37	168	25 700	53 400	2.08	90
IPC-DD	304.38	170	25 900	55 700	2.15	93

$\overline{DP}_n$ , degree of polymerization calculated from  $\overline{M}_n$ ; <sup>(1)</sup> SEC conducted in  $\text{CH}_2\text{Cl}_2$  with PMMA standards; <sup>(2)</sup> dispersity; <sup>(3)</sup> in precipitated polymer; \* product obtained from solution method; + product obtained from toluene method.

Taking these results into account, the conditions used for PDD26-DD in bulk were used to synthesize IPC-DD and PDD25-DD. A high molar mass was obtained for IPC-DD ( $\overline{M}_n = 25\,900\text{ g}\cdot\text{mol}^{-1}$ ), however, PDD25-DD only afforded oligomers ( $\overline{M}_n = 3\,500\text{ g}\cdot\text{mol}^{-1}$ ). This low molar mass may be due to the evaporation of PDD25 evidenced by DSC and TGA (Figure 3-6). Thus, the reaction was conducted in  $\text{CH}_2\text{Cl}_2$  with pyridine under room temperature, but still a low molar mass ( $\overline{M}_n = 6\,400\text{ g}\cdot\text{mol}^{-1}$ ) was obtained. Finally, a high molar mass ( $\overline{M}_n = 25\,700\text{ g}\cdot\text{mol}^{-1}$ ) was achieved when toluene was used as solvent at  $75\text{ }^\circ\text{C}$  (in the presence of pyridine). Thus, these later conditions were kept for PDD25-DD.



**Figure 3-4** Thermal stability of PDD25

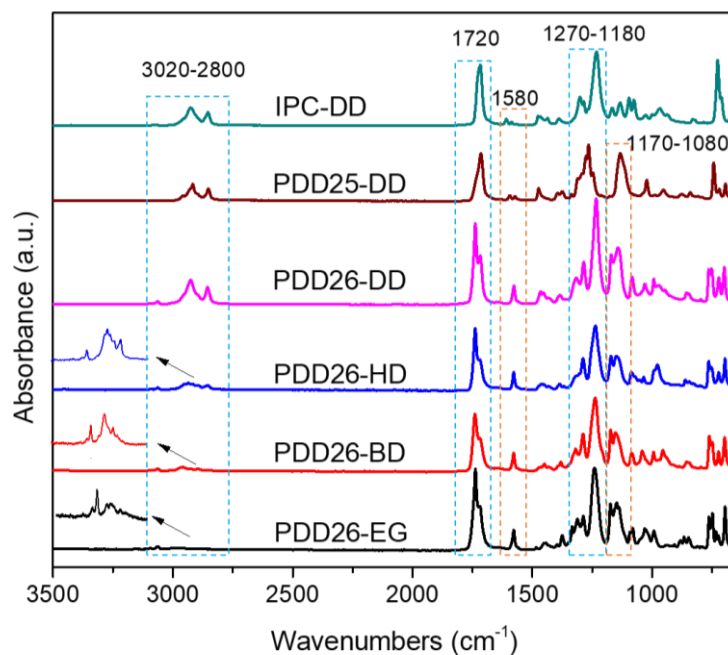
To conclude, the polyesters produced with DD, whatever the aromatic moiety, were obtained with high molar masses and yields, so it seemed the molar masses and yields were much more affected by the nature of the incorporated diol [7].

## 3.2 Characterization of polyesters

### 3.2.1 Structures

#### 3.2.1.1 FTIR analysis

The chemical structures of the obtained polyesters were assessed by FTIR (Figure 3-5). The successful synthesis was first evidenced by the presence of C=O and C-O stretching signals at 1720 and 1270-1180 cm<sup>-1</sup>, respectively, and further confirmed by the occurrence of CH<sub>2</sub> (3020-2800 cm<sup>-1</sup>), C=C (1580 cm<sup>-1</sup>) and C-N (1170-1080 cm<sup>-1</sup>) stretching signals, which corresponded to the alkyl chain of the diol component and the aromatic rings (benzene and pyridine rings).



**Figure 3-5** FTIR spectra of polyesters

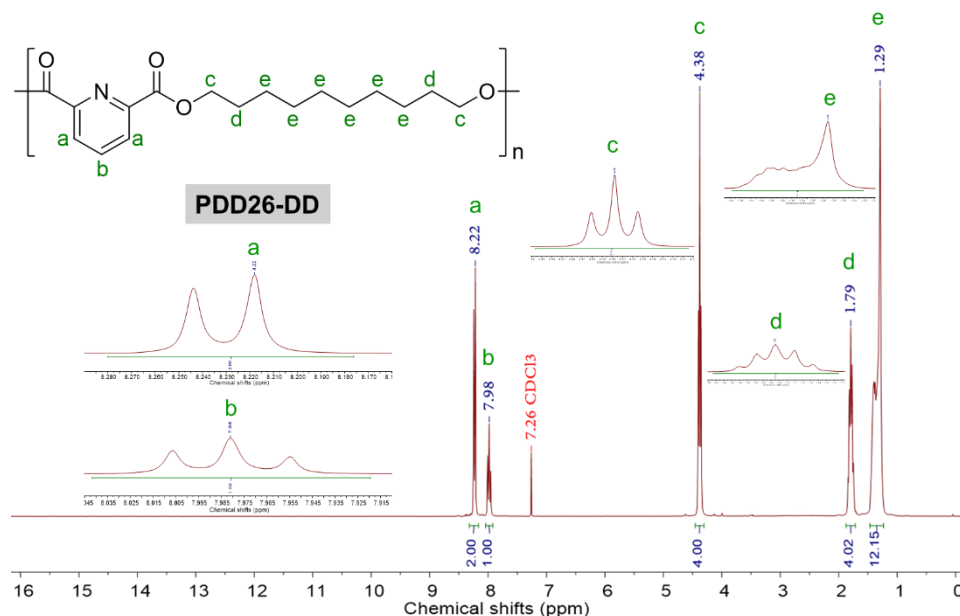
### 3.2.1.2 $^1\text{H}$ NMR analysis

The chemical structures were also investigated by  $^1\text{H}$  NMR. Due to the similarity of chemical structures, but also to avoid redundant explanations, the  $^1\text{H}$  NMR spectrum of PDD26-DD (Figure 3-6) was shown as an example. The other spectra, except PDD26-EG and PDD26-BD which will be discussed later, were listed in Annex 5, and all the corresponding chemical shifts were summarized in Table 3-3.

**Table 3-3**  $^1\text{H}$  NMR chemical shifts of the prepared polyesters

Polyester	$^1\text{H}$ NMR shifts in $\text{CDCl}_3$ (ppm)
PDD26-EG	8.25 (m, 2H), 8.04 (m, 1H), 4.77 (m, 3.7H)
PDD26-BD	8.23 (m, 2H), 8.00 (m, 1H), 4.48 (s, 3.7H), 1.99 (m, 3.7H)
PDD26-HD	8.23 (d, 2H), 7.99 (dd, 1H), 4.41 (t, 4H), 1.85 (m, 4H), 1.51 (m, 4H)
PDD26-DD	8.22 (d, 2H), 7.98 (t, 1H), 4.38 (t, 4H), 1.79 (m, 4H), 1.29 (m, 12H)
PDD25-DD	9.30 (d, 1H), 8.41 (dd, 1H), 8.19 (d, 1H), 4.41 (p, 4H), 1.79 (m, 5H), 1.31 (m, 14H)
IPC-DD	8.67 (t, 1H), 8.20 (dd, 2H), 7.52 (t, 1H), 4.33 (t, 4H), 1.77 (m, 4H), 1.32 (m, 12H)

As observed, the signals at 8.22 and 7.98 ppm corresponded to the protons on the pyridine ring, identified by letters “a” and “b”, respectively. The lower chemical shifts at 4.38, 1.79 and 1.29 ppm related to the protons on the alkyl chain with labels “c”, “d” and “e” accordingly. All the integrations were consistent with the formation of the targeted polyesters.

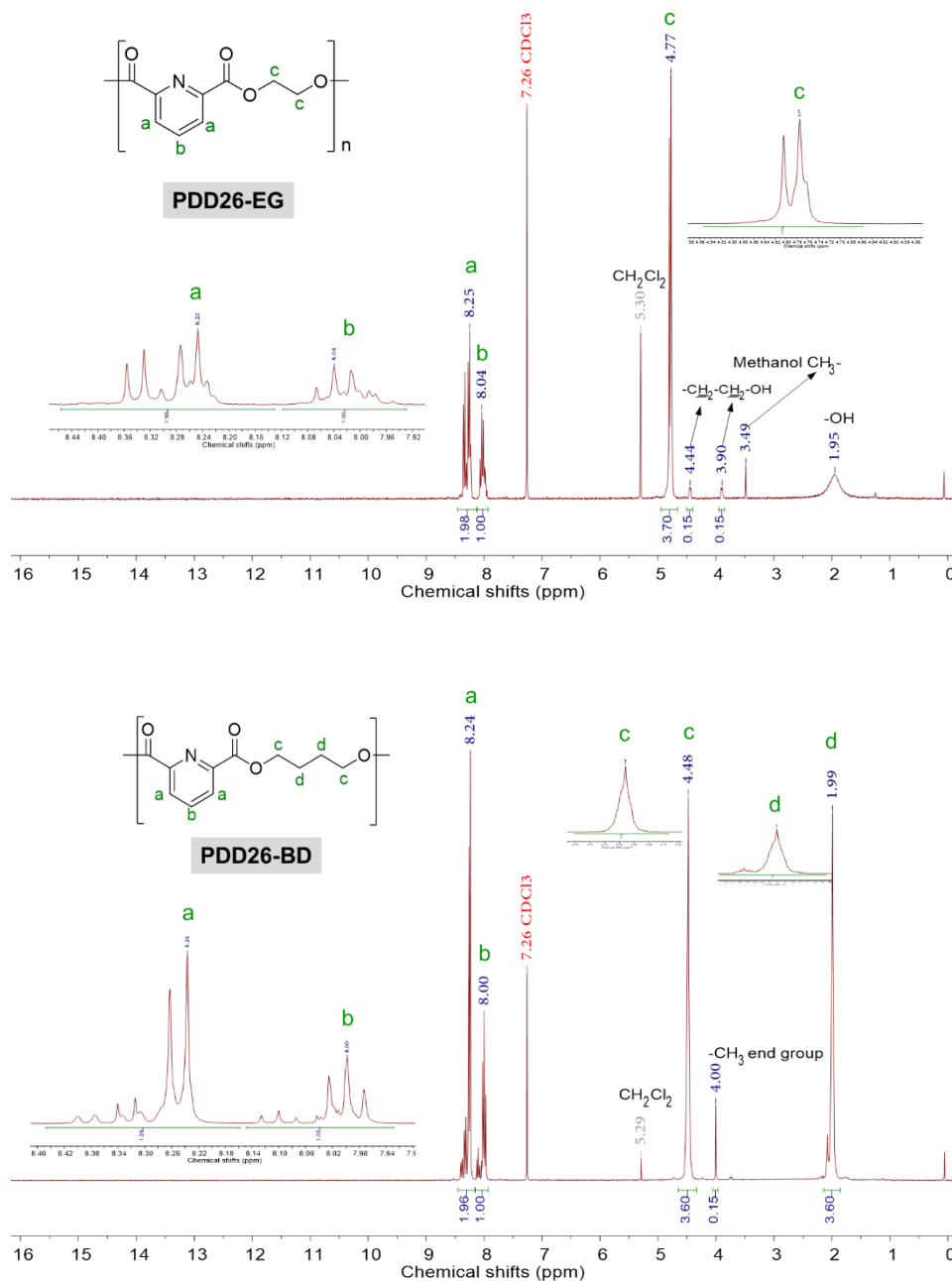


**Figure 3-6**  $^1\text{H}$  NMR spectrum of PDD26-DD

As mentioned before, PDD26-EG and PDD26-BD exhibited low molar masses and complex chromatograms by SEC, so we focused on their  $^1\text{H}$  NMR spectra (Figure 3-7).

As seen for PDD26-EG, excepted the protons at 8.25, 8.04 and 4.77 ppm, which corresponded to the repeating unit, there also existed five additional proton signals at 5.30, 4.44, 3.90, 3.49 and 1.95 ppm. Considering the polyester was recovered by dissolving in dichloromethane ( $\text{CH}_2\text{Cl}_2$ ) then precipitating in methanol ( $\text{CH}_3\text{OH}$ ), the signals at 5.30, 3.49 and 1.95 (partly) ppm could be reasonably attributed to solvent residues. The other peaks at 4.44, 3.90 and 1.95 (partly) ppm could correspond to  $-\text{CH}_2\text{CH}_2\text{OH}$  chain ends. Considering the integrations of both  $\text{CH}_2$  in these end groups, and those in the repeating units were 0.15 and 3.7, respectively, the molar mass of PDD26-EG could be calculated as follows:  $\overline{M}_n = 193.16 \times \frac{4 \times 3.7}{4 \times 0.15} = 4\,800 \text{ g} \cdot \text{mol}^{-1}$ . This result was very different than the molar masses

obtained by SEC, which in fact was not so surprising since the latter were relative molar masses in PMMA equivalent.



**Figure 3-7** <sup>1</sup>H NMR spectra of PDD26-EG and PDD26-BD

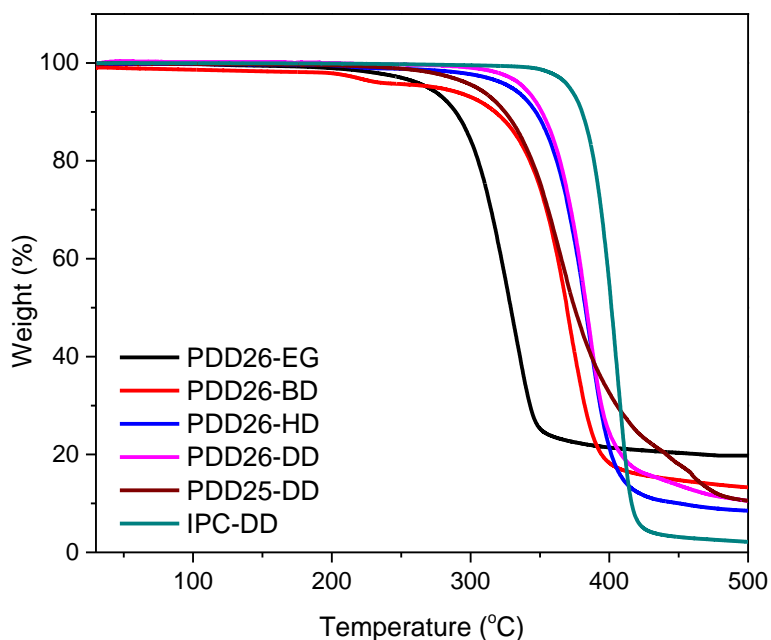
However, this structure with hydroxyl chain ends could not fit for PDD26-BD. Indeed, the obtained spectrum was more consistent with -CH<sub>3</sub> end groups, obtained during the

precipitation by the reaction of acyl chloride chain ends with methanol. The molar mass  $\overline{M}_n = 221.21 \times \frac{6 \times 3.6}{4 \times 0.15} = 8\,000 \text{ g} \cdot \text{mol}^{-1}$  accordingly calculated was also very high compared to the one determined by SEC.

Considering the much higher molar masses calculated from  $^1\text{H}$  NMR for both PDD26-EG and PDD26-BD compared to those obtained by SEC, and combining with the complex chromatograms which exhibited two populations, we could reasonably think that, as already supposed in the literature [1,6], cyclic structures could be obtained as side products. Indeed, such structures would afford an over-estimation of the molar masses calculation by NMR based on chain ends.

### 3.2.2 Thermal degradation

The thermal degradation temperatures of polyesters were determined by thermogravimetric analysis (TGA) in Figure 3-8 and the results were recorded in Table 3-4.



**Figure 3-8** TGA thermograms of polyesters



The thermal stability indicated by 5% weight loss of PDD26 polyesters increased with the molar mass: PDD26-EG < PDD26-BD < PDD26-HD < PDD26-DD. This trend has already been observed for PDD26-BD and PDD26-HD by Pellis *et al* [1]. The polyesters based on DD presented high thermal stability, with 5% weight losses higher than 300 °C, but PDD26-DD was lower than IPC-DD and higher than PDD25-DD. Considering the similar molar masses and the same diol used in these polymers, the thermal stability seemed governed by the aromatic moiety. Even if IPC-DD showed better thermal stability, the char residue at 500 °C was higher for PDD26-DD and PDD25-DD, which indicated a possible application of pyridine aromatic polyesters in fire safety materials.

**Table 3-4** Thermal degradation data recorded from TGA

Polyester	$T_{5\%}$ (°C)	$T_{\max}$ (°C)	Polyester	$T_{5\%}$ (°C)	$T_{\max}$ (°C)
PDD26-EG	269	330	PDD26-DD	341	384
PDD26-BD	275	372	PDD25-DD	304	365
PDD26-HD	329	385	IPC-DD	371	405

$T_{5\%}$ , 5% weight loss temperature;  $T_{\max}$ , maximum degradation rate temperature.

### 3.2.3 Differential scanning calorimetry (DSC)

#### 3.2.3.1 General discussion

The results in Table 3-5 showed that all polyesters were semi-crystalline (all DSC thermograms are presented in Annex 6).  $T_g$ , excepted for IPC-DD ( $T_g = -14$  °C), could not be determined during DSC first heating due to high crystallinities. However, depending on the recrystallization abilities of these polymers,  $T_g$  could occasionally be measured:

- for PDD26-EG and PDD26-DD, the cooling step prevented or decreased, respectively, the crystallization;  $T_g$  of PDD26-EG (80 °C) and PDD26-DD (0 °C) could therefore be measured during the DSC second heating;

- for PDD26-HD, a higher heating or cooling rate (30 °C·min<sup>-1</sup>) enabled to measure  $T_g = 14$  °C;

- for PDD26-BD and PDD25-DD, even a very fast cooling (quenching) did not permit to observe  $T_g$  due to the too-easy recrystallization of these polymers. But fortunately,  $T_g$  were measured by dynamic mechanical analysis (DMA). Assuming a constant shift between the glass transition temperature observed by DSC and DMA for given analysis conditions, this shift was measured for PDD26-DD and enabled us to calculate  $T_g = 65\text{ }^{\circ}\text{C}$  and  $-6\text{ }^{\circ}\text{C}$  for PDD26-BD and PDD25-DD, respectively.

**Table 3-5** Thermal information recorded from DSC

Polyester	First heating			Cooling		Second heating				
	$T_g$	$T_m$	$\Delta H_m$	$T_c$	$\Delta H_c$	$T_g$	$T_{cc}$	$\Delta H_{cc}$	$T_m$	$\Delta H_m$
	( $^{\circ}\text{C}$ )	( $^{\circ}\text{C}$ )	( $\text{J}\cdot\text{g}^{-1}$ )	( $^{\circ}\text{C}$ )	( $\text{J}\cdot\text{g}^{-1}$ )	( $^{\circ}\text{C}$ )	( $^{\circ}\text{C}$ )	( $\text{J}\cdot\text{g}^{-1}$ )	( $^{\circ}\text{C}$ )	( $\text{J}\cdot\text{g}^{-1}$ )
PDD26-EG	-	187	32.4	-	-	80	-	-	-	-
PDD26-BD	-	189	68.2	152	50.5	65 <sup>a</sup>	-	-	183 <sup>c</sup>	49.4
PDD26-HD	-	123	42.1	79	35.4	14 <sup>b</sup>	108	3.1	128	38.1
PDD26-DD	-	110	29.5	49	20.7	0	42	9.8	111	31.2
PDD25-DD	-	124	61.3	90	53.2	-6 <sup>a</sup>	-	-	124	52.5
IPC-DD	-14	45	3.5	-	-	-14	-	-	-	-

$T_g$ , glass transition temperature;  $T_m$ , melting temperature;  $T_c$ , crystallization temperature;  $T_{cc}$ , cold crystallization temperature;  $\Delta H_m$ , melting enthalpy;  $\Delta H_c$ , crystallization enthalpy;  $\Delta H_{cc}$ , cold crystallization enthalpy; <sup>a</sup> calculated from DMA (considering a constant shift, based on PDD26-DD measurements, between DMA and DSC); <sup>b</sup> 30  $^{\circ}\text{C}\cdot\text{min}^{-1}$  heating rate; <sup>c</sup> triplet peak at 168/183/192  $^{\circ}\text{C}$ .

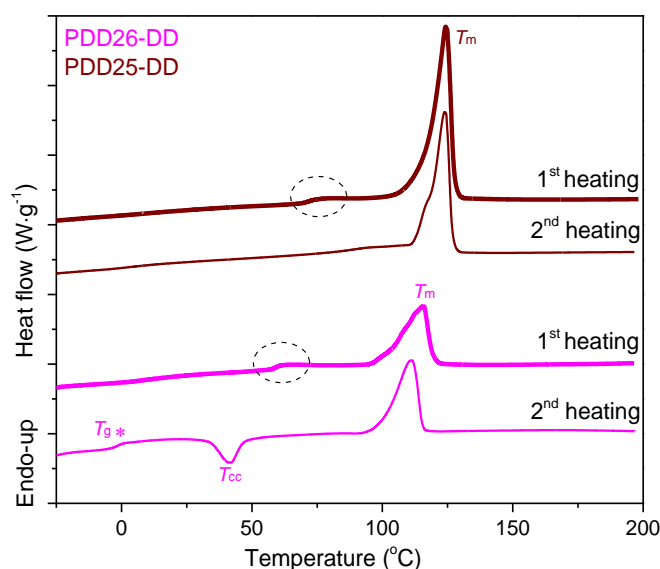
To sum up, concerning the polyesters prepared from PDD26,  $T_g$  naturally decreased with the length of the diol, all the more that shorter diols gave lower molar masses. Moreover, considering the similar molar masses polymers involving PDD26, PDD25 or IPC, notable differences were observed. On the one hand, the PDD26 ring afforded less free volume, hence a higher  $T_g$ , than the PDD25 ring ( $T_g = 0\text{ }^{\circ}\text{C}$  and  $-6\text{ }^{\circ}\text{C}$  for PDD26-DD and PDD25-DD respectively). On the other hand, the PDD26 ring also exhibited less free volume compared to the benzene ring ( $T_g = 0\text{ }^{\circ}\text{C}$  and  $-14\text{ }^{\circ}\text{C}$  for PDD26-DD and IPC-DD respectively).

As noticed in Table 3-5,  $T_m$  and  $\Delta H_m$  varied between first and second heating, which was not surprising since the first heating characterized the polymers crystallized from methanol (precipitation procedure) while the second heating represented the polymers crystallized from the melt.

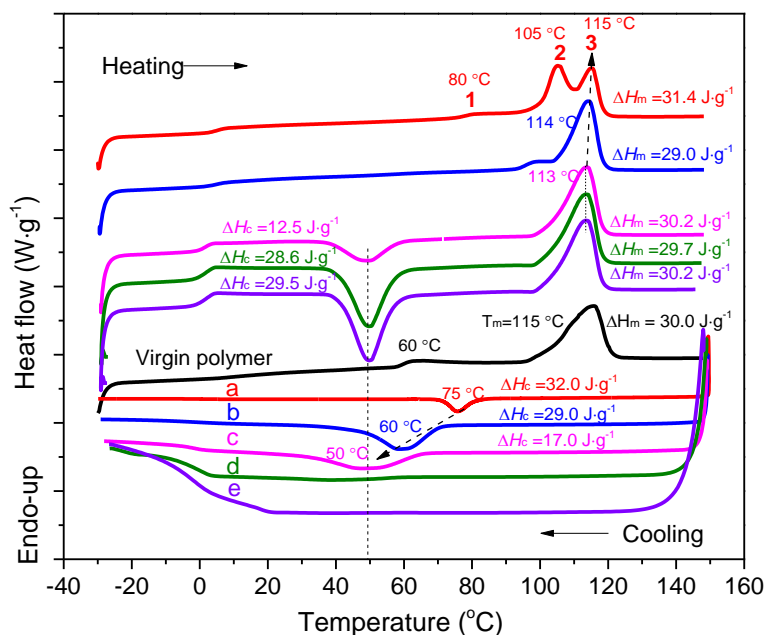
### 3.2.3.2 Investigation of crystallization behavior

The DSC thermograms of PDD26-DD and PDD25-DD were specially studied due to a specificity observed by DSC and their importance in the later investigation.

As noticed in Figure 3-9, except  $T_g$ ,  $T_{cc}$  and  $T_m$ , which have already been discussed before, there is a small signal (marked by dashed circles) on the first heating of both PDD26-DD and PDD25-DD, which looked like a  $T_g$ . However, the temperature (60 °C) was very different from the  $T_g$  measured on the second heating of PDD26-DD. To understand this particular phenomenon, PDD26-DD was deeply investigated (a similar phenomenon was observed for PDD25-DD, which was presented in Annex 6). The cooling rate, which can influence the recrystallization, was controlled at 1, 5, 10, 20 and 30 °C·min<sup>-1</sup> (Figure 3-10). As one could expect, the recrystallization temperatures ( $T_c$ ) and enthalpies decreased when the cooling rate increased from 1 to 10 °C·min<sup>-1</sup>, and even could not be observed at higher rates: a fast cooling left limited time for molecular chains to reorganize properly. At cooling rates higher than 10 °C·min<sup>-1</sup>, the subsequent heating showed a cold crystallization followed by a complete melting. At slower cooling rates (1 and 5 °C·min<sup>-1</sup>), the melting observed during the second heating involved multiple endotherms, probably due to crystalline polymorphism.

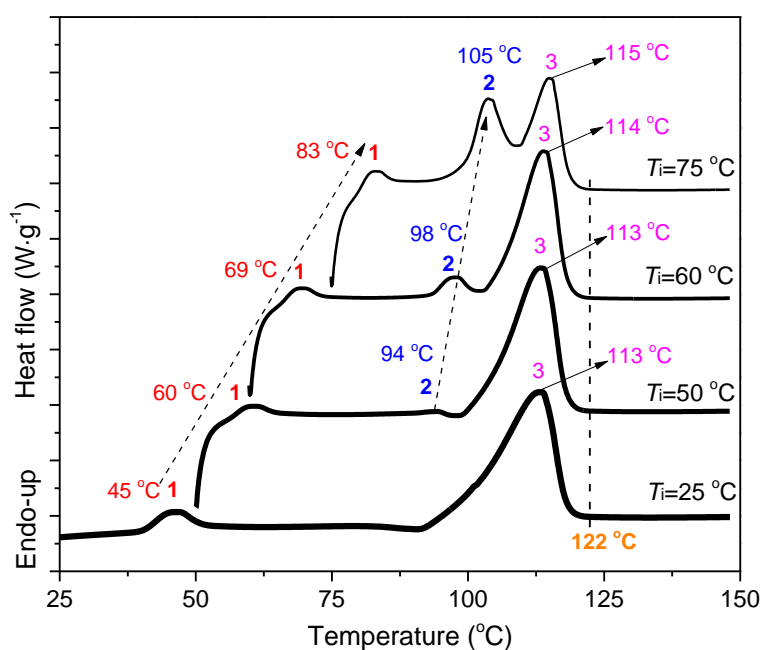


**Figure 3-9** DSC thermograms of PDD26-DD and PDD25-DD



**Figure 3-10** DSC thermograms of PDD26-DD heating (upper) after the melt polymer was cooled (lower) at different rates: (a) 1 °C·min<sup>-1</sup> (b) 5 °C·min<sup>-1</sup> (c) 10 °C·min<sup>-1</sup> (d) 20 °C·min<sup>-1</sup> (e) 30 °C·min<sup>-1</sup>

This supposed polymorphism was further studied by isothermal crystallization ( $T_i$ ) at 25, 50, 60 and 75 °C. Then, each sample was heated directly from the crystallization temperature to 150 °C and their thermograms were shown in Figure 3-11.



**Figure 3-11** DSC thermograms of PDD26-DD: samples heated (10 °C·min<sup>-1</sup>) directly after isothermal step for 120 min at 25 °C, or 30 min at 50, 60 and 75 °C

As seen from Figure 3-11, a small endotherm peak at lower temperature and a big endotherm peak at higher temperature, called "1" and "3" respectively, were always observed. When the crystallization temperature was higher than 50 °C, another endotherm peak, named "2", appeared between peaks "1" and "3". The temperature of all these peaks increased progressively with the isothermal crystallization temperature, indicating thicker crystal lamellae, which agrees with nucleation control [8].

If the recrystallization of sample "a" (red line in Figure 3-10, crystallization centered on 75 °C with a temperature range of 15 °C with 1 °C·min<sup>-1</sup> cooling rate, in other words, 15 min crystallization) is approximated as an isothermal crystallization process at  $T_i = 75$  °C during 15 min and compared to the sample isothermally crystallized at 75 °C for 30 min (Figure 3-11): endotherm "1" shifted to a higher temperature as the increase of the crystallization time, while endotherms "2" and "3" remained constant.

In other words, the temperatures of endotherms "2" and "3" were independent of the crystallization time but increased with the crystallization temperature, which is a typical primary crystallization. Meanwhile, the temperature of endotherm "1" changed with both crystallization temperature and time, which is usually associated with secondary crystallization. The end of peak "3" was independent of the crystallization temperature, signifying that the crystal lamellae were not formed during the isothermal crystallization [8]. It should not be ignored that endotherm "3" showed a complicated temperature dependence: at lower crystallization temperatures ( $\leq 50$  °C), the temperature of endotherm "3" was independent of the crystallization temperature; but at higher crystallization temperatures ( $\geq 50$  °C), it increased progressively. One possible explanation could be that endotherm "3" is a melting of primary crystals followed by recrystallization with a thicker lamella and remelting. This explanation also agreed with the unvaried temperature of the very end of the melting at 122 °C.

Thus, a general conclusion can be drawn: endotherm "1" was the melting of secondary lamellae and endotherm "2" was related to the melting of primary lamellae, while endotherm "3" was attributed to the melting of thickened primary lamellae. The complicated endotherms were related to the balance between primary and secondary crystallizations, their thickness distributions and the melting / recrystallization / remelting occurring during heating.

### 3.3 Characterization of films

#### 3.3.1 Preparation of films

The films were prepared by hot pressing according to their melting temperatures determined by DSC. It was not surprising that the films made of PDD26-EG, PDD26-BD and PDD26-HD were too brittle after pressing due to their low molar masses. The preparation of IPC-DD film was quite difficult due to its very low  $T_g$  and crystallinity coupled with a very slow recrystallization rate from the melt: therefore, the film was kept between two PTFE papers for 7 days under room temperature to induce recrystallization. In contrast, it was easier to obtain PDD26-DD and PDD25-DD films thanks to their fast recrystallization rate. Finally, translucent and flexible films of PDD26-DD, PDD25-DD, and IPC-DD were successfully obtained and presented in Figure 3-12. Further investigations were only focused on these three films.



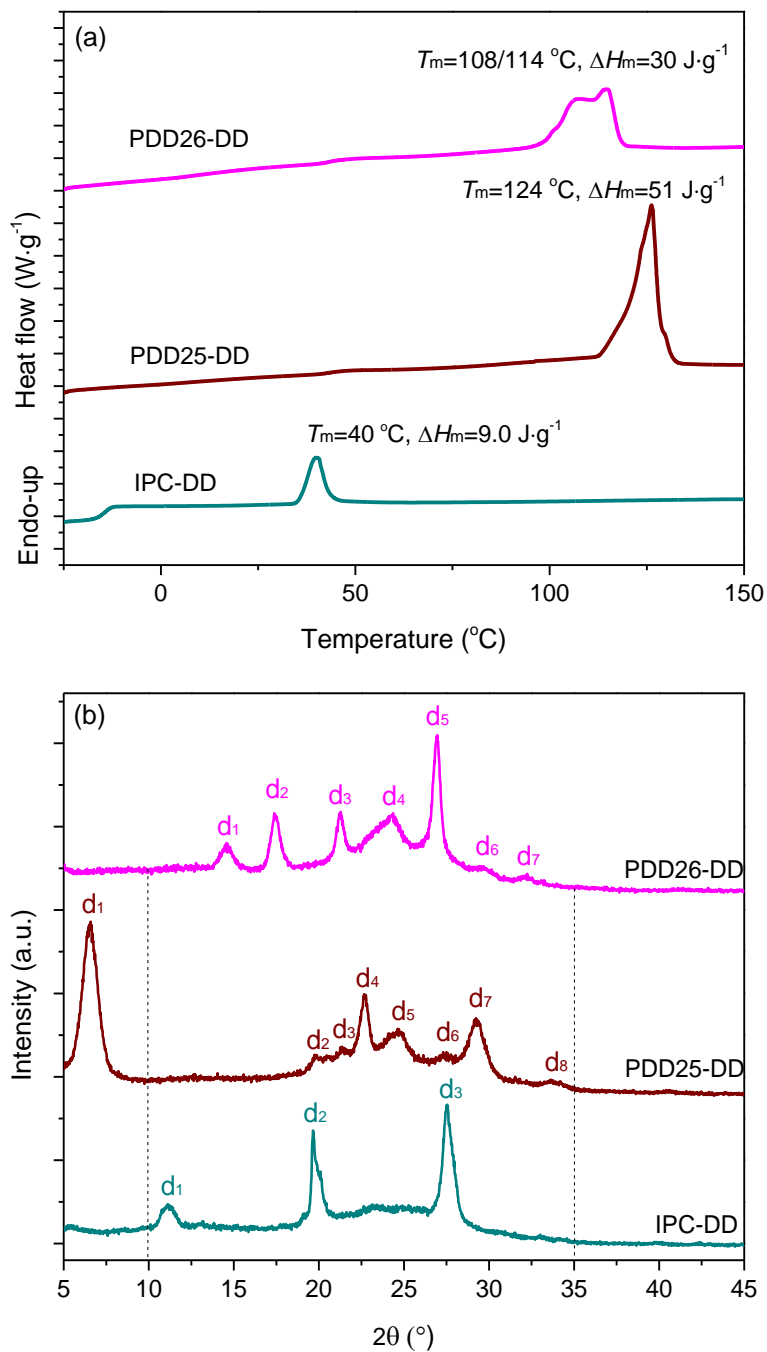
**Figure 3-12** Films prepared by hot pressing

#### 3.3.2 Crystallinity of films

The crystalline properties of films were first examined by DSC and XRD (Figure 3-13) and then confirmed by polarized optical microscopy (POM) (Figure 3-14).

The DSC thermograms in Figure 3-13(a) showed similar melting temperatures and enthalpies for PDD25-DD and PDD26-DD films ( $\Delta H_m = 51 \text{ J}\cdot\text{g}^{-1}$  and  $30 \text{ J}\cdot\text{g}^{-1}$ , respectively) to their precipitated polyesters (DSC second heating). PDD26-DD film displayed a shoulder melting peak, which is a typical phenomenon of melting crystals with different lamellae thicknesses as explained in 3.2.3.2. Contrary to the DSC second heating of IPC-DD, IPC-DD film showed a melting peak. This could be due to the fact mentioned earlier that the film was

strongly packed between two PTFE papers during several days, which acted as an external stretching, and isothermally induced orientated recrystallization and a higher  $\Delta H_m$ .



**Figure 3-13** DSC thermograms (a) and XRD patterns (b) of films

**Table 3-6** XRD data of PDD25-DD, PDD26-DD and IPC-DD films

Polyester film	$2\theta$ (°)	$d$ (nm)	$\chi_c$ (%)
PDD26-DD	14.6	0.70	36.0
	17.4	0.59	
	21.2	0.49	
	24.2	0.43	
	26.9	0.38	
	29.3	0.35	
	32.1	0.32	
PDD25-DD	6.5	1.57	50.4
	20.0	0.52	
	21.5	0.48	
	22.7	0.45	
	24.5	0.42	
	27.6	0.37	
	29.3	0.35	
	33.7	0.29	
IPC-DD	11.1	0.92	20.5
	19.8	0.52	
	27.6	0.37	

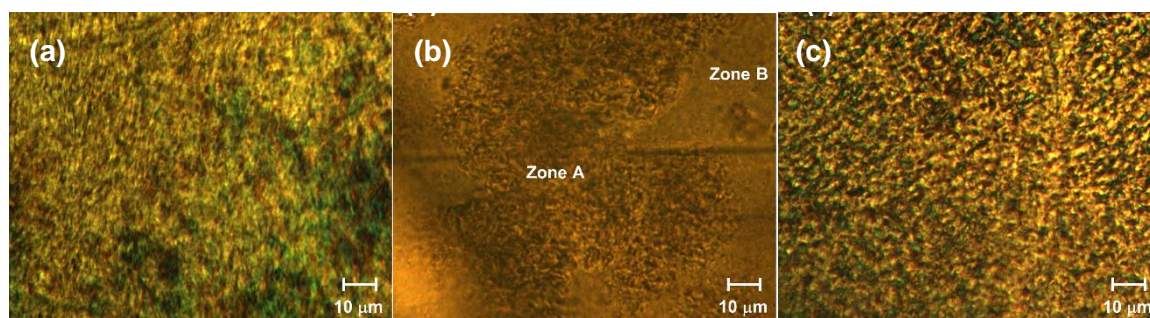
The sharp diffraction peaks on the XRD patterns in Figure 3-13(b) were indicative of a semi-crystalline phase that corroborated the DSC results. Indeed, all films showed several or even many, for PDD25-DD and PDD26-DD films, scattering peaks, which is a result of crystalline polymorphism. The data of diffraction angle ( $2\theta$ ), interplanar distance or  $d$ -spacing ( $d$ ) and crystallinity ( $\chi_c$ ) of films were listed in Table 3-6. In accordance with DSC results, PDD25-DD showed the highest crystallinity ( $\chi_c = 50.4\%$ ) and IPC-DD the lowest ( $\chi_c = 20.5\%$ ). The diffraction pattern of IPC-DD was compared to the corresponding polyesters with shorter diols (BD and octanediol, OD) obtained by Pellis *et al.* [1]: the diffraction peak at  $2\theta \sim 19.8^\circ$  seemed independent of the diol length, which was probably an indication of chain-chain packing ( $d$ -spacing perpendicular to the chain direction); the diffraction peaks corresponding to  $2\theta \sim 11.1^\circ$  and  $27.6^\circ$  shifted to lower  $2\theta$  with the increase of the diol length, and could be assumed to the  $d$ -spacing parallel to the chain direction [9]. PDD26-DD and IPC-DD displayed scattering peaks only in the  $2\theta$  range from  $10 - 35^\circ$ , while PDD25-DD also showed a strong diffraction peak at



lower  $2\theta$  ( $\sim 6.5^\circ$ ), hence related to larger interplane distance. Considering the same diol component in PDD26-DD, PDD25-DD and IPC-DD, it therefore seemed the aromatic moiety determined how the polymer chains pack.

Furthermore, XRD and DSC data exhibited reasonable correspondence. Indeed, the melting enthalpies determined by DSC and  $\chi_c$  calculated by XRD can give an approximation of  $\Delta H_m^{100\%}$  for these new polymers: 44, 83 and 101 J·g<sup>-1</sup> for IPC-DD, PDD26-DD and PDD25-DD respectively.

The crystalline structure of PDD25-DD, PDD26-DD and IPC-DD films was further validated by a polarized optical microscope (POM) as shown in Figure 3-14.

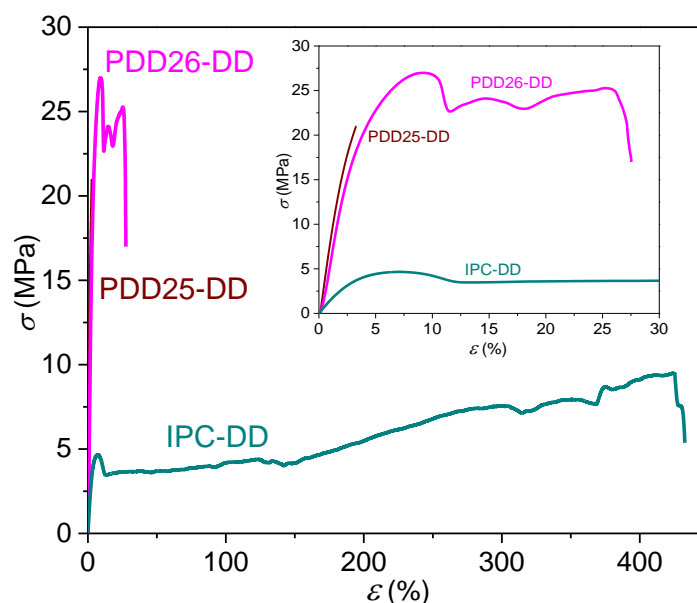


**Figure 3-14** POM images of PDD26-DD (a), PDD25-DD (b) and IPC-DD (c) films

The texture observed by POM further verified the semi-crystalline nature of the three polymer films. However, a less homogeneous crystalline phase was evidenced for PDD25-DD with separated rich (A) and poor (B) crystalline zones. The tiny crystal grains (less than 1  $\mu\text{m}$ ) disclosed in the images were an evidence of the lack of typical spheroid radiating crystal pattern, in other words spherulites, which has also been observed in PBT [10] and PBF [11].

### 3.3.3 Mechanical properties

The representative tensile curves of PDD25-DD, PDD26-DD and IPC-DD films shown in Figure 3-15 first revealed a brittle fracture for PDD25-DD, and a plastic one for PDD26-DD (with a certain degree of ductility) and IPC-DD (with a rubber state strain hardening, which could be correlated to the chain entanglement density and has been disclaimed elsewhere [12]).



**Figure 3-15** Stress-strain curves of PDD25-DD, PDD26-DD and IPC-DD films

The tensile mechanical parameters of films in Table 3-7 showed that PDD25-DD possessed the highest Young's modulus ( $E$ ), while IPC-DD the lowest, in close relation with the higher crystallinity of PDD25-DD. However, large crystalline regions in PDD25-DD restricted the chain mobility, bearing no plastic deformation, thus yielding brittleness. In contrast, plastic deformation was observed for both PDD26-DD and IPC-DD due to their greater amount of amorphous phase.

In addition, it is possible to obtain some information on the plasticity of the film by measuring the area under the curve, which represents the energy needed to break the test specimen (fracture energy  $U$ ). The large value of elongation at break ( $\epsilon_b$ ) for IPC-DD indicated a high amount of energy absorption ( $\sim 2.2 \times 10^6 \text{ kJ}\cdot\text{m}^{-3}$ ) before breaking, which is a result of amorphous chain displacement. However, for packaging film processing, there is a danger of uneven stretching during the unwind operation if the elongation is high. A low elongation should also be avoided because any sudden unbalance in the operation could lead to a break of the film [13]. From this point of view, PDD26-DD seemed the best among the three films. Considering the similar molar masses, and regardless of  $T_g$ , which was lower than the temperature during the tensile tests (21 °C), the difference in rigidity seemed to be consistent with the crystallinity of the films: PDD25-DD > PDD26-DD > IPC-DD. This result was in good agreement with DSC and XRD.

Compared with other food packaging plastics which have  $T_g$  below room temperature, PDD26-DD showed comparable stiffness but more plasticity than PBF ( $E = 1110$  MPa,  $\varepsilon_b = 2.8\%$ ) and PHBV (7 mol% HV) ( $E = 900$  MPa,  $\varepsilon_b = 15\%$ ) [13].

**Table 3-7** Mechanical properties of PDD26-DD, PDD25-DD and IPC-DD films

Polyester film	$E$ (MPa)	$\sigma_b$ (MPa)	$\varepsilon_b$ (%)	$U$ (kJ·m <sup>-3</sup> )
PDD26-DD	$770 \pm 25$	$12.5 \pm 4.8$	$25.0 \pm 6.0$	$4.7 \pm 0.6 \times 10^5$
PDD25-DD	$880 \pm 20$	$21.0 \pm 2.0$	$3.4 \pm 0.6$	$3.0 \pm 0.6 \times 10^4$
IPC-DD	$140 \pm 15$	$5.5 \pm 1.2$	$420 \pm 140$	$2.2 \pm 0.4 \times 10^6$

$E$ , Young's modulus;  $\sigma_b$ , stress at break;  $\varepsilon_b$ , strain at break;  $U$ , fracture energy.

### 3.3.4 Contact angle measurements

The surface properties of films were evaluated by surface energy and water contact angle measurements. The obtained results were given in Table 3-8.

**Table 3-8** Surface energies and contact angles of polymer films

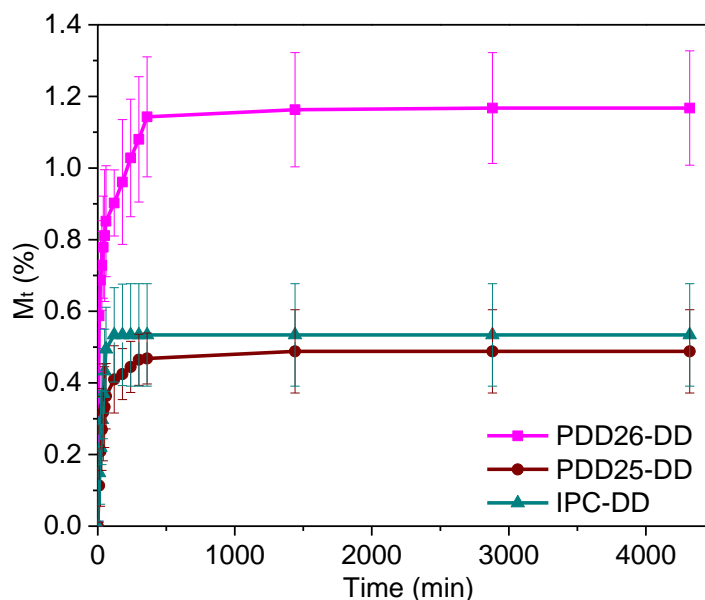
Polyester film	$\gamma^t$ (mN·m <sup>-1</sup> )	$\gamma^d$ (mN·m <sup>-1</sup> )	$\gamma^p$ (mN·m <sup>-1</sup> )	$\theta_w$ (°)
PDD26-DD	$26.0 \pm 0.5$	$23.0 \pm 0.1$	$3.5 \pm 0.1$	$90.0 \pm 0.4$
PDD25-DD	$26.0 \pm 0.2$	$23.0 \pm 0.1$	$3.0 \pm 0.4$	$92.0 \pm 1.0$
IPC-DD	$24.0 \pm 0.2$	$23.0 \pm 0.3$	$1.0 \pm 0.2$	$94.0 \pm 2.0$

$\gamma^t$ , Total surface energy with the dispersive ( $\gamma^d$ ) and polar ( $\gamma^p$ ) parts;  $\theta_w$ , water contact angle.

From the data recorded in Table 3-8, we can conclude that the three films were hydrophobic with quite similar water contact angle values. PDD26-DD presented the lowest water contact angle ( $\theta_w = 90.0 \pm 0.4^\circ$ ) because its polar pyridine sites are accessible to water molecules in its larger amorphous domains. It is not easy to compare the hydrophobicity of PDD25-DD and IPC-DD by their water contact angles considering the experimental errors. However, the total surface energy ( $\gamma^t$ ) was lower for IPC-DD (24 mN·m<sup>-1</sup>) compared to PDD25-DD (26 mN·m<sup>-1</sup>). This reduced  $\gamma^t$  was mainly due to its lower polar component  $\gamma^p$ , which characterized the higher hydrophobicity of IPC-DD.

### 3.3.5 Liquid water and water vapor sorption

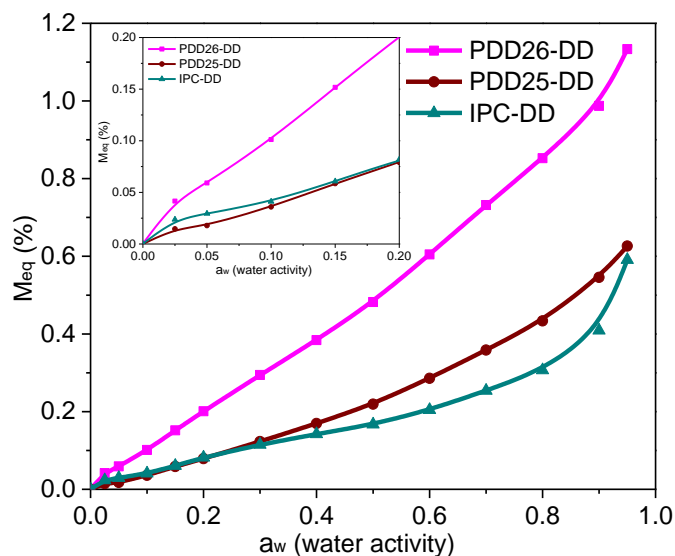
The liquid water sorption results were presented in Figure 3-16.



**Figure 3-16** Liquid water sorption of PDD26-DD, PDD25-DD and IPC-DD

It disclosed a more pronounced water uptake for PDD26-DD ( $M_{eq} = 1.17 \pm 0.16$  %) compared to PDD25-DD ( $M_{eq} = 0.49 \pm 0.12$  %) and IPC-DD ( $M_{eq} = 0.53 \pm 0.14$  %). It is usually reported that the more crystalline a material, the lower the water absorption [14]. Thus, it was not surprising that the higher crystallinity in PDD25-DD compared to PDD26-DD allowed a decrease of the water uptake. Even if PDD26-DD possessed a higher crystallinity than IPC-DD, the polar pyridine ring in PDD26-DD showed a stronger affinity to water molecules compared to the non-polar phenyl ring, thereby holding more water molecules [15]. Taking the experimental errors into account, PDD25-DD displayed almost the same water uptake as IPC-DD, which is a compromise between crystallinity and pyridine ring affinity.

The water vapor sorption isotherms were presented in Figure 3-17.



**Figure 3-17** Water vapor sorption isotherms

All isotherms exhibited a sigmoid shape following Park's model. The corresponding parameters were gathered in Table 3-9. The overall increase of water vapor sorption for PDD26-DD ( $M_{eq} = 1.13$  % at  $a_w = 0.95$ ) was related to its larger amorphous domain and the affinity of polar pyridine sites with water. In a large range of activities ( $a_w > 0.2$ ), the higher water sorption of PDD25-DD compared to IPC-DD was explained by its pyridine sites. At  $a_w < 0.2$  (Langmuir-type sorption), the lower water sorption for PDD25-DD compared to IPC-DD could be explained by its lower number of Langmuir sites ( $A_L = 0.05 \pm 0.02$  vs  $A_L = 1.6 \pm 0.1$ ) due to a higher crystallinity. In the Henry's sorption domain, as stated in the previous chapter, the solubility coefficient  $S$  of water vapor in the film was calculated from the slope of the linear range of the isotherm (reflected by  $k_H$  values in Table 3-9). Considering a linear sorption in the range of  $a_w = 0.1$ - $0.7$  for both PDD26-DD and PDD25-DD,  $S$  values were  $S = 9.5 \times 10^{-3}$  g<sub>H<sub>2</sub>O</sub>/g<sub>pol</sub> and  $S = 4.6 \times 10^{-3}$  g<sub>H<sub>2</sub>O</sub>/g<sub>pol</sub>, respectively. For IPC-DD, the water vapor sorption changed at  $a_w = 0.2$ , thus the calculation of  $S$  was performed in the linear range  $a_w = 0.3$ - $0.7$ :  $S = 1.4 \times 10^{-3}$  g<sub>H<sub>2</sub>O</sub>/g<sub>pol</sub>. It is known that polymers with the same chemical structure (chemical functions in our case), will show lower water vapor solubility when the crystallinity is higher [16]. Thus, it is reasonable that PDD25-DD ( $\chi_c = 50.4$  %) showed a lower solubility coefficient than PDD26-DD ( $\chi_c = 36$  %). The lowest water vapor solubility for IPC-DD regardless of its larger amorphous domain ( $\chi_c = 20.5$  %) revealed that the non-polar phenyl rings were the predominant factor to reduce the water vapor solubility. At high water activities ( $a_w > 0.8$ ), a reduced gap in

water vapor sorption was observed between IPC-DD and PDD25-DD ( $M_{eq} = 0.59\%$  and  $0.63\%$ , respectively). The rapid increase of sorption in IPC-DD was probably due to its larger amorphous domain allowing the accumulation of more water molecules into clusters. Then, stronger attractive forces between water molecules than those between water and polymer induced more and larger water aggregates in IPC-DD ( $K_a = 0.70 \pm 0.04$  and  $n_a = 18.0 \pm 0.1$ ) compared to PDD25-DD ( $K_a = 0.30 \pm 0.02$  and  $n_a = 4.0 \pm 0.3$ ) [17,18].

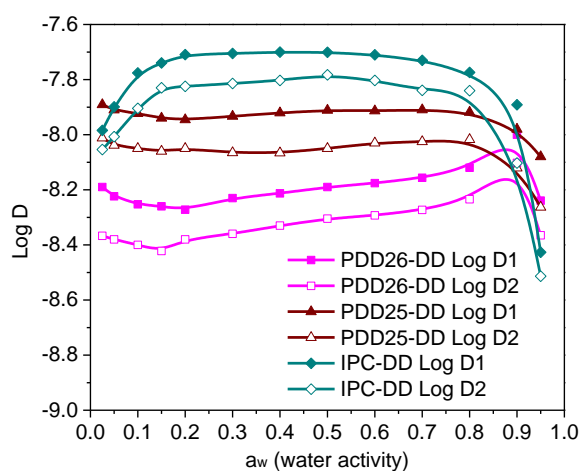
**Table 3-9** Sorption parameters of Park's model

Polyester film	$A_L \times 10^3$ (g/g)	$b_L$	$k_H \times 10^3$ (g/g)	$K_a \times 10^3$ (g/g)	$n_a$
PDD26-DD	$0.15 \pm 0.01$	$1.60 \pm 0.05$	$8.3 \pm 0.3$	$0.35 \pm 0.02$	$6.0 \pm 0.2$
PDD25-DD	$0.05 \pm 0.02$	$1.40 \pm 0.05$	$4.2 \pm 0.2$	$0.30 \pm 0.02$	$4.0 \pm 0.3$
IPC-DD	$1.60 \pm 0.10$	$0.10 \pm 0.04$	$1.5 \pm 0.1$	$0.70 \pm 0.04$	$18.0 \pm 0.1$

$A_L$ , Langmuir's capacity constant;  $b_L$ , Langmuir's affinity constant;  $k_H$ , Henry's type solubility coefficient;  $K_a$ , equilibrium constant for clustering reaction;  $n_a$ , average number of water molecules per cluster.

From a general point of view, with the consideration of higher water vapor sorption of both PDD26-DD and PDD25-DD compared to IPC-DD despite their higher crystallinity, the pyridine rings induced an increased water vapor sorption compared to phenyl rings. This behavior has been already observed for furan rings when compared to phenyl rings [15].

The water vapor diffusion coefficients ( $D$ ) were used to evaluate the water vapor sorption kinetics. The evolution of  $D$  on semilogarithmic scale ( $\log D$ ) as a function of  $a_w$  was presented in Figure 3-18.



**Figure 3-18** Evolution of  $D_1$  and  $D_2$  as a function of  $a_w$

IPC-DD showed the highest diffusion coefficients  $D_1$  and  $D_2$  on a large  $a_w$  range ( $a_w=0.2-0.8$ ) which was in good agreement with its lowest crystallinity. A quicker diffusion process for PDD25-DD compared to PDD26-DD seemed surprising when considering its higher crystallinity, which should increase the diffusion tortuosity [19]. For both, a slight decrease of  $D_1$  and  $D_2$  was observed until  $a_w = 0.2$  probably due to water molecules interactions with polar pyridine rings, leading to hydrogen bonds which increased the cohesion between polymer chains, and then reduced the water mobility [20]. This phenomenon was already observed at low water concentration for flax fibers [20], cereal-based products [21], and tapioca starch film containing a small amount of glycerol [22]. It was explained as an “antiplasticizing effect” of water molecules on the diffusion process [20]. Then PDD26-DD showed an increase for both  $D_1$  and  $D_2$ , which is a common phenomenon of water molecules that induce polymer swelling [17]. For PDD25-DD, small fluctuations that tended to be constant were observed in a large water activity range ( $a_w = 0.2-0.7$ ). This can be explained by the presence of numerous impermeable crystallites acting to stabilize the polymer matrix against swelling [15]. For IPC-DD, at the beginning of the water sorption,  $D_1$  and  $D_2$  increased until a maximum was reached and then stayed constant on a large  $a_w$  domain ( $a_w = 0.2-0.7$ ). The increase of diffusivity for the lowest  $a_w$  was explained by the induced plasticizing of water molecules, which has been noticed in many polymers [17,20]. Then, the relatively constant diffusion process, probably due to the low water concentration inside the film which was not enough to induce polymer swelling, corresponded to Henry’s process (dissolution and diffusion of water molecules). The large decrease of  $D_1$  and  $D_2$  at high  $a_w$  was probably due to the aggregation of water molecules in clusters, which made them less mobile [23,24].

Another observation in Figure 3-18 was the higher diffusion coefficient  $D_1$  than  $D_2$ , whatever the sample.  $D_1$  values (first half-sorption coefficient) should be more characteristic of the diffusion through the surface while  $D_2$  values (second half-sorption coefficient) should be more representative of the diffusion of water in the core of the film. In common cases, due to the swelling effect,  $D_2$  values are higher than  $D_1$  values [20,25,26]. This unusual behavior with  $D_2 < D_1$  might be the result of a structuring effect of water during the water sorption in the films. For PDD26-DD and PDD25-DD, it seemed the diffusion of water was governed by the surface effect (a strong cohesion between the chains to form hydrogen bonds) rather than by the swelling of the core [27]. For IPC-DD, the presence of water molecules in the film induced stronger attractive forces between water molecules than those between water and polymer thus inhibiting the mobility of water molecules [17,18].

The higher diffusion coefficients of PDD25-DD than PDD26-DD were always puzzling, considering the higher crystallinity of the former. This abnormal phenomenon could be explained by the non-homogeneous microstructure of PDD25-DD as shown with the POM images (Figure 3-14): the diffusion of water molecules occurred in the concentrated amorphous domains. Moreover, it is well-known that the molecular geometric symmetry of the polymer will facilitate the diffusion of molecules [28,29]. Thus, if the symmetrical chemical structure of PDD25-DD is taken into consideration, it also contributed to higher diffusion coefficients. This point will be clarified later by dynamic mechanical analysis (DMA).

### 3.3.6 Water vapor permeation

The water barrier properties were evaluated by water vapor permeation measurements and the corresponding results were listed in Table 3-10.

**Table 3-10** Water vapor permeation coefficient ( $P_{\text{H}_2\text{O}}$ ) of PDD26-DD, PDD25-DD and IPC-DD films at different water activities ( $a_w$ )

Polyester film	$a_w$	$P_{\text{H}_2\text{O}} \times 10^5 \text{ (g}\cdot\text{m}^{-1}\cdot\text{d}^{-1}\text{)}$	$P_{\text{H}_2\text{O}}$ (barrer)
PDD26-DD	0.37	$2.0 \pm 0.2$	$13 \pm 1$
	0.52	$49 \pm 5$	$310 \pm 30$
	0.60	$70 \pm 7$	$440 \pm 40$
	0.67	$77 \pm 8$	$470 \pm 45$
PDD25-DD	0.42	$6.0 \pm 0.3$	$40 \pm 3$
	0.49	$10.0 \pm 0.4$	$60 \pm 5$
	0.56	$13 \pm 3$	$80 \pm 8$
	0.63	$17 \pm 2$	$100 \pm 9$
IPC-DD	0.33	$5.0 \pm 0.1$	$30 \pm 3$
	0.45	$8.0 \pm 0.2$	$50 \pm 4$
	0.56	$9.5 \pm 0.3$	$60 \pm 6$
	0.60	$15 \pm 2$	$90 \pm 8$

Low water vapor permeabilities ( $P_{\text{H}_2\text{O}}$ ) were observed for all films (*e.g.*  $P_{\text{H}_2\text{O}} = 440 \pm 40$  barrer,  $P_{\text{H}_2\text{O}} = 100 \pm 9$  barrer and  $P_{\text{H}_2\text{O}} = 90 \pm 8$  barrer at  $a_w \cong 0.6$  for PDD26-DD, PDD25-DD and IPC-DD, respectively). PDD26-DD showed globally a higher water vapor permeability compared to PDD25-DD and IPC-DD, which was contrary to its lowest diffusion coefficients



( $D_1$  and  $D_2$ ), probably due to its much higher water vapor solubility coefficient  $S$  ( $P = D \times S$ ). As reported by Marais *et al.*, the variation in water vapor permeability for polymers can be related to the variations in the water vapor solubility coefficient, which can be qualitatively explained by the hydrophilicity (larger polymer-water interactions) of the polymer. If the total number of polar groups are taken as a criterion, the more polar groups, the higher the water vapor solubility [17]. Considering the crystalline phase impermeable to water vapor, only the polar groups in the amorphous phase are accessible to water molecules [30]. The quantity of polar groups in the amorphous domain in per kilo polymer  $Q_{\text{polar}}$  ( $\text{mol} \cdot \text{kg}^{-1}$ ) was calculated according to the repeating unit molar mass ( $M$ ) and the crystallinity ( $\chi_c$ ) of the polymer films ( $Q_{\text{polar}} = \frac{1000}{M} \times (1 - \chi_c)$ ) (Table 3-11). The largest quantity of polar groups in PDD26-DD ( $6.3 \text{ mol} \cdot \text{kg}^{-1}$ ) induced the highest water vapor solubility and the lowest quantity of polar groups in IPC-DD and PDD25-DD ( $5.2$  and  $4.8 \text{ mol} \cdot \text{kg}^{-1}$  respectively) brought the lowest water vapor solubilities. Consequently, the highest water vapor permeability for PDD26-DD and the lowest for PDD25-DD and IPC-DD were observed.

**Table 3-11** Quantity (mol) of polar groups in per kg polymer

Polymer film	$Q_{\text{polar}}$ ( $\text{mol} \cdot \text{kg}^{-1}$ )		
	Ester groups	Pyridine groups	Total
PDD26-DD	4.2	2.1	6.3
PDD25-DD	3.2	1.6	4.8
IPC-DD	5.2	0	5.2

For PDD26-DD, the increase of the water vapor permeability with the increase of  $a_w$  coupled with the increase of  $D$  (Figure 3-18) confirmed a swelling happened in the polymer matrix [15].

The relatively constant  $P_{\text{H}_2\text{O}}$  values for both PDD25-DD and IPC-DD were consistent with the sorption behavior in the Henry's sorption range with relative constant dissolution ( $S$ ) (Figure 3-17) and diffusion ( $D$ ) (Figure 3-18) [31]. Considering such low water vapor permeation coefficients for these films, it seemed interesting to measure  $P_{\text{H}_2\text{O}}$  values at  $a_w = 1$  for supplementary information: 22 580, 2 620 and 530 barrer for PDD26-DD, PDD25-DD and IPC-DD. The lowest value for IPC-DD was probably due to the decrease in diffusivity observed at large  $a_w$  (Figure 3-18). The overall low water vapor permeability of the polymer films can

be judged by their  $P$  values at  $a_w = 1$ . They were comparable with some common food packaging materials (*e.g.*  $P_{H_2O} = 11\,215$  barrer for PA6,  $P_{H_2O} = 2\,300$  barrer for PEBAX (70 % PTMO),  $P_{H_2O} = 448$  barrer for PET and  $P_{H_2O} = 486$  barrer for PA12) [17].

### 3.3.7 Gas permeation

The gas permeation coefficients ( $P$ ) for  $N_2$ ,  $O_2$  and  $CO_2$  were recorded in Table 3-12.

**Table 3-12** Gas permeation ( $P$ ) and diffusion ( $D$ ) coefficients of polyester films

Polyester film	$N_2$		$O_2$		$CO_2$	
	$P$	$D \times 10^{10}$	$P$	$D \times 10^{10}$	$P$	$D \times 10^{10}$
PDD26-DD	$0.030 \pm 0.003$	$1.7 \pm 0.1$	$0.070 \pm 0.005$	$3.5 \pm 0.2$	$0.30 \pm 0.02$	$64 \pm 4$
PDD25-DD	$0.18 \pm 0.01$	$11 \pm 1$	$0.40 \pm 0.03$	$34 \pm 2$	$1.4 \pm 0.1$	$433 \pm 30$
IPC-DD	$0.22 \pm 0.02$	$11 \pm 1$	$0.90 \pm 0.07$	$50 \pm 4$	$5.4 \pm 0.4$	$580 \pm 41$

$P$  expressed in barrer ( $1 \text{ barrer} = 10^{-10} \text{ cm}^3 \text{ STP} \cdot \text{cm} \cdot \text{cm}^{-2} \cdot \text{s}^{-1} \cdot \text{cmHg}^{-1}$ ),  $D$  expressed in  $\text{cm}^2 \cdot \text{s}^{-1}$ .

The values followed the usual order  $P_{N_2} < P_{O_2} < P_{CO_2}$  for polymers [32]. PDD26-DD showed the lowest gas permeability ( $P_{N_2} = 0.03$  barrer,  $P_{O_2} = 0.07$  barrer and  $P_{CO_2} = 0.3$  barrer), which was contrary to the water vapor permeability. This behavior could be explained by the critical temperature ( $T'_c$ ) of the penetrants: the higher the  $T'_c$ , the higher the condensability and solubility of the penetrant [27]. It is known that  $T'_c (H_2O) (374 \text{ }^\circ\text{C}) > T'_c (CO_2) (31 \text{ }^\circ\text{C}) > T'_c (O_2) (-118 \text{ }^\circ\text{C}) > T'_c (N_2) (-147 \text{ }^\circ\text{C})$ . In other words, water molecules have the highest condensability, and then the highest solubility. Thus, the permeability of water is more influenced by solubility than by diffusion, especially when polar groups are present [30], like the 2,6-pyridine ring in PDD26-DD. In contrast, the much less condensable gases make the permeabilities affected rather by crystallinity than by polar groups [30]. The higher the crystallinity, the lower the solubility and the longer the diffusion pathways [16,33–35]. Thus, it was easy to understand the lower gas permeability for PDD26-DD compared to IPC-DD ( $P_{N_2} = 0.22$  barrer,  $P_{O_2} = 0.9$  barrer and  $P_{CO_2} = 5.4$  barrer): the higher crystallinity of PDD26-DD allowed a lower solubility and diffusivity, and finally a lower permeability ( $P = D \times S$ ). Surprisingly,  $P$  values for PDD26-DD were lower ( $P_{N_2}$ ,  $P_{O_2}$  and  $P_{CO_2}$  were 6, 5.6, and 4.7 times lower, respectively) than those obtained for PDD25-DD. The decrease in permeability seemed related to the lower  $D$  for PDD26-DD (at least 4 times) compared to PDD25-DD. These results were unexpected because the crystallinity

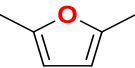
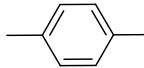
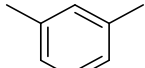
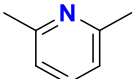
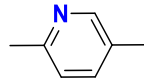
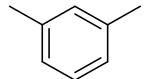
of PDD26-DD was lower ( $\chi_c = 36\%$ ) compared to PDD25-DD ( $\chi_c = 50.4\%$ ). This abnormal behavior for gas diffusion could also be explained by the non-homogeneous microstructure of PDD25-DD and its molecular geometric symmetry [28,29], as previously explained for water diffusion. Moreover, as observed by XRD experiments, the crystals in PDD25-DD showed larger interplane distance than in PDD26-DD, which means less compacted micro-structure [36].

In addition to its best gas barrier properties among the three polymer films, PDD26-DD showed also better gas barrier properties compared to traditional food packaging materials, such as PE ( $P_{N_2} = 0.14\text{--}1.9$  barrer,  $P_{O_2} = 0.6\text{--}6.7$  barrer and  $P_{CO_2} = 1.7\text{--}28$  barrer), PP ( $P_{N_2} = 0.44$  barrer,  $P_{O_2} = 0.9\text{--}2.3$  barrer and  $P_{CO_2} = 9.2$  barrer), and oriented PS ( $P_{N_2} = 0.29\text{--}0.78$  barrer,  $P_{O_2} = 1.1\text{--}2.7$  barrer and  $P_{CO_2} = 8.8\text{--}10.5$  barrer) [13]. Even if PDD26-DD showed less barrier than PEF ( $P_{O_2} = 0.004\text{--}0.01$  barrer and  $P_{CO_2} = 0.026$  barrer), it was still comparable to amorphous PET ( $P_{O_2} = 0.05\text{--}0.11$  barrer and  $P_{CO_2} = 0.21\text{--}0.57$  barrer) and more barrier than bio-based polyester PLA containing 98% L-lactide ( $P_{N_2} = 4.99$  barrer,  $P_{O_2} = 0.11\text{--}0.56$  barrer and  $P_{CO_2} = 1.88$  barrer) [13]. The efficient gas barrier properties for PDD26-DD seemed related to its 2,6-pyridine ring, which will be further discussed.

The absence of  $P$  values for PDD26-EG made it hard to understand the barrier ability of the 2,6-pyridine ring compared to the *p*-phenylene ring in PET and the 2,5-furan ring in PEF. Thus, a comparison between different aromatic skeletons in permeability was given in Table 3-13. Due to the same *m*-phenylene ring, poly(ethylene isophthalate) (PEI) and IPC-DD were taken as references. According to Burgess *et al.* [37], PEF showed a 3-times decrease in  $P_{O_2}$  and a 1.7-times decrease in  $P_{CO_2}$  compared to PEI. Considering their same EG component, we assumed that the reduction in permeability was due to the 2,5-furan ring. Similarly, PDD26-DD showed a 13-times decrease in  $P_{O_2}$  and an 18-times decrease in  $P_{CO_2}$  compared to IPC-DD. This indicated that more barrier to gas was introduced by the 2,6-pyridine ring than the *m*-phenylene ring. Taking this decreased magnitude into consideration, we could indirectly infer that for similar molar masses, PDD26-EG may show better gas barrier than PEF. It needs to mention that even with a lower molar mass (2 400 vs 66 000\* g·mol<sup>-1</sup>), PDD26-EG still showed a  $T_g$  (80 °C) comparable to PEF ( $T_g = 85$  °C) [29]. Considering PEF is more barrier than PET [37,38], we could finally deduce that PDD26-EG may possess the best gas barrier property among PEI, PEF and PET. Since they have the same diol component, we may attribute this improvement in

gas barrier to the 2,6-pyridine ring. Therefore, the 2,6-pyridine ring is highly qualified for preparing high gas barrier materials. (\*Measured by multi-angle laser light scattering)

**Table 3-13** Comparison between different aromatic skeletons in permeability

Literature [37]			
Sample name	PEF	PET	PEI
Aromatic skeleton			
“Polar” ring	Yes	No	No
Hindered ring-flipping	Yes	No	Yes
BIFp (O <sub>2</sub> ) vs. PEI	3.0	0.28	1
BIFp (CO <sub>2</sub> ) vs. PEI	1.7	0.09	1
Our work			
Sample name	PDD26-DD	PDD25-DD	IPC-DD
Aromatic skeleton			
“Polar” ring	Yes	Yes	No
Hindered ring-flipping	Yes	No	Yes
BIFp (O <sub>2</sub> ) vs. IPC-DD	13	2.3	1
BIFp (CO <sub>2</sub> ) vs. IPC-DD	18	3.8	1

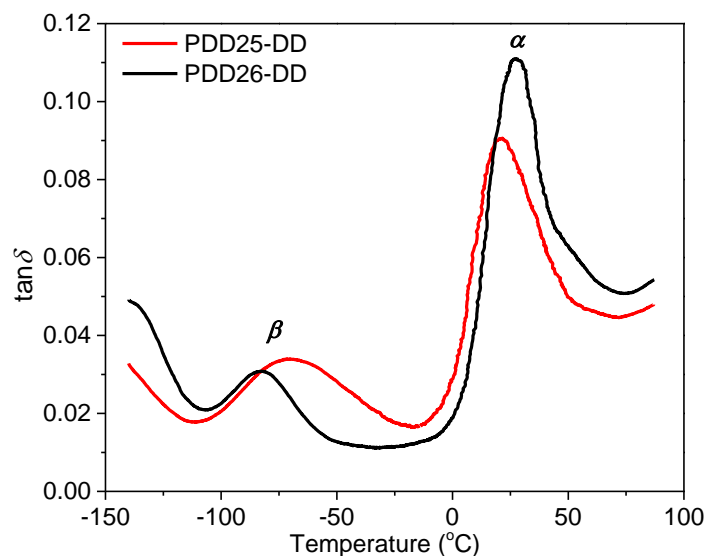
BIFp: Barrier Improvement Factor [37].

### 3.3.8 DMA of films

As mentioned in 3.3.7 the higher barrier property of PDD26-DD than PDD25-DD, with a lower crystallinity, was unexpected due to the known impermeability of crystalline regions. A possible explanation could be found in their amorphous phase, which could exhibit different kinds of movements, depending on the temperature [29,39]:

- at  $T_g$ : chain segments associated with the coordinated motion of 50-100 carbon atoms, namely  $\alpha$  transition or micro-Brownian chain motion,
- and sub- $T_g$ : only localized chain or small units motion, namely  $\beta$  transition.

These transitions can be observed by dynamic mechanical analysis (DMA), as plotted in Figure 3-19.



**Figure 3-19**  $\tan\delta$  versus temperature for PDD26-DD and PDD25-DD films

Relevant transition data for PDD26-DD and PDD25-DD were recorded in Table 3-14.

**Table 3-14** Information of PDD26-DD and PDD25-DD recorded from DMA

Sample	$T$ (°C)		Normalized peak area ( $A_n$ )	
	$\beta$	$\alpha$	$\beta$	$\alpha$
PDD26-DD	-82	27	0.67	4.11
PDD25-DD	-70	21	1.85	4.47

$T$ , temperature of the maximum in  $\tan\delta$ ;  $A_n$ , area normalized to fully amorphous sample (calculated by excluding the crystallinity).

The  $\beta$  transition temperature for PDD26-DD was  $\sim 12$  °C lower than for PDD25-DD, and the lower magnitude of  $\tan\delta$  peak ( $A_n = 0.67$ ) for PDD26-DD could probably be due to the non-symmetrical axis of the 2,6-pyridine ring which resulted in hindered ring-flipping [37].

Concerning the  $\alpha$  transition, it is well established that any structural feature that increases the moving unit size of the molecular chain will increase  $T_g$  [39], and a higher  $T_g$  is linked with a higher activation energy [29]. Thus, a  $T_g$  almost 6 °C higher for PDD26-DD meant a higher activation energy involved to initiate the chain segments movement. Furthermore, the decreased area for PDD26-DD further confirmed more difficulties were encountered in chain segments movement than in PDD25-DD.

According to Light and Seymour, restricted molecular motions in amorphous polymers are related to the decrease of O<sub>2</sub> and CO<sub>2</sub> diffusion coefficients [28]. Therefore, the smaller  $\tan \delta$  areas at sub- $T_g$  and  $T_g$ , combined with the lower diffusion coefficient for PDD26-DD, indicated that the difficulty in molecular motions in the amorphous phase dominated the permeation process by restricting the diffusion and finally decreasing the permeability.

Furthermore, the temperature used for permeation measurements (25 °C) was lower than  $\tan \delta_{\alpha(PDD26-DD)}$  (27 °C) but higher than  $\tan \delta_{\alpha(PDD25-DD)}$  (21 °C): at this temperature, the amorphous phase was much more mobile in PDD25-DD than PDD26-DD, which even amplified the phenomenon discussed above.

### 3.4 Conclusion

Four semi-aromatic bio-based polyesters containing 2,6-pyridinedicarbonyl dichloride (PDD26) and aliphatic diols with different chain length have been synthesized by polycondensation reactions. The highest molar masses and thermal degradation temperature were obtained for the polyester that contained the longest diol chain (PDD26-DD), however,  $T_g$  and  $T_m$  were in reverse. Two analogs of PDD26-DD, named PDD25-DD and IPC-DD, were successfully synthesized with equally satisfying molar masses, in solution and in bulk, respectively. The polyesters containing pyridine rings (PDD26-DD and PDD25-DD) showed lower thermal degradation temperatures compared to the one containing phenyl rings (IPC-DD), however,  $T_g$ ,  $T_m$  and crystallinities were higher. For the polyesters containing pyridine ring, PDD26-DD showed a higher thermal degradation temperature and  $T_g$  compared to PDD25-DD, while, a lower  $T_m$  and crystallinity. Among all, PDD26-DD displayed the lowest water barrier properties but the highest mechanical and gas barrier properties, which have competitive advantage compared with PE, PP, PS and PLA for food packaging applications. To sum up, PDD26-DD has great potential in food packaging, especially when the packaging needs high CO<sub>2</sub> and O<sub>2</sub> barrier.

## References

- [1] A. Pellis, J.W. Comerford, S. Weinberger, G.M. Guebitz, J.H. Clark, T.J. Farmer, Enzymatic synthesis of lignin derivable pyridine based polyesters for the substitution of petroleum derived plastics, *Nat. Commun.* 10 (2019).
- [2] H.N. Isfahani, K. Faghihi, New thermally stable polyesters based on 2,5-pyridinedicarbonyl dichloride and aromatic diols: synthesis and characterization, *Chinese Chem. Lett.* 20 (2009) 885–888.
- [3] M. Okada, Y. Okada, K. Aoi, Dianhydrohexitols and aliphatic dicarboxylic acids, *J. Polym. Sci. Part A Polym. Chem.* 33 (1995) 2813–2820.
- [4] M. Garaleh, T. Yashiro, H.R. Kricheldorf, P. Simon, T. Yashiro, P. Simon, ( Co- ) Polyesters derived from isosorbide and 1,4-cyclohexane dicarboxylic acid and succinic acid, *Macromol. Chem. Phys.* 211 (2010) 1206–1214.
- [5] R. Storbeck, M. Rehahn, M. Ballauff, Synthesis and properties of high-molecular-weight polyesters based on 1,4 : 3,6-dianhydrohexitols and terephthalic acid, 64 (1993) 53–64.
- [6] G.C. East, V.G.R. Gudiguntla, The synthesis and characterization of polyesters based on 2,5-pyridinedicarboxylic acid, *Macromol. Chem. Phys.* 195 (1994) 1851–1864.
- [7] S. Saleh, B. Sweileh, S.O. Taha, R. Mahmoud, M.O. Taha, Preparation of polyester-based metal-cross linked polymeric composites as novel materials resistant to bacterial adhesion and biofilm formation, *Molecules.* 16 (2011) 933–950.
- [8] Y. Kong, J.N. Hay, Multiple melting behaviour of poly(ethylene terephthalate), *Polymer.* 44 (2002) 623–633.
- [9] H. Marubayashi, T. Ushio, S. Nojima, Crystallization of polyesters composed of isohexides and aliphatic dicarboxylic acids: effects of isohexide stereoisomerism and dicarboxylic acid chain length, *Polym. Degrad. Stab.* 146 (2017) 174–183.
- [10] T. Konishi, Y. Miyamoto, Crystallization of poly(butylene terephthalate) from the glass, *Macromolecules.* 43 (2010) 375–383.
- [11] J. Ma, X. Yu, J. Xu, Y. Pang, Synthesis and crystallinity of poly(butylene 2,5-furandicarboxylate), *Polymer.* 53 (2012) 4145–4151.
- [12] H.G.. Van Melick, L.E. Govaert, H.E.H. Meijer, On the origin of strain hardening in glassy polymers, *Polymer.* 44 (2003) 2493–2502.
- [13] Robertson, G. L, *Food packaging-principles and practice*, 3rd ed., Taylor & Francis, 2013.
- [14] R. Crétois, N. Follain, E. Dargent, J. Soulestin, S. Bourbigot, S. Marais, L. Lebrun, Poly (3-hydroxybutyrate-co-4-hydroxybutyrate) based nanocomposites: influence of the microstructure on the barrier properties, *Phys. Chem. Chem. Phys.* 17 (2015) 11313–11323.
- [15] S.K. Burgess, D.S. Mikkilineni, D.B. Yu, D.J. Kim, C.R. Mubarak, R.M. Kriegel, W.J. Koros, Water sorption in poly(ethylene furanoate) compared to poly(ethylene terephthalate) part 1: equilibrium sorption, *Polymer.* 55 (2014) 6861–6869.
- [16] S.W. Lasoski, W.H. Cobbs, Moisture permeability of polymers. I. Role of crystallinity and orientation, *J. Polym. Sci.* 36 (1959) 21–33.

- [17] S. Marais, Q.T. Nguyen, C. Devallencourt, M. Metayer, T.U. Nguyen, P. Schaetzel, Permeation of water through polar and nonpolar polymers and copolymers: determination of the concentration-dependent diffusion coefficient, *J. Polym. Sci. Part B Polym. Phys.* 38 (2000) 1998–2008.
- [18] M. Matsuguchi, S. Umeda, Y. Sadaoka, Y. Sakai, Characterization of polymers for a capacitive-type humidity sensor based on water sorption behavior, *Sensors Actuators, B Chem.* 49 B49 (1998) 179–185.
- [19] N. Follain, S. Belbekhouche, J. Bras, G. Siqueira, S. Marais, A. Dufresne, Water transport properties of bio-nanocomposites reinforced by *Luffa cylindrica* cellulose nanocrystals, *J. Memb. Sci.* 427 (2013) 218–229.
- [20] S. Alix, E. Philippe, A. Bessadok, L. Lebrun, C. Morvan, S. Marais, Effect of chemical treatments on water sorption and mechanical properties of flax fibres, *Bioresour. Technol.* 100 (2009) 4742–4749.
- [21] A. Marzec, P.P. Lewicki, Antiplasticization of cereal-based products by water. Part I. Extruded flat bread, *J. Food Eng.* 73 (2006).
- [22] Y.P. Chang, A. Abd Karim, C.C. Seow, Interactive plasticizing–antiplasticizing effects of water and glycerol on the tensile properties of tapioca starch films, *Food Hydrocoll.* 20 (2006).
- [23] J.A. Barrie, B. Platt, The diffusion and clustering of water vapour in polymers, *Polymer.* 4 (1963) 303–313.
- [24] R. Shi, Q. Liu, D. Tao, H. Yanming, Z. Liqun, C. Dafu, T. Wei, Aging of soft thermoplastic starch with high glycerol content, *J. Appl. Polym. Sci.* 116 (2006) 574–586.
- [25] F. Gouanvé, S. Marais, A. Bessadok, D. Langevin, M. Métayer, Kinetics of water sorption in flax and PET fibers, *Eur. Polym. J.* 43 (2007) 586–598.
- [26] A. Bessadok, S. Roudesli, S. Marais, N. Follain, L. Lebrun, Alfa fibres for unsaturated polyester composites reinforcement: effects of chemical treatments on mechanical and permeation properties, *Compos. Part A Appl. Sci. Manuf.* 40 (2009) 184–195.
- [27] S. Belbekhouche, J. Bras, G. Siqueira, C. Chappey, L. Lebrun, B. Khelifi, S. Marais, A. Dufresne, Water sorption behavior and gas barrier properties of cellulose whiskers and microfibrils films, *Carbohydr. Polym.* 83 (2011) 1740–1748.
- [28] R.R. Light, R.W. Seymour, Effect of sub-T<sub>g</sub> relaxations on the gas transport properties of polyesters, *Polym. Eng. Sci.* 22 (1982) 857–864.
- [29] S.K. Burgess, J.E. Leisen, B.E. Kraftschik, C.R. Mubarak, R.M. Kriegel, W.J. Koros, Chain mobility, thermal, and mechanical properties of poly(ethylene furanoate) compared to poly(ethylene terephthalate), (2014) 1383–1391.
- [30] M. Salame, S. Steingiser, Barrier polymers, *Polym. Plast. Technol. Eng.* 8 (1977) 155–175.
- [31] V. Detallante, D. Langevin, C. Chappey, M. Métayer, R. Mercier, M. Pinéri, Water vapor sorption in naphthalenic sulfonated polyimide membranes, *J. Memb. Sci.* 190 (2001) 227–241.
- [32] D.W. Van Krevelen, K. Te Nijenhuis, *Properties of polymers*, 4th ed., Elsevier, 2009.



- [33] S.K. Burgess, G.B. Wenz, R.M. Kriegel, W.J. Koros, Penetrant transport in semicrystalline poly(ethylene furanoate), *Polymer*. 98 (2016) 305–310.
- [34] A.S. Michaels, W.R. Vieth, J.A. Barrie, Solution of gases in polyethylene terephthalate, *J. Appl. Phys.* 34 (1963) 1–12.
- [35] J. Trifol, D. Plackett, P. Szabo, A.E. Daugaard, M. Giacinti Baschetti, Effect of crystallinity on water vapor sorption, diffusion, and permeation of PLA-based nanocomposites, *ACS Omega*. 5 (2020) 15362–15369.
- [36] L. Shao, T.S. Chung, S.H. Goh, K.P. Pramoda, Polyimide modification by a linear aliphatic diamine to enhance transport performance and plasticization resistance, *J. Memb. Sci.* 256 (2005) 46–56.
- [37] S.K. Burgess, R.M. Kriegel, W.J. Koros, Carbon dioxide sorption and transport in amorphous poly(ethylene furanoate), *Macromolecules*. 48 (2015) 2184–2193.
- [38] S.K. Burgess, O. Karvan, J.R. Johnson, R.M. Kriegel, W.J. Koros, Oxygen sorption and transport in amorphous poly(ethylene furanoate), *Polymer*. 55 (2014) 4748–4756.
- [39] J.E. Mark, *Physical properties of polymers handbook*, 2nd ed., Springer, 1958.

---

## Chapter 4

- ✧ **Copolyesters derived from 1,4:3,6-dianhydrohexitols or 2,6-pyridinedicarbonyl: synthesis, thermal, mechanical and permeation properties** ✧
-



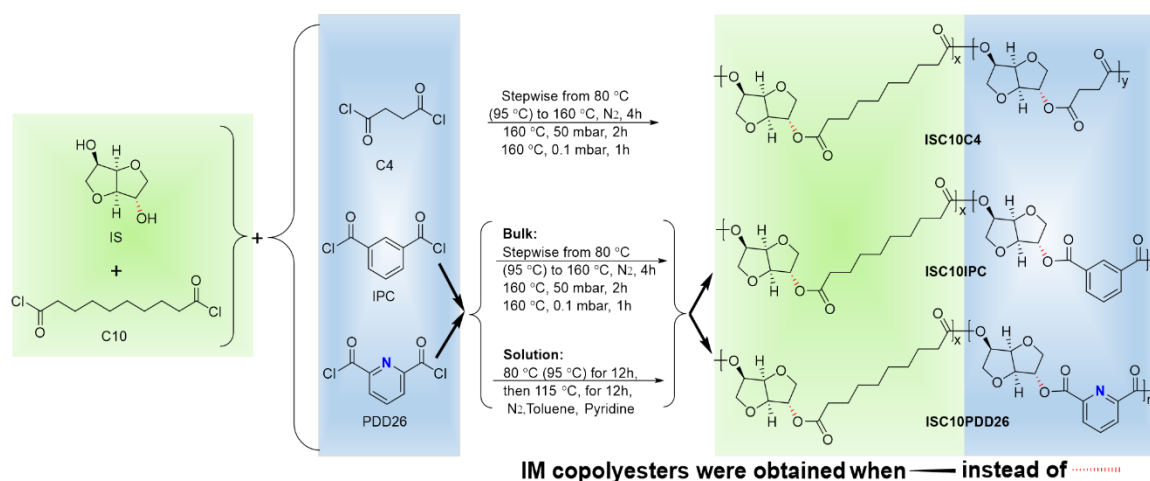
As stated in Chapter 2 and Chapter 3, the semi-crystalline ISC10 (and to a lesser extent IMC10) and PDD26-DD could be good candidates for food packaging applications. However, the low glass transition temperature brought by the long flexible chain (C10 or DD) may be a limitation for their barrier properties. Copolymerization with rigid (cyclic or aromatic) moieties and/or shorter aliphatic segments is usually considered as an effective strategy to obtain polyesters with enhanced  $T_g$  [1–4]. Taking advantage of the results presented in the previous two Chapters, and intending to strengthen the understanding of the barrier properties of those mentioned structures, it first appeared to us that the aromatic structures (PDD26, PDD25, and IPC) investigated in Chapter 3 were interesting as rigid moieties for partially replacing C10. Nevertheless, the unavailability of PDD25 monomer made us finally focus on PDD26 and IPC. Furthermore, Chapter 2 emphasized that C4 can also be a good aliphatic candidate due to the highest  $T_g$  of the corresponding polyesters ISC4 and IMC4. Thus, the acid dichlorides chosen to partially replace C10 were C4, PDD26, and IPC. For the same reason, the diols IS and EG were selected to partially replace DD.

Thus, copolyesters based on ISC10, IMC10 and PDD26-DD were synthesized. Depending on the incorporated moiety, this Chapter will be divided into two parts: in part I, the copolyesters based on ISC10 and IMC10 with rigid acid dichlorides (C4, IPC and PDD26); in part II, the copolyesters based on PDD26-DD with the EG and IS as rigid diol.

## **4.I ISC10 and IMC10 based copolyesters**

### **4.I.1 Synthesis**

Copolyesters with an aliphatic comonomer (ISC10C4 and IMC10C4) were synthesized according to the bulk method already described in Chapter 2 and detailed in Annex 1.5 and Scheme 4-1. The molar masses of the copolyesters along with their dispersities (the corresponding chromatograms were given in Annex 4) and the precipitation yields were presented in Table 4-1.

**Scheme 4-1** Synthesis of IS and IM copolyesters

ISC10C4 ( $\overline{M}_n = 18\,000\text{ g}\cdot\text{mol}^{-1}$ ) showed comparable molar masses to ISC10 ( $\overline{M}_n = 18\,500\text{ g}\cdot\text{mol}^{-1}$ ) but IMC10C4 was lower ( $\overline{M}_n = 13\,000\text{ g}\cdot\text{mol}^{-1}$ ) than IMC10 ( $\overline{M}_n = 19\,000\text{ g}\cdot\text{mol}^{-1}$ ). This was probably due to the decreased reactivity observed in Chapter 2 between IM and C4 which afforded lower molar masses for IMC4.

The copolymerizations involving aromatic moieties were much more difficult to achieve in bulk since their rigidity reduced chain-ends mobility [5]. Taking ISC10PDD26 as an example, the bulk method afforded only low molar masses ( $\overline{M}_n = 4\,300\text{ g}\cdot\text{mol}^{-1}$ ). Thus, the synthesis with toluene as solvent in the presence of pyridine (method established in the previous Chapter) was tried (Scheme 4-1). The best results regarding molar masses were presented in Table 4-1. The higher molar masses obtained with IS compared to IM were probably due to the higher reactivity of IS [6]. Unfortunately, a general decrease in molar masses observed when incorporating aromatic moieties, such as IPC and PDD26, confirmed the difficulty already encountered in producing high molar masses polyesters with 1,4:3,6-dianhydrohexitols and aromatic compounds [6]. High yields of around 90% were obtained for all copolyesters.

**Table 4-1** Molar masses of polyesters and yields of syntheses

Copolyester	$\overline{M}_n^{1)}$ (g·mol <sup>-1</sup> )	$\overline{M}_w^{1)}$ (g·mol <sup>-1</sup> )	$D^{2)}$	Yield <sup>3)</sup> (%)
ISC10C4	18 000	33 600	1.87	91
ISC10IPC	15 300	44 000	2.88	90
ISC10PDD26	11 500	26 900	2.34	85
IMC10C4	13 000	24 700	1.90	89
IMC10IPC	11 000	27 300	2.48	89
IMC10PDD26	10 600	24 200	2.28	86

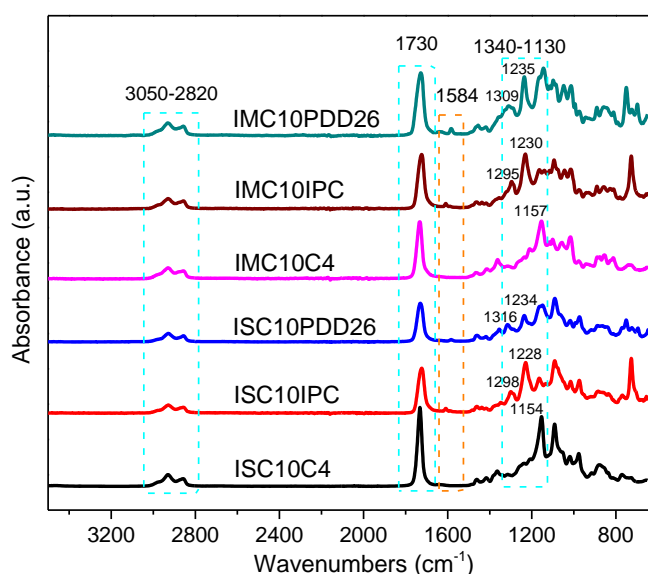
<sup>1)</sup> SEC conducted in CH<sub>2</sub>Cl<sub>2</sub> with PMMA standards. <sup>2)</sup> dispersity. <sup>3)</sup> in precipitated polymer.

## 4.I.2 Characterization of polyesters

### 4.I.2.1 Structures

#### 4.I.2.1.1 FTIR analysis

The chemical structures of the above-mentioned copolyesters with the highest molar masses were first characterized by FTIR in Figure 4-1. The C=O and C-O of ester groups stretching at 1730 and 1340-1130  $\text{cm}^{-1}$ , respectively, first confirmed the successful esterification. Then, the successful copolymerizations were confirmed by the appearance of the functional group signals of the different components: the  $\text{CH}_2$  stretching at 3050-2820  $\text{cm}^{-1}$ , the aromatic C=C stretching at 1584  $\text{cm}^{-1}$ , the ester C-O stretching for aromatics at 1309, 1295, 1316, 1298  $\text{cm}^{-1}$ , and for the aliphatics at 1235, 1230, 1157, 1234, 1228 and 1154  $\text{cm}^{-1}$ .



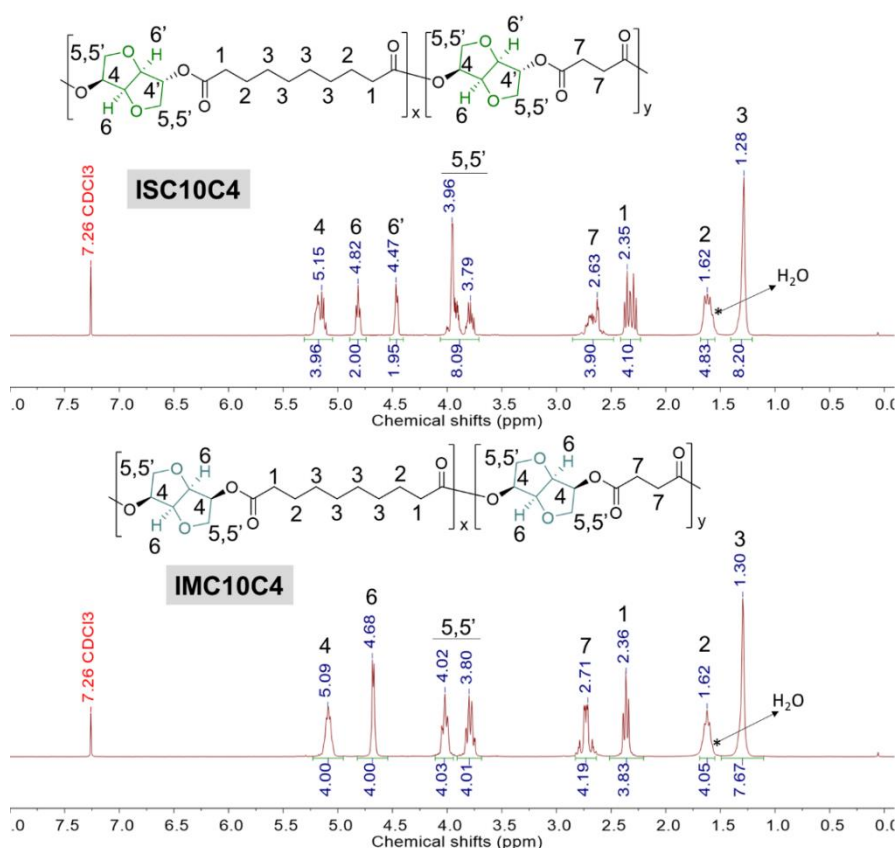
**Figure 4-1** FTIR spectra of copolyesters

#### 4.I.2.1.2 $^1\text{H}$ NMR analysis

The chemical structures were further confirmed by  $^1\text{H}$  NMR and the corresponding spectra were listed in Annex 5 except for ISC10C4 and IMC10C4, which were shown in Figure 4-2.

All proton signals were found at the expected chemical shifts observed in Chapter 2. The integrations globally corresponded to the different comonomers, except the one at 1.62 ppm which was sometimes higher than expected due to the presence of water at 1.56 ppm (denoted

as \*). The more split spectrum of ISC10C4 was due to the exo-endo stereoscopic effect of IS, which induced an irregular structure [7]. Besides, the more complex and split spectra of aromatic copolyesters compared to aliphatic ones (Annex 5) was probably due to a structural difference between aliphatics and aromatics which induced distinct environments for hydrogens in IS and IM. The molar ratio of each component in the polymer was calculated by considering the total proton integrations of each comonomer (except for ISC10C4 and IMC10C4, only H1 and H3 were considered for C10 because of residual water) in Table 4-2.



**Figure 4-2**  $^1\text{H}$  NMR spectra of ISC10C4 and IMC10C4

**Table 4-2** Calculated monomer ratios in polymers

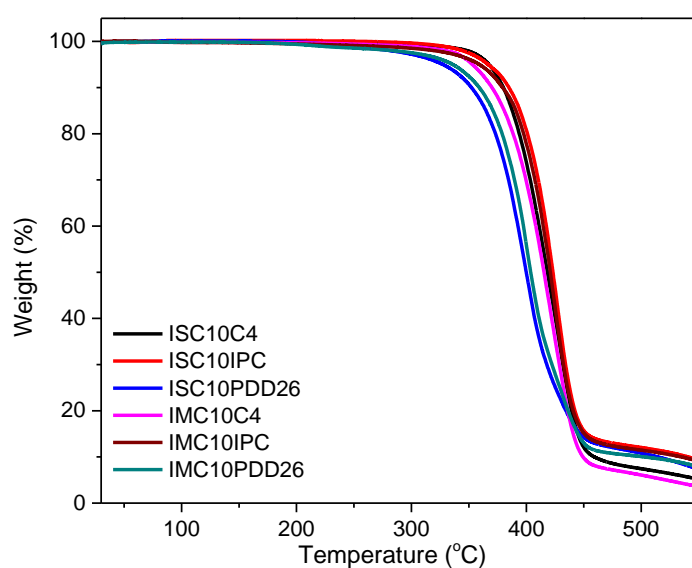
Copolyester	X:C10:Y molar ratio in feeding	X:C10:Y molar ratio in polymer <sup>1)</sup>
ISC10C4	100:50:50	100:51:49
ISC10IPC	100:50:50	100:51:49
ISC10PDD26	100:50:50	100:70:30
IMC10C4	100:50:50	100:48:52
IMC10IPC	100:50:50	100:51:49
IMC10PDD26	100:50:50	100:55:45

<sup>1)</sup> Calculated from  $^1\text{H}$  NMR; X is the diol (IS or IM); Y is the co-acid dichloride.

In general, the molar ratio in the polymer was almost the feeding molar ratio. Considering the reactions were conducted on a small-scale, a slight difference in the monomer weighing cannot be ruled out. Controlling the accuracy of the feeding ratio to ensure the targeted stoichiometric ratio is a challenging factor. However, some bigger differences were observed when using PDD26, which may be linked to its lower reactivity.

#### 4.I.2.2 Thermal degradation

Figure 4-3 showed the thermal stability of copolyesters analyzed by thermogravimetric analysis (TGA) and the corresponding data were recorded in Table 4-3.



**Figure 4-3** TGA thermograms of copolyesters

All copolyesters appeared to be thermally stable up to 330 °C with less than 5% weight loss. The copolyesters containing C4 and IPC showed higher thermal degradation temperatures compared to those containing PDD26, which was consistent with that already observed in Chapter 3 for IPC-DD and PDD26-DD. No important difference could be noticed between the use of IS or IM.

**Table 4-3** Thermal degradation data recorded from TGA

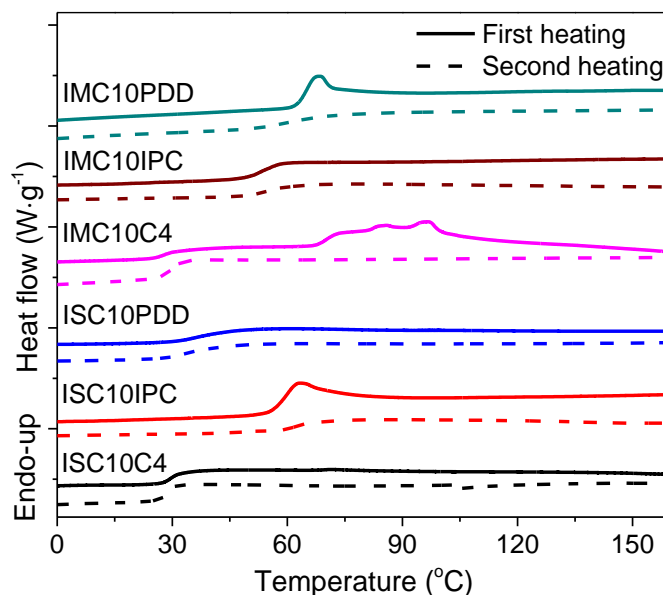
Polyester	$T_{5\%}$ (°C)	$T_{\max}$ (°C)	Polyester	$T_{5\%}$ (°C)	$T_{\max}$ (°C)
ISC10C4	370	428	IMC10C4	354	422
ISC10IPC	369	427	IMC10IPC	361	424
ISC10PDD26	328	398	IMC10PDD26	338	400

$T_{5\%}$ , 5% weight loss temperature;  $T_{\max}$ , maximum degradation rate temperature.



### 4.I.2.3 Differential scanning calorimetry (DSC)

The DSC thermograms of copolyesters were presented in Figure 4-4 and the corresponding  $T_g$ ,  $T_m$  and  $\Delta H_m$  values were recorded in Table 4-4.



**Figure 4-4** DSC thermograms of copolyesters

All copolyesters showed increased  $T_g$  (sometimes with an enthalpic relaxation peak resulting from the thermal history [8,9]) compared to ISC10 ( $T_g = 2$  °C) and IMC10 ( $T_g = 0$  °C). As mentioned in Chapter 2, the stereoscopic difference between IS and IM had little influence on  $T_g$ , nevertheless, some changes could be observed in these copolymers. Considering that ISC10IPC and IMC10IPC had the same molar composition in comonomers (Table 4-2), the higher  $T_g$  of ISC10IPC could be linked to its higher molar mass (Table 4-1). On the contrary, ISC10PDD26 and IMCPDD26 had similar molar masses, but IMC10PDD26 incorporated a much higher amount of PDD26, thus leading to a higher  $T_g$ . Finally, the same  $T_g$  measured for ISC10C4 and IMC10C4 was a cooperation result of molar mass and monomer ratio.

On another side, a higher  $T_g$  was systematically obtained by incorporating aromatic moieties. Excluding ISC10PDD26 which had a low content of PDD26, the pyridine ring ( $T_g = 64$  °C for IMC10PDD26) was more efficient in improving  $T_g$  than the benzene ring ( $T_g = 55$  °C for IMC10IPC). To sum up, the highest  $T_g$  was obtained for IMC10PDD26.

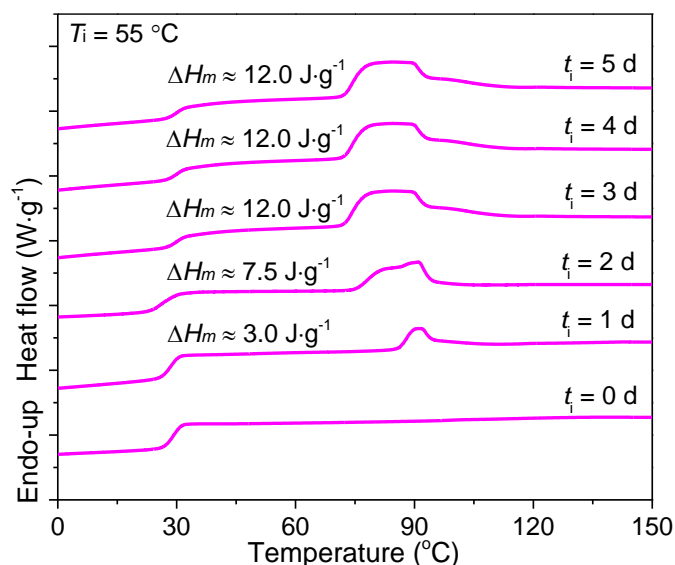
Unfortunately, as one could expect, the incorporation of comonomers prevented the polymers to crystallize, except IMC10C4 which exhibited a melting with  $\Delta H_m = 12 \text{ J}\cdot\text{g}^{-1}$ . Its multiple melting peaks ( $T_m = 74/84/96 \text{ }^\circ\text{C}$ ) with a wide melting range was probably due to the crystallization polymorphism coupling with a melting/crystallization/re-melting process, which is a common trait of linear polyesters comprising both semi-rigid and flexible chains [7,10]. However, the absence of melting on the DSC second heating indicated the difficulty encountered to reorganize the molecular chain orderly from the melt [11].

**Table 4-4** Thermal properties of copolyesters

Copolyester	$T_g^a$ ( $^\circ\text{C}$ )	$T_m^b$ ( $^\circ\text{C}$ )	$\Delta H_m^b$ ( $\text{J}\cdot\text{g}^{-1}$ )	Copolyester	$T_g^a$ ( $^\circ\text{C}$ )	$T_m^b$ ( $^\circ\text{C}$ )	$\Delta H_m^b$ ( $\text{J}\cdot\text{g}^{-1}$ )
ISC10C4	30	-	-	IMC10C4	30	74/84/96*	12
ISC10IPC	61	-	-	IMC10IPC	55	-	-
ISC10PDD26	40	-	-	IMC10PDD26	64	-	-

<sup>a</sup> DSC second heating; <sup>b</sup> DSC first heating; \* multiple peaks.

The crystallization behavior of IMC10C4 was further investigated by isothermal crystallization after a first melting at  $150 \text{ }^\circ\text{C}$ , intended to provide basic information for subsequent polymer film preparation. The isothermal crystallization carried out at  $T_i = 55 \text{ }^\circ\text{C}$  for 0 to 5 days ( $t_i$ ) was presented in Figure 4-5. After a broadening of the endothermic peak and an increase of the melting enthalpy, the crystallization seemed to reach its final state after three days at  $55 \text{ }^\circ\text{C}$ .

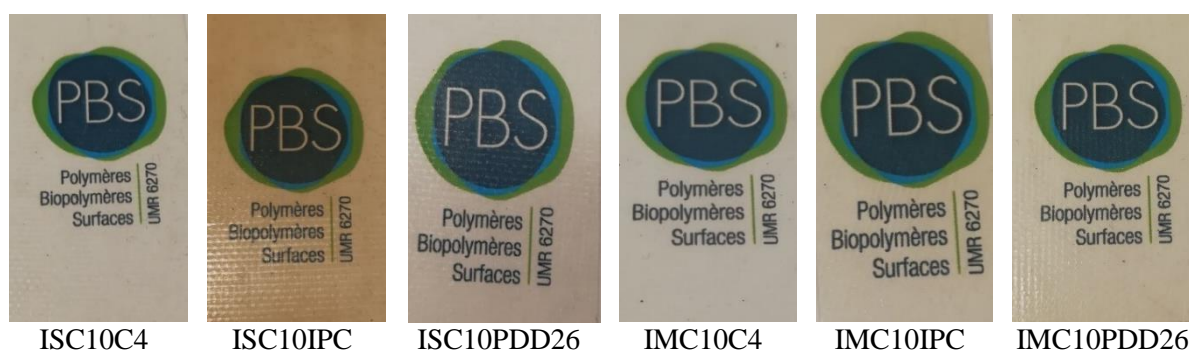


**Figure 4-5** DSC thermograms of IMC10C4: isotherm at  $55 \text{ }^\circ\text{C}$  for an indicated time

### 4.I.3 Characterization of copolyester films

#### 4.I.3.1 Hot pressing

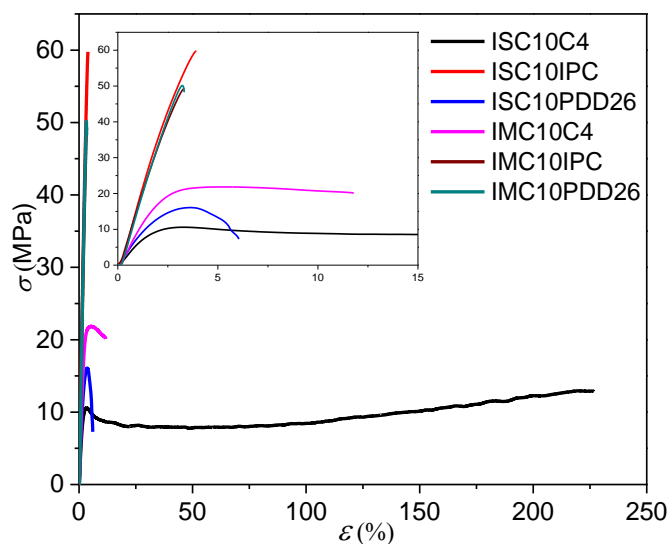
The polymer films shown in Figure 4-6 were prepared by hot pressing according to their thermal properties established by DSC, and then stored at room temperature in dry atmosphere (Annex 2). Due to the slow recrystallization rate of IMC10C4, it was isothermally crystallized at 55 °C for 3 days (DSC thermogram, XRD pattern and POM image presented in Annex 6, 7 and 8, respectively) before storage. All films exhibited good transparency.



**Figure 4-6** Copolyester films prepared by hot pressing

#### 4.I.3.2 Mechanical properties

The representative tensile curves of polymer films were shown in Figure 4-7 and the corresponding tensile parameters were recorded in Table 4-5.



**Figure 4-7** Stress-strain curves of copolyester films

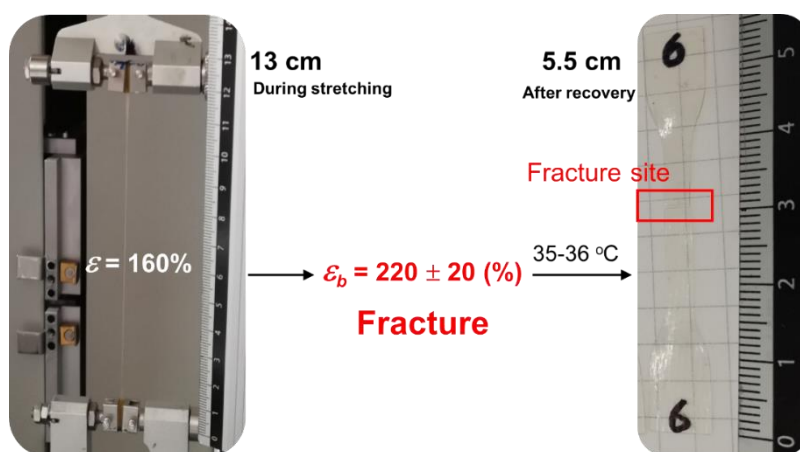
Figure 4-7 disclosed brittle fracture for semi-aromatic copolyesters and plastic fracture for aliphatic ones. The incorporation of rigid comonomers, as C4, IPC and PDD26, naturally increased the stiffness ( $E$  increased at least 6 times) and the tensile strength ( $\sigma_b$  increased at least 3 times) of ISC10 ( $E = 127 \pm 20$  MPa,  $\sigma_b = 4.2 \pm 0.8$  MPa,  $\varepsilon_b = 19 \pm 5$  %) and IMC10 ( $E = 125 \pm 10$  MPa,  $\sigma_b = 1.0 \pm 0.2$  MPa,  $\varepsilon_b = 16 \pm 3$  %), but decreased the elongation at break (except ISC10C4 which will be discussed later). This phenomenon was even more observed for IPC and PDD26 (but to a lesser extent for ISC10PDD26 due to its lower PDD26 content) compared to C4: the aromatic moieties brought more chain stiffness, strength, and brittleness. Furthermore, despite a lower molar mass, IMC10C4 showed higher  $E$  (1180 MPa) and  $\sigma_b$  (21.0 MPa) and restricted elongation at break ( $\varepsilon_b = 12\%$ ) compared to ISC10C4, certainly due to its crystallinity.

**Table 4-5** Tensile parameters of copolyester films

Polyester film	$E$ (MPa)	$\sigma_b$ (MPa)	$\varepsilon_b$ (%)
ISC10C4	$770 \pm 90$	$11.8 \pm 1.1$	$220 \pm 20$
ISC10IPC	$2100 \pm 50$	$59.0 \pm 1.7$	$3.6 \pm 0.4$
ISC10PDD26	$850 \pm 80$	$8.0 \pm 2.6$	$6.0 \pm 1.5$
IMC10C4	$1180 \pm 80$	$21.0 \pm 2.7$	$12.0 \pm 1.0$
IMC10IPC	$1820 \pm 30$	$50.0 \pm 1.7$	$3.0 \pm 0.3$
IMC10PDD26	$1900 \pm 40$	$50.0 \pm 1.2$	$3.0 \pm 0.4$

$E$ , Young's modulus;  $\sigma_b$ , stress at break;  $\varepsilon_b$ , strain at break.

However, ISC10C4 presented a very particular behavior. Indeed, the incorporation of C4 in ISC10C4 not only brought a much higher  $E$  (770 MPa vs 127 MPa) and  $\sigma_b$  (11.8 MPa vs 4.2 MPa) compared to ISC10, but also largely increased  $\varepsilon_b$  (220% vs 19%). The increased  $E$  and  $\sigma_b$  was probably due to the increased  $T_g$ , above room temperature, while the increased  $\varepsilon_b$  may be related to its high molar mass coupled with a  $T_g$  close to the ambient temperature, thus even a slight localized heating due to the tensile stress could favor chain disentanglement [12,13]. Another interesting phenomenon was observed for ISC10C4: the stretched sample, even after being broken at its maximum elongation (220%), recovered almost its original dimensions (5 cm) after being placed around the body external temperature (35-36 °C), as seen in Figure 4-8.



**Figure 4-8** Body external temperature triggered shape recovery of ISC10C4

#### 4.I.3.3 Contact angle

The surface energy  $\gamma^t$  (with dispersive  $\gamma^d$  and polar parts  $\gamma^p$ ) and water contact angle values of copolyester films were gathered in Table 4-6.

**Table 4-6** Surface energies and water contact angles of copolyester films

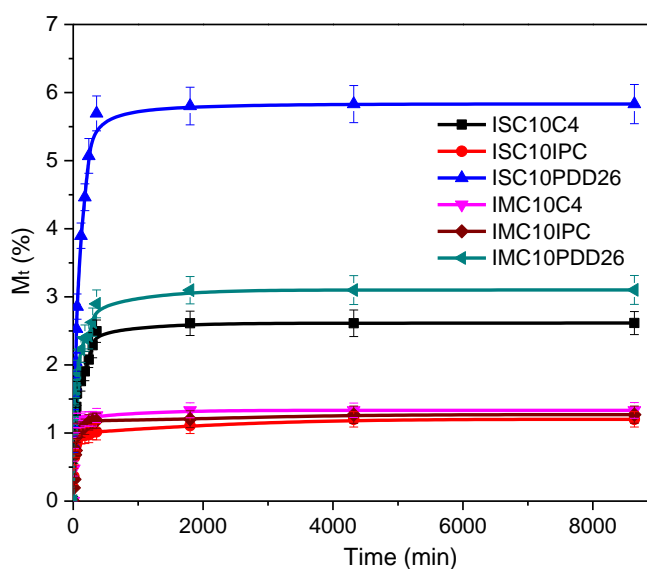
Polyester films	$\gamma^t$ (mN·m <sup>-1</sup> )	$\gamma^d$ (mN·m <sup>-1</sup> )	$\gamma^p$ (mN·m <sup>-1</sup> )	$\theta_w$ (°)
ISC10C4	28.8	23.4	5.4	86 ± 1.7
ISC10IPC	28.6	23.2	5.4	87 ± 1.2
ISC10PDD26	30.5	24.2	6.3	84 ± 1.5
IMC10C4	28.8	23.3	5.5	86 ± 0.8
IMC10IPC	28.3	23.1	5.2	87 ± 1.0
IMC10PDD26	31.2	24.3	6.9	83 ± 1.3

$\gamma^t$ , Total surface energy with dispersive ( $\gamma^d$ ) and polar ( $\gamma^p$ ) parts;  $\theta_w$ , water contact angle.

The copolyesters showed no obvious difference in surface properties compared to ISC10 ( $\gamma^t = 31.0$  mN·m<sup>-1</sup>,  $\theta_w = 85 \pm 1.0^\circ$ ) and IMC10 ( $\gamma^t = 29.6$  mN·m<sup>-1</sup>,  $\theta_w = 83 \pm 0.5^\circ$ ). Only a slightly lower  $\theta_w$  (or higher  $\gamma^t$ ) was observed for ISC10PDD26 and IMC10PDD26 compared to other copolyesters, probably due to the presence of polar pyridine sites.

#### 4.I.3.4 Liquid water sorption

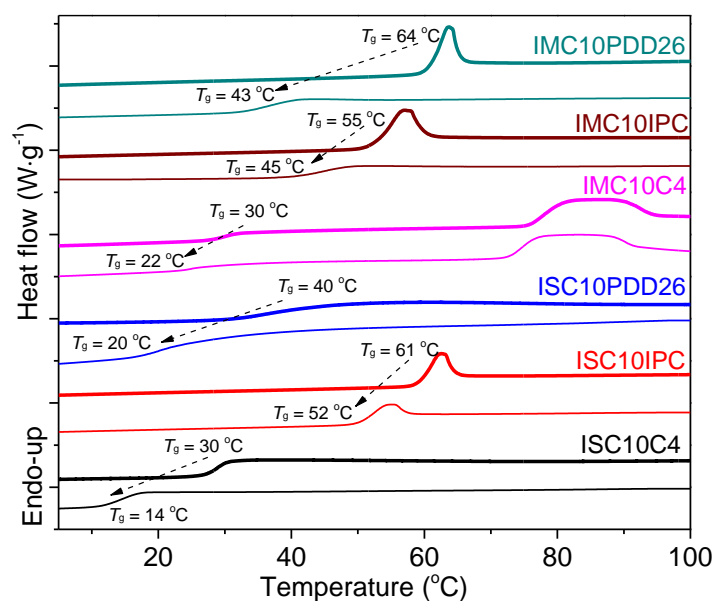
Figure 4-9 presented the liquid water sorption results. All copolyesters showed increased liquid water sorption compared to ISC10 ( $M_{eq} = 0.55 \pm 0.05$  %) and IMC10 ( $M_{eq} = 1.03 \pm 0.09$  %) due to their large amorphous domain that probably allowed a larger water uptake [14]. ISC10PDD26 ( $M_{eq} = 5.8 \pm 0.5$  %) and IMC10PDD26 ( $M_{eq} = 3.1 \pm 0.3$  %) showed the higher liquid water sorption, which could be explained by the hydrophilic pyridine sites in the polymer films. However, the higher water uptake of ISC10PDD26 compared to IMC10PDD26 was unexpected since ISC10PDD26 contained less pyridine moieties (30 mol % for ISC10PDD26, 45 mol % for IMC10PDD26). It should be mentioned that water sorption in polyesters is complex since water molecules show great interactions with the polymer matrix [15]. Thereby, the sorption of water molecules in polymers can lead to dimensional changes, through the swelling of the polymer matrix, and the decrease of the glass transition temperature ( $T_g$ ) [16], which will in turn result in larger water sorption [15,17].



**Figure 4-9** Liquid water sorption of copolyester films

Thus, the effect of liquid water sorption on  $T_g$  for ISC10PDD26 and IMC10PDD26 was checked by DSC measurements (Figure 4-10).  $T_g$  after sorption ( $T_{g, H_2O}$ ) for ISC10PDD26 ( $T_{g, H_2O} = 20$  °C) was below the experimental temperature ( $T = 25$  °C), while for IMC10PDD26 ( $T_{g, H_2O} = 43$  °C) it retained above 25 °C. Even if  $T_{g, H_2O}$  for both ISC10PDD26 and IMC10PDD26 was decreased by 20 °C, the high initial  $T_g$  of IMC10PDD26 (64 °C) allowed its  $T_{g, H_2O}$  to stay above 25 °C, contrary to ISC10PDD26. The lower  $T_{g, H_2O}$  of ISC10PDD26 than 25 °C meant

the sample was in rubber state with larger free volume, which allowed higher water uptake [18,19].



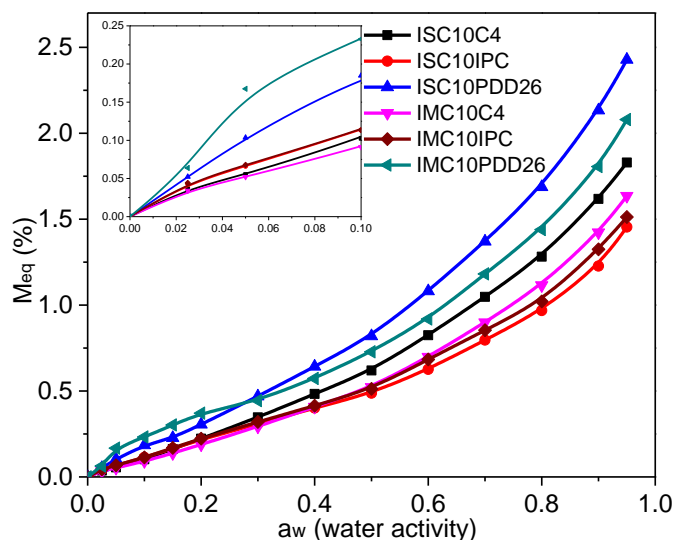
**Figure 4-10** DSC thermograms of copolyester films before (bold) and after (fine line) liquid water sorption

More generally, we noticed that all samples showed a decreased  $T_g$  after water sorption, which is known as water-induced plasticization [20–23]. For ISC10IPC, IMC10IPC and IMC10PDD26, their high initial  $T_g$  allowed preserving their glassy state because their final  $T_{g-H_2O}$  stayed above 25 °C, contrary to ISC10C4, ISC10PDD26 and IMC10C4. IMC10C4, IMC10IPC and ISC10IPC showed better resistance to water plasticization with a lower decrease of  $T_g$ . Consequently, the liquid water sorption was less pronounced for them (Figure 4-9). The nonpolar aromatic benzene ring in IPC and the semi-crystalline nature of IMC10C4 can explain this behavior.

Finally, combining the changes in  $T_g$  with the water sorption behavior, we can conclude that the ability to resist water plasticization is an important factor determining the water sorption of these glassy state copolyesters.

#### 4.I.3.5 Dynamic vapor sorption

The water vapor sorption isotherms of copolyester films were presented in Figure 4-11.



**Figure 4-11** Water vapor sorption isotherms of copolyester films

All copolyesters showed an increase of water vapor sorption compared to ISC10 and IMC10 (*e.g.*  $M_{eq} = 0.58\%$  and  $M_{eq} = 1.08\%$  at water activity  $a_w = 0.95$ , respectively). The values at  $a_w = 0.95$  followed the same order as observed for liquid water sorption with the highest sorption value for ISC10PDD26 and the lowest for ISC10IPC. All isotherms displayed sigmoid profiles and obeyed the three steps of Park's model. The corresponding Park's model parameters were gathered in Table 4-7. At  $a_w < 0.1$ , typical Langmuir-type sorption is related to the adsorption of water molecules onto specific hydrophilic sites, such as polar groups or micro-voids on the surface of films [24]. At this  $a_w$ , ISC10PDD26 and IMC10PDD26 showed higher sorption with larger  $b_L$  values compared to other copolyesters due to their hydrophilic pyridine sites. The higher Langmuir constants of ISC10IPC compared to ISC10C4 is related to the Langmuir sites of the former ( $A_L = 1.20$  vs  $A_L = 0.55$ ). A possible explanation could be found in their structure: even though the whole benzene ring is a non-polar structure, the IPC ring has a dipolar moment greater than the C4 unit. The lowest Langmuir-type sorption of IMC10C4 was probably due to the presence of crystallites that reduced the value of  $A_L$  [15,27,28]. When the preferential sites were occupied, the isotherms became linear owing to random dissolution / diffusion (Henry's type sorption) of water molecules in the polymer matrix [29]. The solubility coefficients  $S$  (analogous to  $k_H$  in Table 4-7) can be then calculated from the slope of the linear part ( $a_w = 0.2-0.7$ ) of isotherms. The large  $S$  values for ISC10PDD26 ( $S = 10.6 \times 10^{-3} \text{ g}_{\text{H}_2\text{O}}/\text{g}_{\text{pol}}$ ) and IMC10PDD26 ( $S = 8.1 \times 10^{-3} \text{ g}_{\text{H}_2\text{O}}/\text{g}_{\text{pol}}$ ) were reasonable due to their hydrophilic pyridine sites. ISC10IPC ( $S = 6.3 \times 10^{-3} \text{ g}_{\text{H}_2\text{O}}/\text{g}_{\text{pol}}$ ) and IMC10IPC ( $S = 5.8 \times 10^{-3}$



$g_{H_2O}/g_{pol}$ ) showed lower solubility compared to ISC10C4 ( $S = 8.3 \times 10^{-3} g_{H_2O}/g_{pol}$ ) and IMC10C4 ( $S = 7.1 \times 10^{-3} g_{H_2O}/g_{pol}$ ), which was contrary to their Langmuir-type sorption. This was probably due to a larger water-induced polymer swelling for the latter [15,17], which has been previously discussed for the liquid water sorption. At  $a_w > 0.7$ , an exponential increase of sorbed water concentration was observed due to the formation of water aggregates.  $K_a$  values were larger for ISC10PDD26 and IMC10PDD26 indicating more water aggregates but with similar sizes whatever the sample.

It disclosed that ISC10PDD26 and IMC10PDD26 were more hydrophilic than other copolyesters for the whole range of water vapor activity. This was not surprising that polar pyridine sites showed strong affinities to water molecules.

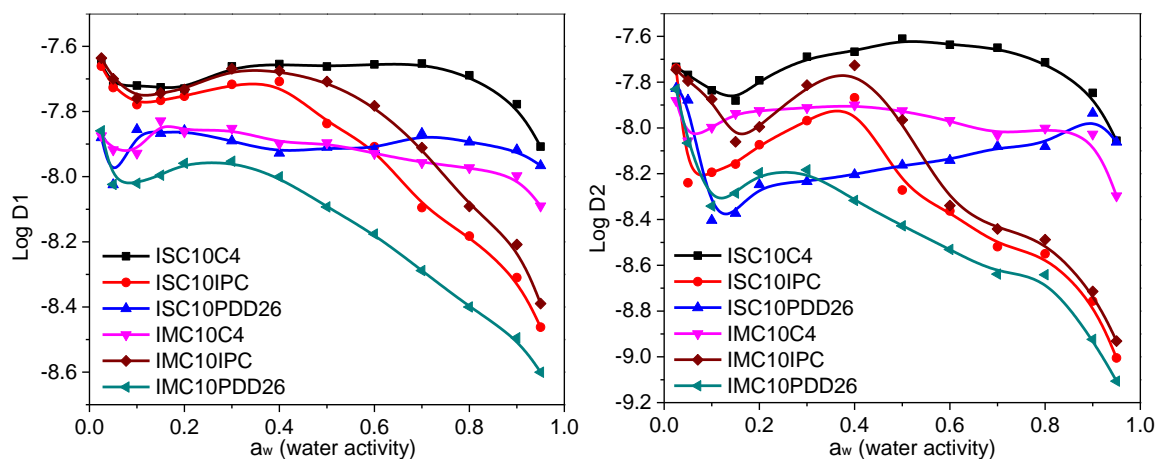
**Table 4-7** Sorption parameters of Park's model

Polyester film	$A_L \times 10^3$ (g/g)	$b_L$	$k_H \times 10^3$ (g/g)	$K_a \times 10^3$ (g/g)	$n_a$
ISC10C4	$0.55 \pm 0.03$	$0.42 \pm 0.01$	$10.6 \pm 1.1$	$0.92 \pm 0.05$	$4.0 \pm 0.1$
ISC10IPC	$1.20 \pm 0.07$	$0.47 \pm 0.04$	$3.9 \pm 0.2$	$0.85 \pm 0.03$	$4.0 \pm 0.2$
ISC10PDD26	$0.55 \pm 0.05$	$3.00 \pm 0.20$	$15.5 \pm 1.3$	$1.32 \pm 0.13$	$3.0 \pm 0.1$
IMC10C4	$0.35 \pm 0.02$	$0.40 \pm 0.01$	$9.0 \pm 0.5$	$0.87 \pm 0.04$	$4.0 \pm 0.1$
IMC10IPC	$1.30 \pm 0.09$	$0.50 \pm 0.03$	$3.7 \pm 0.2$	$0.80 \pm 0.03$	$5.0 \pm 0.2$
IMC10PDD26	$0.12 \pm 0.01$	$38.4 \pm 2.0$	$10.4 \pm 0.9$	$1.00 \pm 0.07$	$4.0 \pm 0.1$

$A_L$ , Langmuir's capacity constant ;  $b_L$ , Langmuir affinity constant;  $k_H$ , Henry's type solubility coefficient;  $K_a$ , equilibrium constant for clustering reaction;  $n_a$ , average number of water molecules per cluster.

To evaluate the water vapor sorption kinetics, the evolution of water diffusion coefficients,  $D_1$  and  $D_2$ , in semi-logarithmic scale ( $\log D$ ) as a function of water activity for copolyester films was reported in Figure 4-12. The diffusion coefficients evolution generally followed three steps: a decrease followed by an increase and a final decrease. Considering the presence of "oxygen" atoms in IS and IM structure, the first decrease in  $D$  values was probably due to water molecules interactions with the polar "oxygen" atoms in IS and IM, leading to hydrogen bonds that increase the cohesion between polymer chains, and then reduce the water mobility ("antiplasticizing effect") [30–32]. Then, water reverted to its role as a typical plasticizer, thus a subsequent increase in  $D$  values was observed [30]. The final decrease in  $D$  was due to water molecule clustering [30,33,34]. These behaviors were indicative of water sorption mechanism complying with Park's model: part of the water was adsorbed on specific sites (low mobility of the fixed water molecules) and the rest dissolved according to Henry's process (higher mobility of the dissolved molecules) later forming aggregates at a high water activity (low mobility of the aggregates) [30].

The highest  $D$  values for ISC10C4 was probably due to its lowest resistance to swelling and the lowest  $D$  values for IMC10PDD26 perhaps to its high resistance to swelling, besides the polar pyridine sites reduced water mobility. Usually,  $D$  values are considered to increase with the local permeant concentration in polymer films during water penetration (well-known plasticizing effect) [30,33,35]. It was observed that  $D$  values of ISC10IPC, IMC10IPC and IMC10PDD26 increased in a narrow  $a_w$  range and decreased immediately after the maximum. This behavior indicated a strong resistance to water plasticization of these polymer films [36]. In contrast, ISC10PDD26 showed a prolonged ( $a_w = 0.1-0.9$ ) increase in  $D_2$  values, which indicated a continuous swelling of the polymer matrix. This variation of  $D$  was generally attributed to an increase of free volume due to the plasticization effect [37,38]. The low ability to resist swelling can be used to explain the higher water vapor sorption of ISC10PDD26 than IMC10PDD26, which is consistent with their liquid water sorption. The presence of crystallites in IMC10C4, on the one hand, stabilized the film from swelling and on the other hand, increased diffusion tortuosity, thus IMC10C4 showed lower  $D$  values than ISC10C4. For selected  $a_w$ , larger  $D$  values for ISC10IPC and IMC10IPC compared to IMC10PDD26 was probably due to the higher inter/intrachain attractions in the latter which brought more compact microstructures [39,40]. In addition, the polar pyridine sites will also reduce the mobility of water molecules, and then decrease  $D$  values [41]. The lowest water vapor sorption of ISC10IPC and IMC10IPC seemed related to their high  $T_g$  and low polarity. An excellent agreement was observed between the two independent (liquid and vapor water) sorption measurement techniques, providing a consistency check for the reported data. These results supported us to conclude that the resistance to swelling, polymer polarity, and crystallinity are three major factors that influenced the water (vapor) sorption of these copolyesters.



**Figure 4-12** Evolution of  $D_1$  and  $D_2$  as a function of  $a_w$

Another observation was that  $D_2$  didn't follow exactly the same profile as  $D_1$ .  $D_2$  value (second half sorption) should be more representative of the diffusion of water in the core of the film, while  $D_1$  (first half sorption) should be more characteristic of the diffusion through the surface [30]. The generally lower  $D_2$  than  $D_1$  values have also been observed in the previous two chapters and is understandable: the diffusion of water was governed by the surface effect (a strong cohesion between the chains to form hydrogen bonds) rather than by the core of the swelling [33].

#### 4.I.3.6 Water vapor permeation

The water barrier properties were further evaluated by water vapor permeation measurements and the corresponding results were given in Table 4-8.

**Table 4-8** Water vapor permeation coefficient ( $P_{H_2O}$ ) of copolyester films at different water activities ( $a_w$ )

Polyester film	$a_w$	$P_{H_2O} \times 10^3$ (g·m <sup>-1</sup> ·d <sup>-1</sup> )	$P_{H_2O}$ (barrer)
ISC10C4	0.35	5.9 ± 0.6	4130 ± 340
	0.86	132 ± 9	79730 ± 5830
	0.94	195 ± 19	118000 ± 9800
ISC10IPC	0.34	1.2 ± 0.1	730 ± 60
	0.63	1.6 ± 0.2	970 ± 80
	0.73	2.1 ± 0.2	1260 ± 110
ISC10PDD26	0.40	6.8 ± 0.7	3570 ± 216
	0.63	34.5 ± 2.8	20930 ± 1950
	0.71	87.6 ± 5.7	53110 ± 4800
IMC10C4	0.50	1.9 ± 0.1	1090 ± 100
	0.65	7.4 ± 0.6	4480 ± 340
	0.89	53.1 ± 4.6	32220 ± 2800
IMC10IPC	0.39	1.3 ± 0.1	770 ± 60
	0.60	1.7 ± 0.2	1050 ± 90
	0.74	2.4 ± 0.2	1440 ± 100
IMC10PDD26	0.55	4.5 ± 0.3	2760 ± 210
	0.67	4.8 ± 0.4	2900 ± 270
	0.75	4.8 ± 0.4	2930 ± 270

All copolyesters showed reduced water vapor permeabilities ( $P_{\text{H}_2\text{O}}$ ) compared to ISC10 ( $P_{\text{H}_2\text{O}} = 5.10 \text{ g}\cdot\text{m}^{-1}\cdot\text{d}^{-1}$  at  $a_w = 0.65$ ) and IMC10 ( $P_{\text{H}_2\text{O}} = 5.95 \text{ g}\cdot\text{m}^{-1}\cdot\text{d}^{-1}$  at  $a_w = 0.60$ ), which was probably due to the increased  $T_g$ . The water vapor permeation results were different from the water (vapor) sorption results. Taking IS samples as examples, the  $P_{\text{H}_2\text{O}}$  values at  $a_w \cong 0.35$  were ISC10C4 ( $P_{\text{H}_2\text{O}} = 4130$  barrer) > ISC10PDD26 ( $P_{\text{H}_2\text{O}} = 3570$  barrer). To explain this behavior, we should keep in mind that permeation ( $P$ ) is a result of dissolution ( $S$ ) and diffusion ( $D$ ). Thus, even if a higher  $S$  value was obtained for ISC10PDD26, the much lower  $D$  value (Figure 4-12) resulted in a lower  $P$  value. The high  $P_{\text{H}_2\text{O}}$  values over the entire water activity range for both ISC10C4 and ISC10PDD26 could be attributed to the polymer swelling. It is surprising to obtain a large  $P_{\text{H}_2\text{O}}$  value for IMC10C4 because this polyester is semi-crystalline. This could be explained by its low  $T_g$  that decreased in presence of water (Figure 4-10) and consequently induced large swelling at high  $a_w$  values. The  $P_{\text{H}_2\text{O}}$  values of ISC10IPC, IMC10IPC, and IMC10PDD26 were generally lowest and constant, which validated the ability to resist swelling of these polymers. The higher  $P_{\text{H}_2\text{O}}$  values of IMC10PDD26 compared to ISC10IPC and IMC10IPC could be due to the higher water solubility brought by polar pyridine sites. Then the lowest  $P_{\text{H}_2\text{O}}$  values for ISC10IPC and IMC10IPC seemed reasonable, due to their resistance to swelling and low polarity. Thus, we can generally conclude that the  $T_g$  and polarity of these copolyesters were the two dominant factors that influence their water vapor permeation behaviors.

#### 4.I.3.7 Gas permeation

As described in Annex 3, the gas permeation was conducted under differential pressure (upstream pressure  $p_1 = 4$  bar and downstream compartment initially under vacuum). However, IMC10IPC and IMC10PDD26 were not resistant enough to the experimental pressure. Consequently, a PDMS membrane was used as support to assist their gas permeation measurements. In this case,  $D$  values cannot be accurately calculated by the time-lag method, thus only permeation coefficients ( $P$ ) were discussed for these samples. Their  $P$  values were calculated according to the law of resistors in series  $\frac{P_t}{l_t} = \frac{P}{l} + \frac{P_{\text{PDMS}}}{l_{\text{PDMS}}}$ , where  $P_t$  and  $l_t$  are the total permeability and thickness,  $P_{\text{PDMS}}$  and  $l_{\text{PDMS}}$  are the permeability and thickness of PDMS membrane,  $P$  and  $l$  are the permeability and thickness of the tested film. The gas permeation coefficients ( $P$ ) for  $\text{N}_2$ ,  $\text{O}_2$  and  $\text{CO}_2$  were presented in Table 4-9.

**Table 4-9** Gas permeation coefficients ( $P$ ) of copolyester films

Polyester film	$P$ (barrer)		
	N <sub>2</sub>	O <sub>2</sub>	CO <sub>2</sub>
ISC10C4	0.085 ± 0.006	0.161 ± 0.011	0.63 ± 0.04
ISC10IPC	0.045 ± 0.003	0.079 ± 0.005	0.40 ± 0.03
ISC10PDD26	0.043 ± 0.003	0.077 ± 0.005	0.37 ± 0.02
IMC10C4	0.019 ± 0.001	0.042 ± 0.003	0.26 ± 0.02
IMC10IPC	0.051 ± 0.003	0.096 ± 0.007	0.59 ± 0.04
IMC10PDD26	0.014 ± 0.001	0.025 ± 0.002	0.12 ± 0.01

$P$  expressed in barrer (1 barrer =  $10^{-10}$  cm<sup>3</sup> STP·cm·cm<sup>-2</sup>·s<sup>-1</sup>·cmHg<sup>-1</sup>).

Even with the loss of crystallinity, all copolyesters showed increased gas barrier properties (decreased  $P$  values) compared to ISC10 ( $P_{N_2}$  = 0.09 barrer,  $P_{O_2}$  = 0.26 barrer,  $P_{CO_2}$  = 1.32 barrer) and IMC10 ( $P_{N_2}$  = 0.18 barrer,  $P_{O_2}$  = 0.46 barrer,  $P_{CO_2}$  = 2.04 barrer). This was due to the increase of  $T_g$  values for all copolyesters: their glassy state at 25 °C (experimental temperature) allowed limited chain movements for the gas penetration. All copolyesters showed  $P$  values following the well-known order reported by Van Krevelen [42]:  $P_{N_2} < P_{O_2} < P_{CO_2}$ . This ranking is a result of the double dependence of permeability on diffusivity, mainly on the kinetic diameter of permeants ( $d_{N_2}$  (0.364 nm) >  $d_{O_2}$  (0.346 nm) >  $d_{CO_2}$  (0.33 nm)), and solubility, mainly on the critical temperature of permeants ( $T'_{c (CO_2)}$  (31 °C) >  $T'_{c (O_2)}$  (-118 °C) >  $T'_{c (N_2)}$  (-147 °C)) [19].

It is known that the large sorption of CO<sub>2</sub> molecules will plasticize a glassy polymer matrix [43–45]. However, CO<sub>2</sub> ( $T'_{c (CO_2)}$  = 31 °C) is much less condensable than water ( $T'_{c (H_2O)}$  = 374 °C), thus the plasticization by CO<sub>2</sub> usually needs high feeding pressure (depending on the polymer, but usually > 10 bar) [46]. Considering the low CO<sub>2</sub> feeding pressure (3 bar) in our case, the CO<sub>2</sub> plasticization effect will be ignored in our discussion.

It should always be kept in mind that  $P$  is a combined result of  $D$  (obtained by time-lag method) and  $S$  (deduced from  $P$  and  $D$  coefficients), any factor that affects  $D$  and  $S$  can consequently influence  $P$ . To support our discussion, the  $S$  and  $D$  values of ISC10C4, ISC10IPC, ISC10PDD26, and IMC10C4 were provided in Table 4-10.

**Table 4-10** Gas solubility and diffusion coefficients ( $S$  and  $D$ ) of IS copolyester films and IMC10C4 film

	$D \times 10^{10} (\text{cm}^2 \cdot \text{s}^{-1})$			$S \times 10^3 (\text{cm}^3(\text{STP}) \cdot \text{cm}^{-3} \cdot \text{cmHg}^{-1})$		
	N <sub>2</sub>	O <sub>2</sub>	CO <sub>2</sub>	N <sub>2</sub>	O <sub>2</sub>	CO <sub>2</sub>
ISC10C4	9.4 ± 0.6	16 ± 1	76 ± 5	9.0 ± 0.6	10.1 ± 0.6	8.3 ± 0.7
ISC10IPC	4.9 ± 0.3	8.2 ± 0.6	48 ± 3	9.2 ± 0.7	9.6 ± 0.6	8.3 ± 0.6
ISC10PDD26	4.5 ± 0.3	6.8 ± 0.5	28 ± 2	9.5 ± 0.7	11.3 ± 0.8	13.3 ± 0.9
IMC10C4	2.5 ± 0.2	5.4 ± 0.4	35 ± 2	7.7 ± 0.5	7.8 ± 0.6	7.4 ± 0.5

Then, the influence of the following factors on the gas permeation properties was discussed:

- (1) Main chain type (aliphatic vs aromatic): the incorporation of aromatic moieties (ISC10IPC and ISC10PDD26) was generally more efficient in increasing gas barrier properties than the aliphatic one (ISC10C4). This was probably due to the higher chain stiffness which caused lower mobility of chain segments, thus creating diffusion restriction [40].
- (2) Structurally different aromatic moieties (*m*-phenylene ring vs 2,6-pyridine ring): the lower  $P$  values for ISC10PDD26 and IMC10PDD26 compared to ISC10IPC and IMC10IPC indicated the 2,6-pyridine ring structure brought more barrier properties. This result is highly consistent with those discussed in Chapter 3 for PDD26-DD and IPC-DD. However, in Chapter 3, it was explained by their difference in crystallinity. Considering that the copolyesters were amorphous, the lower gas permeability for ISC10PDD26 and IMC10PDD26 seemed due to the polar pyridine ring which induced chain-chain (inter/intrachain) attractions, thus allowing a close chain-chain packing and restricting chain segmental motions [47]. Similarly, the higher PDD26 incorporation ratio could explain the higher gas barrier properties of IMC10PDD26 compared to ISC10PDD26.
- (3) Crystallinity: semi-crystalline IMC10C4 was more barrier ( $P_{\text{N}_2} = 0.019$  barrer,  $P_{\text{O}_2} = 0.04$  barrer,  $P_{\text{CO}_2} = 0.26$  barrer) than amorphous ISC10C4 ( $P_{\text{N}_2} = 0.084$  barrer,  $P_{\text{O}_2} = 0.12$  barrer,  $P_{\text{CO}_2} = 0.59$  barrer), which was expected since crystallites are generally impermeable to gases [48–50]. This explanation was verified by both lower  $S$  and  $D$  values for IMC10C4.

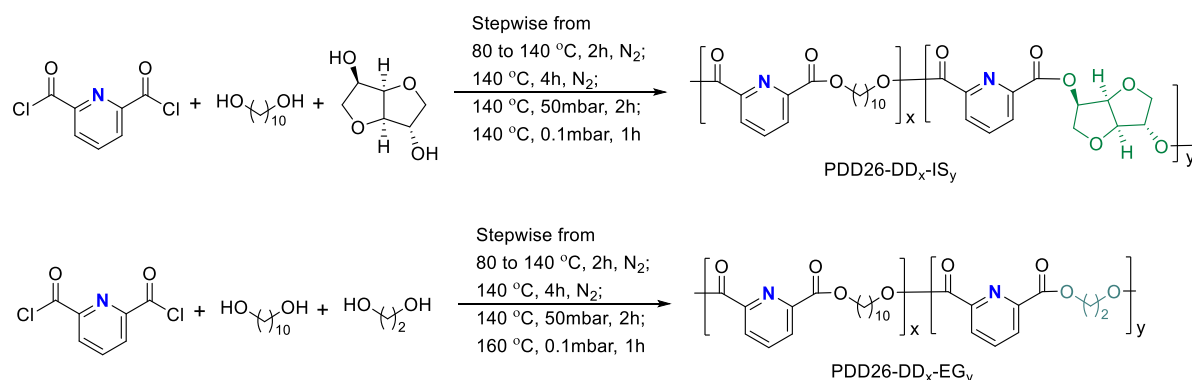
- (4) Exo/endo stereoscopy: even if ISC10IPC showed slightly higher gas barrier properties than IMC10IPC, we cannot generally conclude that the exo/endo stereoscopic structure of IS was more barrier to gases than the endo-endo stereoscopic structure of IM, because the higher chain entanglement caused by the larger molar masses of ISC10IPC also decreases gas permeability.

To sum up, the increased  $T_g$  effectively decreased the gas permeability of IS and IM polyesters, and retaining crystallinity is a supplemental positive factor. At the same time, regardless of the semi-crystalline nature of IMC10C4, the chemical structures of the introduced rigid moieties showed the abilities ( $A_p$ ) to decrease  $P$  values in the order  $A_p(\text{PDD26}) > A_p(\text{IPC}) > A_p(\text{C4})$ . Moreover, all the synthesized copolyesters showed better gas barrier properties than the common food packaging materials, such as PE ( $P_{\text{N}_2} = 0.14\text{-}1.9$  barrer,  $P_{\text{O}_2} = 0.6\text{-}6.7$  barrer and  $P_{\text{CO}_2} = 1.7\text{-}28$  barrer), PP ( $P_{\text{N}_2} = 0.44$  barrer,  $P_{\text{O}_2} = 0.9\text{-}2.3$  barrer and  $P_{\text{CO}_2} = 9.2$  barrer), oriented PS ( $P_{\text{N}_2} = 0.29\text{-}0.78$  barrer,  $P_{\text{O}_2} = 1.1\text{-}2.7$  barrer and  $P_{\text{CO}_2} = 8.8\text{-}10.5$  barrer) and PC ( $P_{\text{O}_2} = 1.5$  barrer and  $P_{\text{CO}_2} = 6.4$  barrer) [40]. Furthermore, IMC10PDD26 showed better gas barrier than PLA containing 98% L-lactide ( $P_{\text{N}_2} = 4.99$  barrer,  $P_{\text{O}_2} = 0.11\text{-}0.56$  barrer and  $P_{\text{CO}_2} = 1.88$  barrer) [40] and comparable  $\text{O}_2$  and  $\text{CO}_2$  barrier to semi-crystalline PET ( $P_{\text{O}_2} = 0.018\text{-}0.030$  barrer and  $P_{\text{CO}_2} = 0.12\text{-}0.16$  barrer). Such efficient gas barrier properties for IMC10PDD26 seemed related to its 2,6-pyridine ring, which has been discussed in Chapter 3.

## 4.II PDD26-DD copolyesters

### 4.II.1 Synthesis

PDD26-DD based copolyesters were synthesized analogously to PDD26-DD in bulk, as shown in Scheme 4-2, using several feeding ratios. Detailed procedures were referred to Annex 1.7.



**Scheme 4-2** Synthesis of PDD26-DD copolyesters

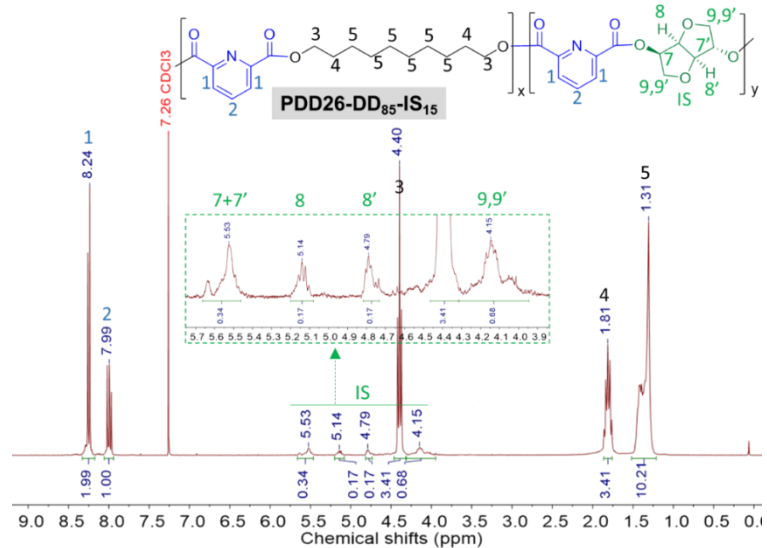
### 4.II.2 Characterization of copolyesters

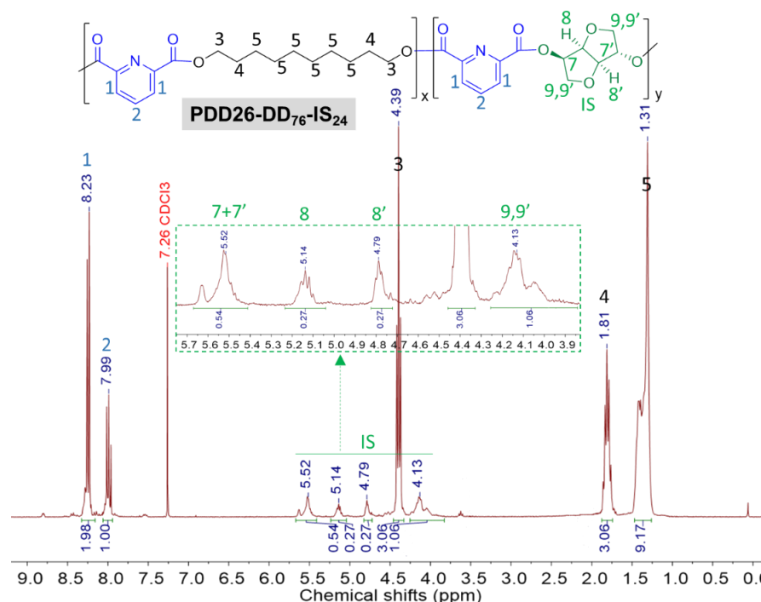
#### 4.II.2.1 <sup>1</sup>H NMR analysis

The structures of the obtained copolyesters were evaluated by <sup>1</sup>H NMR as shown in Figure 4-13. Using the previous Chapters, all proton signals confirmed the targeted structures, and the intense and well-defined integrations H2 for PDD26 and H5 for DD enabled to determine the composition of the copolymers (IS and EG amount were deduced), which were always close to the feeding ratios (Table 4-11). All copolyesters were subsequently named according to their monomer ratio in the polymer as PDD26-DD<sub>x</sub>-X<sub>y</sub>.

The spectrum of PDD26-DD<sub>33</sub>-EG<sub>67</sub> showed two extra proton signals at 4.65 and 3.83 ppm, which could correspond to CH<sub>2</sub>CH<sub>2</sub>OH end-groups.







**Figure 4-13**  $^1\text{H}$  NMR Spectra of PDD26-DD<sub>33</sub>-EG<sub>67</sub> and PDD26-DD<sub>x</sub>-IS<sub>y</sub>

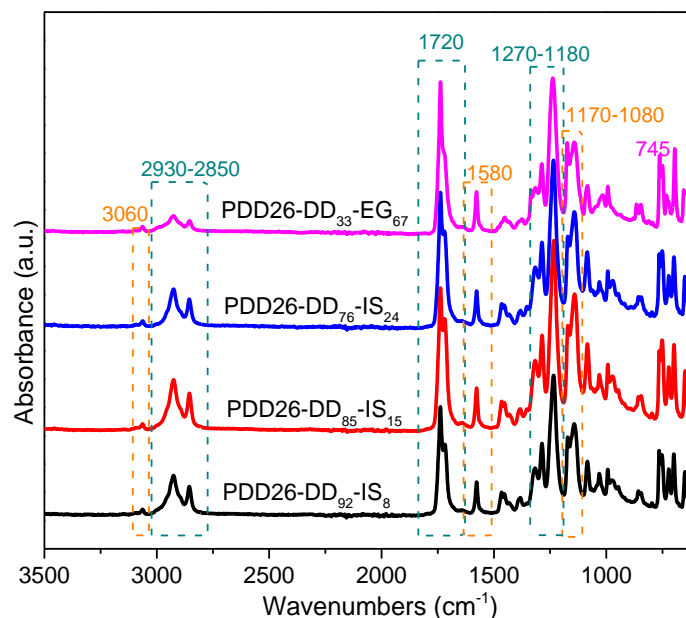
**Table 4-11** PDD26-DD<sub>x</sub>-X<sub>y</sub> copolyesters

Copolyester	PDD26:DD:X molar ratio in feeding	PDD26:DD:X molar ratio in polymer <sup>1)</sup>
PDD26-DD-IS	100:90:10	100:92:8
	100:80:20	100:85:15
	100:70:30	100:76:24
PDD26-DD-EG	100:30:70	100:33:67

X means IS or EG; <sup>1)</sup> calculated from  $^1\text{H}$  NMR spectra.

#### 4.II.2.2 FTIR analysis

Figure 4-14 showed the FTIR spectra with the expected bands: the ester C=O and C-O stretching signals appeared at 1720 and 1270-1180  $\text{cm}^{-1}$  respectively. Furthermore, C-H stretching vibrations at 2930  $\text{cm}^{-1}$  (asymmetrical) and 2850  $\text{cm}^{-1}$  (symmetrical), and C-H stretching and C-H out-of-plane deformation vibrations of the pyridine ring were observed at 3060 and 745  $\text{cm}^{-1}$  respectively. All copolyesters showed signals at 1580 and 1170-1080  $\text{cm}^{-1}$ , which were assignable to C=C plus C=N skeletal vibrations and C-N stretching signals of the pyridine ring, respectively.



**Figure 4-14** FTIR spectra of PDD26-DD<sub>x</sub>-IS<sub>y</sub> and PDD26-DD<sub>33</sub>-EG<sub>67</sub>

#### 4.II.2.3 SEC analysis

The molar masses of the copolyesters were evaluated by SEC, and the corresponding results were recorded in Table 4-12 (chromatograms referred to Annex 4). The molar masses of PDD26-DD<sub>x</sub>-IS<sub>y</sub> were strongly influenced by the feeding ratio: the more the IS, the lower the molar mass. This could be explained by the lower reactivity of IS [6]. The low molar mass of PDD26-DD<sub>33</sub>-EG<sub>67</sub> confirmed the difficulty encountered to obtain high molar masses with PDD26 and EG (PDD26-EG was already discussed in Chapter 3). The complex distribution, with two populations, was highly consistent with that obtained for PDD26-EG, and the lower one probably corresponded to cyclic species [51,52]. The variation in yields was probably due to the higher solubility of the low molar mass components [52].

**Table 4-12** Molar masses of copolyesters and yields of syntheses

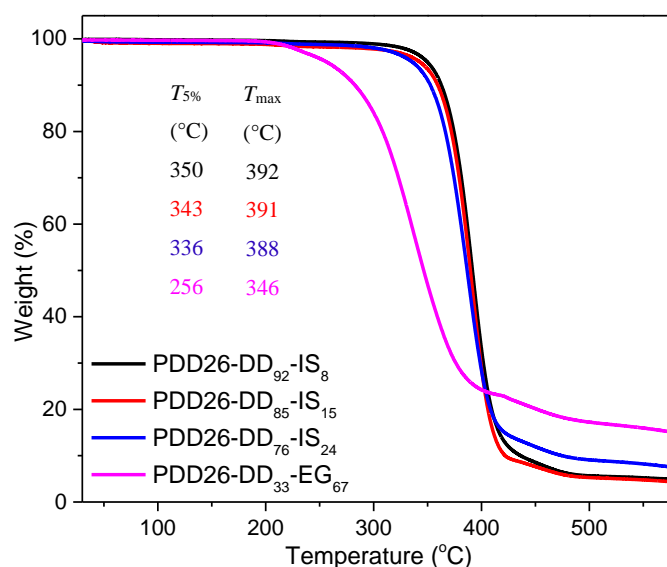
Copolyester	$\overline{M}_n^{1)}$ (g·mol <sup>-1</sup> )	$\overline{M}_w^{1)}$ (g·mol <sup>-1</sup> )	$\overline{D}^{2)}$	Yield <sup>3)</sup> (%)
PDD26-DD <sub>92</sub> -IS <sub>8</sub>	17 100	38 100	2.23	90
PDD26-DD <sub>85</sub> -IS <sub>15</sub>	11 100	24 300	2.19	83
PDD26-DD <sub>76</sub> -IS <sub>24</sub>	4 000	8 000	2.00	76
PDD26-DD <sub>33</sub> -EG <sub>67</sub>	2 700/320	4 100/330	1.51/1.00	66

<sup>1)</sup> SEC conducted in CH<sub>2</sub>Cl<sub>2</sub> with PMMA standards; <sup>2)</sup> dispersity; <sup>3)</sup> in precipitated polymer.

#### 4.II.2.4 Thermal degradation

The thermal stability of the copolyesters was analyzed by TGA as shown in Figure 4-15.

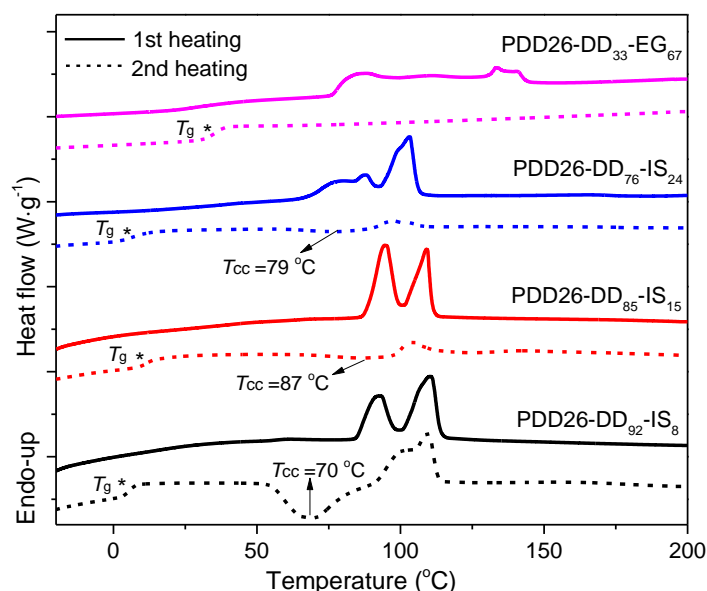
All PDD26-DD<sub>x</sub>-IS<sub>y</sub> copolyesters appeared thermally stable up to 336 °C and showed similar thermal decomposition profiles. PDD26-DD<sub>92</sub>-IS<sub>8</sub> and PDD26-DD<sub>85</sub>-IS<sub>15</sub> showed higher thermal stability with even much lower molar masses than PDD26-DD ( $T_{5\%} = 341$  °C,  $T_{\max} = 384$  °C), suggesting a higher thermal stability brought by IS. It seemed the lower the molar mass, the lower  $T_{5\%}$  and  $T_{\max}$ :  $T(\text{PDD26-DD}_{92}\text{-IS}_8) > T(\text{PDD26-DD}_{85}\text{-IS}_{15}) > T(\text{PDD26-DD}_{76}\text{-IS}_{24})$ . PDD26-DD<sub>33</sub>-EG<sub>67</sub> was much less stable than PDD26-DD, which could be linked to its very low molar mass.



**Figure 4-15** TGA thermograms of PDD26-DD<sub>x</sub>-IS<sub>y</sub> and PDD26-DD<sub>33</sub>-EG<sub>67</sub>

#### 4.II.2.5 Differential scanning calorimetry (DSC)

The thermal behavior of copolyesters was investigated by DSC as shown in Figure 4-16 and Table 4-13.



**Figure 4-16** DSC thermograms of PDD26-DD<sub>x</sub>-IS<sub>y</sub> and PDD26-DD<sub>33</sub>-EG<sub>67</sub>

PDD26-DD<sub>x</sub>-IS<sub>y</sub> copolyesters were quite similar during the first heating, with close melting temperatures ( $\sim 100$  °C) and enthalpies ( $\sim 30$  J·g<sup>-1</sup>), and multiple or prolonged melting explainable by a crystallization polymorphism coupled with a melting/crystallization/remelting as discussed in Chapter 3. PDD26-DD<sub>33</sub>-EG<sub>67</sub> showed a very complex and broad endotherm, which could hardly be linked with a classical melting. Every copolyester revealed the difficulty to crystallize from the melt (cooling presented in Annex 6). Only PDD26-DD<sub>92</sub>-IS<sub>8</sub> exhibited an important cold crystallization.

**Table 4-13** Thermal properties of copolyesters

Copolyester	First heating		Second heating				
	$T_m$ (°C)	$\Delta H_m$ (J·g <sup>-1</sup> )	$T_g$ (°C)	$T_{cc}$ (°C)	$\Delta H_{cc}$ (J·g <sup>-1</sup> )	$T_m$ (°C)	$\Delta H_m$ (J·g <sup>-1</sup> )
PDD26-DD <sub>92</sub> -IS <sub>8</sub>	92/110	32.3	6	70	22.6	102/110	21.9
PDD26-DD <sub>85</sub> -IS <sub>15</sub>	94/109	32.1	12	87	2.6	104	3.1
PDD26-DD <sub>76</sub> -IS <sub>24</sub>	79/88/103	28.2	8	79	2.0	97	2.3
PDD26-DD <sub>33</sub> -EG <sub>67</sub>	75-146*	30.5	35	-	-	-	-

$T_g$ , glass transition temperature;  $T_m$ , melting temperature;  $T_c$ , crystallization temperature;  $T_{cc}$ , cold crystallization temperature;  $\Delta H_m$ , melting enthalpy;  $\Delta H_c$ , crystallization enthalpy;  $\Delta H_{cc}$ , cold crystallization enthalpy; \*large melting range.

Determined on the DSC second heating, the  $T_g$  of all copolyesters was higher than PDD26-DD ( $T_g = 0\text{ }^{\circ}\text{C}$ ). According to Storbeck *et al.* [53], the incorporation of 6 mol% isosorbide was enough to increase the  $T_g$  of PBT by  $10\text{ }^{\circ}\text{C}$ . Our result was close but lower, which was probably due to the decreased molar mass of PDD26-DD<sub>92</sub>-IS<sub>8</sub> ( $\overline{M}_n = 17\,100\text{ g}\cdot\text{mol}^{-1}$ ) compared to PDD26-DD ( $\overline{M}_n = 24\,500\text{ g}\cdot\text{mol}^{-1}$ ).  $T_g$  continued to increase with PDD26-DD<sub>85</sub>-IS<sub>15</sub>, despite its lower molar mass, but finally decreased with the too low PDD26-DD<sub>76</sub>-IS<sub>24</sub>. Consequently, the highest  $T_g$  of PDD26-DD<sub>x</sub>-IS<sub>y</sub> was limited to  $12\text{ }^{\circ}\text{C}$ . Despite its very low molar mass, PDD26-DD<sub>33</sub>-EG<sub>67</sub> gave a much higher  $T_g$ , which might be explained by the much higher EG ratio in the polymer.

### 4.II.3 Characterization of films

#### 4.II.3.1 Preparation of films

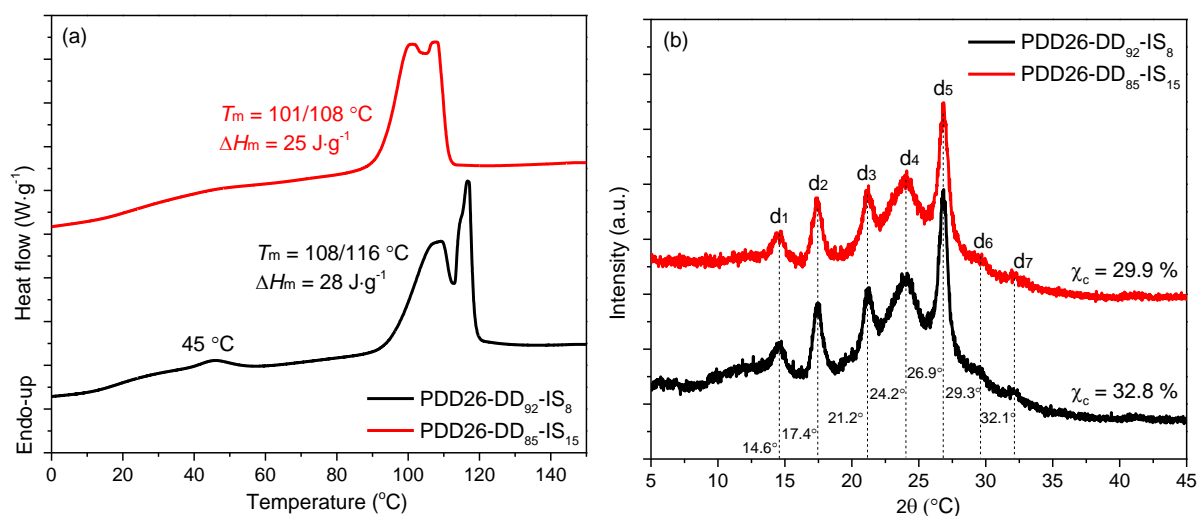
The films were prepared by hot pressing according to their melting temperatures determined by DSC. It was not surprising that the films from PDD26-DD<sub>76</sub>-IS<sub>24</sub> and PDD26-DD<sub>33</sub>-EG<sub>67</sub> were too brittle after pressing due to their low molar masses. Finally, only the films from PDD26-DD<sub>92</sub>-IS<sub>8</sub> and PDD26-DD<sub>85</sub>-IS<sub>15</sub> were successfully obtained and presented in Figure 4-17. Although these copolyesters did not fulfill the expected increase in  $T_g$ , it was still worth understanding the impact of IS on the mechanical and permeation properties of such materials. Thus, further investigations were focused on these two films.



**Figure 4-17** Films prepared by hot pressing at  $120\text{ }^{\circ}\text{C}$

### 4.II.3.2 Crystallinity of films

The crystallinity of the films was examined by both DSC and XRD (Figure 4-18).



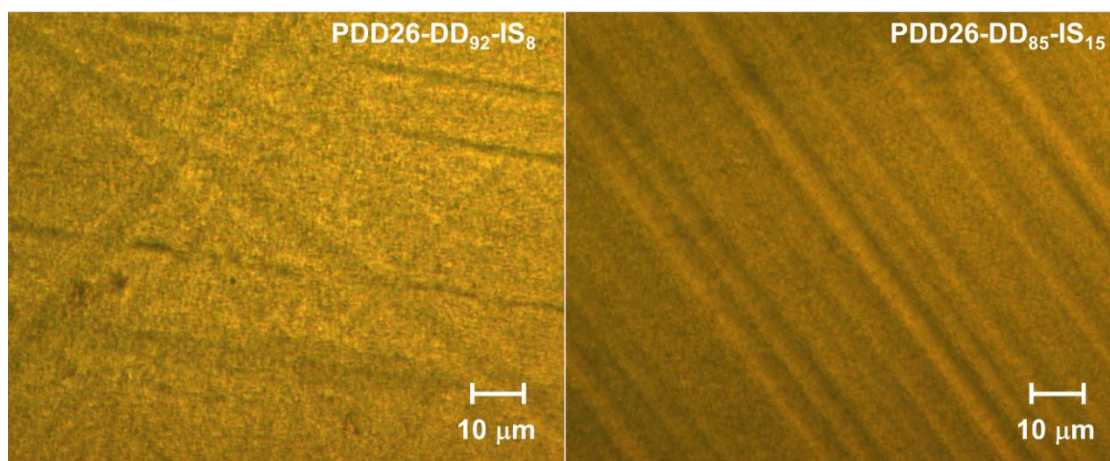
**Figure 4-18** DSC thermograms (a) and XRD patterns (b) of films

Despite the difficult crystallization from the melt observed by DSC, Figure 4-18(a) showed that both PDD26-DD<sub>92</sub>-IS<sub>8</sub> and PDD26-DD<sub>85</sub>-IS<sub>15</sub> films were semi-crystalline and presented complex melting peaks. Besides, PDD26-DD<sub>92</sub>-IS<sub>8</sub> showed a small endotherm at 45 °C, probably due to a melting of secondary lamellae [54], which was already explained in Chapter 3 and verified by DSC isothermal crystallization (Annex 6). Furthermore, both films showed increased melting enthalpies compared to the original polymers (Table 4-13). This was not surprising since the polymer chains in the films could reorganize during a prolonged time (stored more than 7 days before measurements) compared to the time given to the original polymer during DSC analysis (~25 min). The melting enthalpy was lower for PDD26-DD<sub>85</sub>-IS<sub>15</sub> than for PDD26-DD<sub>92</sub>-IS<sub>8</sub>, and both were lower than PDD26-DD (30 J·g<sup>-1</sup>). The XRD patterns in Figure 4-18(b) showed similar profiles to PDD26-DD, indicating similar crystallization units [55,56]. The crystallinity of PDD26-DD<sub>85</sub>-IS<sub>15</sub> ( $\chi_c = 29.9\%$ ) was slightly lower than PDD26-DD<sub>92</sub>-IS<sub>8</sub> ( $\chi_c = 32.8\%$ ), and both of them were lower than PDD26-DD ( $\chi_c = 36.0\%$ ), which was consistent with the melting enthalpies on DSC thermograms, and would give an approximation of  $\Delta H_m^{100\%}$  of 85 and 84 J·g<sup>-1</sup> for PDD26-DD<sub>92</sub>-IS<sub>8</sub> and PDD26-DD<sub>85</sub>-IS<sub>15</sub>, respectively. These



values are very close to the previously determined  $83 \text{ J}\cdot\text{g}^{-1}$  for PDD26-DD, thus further confirmed the similar crystallization units of these polyesters.

The crystalline morphologies were then checked by POM, as shown in Figure 4-19.



**Figure 4-19** POM images of PDD26-DD<sub>92</sub>-IS<sub>8</sub> and PDD26-DD<sub>85</sub>-IS<sub>15</sub> films

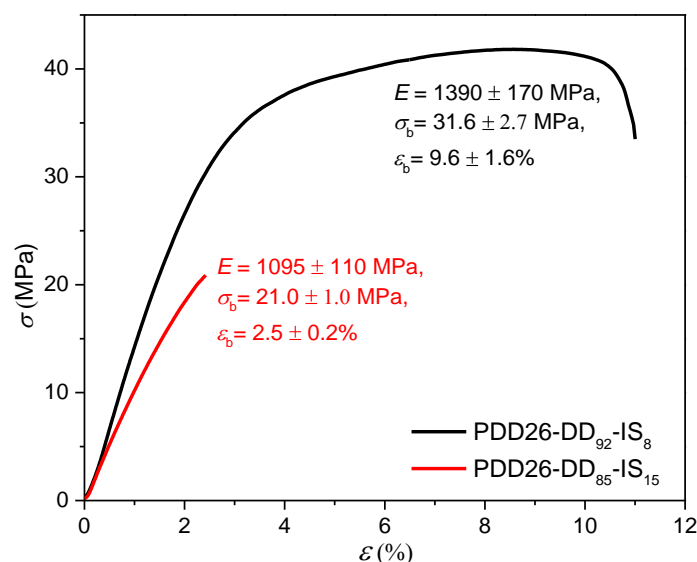
It was difficult to obtain very clear POM images. As described in Annex 2, the films were sandwiched between two PTFE sheets, whose texture caused the unevenness of the film surface. Moreover, the films were too thick (controlled around  $150 \mu\text{m}$ ). Nevertheless, some useful information could still be obtained from Figure 4-19: the homogeneous but small crystal grains without spherulites for both PDD26-DD<sub>92</sub>-IS<sub>8</sub> and PDD26-DD<sub>85</sub>-IS<sub>15</sub> were similar to that observed for PDD26-DD and also similar to PBT [57] and PBF [58].

### 4.II.3.3 Mechanical properties

The representative stress-strain curves of PDD26-DD<sub>92</sub>-IS<sub>8</sub> and PDD26-DD<sub>85</sub>-IS<sub>15</sub> were given in Figure 4-20. It revealed a plastic fracture for PDD26-DD<sub>92</sub>-IS<sub>8</sub> but a brittle one for PDD26-DD<sub>85</sub>-IS<sub>15</sub>. Both PDD26-DD<sub>92</sub>-IS<sub>8</sub> and PDD26-DD<sub>85</sub>-IS<sub>15</sub> showed higher  $E$  and  $\sigma_b$  than PDD26-DD ( $E = 770 \pm 25 \text{ MPa}$ ,  $\sigma_b = 12.5 \pm 4.8 \text{ MPa}$ ), which indicated a stiffer and stronger chain brought by IS. However, the rigidity of IS decreased  $\epsilon_b$  for both PDD26-DD<sub>92</sub>-IS<sub>8</sub> and PDD26-DD<sub>85</sub>-IS<sub>15</sub> compared to PDD26-DD ( $\epsilon_b = 25.0 \pm 6.0\%$ ). The increased  $E$  and  $\sigma_b$  revealed



globally better mechanical properties of PDD26-DD<sub>92</sub>-IS<sub>8</sub> compared to the bio-based food packaging plastic PBF ( $E = 1110$  MPa,  $\sigma_b = 19.8$  MPa,  $\varepsilon_b = 2.8\%$ ).



**Figure 4-20** Stress-strain curves of PDD26-DD<sub>92</sub>-IS<sub>8</sub> and PDD26-DD<sub>85</sub>-IS<sub>15</sub>

#### 4.II.3.4 Contact angle measurements

The surface properties of films were accessed by surface energy ( $\gamma^t$ ) and water contact angle ( $\theta_w$ ). The corresponding results were gathered in Table 4-14. The general large values of  $\theta_w$  indicated hydrophobicity for both PDD26-DD<sub>92</sub>-IS<sub>8</sub> and PDD26-DD<sub>85</sub>-IS<sub>15</sub>. PDD26-DD<sub>85</sub>-IS<sub>15</sub> showed slightly smaller  $\theta_w$  ( $86.0 \pm 1.2^\circ$ ) and larger  $\gamma^t$  ( $29.4$  mN·m<sup>-1</sup>) compared to PDD26-DD<sub>92</sub>-IS<sub>8</sub> ( $\theta_w = 88.0 \pm 0.8^\circ$ ,  $\gamma^t = 27.4$  mN·m<sup>-1</sup>), which was probably due to the presence of the polar “oxygen” atoms of IS. In addition, both PDD26-DD<sub>92</sub>-IS<sub>8</sub> and PDD26-DD<sub>85</sub>-IS<sub>15</sub> displayed a decrease in  $\theta_w$  and an increase in  $\gamma^t$  compared to PDD26-DD ( $\theta_w = 90.0 \pm 0.4^\circ$ ,  $\gamma^t = 26.0 \pm 0.5$  mN·m<sup>-1</sup>), which further confirmed the hydrophilicity brought by IS [59].

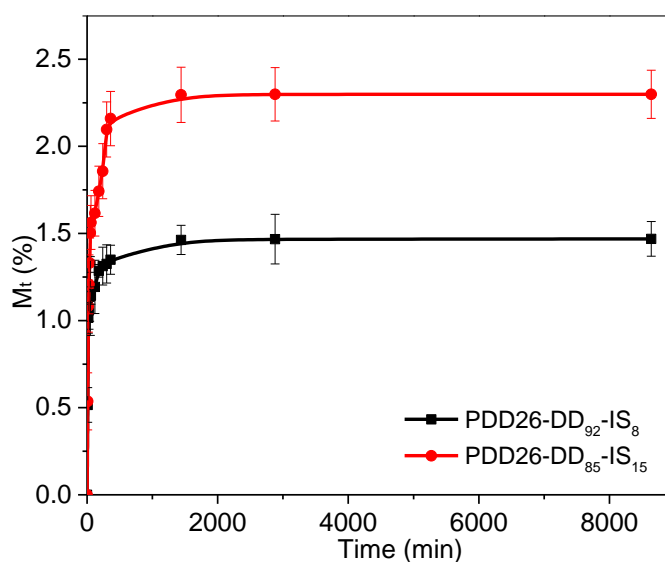
**Table 4-14** Surface energies and water contact angle values of films

Polyester films	$\gamma^t$ (mN·m <sup>-1</sup> )	$\gamma^d$ (mN·m <sup>-1</sup> )	$\gamma^p$ (mN·m <sup>-1</sup> )	$\theta_w$ (°)
PDD26-DD <sub>92</sub> -IS <sub>8</sub>	27.4	23.1	4.3	88.0 ± 0.8
PDD26-DD <sub>85</sub> -IS <sub>15</sub>	29.4	24.5	4.9	86.0 ± 1.2

$\gamma^t$ , Total surface energy with dispersive ( $\gamma^d$ ) and polar ( $\gamma^p$ ) parts;  $\theta_w$ , water contact angle.

#### 4.II.3.5 Liquid water and water vapor sorption

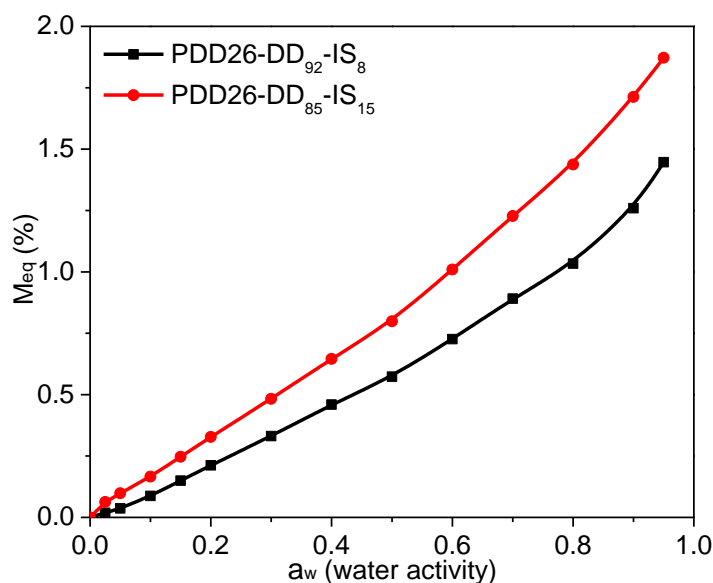
The liquid water sorption results (Figure 4-21) showed a larger water uptake for PDD26-DD<sub>85</sub>-IS<sub>15</sub> ( $M_{eq} = 2.30 \pm 0.14$  %) compared to PDD26-DD<sub>92</sub>-IS<sub>8</sub> ( $M_{eq} = 1.46 \pm 0.10$  %). In addition, both of them showed larger water sorption than PDD26-DD ( $M_{eq} = 1.17 \pm 0.16$  %), which could be explained by a combined result of the larger amorphous domain and polar IS “oxygen” atoms (ether linkages) affinity with water. The affinity effect of the ether linkages was already observed for aromatic polyamides containing benzimidazole and ethylene oxide moieties [60].

**Figure 4-21** Liquid water sorption of PDD26-DD<sub>92</sub>-IS<sub>8</sub> and PDD26-DD<sub>85</sub>-IS<sub>15</sub>

The water vapor sorption (Figure 4-22) was consistent with the liquid water sorption. PDD26-DD<sub>85</sub>-IS<sub>15</sub> (e.g.  $M_{eq} = 1.87$  % at  $a_w = 0.95$ ) exhibited globally larger water vapor sorption than PDD26-DD<sub>92</sub>-IS<sub>8</sub> (e.g.  $M_{eq} = 1.44$  % at  $a_w = 0.95$ ), and both of them sorbed more

water molecules than PDD26-DD (*e.g.*  $M_{eq} = 1.13\%$  at  $a_w = 0.95$ ). As previously discussed, the lower crystallinity and the presence of polar “oxygen” atoms in IS could explain these results.

Both isotherms showed sigmoid profiles following Park’s model. The corresponding parameters were listed in Table 4-15.



**Figure 4-22** Water vapor sorption isotherms

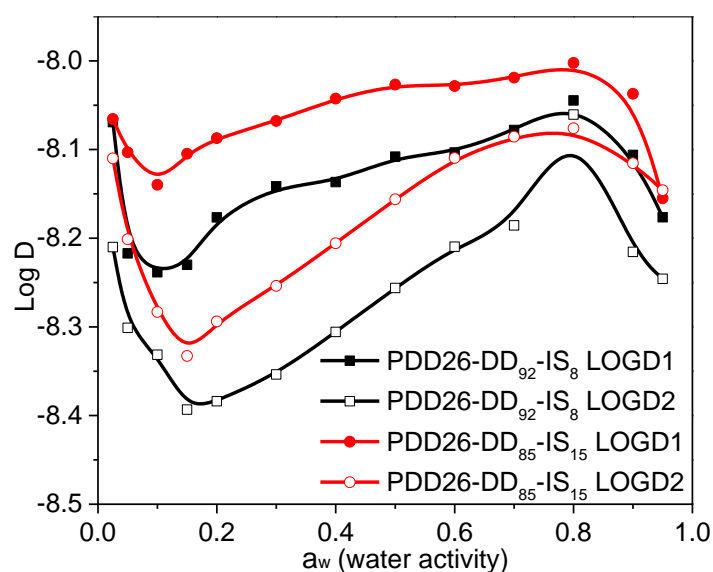
At  $a_w < 0.1$ , PDD26-DD<sub>85</sub>-IS<sub>15</sub> showed higher Langmuir-type sorption compared to PDD26-DD<sub>92</sub>-IS<sub>8</sub> ( $b_L = 5.3 \pm 0.4$  vs  $b_L = 3.4 \pm 0.3$ ). Considering the impermeable crystallites should not affect the thermodynamic interactions ( $b_L$ ) between the penetrant and polymer sites in the amorphous phase [15,48], the higher  $b_L$  value for PDD26-DD<sub>85</sub>-IS<sub>15</sub> could be due to the numerous polar oxygen atoms in IS. With larger  $a_w$ , the Langmuir sites were occupied and the isotherms became linear owing to random dissolution / diffusion (Henry’s type sorption) of water molecules in the polymer matrix [29]. The solubility coefficients  $S$  (analogous to  $k_H$  in Table 4-15) could be then calculated from the slope of the linear part ( $a_w = 0.1$ - $0.8$ ) of isotherms. The larger  $S$  values for PDD26-DD<sub>85</sub>-IS<sub>15</sub> ( $S = 18.2 \times 10^{-3} \text{ g}_{\text{H}_2\text{O}}/\text{g}_{\text{pol}}$ ) than for PDD26-DD<sub>92</sub>-IS<sub>8</sub> ( $S = 13.5 \times 10^{-3} \text{ g}_{\text{H}_2\text{O}}/\text{g}_{\text{pol}}$ ) were expected due to larger amorphous domains and more IS moieties in the former. At  $a_w > 0.8$ , upward sorption of water molecules was observed due to the formation of water “clusters”. The number of water molecules in each cluster was larger for PDD26-DD<sub>92</sub>-IS<sub>8</sub>.

**Table 4-15** Liquid water and water vapor sorption parameters of Park's model

Polyester film	$A_L \times 10^3$ (g/g)	$b_L$	$k_H \times 10^3$ (g/g)	$K_a \times 10^3$ (g/g)	$n_a$
PDD26-DD <sub>92</sub> -IS <sub>8</sub>	$0.15 \pm 0.01$	$3.4 \pm 0.3$	$11.0 \pm 0.7$	$0.46 \pm 0.01$	$5.0 \pm 0.2$
PDD26-DD <sub>85</sub> -IS <sub>15</sub>	$0.17 \pm 0.02$	$5.3 \pm 0.4$	$15.0 \pm 0.9$	$0.50 \pm 0.01$	$3.5 \pm 0.1$

$A_L$ , Langmuir's capacity constant;  $b_L$ , Langmuir's affinity constant;  $k_H$ , Henry's type solubility coefficient;  $K_a$ , equilibrium constant for clustering reaction;  $n_a$ , average number of water molecules per cluster.

To evaluate the dynamic aspect of water vapor sorption, the water vapor diffusion coefficients ( $D$ ) were calculated from the sorption kinetics. The evolution of  $D$  on semilogarithmic scale (Log  $D$ ) as a function of  $a_w$  was presented in Figure 4-23.

**Figure 4-23** Evolution of  $D_1$  and  $D_2$  as a function of  $a_w$ 

PDD26-DD<sub>92</sub>-IS<sub>8</sub> and PDD26-DD<sub>85</sub>-IS<sub>15</sub> followed a similar behavior *vs*  $a_w$ : a decrease followed by an increase on a large domain of  $a_w$  and then a final decrease. For both, a decrease of  $D_1$  and  $D_2$  was observed until  $a_w = 0.1$  probably due to water molecules interactions with polar oxygen atoms, leading to hydrogen bonds that increased the cohesion between polymer chains, and then reduced the water mobility [30–32]. As mentioned in Chapter 3, this phenomenon was explained as an “antiplasticizing effect” of the water molecules on the diffusion process [30]. Then, both samples showed an increase in  $D$  values on a large domain of  $a_w$ , which is a common phenomenon of water molecules that induce polymer swelling [41].

The decrease of  $D_1$  and  $D_2$  at high  $a_w$  was probably due to the aggregation of water molecules in clusters, which made them less mobile [61,62]. A quicker diffusion process (higher diffusion coefficients  $D_1$  and  $D_2$ ) for PDD26-DD<sub>85</sub>-IS<sub>15</sub> compared to PDD26-DD<sub>92</sub>-IS<sub>8</sub>, can be explained by the lower crystallinity of the former, because the crystals increase the diffusion pathway [29]. Both PDD26-DD<sub>92</sub>-IS<sub>8</sub> and PDD26-DD<sub>85</sub>-IS<sub>15</sub> followed the same diffusion behavior as PDD26-DD but more marked due to the presence of hydrophilic IS.

The higher diffusion coefficient  $D_1$  than  $D_2$  seemed to be a common trait of these polyesters. As discussed in the previous chapters, the diffusion of water was governed by the surface effect (a strong cohesion between the chains to form hydrogen bonds) rather than by the swelling of the core [33].

#### 4.II.3.6 Water vapor permeation

Water vapor permeation coefficients ( $P$ ) of films at different water activities ( $a_w$ ) were given in Table 4-16.

**Table 4-16** Water vapor permeation coefficients ( $P_{H_2O}$ ) of films

Polyester film	$a_w$	$P_{H_2O} \times 10^4$ (g·m <sup>-1</sup> ·d <sup>-1</sup> )	$P_{H_2O}$ (barrer)
PDD26-DD <sub>92</sub> -IS <sub>8</sub>	0.45	$3.06 \pm 0.33$	$190 \pm 10$
	0.52	$9.46 \pm 0.82$	$570 \pm 30$
	0.64	$11.1 \pm 0.90$	$670 \pm 50$
PDD26-DD <sub>85</sub> -IS <sub>15</sub>	0.47	$4.74 \pm 0.55$	$280 \pm 30$
	0.51	$20.4 \pm 1.87$	$1220 \pm 110$
	0.67	$85.1 \pm 6.53$	$5370 \pm 320$

PDD26-DD<sub>85</sub>-IS<sub>15</sub> showed globally higher water permeability compared to PDD26-DD<sub>92</sub>-IS<sub>8</sub>, and both showed higher  $P$  values than PDD26-DD (e.g.  $P_{H_2O} = 310$  barrer, at  $a_w = 0.52$ ). This increase in permeability was expected because of the lowest crystallinity of PDD26-DD<sub>85</sub>-IS<sub>15</sub> and its largest number of IS monomers containing polar oxygen sites favoring the solubility of the highly condensable water molecules [41]. For both films, the increase in water vapor permeability, coupled with the increase of  $D$  (Figure 4-23), with the increase of  $a_w$  confirmed that a swelling happened in the polymer matrix [15].

### 4.II.3.7 Gas permeation

The gas permeation coefficients ( $P$ ) for  $N_2$ ,  $O_2$  and  $CO_2$  were gathered in Table 4-17 and the corresponding diffusion and solubility coefficients ( $D$  and  $S$ ) were listed in Table 4-18. As expected, the gas permeabilities followed the usual order  $P_{N_2} < P_{O_2} < P_{CO_2}$  for polymers [42]. Both PDD26-DD<sub>92</sub>-IS<sub>8</sub> and PDD26-DD<sub>85</sub>-IS<sub>15</sub> showed very low permeabilities, but higher than those of PDD26-DD ( $P_{N_2} = 0.03$  barrer,  $P_{O_2} = 0.07$  barrer and  $P_{CO_2} = 0.3$  barrer). The slight increase in  $P$  values with the number of IS seemed related to the increase of  $D$  values (Table 4-18), which is probably due to the decreased crystallinity. The increase in permeability and diffusion coefficients for PDD26-DD<sub>85</sub>-IS<sub>15</sub> is more marked for  $N_2$  than for  $CO_2$  and  $O_2$  while these last two gases have more affinity with IS.  $N_2$  molecules behave as probes that have no affinity with the polyester matrix and are only affected by the increase of tortuosity caused by crystallinity.

**Table 4-17** Gas permeation ( $P$ ) coefficient of polyester films

Polyester film	$P$ (barrer)		
	$N_2$	$O_2$	$CO_2$
PDD26-DD <sub>92</sub> -IS <sub>8</sub>	$0.027 \pm 0.002$	$0.08 \pm 0.005$	$0.36 \pm 0.02$
PDD26-DD <sub>85</sub> -IS <sub>15</sub>	$0.037 \pm 0.002$	$0.11 \pm 0.007$	$0.45 \pm 0.03$

1 barrer =  $10^{-10}$  cm<sup>3</sup> STP·cm·cm<sup>-2</sup>·s<sup>-1</sup>·cmHg<sup>-1</sup>.

Although the  $P$  values slightly increased compared to PDD26-DD, they were still lower than those of some common food packaging materials, such as PE ( $P_{N_2} = 0.14$ -1.9 barrer,  $P_{O_2} = 0.6$ -6.7 barrer and  $P_{CO_2} = 1.7$ -28 barrer), PP ( $P_{N_2} = 0.44$  barrer,  $P_{O_2} = 0.9$ -2.3 barrer and  $P_{CO_2} = 9.2$  barrer), oriented PS ( $P_{N_2} = 0.29$ -0.78 barrer,  $P_{O_2} = 1.1$ -2.7 barrer and  $P_{CO_2} = 8.8$ -10.5 barrer) and PLA ( $P_{N_2} = 4.99$  barrer,  $P_{O_2} = 0.11$ -0.56 barrer and  $P_{CO_2} = 1.88$  barrer) [40], and competitive to amorphous PET ( $P_{O_2} = 0.05$ -0.11 barrer and  $P_{CO_2} = 0.21$ -0.57 barrer).

**Table 4-18** Gas diffusion ( $D$ ) and solubility ( $S$ ) coefficients of films

Polyester film	$D \times 10^{10}$ (cm <sup>2</sup> ·s <sup>-1</sup> )			$S \times 10^3$ (cm <sup>3</sup> (STP)·cm <sup>-3</sup> ·cmHg <sup>-1</sup> )		
	$N_2$	$O_2$	$CO_2$	$N_2$	$O_2$	$CO_2$
PDD26-DD <sub>92</sub> -IS <sub>8</sub>	$1.78 \pm 0.12$	$5.16 \pm 0.36$	$76.2 \pm 5.3$	$15.4 \pm 1.08$	$16.0 \pm 1.12$	$4.77 \pm 0.45$
PDD26-DD <sub>85</sub> -IS <sub>15</sub>	$2.36 \pm 0.16$	$6.79 \pm 0.47$	$96.7 \pm 6.8$	$15.7 \pm 1.18$	$15.9 \pm 1.11$	$4.69 \pm 0.33$

### 4.III Conclusion

Six bio-based copolyesters, involving isosorbide (IS) (or isomannide (IM)), sebacoyl dichloride (C10), and a second acid dichloride were synthesized by polycondensation reactions in bulk or solution. The second acid dichloride was either aliphatic (C4) or aromatic (IPC and PDD26).  $^1\text{H}$  NMR spectroscopy enabled to calculate the respective monomer ratios in the copolymers, and  $\overline{M}_n$  ranged from 10 600 to 18 000  $\text{g}\cdot\text{mol}^{-1}$ . All copolyesters were thermally stable with  $T_{5\%}$  higher than 328 °C and  $T_g$  ranging from 30 to 64 °C. DSC results showed that the second acid dichloride component significantly improved the  $T_g$  of ISC10 and IMC10. Generally, the aromatic skeleton, and especially the pyridine skeleton, was more efficient in improving  $T_g$ . The tensile test revealed plastic fractures for aliphatic copolyesters and brittle fractures for aromatic ones. The highest Young's modulus and tensile strength were obtained for the aromatic copolyesters, whereas, the largest elongation at break was observed for the aliphatic ones. All copolyesters showed improved barrier properties (for both water and gases) compared to ISC10 and IMC10. The copolyester containing *m*-phenylene moiety (ISC10IPC) exhibited the highest water barrier properties, whereas the one containing 2,6-pyridine moiety (IMC10PDD26) was more barrier to gases. The excellent water and gas barrier property was mainly linked to their high  $T_g$  as well as their chemical structures. The 2,6-pyridine structure coupling with high  $T_g$  brought much better gas barrier properties than commonly used food packaging materials, such PE, PP, PS, PC, and PLA, and comparable to semi-crystalline PET.

Copolyesters involving 2,6-pyridinedicarbonyl dichloride (PDD26), 1,10-decanediol (DD), and a second bicyclic (IS) or short-chain linear (EG) diol were synthesized by melt polycondensation. However, difficulties were encountered to incorporate the second rigid diol. PDD26-DD<sub>x</sub>-IS<sub>y</sub> showed limited  $T_g$  at 12 °C and large decreases in molar masses. PDD26-DD<sub>33</sub>-EG<sub>67</sub> showed satisfying  $T_g$  (35 °C) but the molar mass was not sufficient to prepare usable films. Although the  $T_g$  of PDD26-DD<sub>x</sub>-IS<sub>y</sub> copolyesters were not compliant with the expected ones, the successful preparation of films containing 8 mol% (PDD26-DD<sub>92</sub>-IS<sub>8</sub>) and 15 mol% IS (PDD26-DD<sub>85</sub>-IS<sub>15</sub>) were encouraging for further investigation of IS influence on mechanical and permeation properties. The incorporation of IS generally decreased the crystallinity as well as the water and gas barrier. However, the mechanical properties in terms of  $E$  and  $\sigma_b$  were strongly improved. Considering the slight sacrifice in barrier properties but much improvement in mechanical properties when incorporating 8 mol% of IS, PDD26-DD<sub>92</sub>-

IS<sub>8</sub> provides supplementary properties to PDD26-DD when considering mostly the mechanical properties for food packaging applications.

## References

- [1] F.R. Mayo, C. Walling, Copolymerization, *Chem. Rev.* 46 (1950) 191–287.
- [2] M. Garaleh, T. Yashiro, H.R. Kricheldorf, P. Simon, T. Yashiro, P. Simon, ( Co- ) Polyesters Derived from Isosorbide and 1,4-Cyclohexane Dicarboxylic Acid and Succinic Acid, (2009) 1206–1214.
- [3] C. Lavilla, S. Muñoz-Guerra, Sugar-based aromatic copolyesters: A comparative study regarding isosorbide and diacetalized alditols as sustainable comonomers, *Green Chem.* 15 (2013) 144–151.
- [4] W. Shiao, C.K. Hsin, C.C. Feng, Thermal behavior and specific interaction in high glass transition temperature PMMA copolymer, *Polymer.* 44 (2003) 6873–6882.
- [5] S.N. Vouyiouka, E.K. Karakatsani, C.D. Papaspyrides, Solid state polymerization, *Prog. Polym. Sci.* 30 (2005) 10–37.
- [6] F. Fenouillot, A. Rousseau, G. Colomines, R. Saint-Loup, J.P. Pascault, Polymers from renewable 1,4:3,6-dianhydrohexitols (isosorbide, isomannide and isoidide): A review, *Prog. Polym. Sci.* 35 (2010) 578–622.
- [7] H. Marubayashi, T. Ushio, S. Nojima, Crystallization of polyesters composed of isohexides and aliphatic dicarboxylic acids: effects of isohexide stereoisomerism and dicarboxylic acid chain length, *Polym. Degrad. Stab.* 146 (2017) 174–183.
- [8] B. Wunderlich, D.M. Bodily, M.H. Kaplan, Theory and measurements of the glass-transformation interval of polystyrene, *J. Appl. Phys.* 35 (1964) 95–102.
- [9] S.Z.D. Cheng, B. Wunderlich, Glass Transition and Melting Behavior of Poly(Ethylene-2,6-Naphthalenedicarboxylate), *Macromolecules.* 21 (1988) 789–797.
- [10] G.Z. Papageorgiou, D.G. Papageorgiou, Z. Terzopoulou, D.N. Bikiaris, Production of bio-based 2,5-furan dicarboxylate polyesters: recent progress and critical aspects in their synthesis and thermal properties, *Eur. Polym. J.* 83 (2016) 202–229.
- [11] Q. Lu, Z. Yang, X. Li, S. Jin, Synthesis, morphology, and melting behavior of poly(ether ether ketone) of different molecular weights, *J. Appl. Polym. Sci.* 116 (2010) 2060–2070.
- [12] H.G. Van Melick, L.E. Govaert, H.E.H. Meijer, On the origin of strain hardening in glassy polymers, *Polymer.* 44 (2003) 2493–2502.
- [13] D.C. Prevorsek, B.T. De Bona, On chain entanglement in high- T<sub>g</sub> amorphous polymers, *J. Polym. Sci. Part B Polym. Phys.* 19 (1981) 605–622.
- [14] S.K. Burgess, G.B. Wenz, R.M. Kriegel, W.J. Koros, Penetrant transport in semicrystalline poly(ethylene furanoate), *Polymer.* 98 (2016) 305–310.
- [15] S.K. Burgess, D.S. Mikkilineni, D.B. Yu, D.J. Kim, C.R. Mubarak, R.M. Kriegel, W.J.



- Koros, Water sorption in poly(ethylene furanoate) compared to poly(ethylene terephthalate). part 1: equilibrium sorption, *Polymer*. 55 (2014) 6861–6869.
- [16] D. Langevin, J. Grenet, J. Saiter, Moisture sorption in PET influence on the thermokinetic parameters, 30 (1994) 339–345.
- [17] K. Galić, N. Ciković, Permeability characterisation of solvent treated polymer materials, *Polym. Test*. 20 (2001) 599–606.
- [18] B. Ben Doudou, E. Dargent, S. Marais, J. Grenet, Y. Hirata, Barrier properties and microstructure modifications induced by liquid water for a semiaromatic polyamide, *J. Polym. Sci. Part B Polym. Phys.* 43 (2005) 2604–2616.
- [19] T. Messin, N. Follain, A. Guinault, G. Miquelard-Garnier, C. Sollogoub, N. Delpouve, V. Gaucher, S. Marais, Confinement effect in PC/MXD6 multilayer films: Impact of the microlayered structure on water and gas barrier properties, *J. Memb. Sci.* 525 (2017) 135–145.
- [20] R.M. Hodge, T.J. Bastow, G.H. Edward, G.P. Simon, A.J. Hill, Free volume and the mechanism of plasticization in water-swollen poly(vinyl alcohol), *Macromolecules*. 29 (1996) 8137–8143. <https://doi.org/10.1021/ma951073j>.
- [21] D. Langevin, J. Grenet, J.M. Saiter, Moisture sorption in pet influence on the thermokinetic parameters, *Eur. Polym. J.* 30 (1994) 339–345.
- [22] C.L. Buquet, B. Ben Doudou, C. Chappey, E. Dargent, S. Marais, Permeation properties of poly(m-xylene adipamide) membranes, *J. Phys. Chem. B*. 113 (2009) 3445–3452.
- [23] R. Crétois, N. Follain, E. Dargent, J. Soulestin, S. Bourbigot, S. Marais, L. Lebrun, Structure and barrier properties of biodegradable polyhydroxyalkanoate films, *Phys. Chem. Chem. Phys.* 17 (2015) 11313–11323.
- [24] J. Grank, G.S. Park, *Diffusion in Polymers*, Academic Press, London and New- York, 1968.
- [25] B. Freeman, Y. Yampolskii, I. Pinnau, *Materials science of membranes for gas and vapor separation*, John Wiley & Sons, Ltd, Chichester, 2006.
- [26] C. Fuhrman, M. Nutt, K. Vichtovonga, M.R. Coleman, Effect of Thermal Hysteresis on the Gas Permeation Properties of 6FDA-Based Polyimides, *J. Appl. Polym. Sci.* 91 (2004) 1174–1182.
- [27] I. Erukhimovich, M.O. de la Cruz, Phase equilibria and charge fractionation in polydisperse polyelectrolyte solutions, (2004) 1798–1807.
- [28] A.S. Michaels, W.R. Vieth, J.A. Barrie, Solution of gases in polyethylene terephthalate, *J. Appl. Phys.* 34 (1963) 1–12.
- [29] N. Follain, S. Belbekhouche, J. Bras, G. Siqueira, S. Marais, A. Dufresne, Water transport properties of bio-nanocomposites reinforced by *Luffa cylindrica* cellulose nanocrystals, *J. Memb. Sci.* 427 (2013) 218–229.
- [30] S. Alix, E. Philippe, A. Bessadok, L. Lebrun, C. Morvan, S. Marais, Effect of chemical treatments on water sorption and mechanical properties of flax fibres, *Bioresour. Technol.* 100 (2009) 4742–4749.
- [31] A. Marzec, P.P. Lewicki, Antiplasticization of cereal-based products by water. Part I.

- Extruded flat bread, *J. Food Eng.* 73 (2006).
- [32] Y.P. Chang, A. Abd Karim, C.C. Seow, Interactive plasticizing–antiplasticizing effects of water and glycerol on the tensile properties of tapioca starch films, *Food Hydrocoll.* 20 (2006).
- [33] S. Belbekhouche, J. Bras, G. Siqueira, C. Chappey, L. Lebrun, B. Khelifi, S. Marais, A. Dufresne, Water sorption behavior and gas barrier properties of cellulose whiskers and microfibrils films, *Carbohydr. Polym.* 83 (2011) 1740–1748.
- [34] A. Bessadok, S. Roudesli, S. Marais, N. Follain, L. Lebrun, Alfa fibres for unsaturated polyester composites reinforcement: Effects of chemical treatments on mechanical and permeation properties, *Compos. Part A Appl. Sci. Manuf.* 40 (2009) 184–195.
- [35] S. Belbekhouche, J. Bras, G. Siqueira, C. Chappey, L. Lebrun, B. Khelifi, S. Marais, A. Dufresne, Water sorption behavior and gas barrier properties of cellulose whiskers and microfibrils films, *Carbohydr. Polym.* 83 (2011) 1740–1748.
- [36] L. Shao, T.S. Chung, S.H. Goh, K.P. Pramoda, Polyimide modification by a linear aliphatic diamine to enhance transport performance and plasticization resistance, *J. Memb. Sci.* 256 (2005) 46–56.
- [37] S. Prager, F.A. Long, Diffusion of Hydrocarbons in Polyisobutylene, *J. Am. Chem. Soc.* 73 (1951) 4072–4075.
- [38] W.J. Koros, Barrier Polymers and Structures, *Anal. Chem.* 62 (1990) 22–59.
- [39] M. Gilbert, States of Aggregation in Polymers, *Brydson's Plast. Mater.* Eighth Ed. (2017) 39–57.
- [40] Robertson, G. L, Food packaging-Principles and practice, 3rd ed., Taylor & Francis, 2013.
- [41] S. Marais, Q.T. Nguyen, C. Devallencourt, M. Metayer, T.U. Nguyen, P. Schaetzel, Permeation of water through polar and nonpolar polymers and copolymers: determination of the concentration-dependent diffusion coefficient, *J. Polym. Sci. Part B Polym. Phys.* 38 (2000) 1998–2008.
- [42] D.W. Van Krevelen, K. Te Nijenhuis, Properties of polymers, 4th ed., Elsevier, 2009.
- [43] E.S. Sanders, Penetrant-induced plasticization and gas permeation in glassy polymers, *J. Memb. Sci.* 37 (1988) 63–80.
- [44] A. Bos, I. Pünt, H. Strathmann, M. Wessling, Suppression of gas separation membrane plasticization by homogeneous polymer blending, *AIChE J.* 47 (2001) 1088–1093.
- [45] R. Swaidan, B. Ghanem, E. Litwiller, I. Pinnau, Physical Aging, Plasticization and Their Effects on Gas Permeation in “rigid” Polymers of Intrinsic Microporosity, *Macromolecules.* 48 (2015) 6553–6561.
- [46] A.F. Ismail, W. Lorna, Penetrant-induced plasticization phenomenon in glassy polymers for gas separation membrane, *Sep. Purif. Technol.* 27 (2002) 173–194.
- [47] L. Jja, J. Xu, A simple method for prediction of gas permeability of a method for the prediction of gas permeabilities, *Polym. J.* 23 (1991) 417–425.
- [48] A.S. Michaels, W.R. Vieth, J.A. Barrie, Solution of gases in polyethylene terephthalate,

- J. Appl. Phys. 34 (1963) 1–12.
- [49] J. Trifol, D. Plackett, P. Szabo, A.E. Daugaard, M. Giacinti Baschetti, Effect of Crystallinity on Water Vapor Sorption, Diffusion, and Permeation of PLA-Based Nanocomposites, *ACS Omega*. 5 (2020) 15362–15369.
  - [50] S.W. Lasoski, W.H. Cobbs, Moisture permeability of polymers. I. Role of crystallinity and orientation, *J. Polym. Sci.* 36 (1959) 21–33.
  - [51] G.C. East, V.G.R. Gudiguntla, The synthesis and characterization of polyesters based on 2,5 - pyridinedicarboxylic acid, *Macromol. Chem. Phys.* 195 (1994) 1851–1864.
  - [52] A. Pellis, J.W. Comerford, S. Weinberger, G.M. Guebitz, J.H. Clark, T.J. Farmer, Enzymatic synthesis of lignin derivable pyridine based polyesters for the substitution of petroleum derived plastics, *Nat. Commun.* 10 (2019).
  - [53] R. Storbeck M. Ballauff, Synthesis and thermal analysis of copolyesters deriving from 1,4:3,6- dianhydrosorbitol, ethylene glycol, and terephthalic acid, *J. Appl. Polym. Sci.* 59 (1996) 1199–1202.
  - [54] Y. Kong, J.N. Hay, Multiple melting behaviour of poly(ethylene terephthalate), *Polymer*. 44 (2002) 623–633.
  - [55] V. Tserki, P. Matzinos, E. Pavlidou, D. Vachliotis, C. Panayiotou, Biodegradable aliphatic polyesters. Part I. Properties and biodegradation of poly(butylene succinate-co-butylene adipate), *Polym. Degrad. Stab.* 91 (2006) 367–376.
  - [56] V. Tserki, P. Matzinos, E. Pavlidou, C. Panayiotou, Biodegradable aliphatic polyesters. Part II. Synthesis and characterization of chain extended poly(butylene succinate-co-butylene adipate), *Polym. Degrad. Stab.* 91 (2006) 377–384.
  - [57] T. Konishi, Y. Miyamoto, Crystallization of Poly(butylene terephthalate) from the glass, *Macromolecules*. 43 (2010) 375–383.
  - [58] J. Ma, X. Yu, J. Xu, Y. Pang, Synthesis and crystallinity of poly(butylene 2,5-furandicarboxylate), *Polymer*. 53 (2012) 4145–4151.
  - [59] D. Kim, I.-C. Kim, Y.-N. Kwon, S. Myung, Novel bio-based polymer membranes fabricated from isosorbide-incorporated poly(arylene ether)s for water treatment, *Eur. Polym. J.* 136 (2020).
  - [60] V. Ayala, E.M. Maya, J.M. García, J.G. De La Campa, A.E. Lozano, J. De Abajo, Synthesis, characterization, and water sorption properties of new aromatic polyamides containing benzimidazole and ethylene oxide moieties, *J. Polym. Sci. Part A Polym. Chem.* 43 (2005) 112–121.
  - [61] J.A. Barrie, B. Platt, The diffusion and clustering of water vapour in polymers, *Polymer*. 4 (1963) 303–313.
  - [62] R. Shi, Q. Liu, D. Tao, H. Yanming, Z. Liqun, C. Dafu, T. Wei, Aging of soft thermoplastic starch with high glycerol content, *J. Appl. Polym. Sci.* 116 (2006) 574–586.

---

## ∞ General Conclusion ∞

---



In this thesis, several new fully bio-based polyesters, intended for food packaging applications, were synthesized and investigated in terms of thermal, mechanical, and particularly transport properties toward water and gases (N<sub>2</sub>, O<sub>2</sub> and CO<sub>2</sub>). Relationships between microstructure, morphology, physicochemical and functional properties were also established.

Firstly, six aliphatic bio-based polyesters were obtained by melt polycondensation reactions of isosorbide (IS) or isomannide (IM) with succinyl chloride (C4), adipoyl chloride (C6) and sebacoyl chloride (C10), respectively. Molar masses varying from 4 300 to 19 000 g·mol<sup>-1</sup>, thermal stabilities higher than 325 °C,  $T_g$  ranging from 0 °C to 65 °C, and occasionally crystallinity, were obtained. It was established that the stereoisomerism of IS and IM mainly influenced the crystallization properties, while the chain length of the diacid units influenced the thermal degradation and glass transition temperatures as well as the crystallization. Flexible films could be obtained only with ISC10 and IMC10. The remarkable ISC10 exhibited larger crystal size and higher crystallinity, contributing to the highest tensile stress at break ( $\sigma_b$ ) and the best barrier properties to water and gases, the latter being similar to those of PLA. Even if the barrier properties of ISC10 were lower than PET and PEF, the selectivity to CO<sub>2</sub> and O<sub>2</sub> was nevertheless at least as good as PET and PEF, which is very favorable for fruits and vegetables preservation.

Secondly, four semi-aromatic bio-based polyesters containing 2,6-pyridinedicarbonyl dichloride (PDD26) and aliphatic diols (ethylene glycol, EG; 1,4-butanediol, BD; 1,6-hexanediol, HD; 1,10-decanediol, DD) were synthesized by polycondensation. Only PDD26-DD afforded high molar masses. So, two analogs, named PDD25-DD and IPC-DD, were synthesized with satisfying molar masses (around 25 000 g·mol<sup>-1</sup>) and were compared to PDD26-DD. Polyesters containing pyridine rings (PDD26-DD and PDD25-DD) showed lower thermal degradation temperatures (341 and 304 °C) than the one containing phenyl rings (IPC-DD, 371 °C), but  $T_g$  (always below room temperature),  $T_m$  and crystallinities were higher. Among all, PDD26-DD displayed the preferred mechanical properties with the highest gas barrier properties, better than PLA and comparable to amorphous PET. As conclusion, PDD26-DD shows a great potential in the field of food packaging, especially when high CO<sub>2</sub> and O<sub>2</sub> barrier are needed.

Finally, the work was focused on improving the barrier properties of ISC10, IMC10 and PDD26-DD by increasing their  $T_g$ . The general idea was to incorporate a third rigid or short-

chain monomer via copolycondensation, and two scenarios were considered: one was based on ISC10 and IMC10, and the other was based on PDD26-DD. In the first part, six copolyesters, involving ISC10 or IMC10 and a second acid dichloride, were synthesized. The second acid dichloride component was either aliphatic (C4) or aromatic (IPC and PDD26).  $\overline{M}_n$  of synthesized copolyesters ranged from 10 600 to 18 000 g·mol<sup>-1</sup>. All were thermally stable with  $T_{5\%}$  higher than 328 °C and  $T_g$  ranged from 30 to 64 °C. The second acid dichloride component significantly improved the  $T_g$  of ISC10 and IMC10, and more generally the aromatic skeleton, especially the pyridine skeleton. All copolyesters showed improved barrier properties (both to water and gases) compared to ISC10 and IMC10. Focusing on gas barrier properties, IMC10PDD26 was the best, which was linked to its high  $T_g$  ( $T_g = 64$  °C) and its pyridine chemical structure. This high gas barrier properties were much better than those of commonly used food packaging materials, such as PE, PP, PS, and PLA, and comparable to the widely used semi-crystalline PET. In the second part, copolyesters involving PDD26-DD and a second bicyclic or short-chain linear diol (IS or EG) were synthesized. However, difficulties were encountered to incorporate the second rigid diol and a general decrease in molar masses was observed. For this reason, PDD26-DD<sub>33</sub>-EG<sub>67</sub>, despite its satisfying  $T_g$  at 35 °C, could not afford usable films. Even though the  $T_g$  of PDD26-DD<sub>x</sub>-IS<sub>y</sub> could not be increased beyond 12 °C, the successful preparation of films containing 8 mol% (PDD26-DD<sub>92</sub>-IS<sub>8</sub>) and 15 mol% IS (PDD26-DD<sub>85</sub>-IS<sub>15</sub>) was encouraging for further investigations. Even if the incorporation of IS generally decreased the crystallinity and slightly the water and gas barrier of the films compared to PDD26-DD, the mechanical properties in terms of  $E$  and  $\sigma_b$  were strongly improved. Thus, PDD26-DD<sub>92</sub>-IS<sub>8</sub> will provide supplementary properties to PDD26-DD when considering mainly the mechanical properties for applications in food packaging.

To sum up, a series of bio-based polyesters and copolyesters based on 1,4:3,6-dianhydrohexitols and/or 2,6-pyridinedicarbonyl dichloride were synthesized by polycondensation reactions. Important characteristics, such as thermal, tensile and water/gases transport properties, regarding food packaging applications, were investigated. A wide variety of thermal and mechanical properties has been observed, and good to excellent water and gas (N<sub>2</sub>, O<sub>2</sub>, CO<sub>2</sub>) barrier properties, sometimes at PET level, suggesting a large range of applications in food packaging.

## **Perspectives**

To extend this work and continue to gather information on these promising polymers, several perspectives could be drawn.

Considering that increasing  $T_g$  via copolymerization improved the mechanical and water/gas barrier properties, it would be attractive to use ISC4 and IMC4, which have already high  $T_g$ , to develop high barrier food packaging materials. However, the polyesters did not show film forming properties. So, it would be interesting to improve the synthesis conditions in order to obtain high molar masses polyesters, which are more able to give films.

The presence of 2,6-pyridine rings in the structure of polyester chains has shown efficiency in increasing  $T_g$  and crystallinity, as well as good mechanical and excellent gas barrier properties. Thus, 2,6-pyridine ring monomers could be a platform to develop new and promising bio-based polyesters for food packaging. In particular, PDD26-EG may have better gas barrier properties than the unrivaled PEF. Besides, polymers containing pyridine structures can also show interests in antibacterial materials. Thus, investigating the antibacterial properties of the above-mentioned 2,6-pyridine and 2,5-pyridine based polyesters may bring additional values and broaden their applications in food packaging.

It should be emphasized in this work that we did not control the crystallization during the preparation of the films. In-depth crystallization and annealing studies, and their consequences on crystallinity, polymorphism, and on mechanical and transport properties, could be highly relevant on these particular structures based on the 2,6 and 2,5-pyridine, such as PDD26-EG, PDD26-BD, PDD26-DD and PDD25-DD.

Another point of interest could be to study the gas barrier properties of the films under different moisture contents. Indeed, the hydrophilicity induced by polar groups of polyesters could change their permeation properties when being used in a humid environment.

Finally, taking green chemistry and the environmental issues into consideration, it remains several works: optimizing the synthesis conditions by starting from diacids or diesters instead of acid dichlorides; investigating the biodegradability of the obtained polyesters; chemically or mechanically evaluating the recyclability of these polyesters.





---

## ❧ Annexes ❧

---



---

## Annex 1 Synthesis

### A1.1 1,4:3,6-dianhydrohexitols-based aliphatic polyesters

#### A1.1.1 Operation 1

8.948 g of isosorbide (IS, 60 mmol) and 13.5 mL of sebacoyl chloride (C10, 60 mmol) were weighed into a 100 mL three-necked round-bottomed flask equipped with a mechanical stirrer and a HCl capture tube (filled with calcium oxide and communicating with atmosphere). The flask was dipped into a 160 °C oil bath and kept under normal pressure for 6 h. Then, reduced pressure was applied: 50 mbar for 2 h, then 0.1 mbar for 15 h. The corresponding product was named ISC10\* (18.6 g).

#### A1.1.2 Operation 2

8.948 g of isosorbide (IS, 60 mmol) were weighed into a 100 mL three-necked round-bottomed flask equipped with a mechanical stirrer. A continuous N<sub>2</sub> flow was introduced and the flask was dipped into a 160 °C oil bath. 13.5 mL of sebacoyl chloride (C10, 60 mmol) were added when IS was fully molten. The mixture was kept under normal pressure for 6 h with continuous N<sub>2</sub>. Then, reduced pressure was applied: 50 mbar for 2 h, then 0.1 mbar for 15 h. After cooling to room temperature, the media was dissolved in dichloromethane (50 mL) and the polymer was precipitated in methanol (500 mL). The product was purified by 3 times repeated dissolution/precipitation. Finally, it was dried for 2 days at 40 °C under reduced pressure. The corresponding polymer was named ISC10\*\* (16.9 g).

#### A1.1.3 Operation 3

8.948 g of isosorbide or 9.230 g of isomannide (IS or IM, 60 mmol) were weighed into a 100 mL three-necked round-bottomed flask equipped with a mechanical stirrer. A continuous N<sub>2</sub> flow was introduced and the flask was dipped into an oil bath (80 and 95 °C for IS and IM, respectively) ( $T_{m(IS)}=60-63$  °C,  $T_{m(IM)}=80-85$  °C). 13.5 mL of sebacoyl chloride (C10, 60 mmol) were added when IS or IM was fully molten. The temperature was kept at 80 °C (or 95 °C) for 15 min, 100 °C for 15 min, 120 °C for 30 min, 140 °C for 30 min, then raised to 160 °C (the decrease of the release of HCl set the duration of each step) and kept at 160 °C under normal

pressure for 4 h with continuous N<sub>2</sub> flow. Then, reduced pressure was applied: 50 mbar for 2 h, then 0.1 mbar for 15 h. After cooling to room temperature, the media was dissolved in dichloromethane (50 mL) and the polymer was precipitated in methanol (500 mL). The product was purified by 3 times repeated dissolution/precipitation. Finally, it was dried for 2 days at 40 °C under reduced pressure. The corresponding polymer was named ISC10 (17.7 g) or IMC10 (17.5 g).

Following the same procedure, the use of succinyl (C4) and adipoyl (C6) chlorides afforded the polymers named ISC4 (11.5 g), ISC6 (13.9 g), IMC4 (8.9 g), and IMC6 (13.4 g).

## **A1.2 2,6-pyridinedicarbonyl dichloride-based polyesters**

### **A1.2.1 Solution method**

1.052 g of PDD26 (5 mmol), 0.28 mL of EG (5 mmol) or 0.45 mL of BD (5 mmol) or 0.871 g of DD (5 mmol), were weighed into a 50 mL two-necked round-bottomed flask equipped with a magnetic stirrer. A continuous N<sub>2</sub> flow was introduced and 10 mL of dry CH<sub>2</sub>Cl<sub>2</sub> were added. Then, the flask was dipped into an ice bath and 2.5 mL of dry pyridine were dropwise added into the mixture. Then, the ice bath was removed and the reaction was kept under a N<sub>2</sub> atmosphere at room temperature for 24 h. Finally, the products were purified by 3 times repeated dissolution/precipitation (CH<sub>2</sub>Cl<sub>2</sub> / CH<sub>3</sub>OH) and were dried for 2 days at 40 °C under reduced pressure. The corresponding polymers PDD26-EG (0.3 g) and PDD26-BD (0.7 g).

### **A1.2.2 Bulk method**

4.080 g of 2,6-pyridinedicarbonyl dichloride (PDD26, 20 mmol) and 2.363 g of 1,6-hexanediol (HD, 20 mmol), or 3.154 g of PDD26 (15 mmol) and 2.667 g of 1,10-decanediol (DD, 15 mmol) were weighed into a 100 mL three-necked round-bottomed flask equipped with a mechanical stirrer and a continuous N<sub>2</sub> flow. Then, the flask was dipped into an 80 °C oil bath. The temperature was kept at 80 °C for 30 min, 100 °C for 30 min, 120 °C for 1h, then raised to 140 °C and kept at 140 °C under normal pressure for 4 h with continuous N<sub>2</sub>. Finally, reduced pressure was applied: 50 mbar for 2h and 0.1 mbar for 1h. After cooling to room temperature, the media was dissolved in dichloromethane (20 mL) and the polymer was precipitated in

methanol (200 mL). The products were purified by 3 times repeated dissolution/precipitation ( $\text{CH}_2\text{Cl}_2$  /  $\text{CH}_3\text{OH}$ ) and were dried for 2 days at 40 °C under reduced pressure. The corresponding polymers were named PDD26-HD (3.6 g) and PDD26-DD (4.2 g).

When ethylene glycol (EG) (20 mmol) or 1,4-butanediol (BD) (20 mmol) were used as diols, the syntheses were performed similar to HD and DD, except the temperature procedure was: 80 °C for 30 min, 100 °C for 30 min, 120 °C for 1h, 140 °C for 4h, under normal pressure with continuous  $\text{N}_2$  and 200 °C with reduced pressure (50 mbar for 2h and 0.1 mbar for 1h). The corresponding polymers PDD26-EG (1.5 g) and PDD26-BD (3.9 g).

### **A1.3 Isophthaloyl dichloride-based polyester**

The synthesis was performed the same as PDD26-DD in bulk (A1.2.2). 3.024 g of isophthaloyl dichloride (IPC, 14.6 mmol) and 2.614 g of 1,10-decanediol (DD, 14.7 mmol) were used and the corresponding polymer was named IPC-DD (4.2 g).

### **A1.4 2,5-pyridinedicarbonyl dichloride-based polyester**

#### **A1.4.1 Synthesis of 2,5-pyridinedicarbonyl dichloride**

10.013 g of 2,5-pyridinedicarboxylic acid (PDA25, 59.9 mmol) were weighed into a round-bottomed flask equipped with a magnetic stirrer and a condenser.  $\text{N}_2$  and 70 mL of  $\text{SOCl}_2$  were introduced. The suspension mixture was heated in an oil bath at 70 °C until it turned orange and clear (48 h), and then was transferred to a rotating evaporator to remove the excess  $\text{SOCl}_2$ . Thereafter, the obtained product was connected to a pump, equipped with a trap filled with aqueous NaOH, and was further purified by continuously removing  $\text{SOCl}_2$  for 6 h. The ultimate product was named PDD25 (12.0 g).

#### **A1.4.2 Synthesis of polyester**

##### **A1.4.2.1 Bulk method**

The synthesis procedure was the same as PDD26-DD (A1.2.2) : 2.003 g (9.80 mmol) of PDD25 and 1.710 g of DD (9.81 mmol) were used and the production was 1.9 g.

**A1.4.2.2 In CH<sub>2</sub>Cl<sub>2</sub> with pyridine at room temperature**

The procedure was the same as PDD26-DD in A1.2.1 PDD25 (2.0150 g, 9.87 mmol) and DD (1.723g, 9.89 mmol) were used, and the amounts of solvent and pyridine were increased accordingly (2.6 g).

**A1.4.2.3 In toluene with pyridine**

3.009 g (14.7 mmol) of PDD25 and 2.580 g (14.8 mmol) of DD were weighed into a 100 mL three-necked round-bottomed flask equipped with a mechanical stirrer and a condenser. With the introduction of a continuous N<sub>2</sub> flow, 20 mL of toluene were added and the flask was dipped into a 75 °C oil bath. When the solid particles disappeared, 5 mL of pyridine was dropwise added. When the solution turned turbulent then brown clear, the temperature was increased to 85 °C and kept for 24 h, and then increased to 115 °C for 3 h under N<sub>2</sub> atmosphere. After cooling to room temperature, the media was precipitated in methanol and purified by 3 times repeated dissolution/precipitation (CH<sub>2</sub>Cl<sub>2</sub> / CH<sub>3</sub>OH). Finally, it was dried for 2 days at 40 °C under reduced pressure. The corresponding polyester was named PDD25-DD (4.1 g).

**A1.5 1,4:3,6-dianhydrohexitols-based aliphatic/aliphatic copolyesters**

2.983 g of isosorbide or 3.077 g of isomannide (IS or IM, 20 mmol), 1.16 mL of succinyl chloride (C4, 10 mmol) and 2.25 mL of sebacoyl chloride (C10, 10 mmol) were weighed into a 100 mL three-necked round-bottomed flask equipped with a mechanical stirrer. A continuous N<sub>2</sub> flow was introduced and the flask was dipped into an oil bath (80 and 95 °C for IS and IM, respectively). The temperature was kept at 80 °C (or 95 °C) for 15 min, 100 °C for 15 min, 120 °C for 30 min, 140 °C for 30 min, then raised to 160 °C (the decrease of the release of HCl set the duration of each step) and kept at 160 °C under normal pressure for 4 h with continuous N<sub>2</sub> flow. Then, reduced pressure was applied: 50 mbar for 2 h, then 0.1 mbar for 1 h. After cooling to room temperature, the media was dissolved in dichloromethane (20 mL) and the polymer was precipitated in methanol (200 mL). The polymers were purified by 3 times repeated dissolution/precipitation. Finally, they were dried for 2 days at 40 °C under reduced pressure. The corresponding polymers were named ISC10C4 (5.2 g) and IMC10C4 (5.1 g).

## **A1.6 1,4:3,6-dianhydrohexitols-based aliphatic/aromatic copolyesters**

### **A1.6.1 Bulk method**

The bulk syntheses of aliphatic/aromatic copolyesters were performed the same as the aliphatic/aliphatic ones: 1.492 g (10.01 mmol) of IS, 1.13 mL (5.00 mmol) of C10 and 1.052 g of PDD26 (5.00 mmol) were used for ISC10PDD26 (2.2 g).

### **A1.6.2 Toluene as solvent**

1.491 g of IS (or 1.538 g of IM), 1.13 mL of C10 and 1.052 g of PDD26 (IS or IM : C10 : PDD26 = 10 mmol : 5 mmol : 5 mmol, respectively) were weighed into a 100 mL three-necked round-bottomed flask equipped with a mechanical stirrer and a condenser. With the introduction of a continuous N<sub>2</sub> flow, 15 mL of toluene were added and the flask was dipped into an oil bath (80 and 95 °C for IS and IM, respectively). When the solid particles (IS and PDD26) disappeared, 5 mL of pyridine were dropwise added and the temperature was kept at 80 °C (or 95 °C) for 12 h, then raised to 115 °C and maintained for 12 h under N<sub>2</sub> atmosphere. After cooling to room temperature, the medium was precipitated in methanol and purified by 3 times repeated dissolution/precipitation (CH<sub>2</sub>Cl<sub>2</sub> / CH<sub>3</sub>OH). Finally, it was dried for 2 days at 40 °C under reduced pressure. The corresponding polymers were named ISC10PPD26 (2.6 g) and IMC10PDD26 (2.7 g).

Other polymers, using isophthaloyl dichloride (IPC), were synthesized analogously. They were named ISC10IPC (2.8 g) (1.492 g (10.01 mmol) of IS, 1.13 mL (5.00 mmol) of C10 and 1.036 g of IPC (5.00 mmol) were used) and IMC10IPC (2.8 g) (1.539 g (10.00 mmol) of IM, 1.13 mL (5.00 mmol) of C10 and 1.037 g of IPC (5.00 mmol) were used).

## **A1.7 2,6-pyridinedicarbonyl dichloride-based copolyesters**

The conditions were analogous to PDD26-DD in bulk (A1.2.2 2.103 g of PDD26 (10 mmol) were reacted with different molar ratios of DD and IS: (1) DD : IS = 9 mmol : 1 mmol, 1.568 g and 0.149 g, respectively; (2) DD : IS = 8 mmol : 2 mmol, 1.394 g and 0.298 g respectively; (3) DD : IS = 7 mmol : 3 mmol, 1.219 g and 0.447 g respectively. The obtained quantities were 2.8, 2.5, 2.3 g, respectively.

A similar procedure was implemented for PDD26, DD and EG with a ratio of 10 mmol (2.104 g): 3 mmol (0.534 g): 7 mmol (0.439 g) and a final temperature (at 0.1 mbar) of 160 °C with the production of 1.5 g





---

## Annex 2 Films preparation

The polyester films were prepared by compression molding using a hot press from Scamex (Presse 20 Tons 300 × 300).

The detailed procedure consisted of 6 steps (Figure A2-1):

Step 1: the polyesters were placed within an aluminum window and sandwiched between two steel plates. To avoid the polyester film sticking onto the steel plate, two protective layers were used. The first layer was PTFE sheet, from which the film could be easily taken off. The second layer was an aluminum foil, which was used to protect the steel plate against stains caused by the polymer spilling over the PTFE sheets at high temperature;

Step 2: the sandwich packed steel plates were put into the hot press for 5 min with 50 bars pressure. The pressing temperature varied depending on the thermal properties of the different polyesters (Table A2-1);

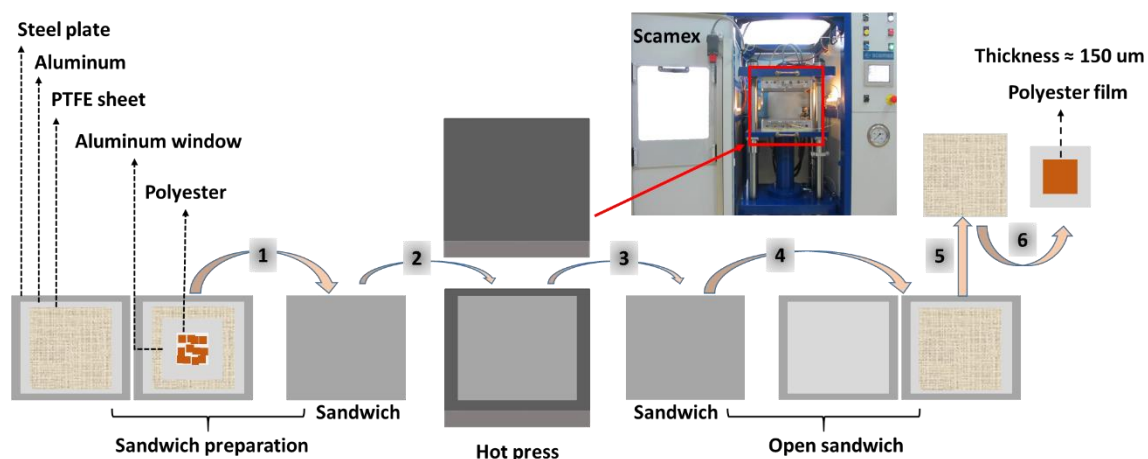
Step 3: after pressing, the sandwich was taken out from the press;

Step 4: the sandwich was opened (without opening the PTFE sheets);

Step 5: the PTFE sheets (including the polyester film) were kept at room temperature (RT) for 60 min (except for IMC10C4 it was put into a 55 °C oven for 3 days, and for IPC-DD it was kept at RT for more than 7 days);

Step 6: the PTFE sheets were opened and the polyester film was taken off from the PTFE paper.

The thickness of the films was controlled to around 150 µm by the thickness of the aluminum window. The films were stored in a desiccator at room temperature under vacuum with P<sub>2</sub>O<sub>5</sub> protection before measurements.



**Figure A2-1** Hot pressing procedure

**Table A2-1** Hot pressing temperatures

Sample name	Press temperature (°C)	Sample name	Press temperature (°C)
ISC4	100	PDD26-EG	200
ISC6	60	PDD26-BD	200
ISC10	50	PDD26-HD	140
IMC4	190	PDD26-DD	120
IMC6	60	PDD25-DD	140
IMC10	45	IPC-DD	55
Sample name	Press temperature (°C)	Sample name	Press temperature (°C)
ISC10C4	60	PDD26-DD <sub>92</sub> -IS <sub>8</sub>	120
ISC10IPC	120	PDD26-DD <sub>85</sub> -IS <sub>15</sub>	120
ISC10PDD26	80	PDD26-DD <sub>76</sub> -IS <sub>24</sub>	120
IMC10C4	100	PDD26-DD <sub>33</sub> -EG <sub>67</sub>	160
IMC10IPC	120		
IMC10PDD26	120		

---

## Annex 3 Characterizations

### A3.1 Size Exclusion Chromatography (SEC)

Average molar masses (number average molar mass  $\overline{M}_n$ , weight average molar mass  $\overline{M}_w$ ) and dispersity ( $D$ ) were measured by size exclusion chromatography (PL-GPC50 from Varian) at 25 °C using two PLgel MIXED-C 5  $\mu\text{m}$  (300  $\times$  7.5 mm) columns and a RI detector. The samples were prepared by dissolving polymers ( $\cong$  10 mg) in dichloromethane (1.7 mL, HPLC grade), and the analysis was carried out using PMMA calibration. The solvent flow rate in the columns was 1.0 mL/min.

### A3.2 Nuclear Magnetic Resonance (NMR)

Chemical structures were determined by  $^1\text{H}$  NMR (Bruker, 300 MHz) with a TopSpin acquisition system at room temperature in  $\text{CDCl}_3$ , unless otherwise stated. Chemical shifts ( $\delta$ ) were expressed in parts per million (ppm) and referenced to the non-deuterated residual solvent peak ( $\delta = 7.26$  ppm) as the internal standard. Around 10 mg polyester was dissolved in  $\sim$ 1.7 mL deuterated solvent.

### A3.3 Fourier Transform Infrared (FTIR)

FTIR measurements were performed on a Spectrum Two from Perkin Elmer, in ATR mode (diamond cell) at 25 °C. Each sample was scanned 10 times from 4000 to 650  $\text{cm}^{-1}$ .

### A3.4 Thermogravimetric Analysis (TGA)

The thermal decomposition of the polymers was investigated by TGA (Q500 from TA Instruments) under a nitrogen atmosphere. To protect the platinum pan from corroding by the potentially released chlorine, the platinum pan was covered with two aluminum layers. 5-10 mg of sample was loaded in the pan and heated from 30 to 600 °C with a heating rate of 10  $^{\circ}\text{C}\cdot\text{min}^{-1}$ .

### A3.5 Differential Scanning Calorimetry (DSC)

The thermal properties of the polymers were investigated by DSC (Q2000 from TA Instruments).  $T_g$  was determined at the mid-point, and  $T_c$  and  $T_m$  at the maximum of the peaks. The sample (5-10 mg) was enclosed in an aluminum pan, and heated under  $N_2$  atmosphere (50 mL·min<sup>-1</sup>) from -30 °C (or 0 °C) to a temperature below degradation previously determined by TGA, followed by a cooling and second heating, at 10 °C·min<sup>-1</sup>. Other running procedures were occasionally applied depending on specific purposes.

### A3.6 X-Ray Diffraction (XRD)

The crystal structures and crystallinity ( $\chi_c$ ) were evaluated using an X-Ray diffractometer D5000 from Bruker AXS. The radiation was  $\lambda_{Co} = 1.789 \text{ \AA}$  powered by a current of 40 mA and a voltage of 40 kV. The data were acquired on a scanning range  $2\theta = 5^\circ$ - $55^\circ$  with a scanning speed of  $0.004^\circ \text{ s}^{-1}$ . The crystallinity determination was performed using PeakFit<sup>®</sup> software.

X-ray diffraction (XRD) can be used to characterize the crystal structures according to Bragg's law:

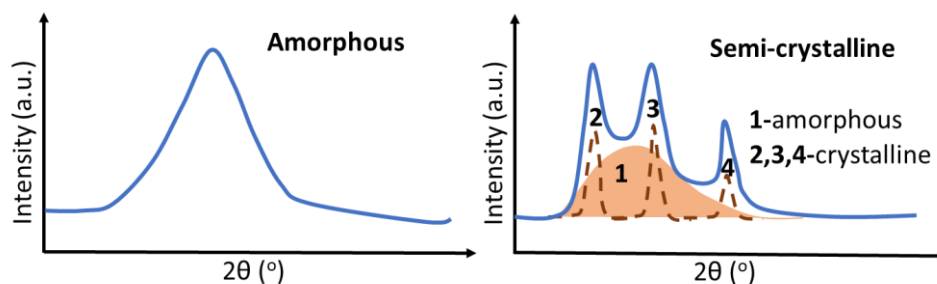
$$2d\sin\theta = n\lambda \quad (\text{Eq. 2-1})$$

where  $d$  is the interplanar distance,  $\theta$  ( $^\circ$ ) is the diffraction angle,  $n$  is a positive integer,  $\lambda$  ( $\text{\AA}$ ) is the wavelength of the incident beam.

Typical XRD spectra of polymers are shown in Figure A3-1: an amorphous polymer only displays a broad signal, while a semi-crystalline one presents both sharp peaks (crystalline phase) and broad halo (amorphous phase). The crystallinity ( $\chi_c$ ) describes the percentage of the crystalline phase that can be calculated as follows:

$$\chi_c = S_c / (S_a + S_c) \quad (\text{Eq. 2-2})$$

where  $S_c$  is the area of the crystalline phase ( $S_c = S_2 + S_3 + S_4$ ) and  $S_a$  is the area of the amorphous phase numbered 1 in Figure A3-1.



**Figure A3-1** Typical XRD spectra of polymers

### A3.7 Dynamic Mechanical Analysis (DMA)

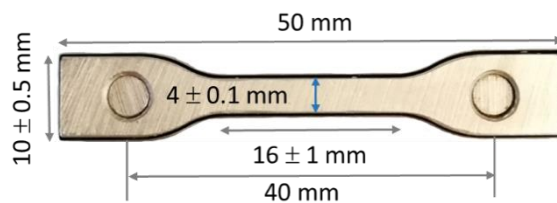
DMA measurements were performed on a Q800 from TA Instruments. The temperature ramp was set from  $-140\text{ }^{\circ}\text{C}$  to the temperature just before melting, at  $3\text{ }^{\circ}\text{C}\cdot\text{min}^{-1}$  and with the frequency of 1 Hz. Rectangular samples ( $21.0\pm0.5 \times 6.6\pm0.01 \times 0.15\pm0.03\text{ mm}$ ) were scanned for PDD26-DD and PDD25-DD films using the tensile mode, while powder was used with PDD26-BD in dual cantilever mode (powder kit).

### A3.8 Polarized Optical Microscopy (POM)

Crystals in polymer films were observed by a Leica DM2500 M polarized optical microscope. Image acquisition and analysis were performed with Archimed<sup>®</sup> software.

### A3.9 Mechanical properties

Young's modulus  $E$  (MPa), stress at break  $\sigma_b$  (MPa) and elongation at break  $\varepsilon_b$  (%) of the polymer films were determined by tensile tests at room temperature ( $23\text{ }^{\circ}\text{C}$ ) using a ZwickRoell Z010 apparatus with testXpert II software. A 500 N load cell,  $10\text{ mm}\cdot\text{min}^{-1}$  crosshead speed and 40 mm distance between grips were used. The dumbbell-shaped specimens were 1BB type according to ISO 527-2 (main dimensions given in Figure A3-2). More than 8 tests were performed on each sample and the obtained values were averaged.

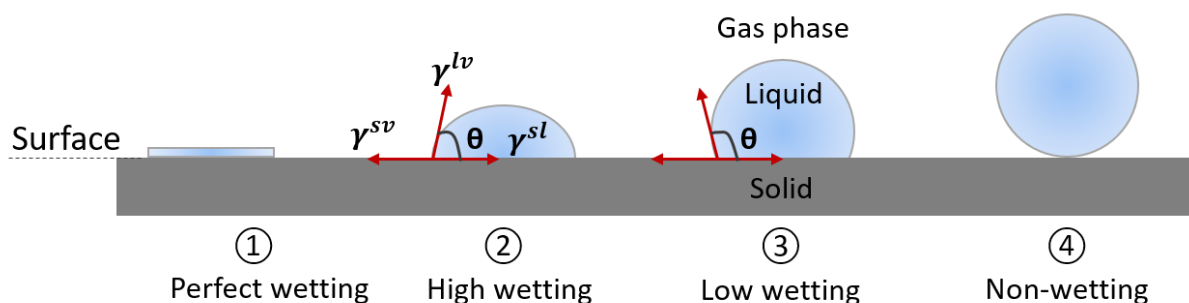


**Figure A3-2** 1BB dumbbell-shaped specimens' dimensions

### A3.10 Surface energy

Water contact angle  $\theta_w$  ( $^\circ$ ) and surface energy  $\gamma^t$  ( $\text{mN}\cdot\text{m}^{-1}$ ) with polar ( $\gamma^p$ ) and dispersive ( $\gamma^d$ ) parts were determined on the films at room temperature ( $23\text{ }^\circ\text{C}$ ) with three different liquids: water (MilliQ Millipore<sup>®</sup> Water system), ethylene glycol ( $> 99\%$ ), and decane ( $> 99\%$ ). The size of the droplet was controlled to  $3\text{ }\mu\text{L}$  and the photo time within 500 ms. Each result was averaged from at least five measurements. The surface energy was calculated by Windrop++ Carrousel software according to Owens & Wendt method [2].

As shown in Figure A3-3, a liquid drop onto a solid surface shows three types of surface energy or tension, denoted as  $\gamma^{sl}$ ,  $\gamma^{sv}$  and  $\gamma^{lv}$ , which correspond to the solid-liquid interfacial force, solid-vapor interfacial force and liquid-vapor interfacial force, respectively. Contact angle ( $\theta$ ) is defined as the angle between  $\gamma^{sl}$  and  $\gamma^{lv}$ . In the case of water, the value of  $\theta$  distinguishes materials into four types: superhydrophilic ( $\theta \leq 5^\circ$ ), hydrophilic ( $5^\circ < \theta < 90^\circ$ ), hydrophobic ( $90^\circ \leq \theta \leq 150^\circ$ ) and superhydrophobic ( $150^\circ < \theta \leq 180^\circ$ ).



**Figure A3-3** Profiles of liquids on different types of surface

### A3.11 Sorption and permeation

When small molecules cross a dense polymer material, the transport phenomena are governed by a dissolution-diffusion process and result from the continuity of:

- the dissolution of molecules within the polymer: this first thermodynamic phenomenon is characterized by a solubility coefficient ( $S$ );
- the diffusion of molecules: this kinetic phenomenon is characterized by a diffusion coefficient ( $D$ ), which reflects the ability of the diffused molecules to disperse in the polymer.

In the ideal case, a homogeneous polymer material presents weak interactions with the diffusing molecules, for which the diffusion remains constant. Thus, the permeability coefficient ( $P$ ) can be obtained from the solubility ( $S$ ) and diffusion ( $D$ ) coefficients:

$$P = D \cdot S \quad (\text{Eq. 2-3})$$

These three parameters can be determined directly or indirectly by sorption and/or permeation measurements.

The transport phenomena of small molecules in polymers are generally observed by sorption and permeation isotherms under the following conditions:

- the polymer is in the form of a film, whose thickness ( $L$ ) is negligible compared to its two other dimensions, and it is exposed to the diffusion or permeation with a surface area  $A$ ;
- the polymer is initially empty of penetrant;
- the activity ( $a$ ) or pressure ( $p$ ) of the penetrant is maintained constant. For a pure liquid,  $a = 1$ , and for a vapor,  $a = p/p_{\text{sat}}$ , where,  $p_{\text{sat}}$  is the saturated vapor pressure.

It is supposed that the diffusion in the polymer film obeys the two Fick's laws [3,4]:

$$J(x, t) = -D \frac{\partial C(x, t)}{\partial x} \quad (\text{Eq. 2-4})$$

$$\text{and,} \quad \frac{\partial C(x, t)}{\partial t} = - \frac{\partial J(x, t)}{\partial x} \quad (\text{Eq. 2-5})$$

$J$  is the local diffusion flux and  $C$  is the local concentration of the penetrant at time  $t$  and  $x$  (coordinate perpendicular to the surface of the film),  $D$  is the local diffusion coefficient of the



penetrant. Frisch [5] distinguishes two Fickian mechanisms, one for a constant  $D$  and the other for a  $D$  depending on the concentration.

If the two interfaces are located at  $x = 0$  and  $x = L$ , the hypotheses are as follows:

- the polymer film is dense and homogeneous;
- the diffusion process is independent of time (the swelling of the film is negligible);
- the sorption equilibrium on the film surface is almost instantaneous;
- the diffusion of the penetrant is supposed to be unidirectional in the film, i.e. the material transfer takes place perpendicular to its the surface.

A general description of the sorption and the permeation mechanisms as well as the description of the obtaining parameters are presented in the following paragraphs.

### A3.11.1 Water sorption

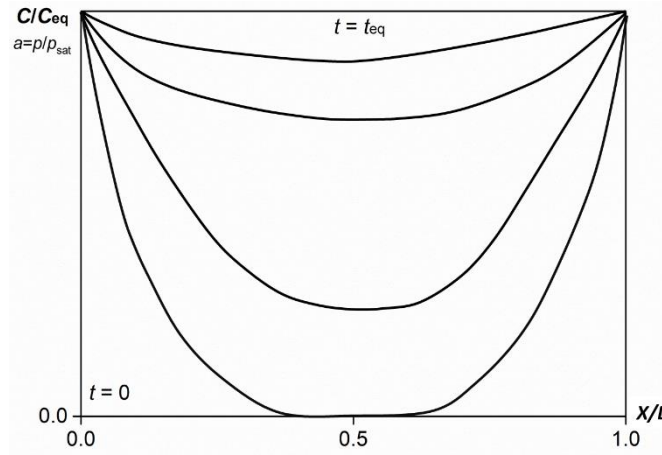
Two types of water sorption measurements have been performed: liquid water sorption and water vapor sorption. In both cases, the sample showed a mass gain in the penetrant environment containing either liquid water or a controlled humidity. The measurements were performed at the same temperature (25 °C) but with different experimental protocols.

#### A3.11.1.1 Sorption mechanisms

The sorption measurements are made by immersing the film in the penetrant phase. The amount of the penetrant accumulates  $M_t$  over time ( $t$ ) in the film. At the end of the kinetic stage,  $M_t$  reaches  $M_{eq}$  which characterizes the equilibrium of sorption. By reducing  $M_{eq}$  to the volume of the film, it becomes the equilibrium concentration ( $C_{eq}$ ), which varies with the penetrant activity ( $a$ ) or pressure ( $p$ ). The corresponding diagram is named sorption isotherm. The limit conditions of sorption are:

$$\begin{aligned}
 &\text{when, } t = 0, \quad C(x, 0) = 0, \quad \forall x \in ]0, L[ \\
 &\text{when, } x = 0, \quad C(0, t) = C_{eq}, \quad \forall t \\
 &\text{when, } x = L, \quad C(L, t) = C_{eq}, \quad \forall t
 \end{aligned}
 \tag{Eq. 2-6}$$

According to Fick equations ((Eq. 2-4) and (Eq. 2-5)), when  $D$  is constant, the profile of concentration in sorption can be established from the initial time  $t = 0$  to  $t_{eq}$  (time at equilibrium of sorption) in reduced scales (Figure A3-4).



**Figure A3-4** Concentration profiles of sorption

In sorption,  $M_t$  is linked to the exposed area of film ( $A$ ) and the concentration ( $C$ ) of penetrant by integration:

$$M_t = A \cdot \int_{x=0}^L C(x, t) \cdot dx \quad (\text{Eq. 2-7})$$

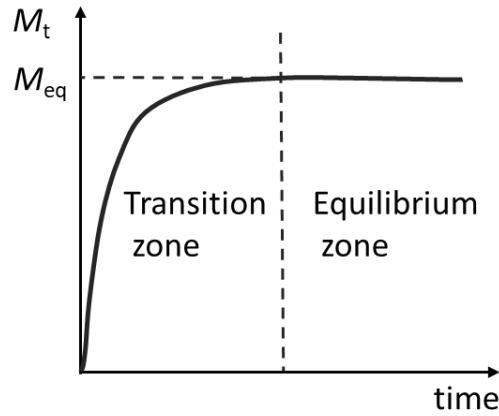
At equilibrium,

$$M_{eq} = A \cdot C_{eq} \cdot L \quad (\text{Eq. 2-8})$$

Then, solubility coefficient ( $S$ ) can be defined as:

$$S_a = \frac{C_{eq}}{a} \quad \text{or} \quad S_p = \frac{C_{eq}}{p} \quad (\text{Eq. 2-9})$$

The sorption kinetics are generally obtained by gravimetric measurements. This method consists of measuring the quantity ( $M_t$  or  $C$ ) of penetrant retained by the material over time up to the equilibrium ( $M_{eq}$  or  $C_{eq}$ ) for a given applied activity ( $a$ ) or pressure ( $p$ ). A typical sorption kinetics is drawn in Figure A3-5.



**Figure A3-5** Example of sorption kinetics at one given activity

At equilibrium, the penetrant concentration ( $C_{eq}$ ) in the material can be directly related to the activity ( $a$ ) by the solubility coefficient ( $S$ ) according to (Eq. 2-9), if the swelling of the sample is negligible. The analysis of the transient zone leads to the determination of the diffusion coefficient ( $D$ ). Finally, the study of sorption equilibria as a function of activity ( $M_{eq}$  vs  $a$ ) makes it possible to establish sorption isotherms. The shapes of these isotherms show the behavior of the diffusing molecules in the material, and particularly, the various types of interactions existing between the diffusing molecules and the material, and also between the molecules.

If  $D$  is constant, (Eq. 2-4) and (Eq. 2-5) allow to establish a relationship between the mass gain ( $m = (M_t/M_{eq})$ ) and the dimensionless time  $\tau$ , where  $\tau$  is defined as

$$\tau = \frac{D \cdot t}{L^2} \quad (\text{Eq. 2-10})$$

and

$$m = \frac{4}{\sqrt{\pi}} \sqrt{\tau} \left( 1 + 2\sqrt{\pi} \sum_{n=1}^{\infty} (-1)^n \operatorname{ierfc} \frac{n}{2\sqrt{\pi}} \right)$$

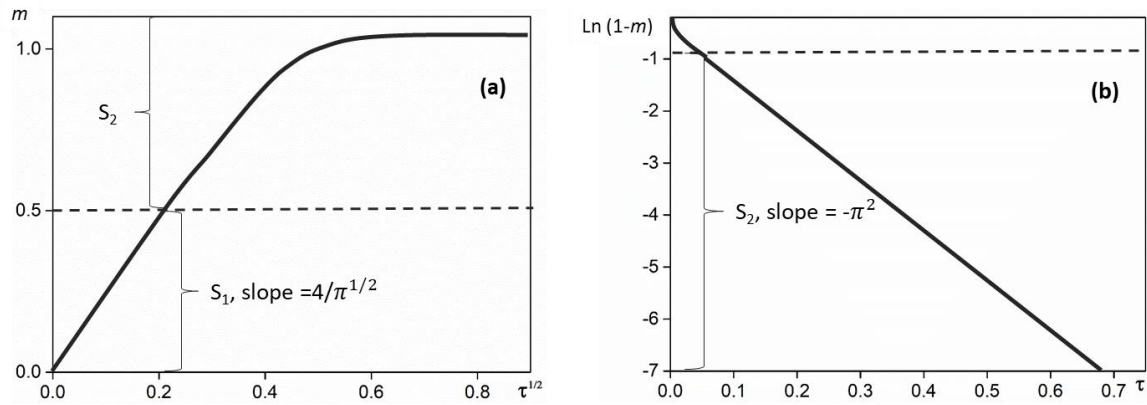
$$m = 1 - \frac{8}{\pi^2} \sum_{n=0}^{\infty} \frac{e^{[-(2n+1)^2 \pi^2 \tau]}}{(2n+1)^2} \quad (\text{Eq. 2-11})$$

For the first half-sorption  $S_1$  ( $m < 1/2$ , Figure A3-6(a)), (Eq. 2-11) is limited to the first term and can be described as:

$$m \approx \frac{4}{\sqrt{\pi}} \cdot \sqrt{\tau} \quad \text{or} \quad m \approx \frac{4}{L} \sqrt{\frac{D_1}{\pi}} \cdot \sqrt{t} \quad (\text{Eq. 2-12})$$

For the second half-sorption  $S_2$  ( $m > 1/2$ , Figure A3-6(b)), (Eq. 2-11) can be reduced to:

$$\begin{aligned} \text{Ln}(1-m) &\approx -\pi^2 \tau - \text{Ln} \frac{\pi^2}{8} \quad \text{or} \\ \text{Ln}(1-m) &\approx -\pi^2 \frac{D_2 \cdot t}{L^2} - \text{Ln} \frac{\pi^2}{8} \end{aligned} \quad (\text{Eq. 2-13})$$

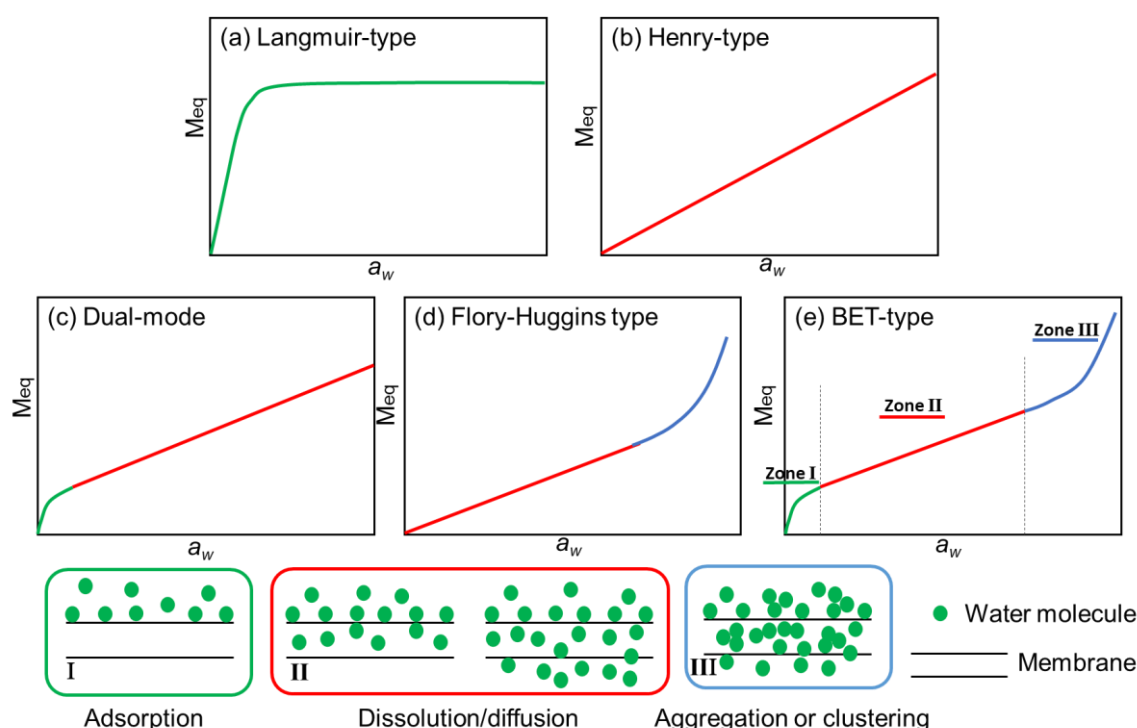


**Figure A3-6** Kinetics of sorption: (a) first half-sorption  $m$  vs  $\sqrt{\tau}$  and (b) second half-sorption  $\text{Ln}(1-m)$  vs  $\tau$

Then, the diffusion coefficient ( $D$ ) can be accessed by two ways: determining  $D_1$  from the first half-sorption and  $D_2$  from the second half-sorption. If  $D_1 = D_2$ , the diffusion coefficient is assumed to be constant. If  $D_2 > D_1$  or vice versa, the diffusion coefficient is dependent on the concentration. In the latter case, the representation  $m = f(\sqrt{t})$  is only valid at the beginning of sorption, and the slope gives an average value of  $D$ . Different types of concentration dependency laws  $D = f(C)$  will be introduced in A3.10.2.1

### Description of sorption isotherms

The solubility ( $S$ ) is a thermodynamic parameter of the penetrants through a material. It depends on the interactions between the penetrant and the material as well as on the temperature. In order to obtain information on the general behavior of the material with respect to the penetrant/polymer interactions, it is necessary to represent the sorption isotherms ( $M_{eq}$  or  $C_{eq}=f(a)$ ). According to Rogers [6] and Brunauer [7], different types of isotherms can be identified and classified depending on the interactions between the penetrants and the materials, and within the penetrants. There are different isotherms (Figure A3-7) for different absorbents, then, numerous sorption theories. They are shown and briefly reviewed below.



**Figure A3-7** Classification of isotherms

#### (a) Langmuir-type

Langmuir sorption (Figure A3-7(a)) is defined when atoms or molecules on a solid surface have outward valence forces that can trap molecules. The range of this residual valence force is equivalent to the molecular diameter, so only single molecular layer adsorption can occur on the surface of the adsorbent (monolayer sorption). Physically, it is observed when sorption takes place in specific sites (hydrophilic groups) or on the surface of microcavities.

The concentration of the adsorbed molecules is given by (Eq. 2-14).

$$C = \frac{A_L \cdot b_L \cdot a}{1 + b_L \cdot a} \quad (\text{Eq. 2-14})$$

The maximum concentration is reached at the saturation of these sites.  $A_L$  corresponds to the average concentration of Langmuir sites and  $b_L$  is the affinity constant between the penetrating molecules and the sites. This type of sorption usually appears for the sorption of dyes in ionic polymers or in polymers containing porous particles (black carbon, silica gel, etc.).

(b) Henry-type

This sorption model describes the ideal case when the penetrant-penetrant interactions and the penetrant-polymer interactions are weak. It usually describes the behavior of the penetrant in a rubbery polymer. In that case sorption of penetrants occurs randomly in the polymer matrix (amorphous areas) and the solubility coefficient ( $S$ ) introduced in (Eq. 2-9) is usually quite low and constant (Figure A3-7(b)). Therefore,  $S$  can be obtained from Henry's law (Eq. 2-15), where the Henry's coefficient  $k_H$  reflects  $S$  and signifies the ability of the penetrant to “condense” in the matrix.

$$C = k_H \cdot a \quad (\text{Eq. 2-15})$$

(c) Henry-Langmuir type (Dual-Mode)

This type of sorption is a combination of Henry and Langmuir (Figure A3-7(c)). It generally concerns glassy polymers and obeys to the law of additivity as follows:

$$C = k_H \cdot a + \frac{A_L \cdot b_L \cdot a}{1 + b_L \cdot a} \quad (\text{Eq. 2-16})$$

(d) Flory-Huggins type

In this case, the penetrant-penetrant interactions are stronger compared to those existing between penetrant and polymer. The presence of this type of interactions generate higher penetrant solubility which exponentially increases with the increase of activity. The sorption described by the Flory-Huggins relation mainly concerns non-polar solvents. It is also found during the sorption of water in hydrophobic polymers containing some polar groups.

$$\ln a = \ln \Phi_1 + (1 - \Phi_1) + \chi \cdot (1 - \Phi_1)^2 \quad (\text{Eq. 2-17})$$

$\Phi_1$  is the penetrant volume fraction in the polymer and  $\chi$  is the Flory-Huggins interaction parameter (between penetrant and polymer) assumed to be constant. Such isotherm presents an upwards concavity (Figure A3-7(d)). This behavior is also found for high water activity when the penetrants aggregate in the polymer. It results in an increase of penetrant solubility in the polymer.

(e) BET-type (Park model)

This type of sorption is named from the authors' names Brunauer, Emmett and Teller. BET-type sorption isotherms always present a "sigmoid" shape as shown in Figure A3-7(e).

It may correspond to the additivity of Langmuir and Flory-Huggins sorption. This behavior is encountered when the penetrant-polymer interactions are strong. The result is a significant swelling of the polymer matrix.

In accordance with Park's model [8], this isotherm is observed when the aggregation of water molecules is observed after Langmuir and Henry sorptions.

$$C = \frac{A_L \cdot b_L \cdot a}{1 + b_L \cdot a} + k_H \cdot a + K_a \cdot a^{n_a} \quad (\text{Eq. 2-18})$$

$K_a$  is the equilibrium constant for the clustering reaction and  $n_a$  is the average number of water molecules per cluster. This equation is often used to describe the sorption of water molecules in hydrophilic polymers.

### A3.11.1.2 Liquid water sorption

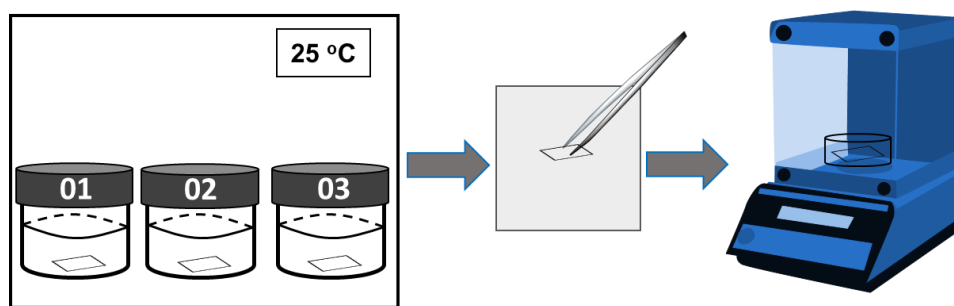
The liquid water sorption measurements were performed at 25 °C by measuring the variation of the mass gain ( $M_t$ ) vs time ( $t$ ) of samples (initially dry) immersed in pure water (MilliQ Millipore® Water system). The measurement was triplicated for each sample ( $A = 1 \text{ cm}^2$ ) using a balance (precision 0.1 mg).  $M_t$  can be calculated according to:

$$M_t = \frac{m_t - m_d}{m_d} \cdot 100 \quad (\text{Eq. 2-19})$$

with  $m_t$  the film mass at  $t$  time and  $m_d$  the dry film mass. The accuracy of  $M_t$  value was estimated lower than 10%.

### Measurement procedures

The detailed procedure is presented in Figure A3-8. Three numbered wide-mouth plastic bottles (volume ~10 mL) were prepared and filled with 7 mL pure water (MilliQ Millipore® Water system). The film sample (~ 30 mg) was first weighed to determine its initial mass  $m_d$  (taken in a dry state). Then, the film sample was immersed into water and kept under 25 °C, periodically removed from the water, cautiously wiped away the surface water and then weighed ( $m_t$ ). This operation was repeated every 10 min for the first hour, then every hour for 5 hours, finally every day until the equilibrium (the weight of the film became constant,  $m_{eq}$ ) was obtained.



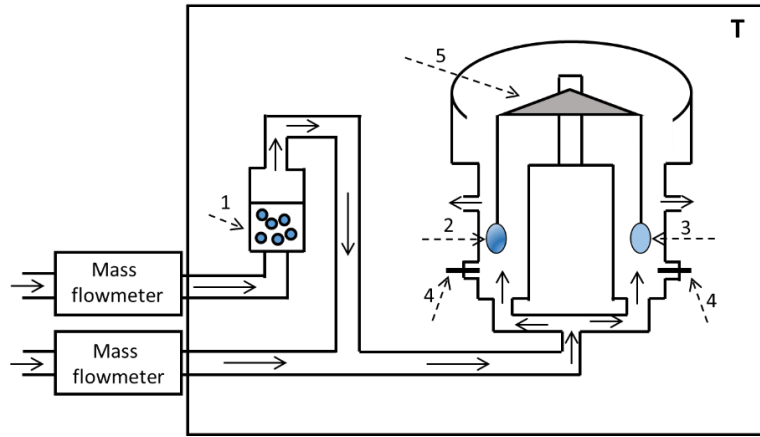
**Figure A3-8** Flow chart of liquid water sorption measurement

#### **A3.11.1.3 Water vapor sorption**

Water vapor sorption measurements were conducted with the automatic gravimetric dynamic vapor sorption DVS (Surface Measurement Systems Ltd). This device can continuously measure the weight change of a sample at controlled water activities.

The simplified DVS device is given in Figure A3-9. It consists of a microbalance in a thermoregulated chamber. Two quartz nacelles are connected to the microbalance by alloy wires that do not absorb water. The nacelle on the left is used to load samples and the one on the right serves as a reference (empty). During the measurement, the two compartments of the microbalance are swept by a certain gas humidity (a mixture of dry gas (nitrogen) and humid gas (nitrogen with saturated water vapor)) controlled by mass flowmeters. The temperature and relative humidity in both compartments are checked by probes below the nacelles.





**Figure A3-9** DVS device simplification

With,

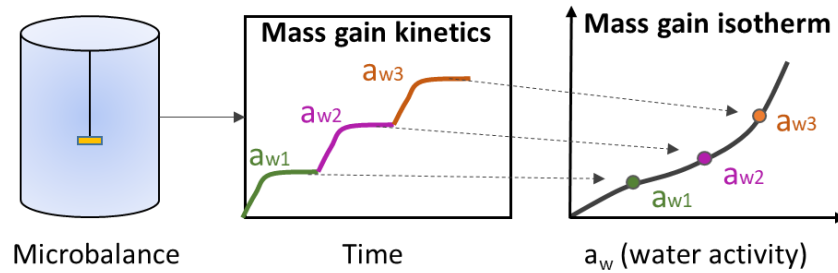
- 1- Humidifier ( $\pm 1.5\%$ )
- 2- Sample nacelle
- 3- Reference nacelle
- 4- Temperature and humidity detector
- 5- Microbalance ( $\pm 0.1 \mu\text{g}$ )

### **Measurement procedures**

The measurements were performed at 25 °C. Before each measurement the microbalance was calibrated and tared. Then, a film sample (about 15 mg) previously stored in a desiccator was loaded in the measuring nacelle. The film was dried until a constant weight ( $m_d$ ) by a dry nitrogen flow (200 cm<sup>3</sup>/min) before measurement. Then, different water activity ( $a_w$ ) steps ranging from 0 to 0.95 were applied to the film. At each step, the mass gain was measured as a function of time until the equilibrium was reached. The mass gain at equilibrium  $M_{eq}$  was calculated for each  $a_w$  according to (Eq. 2-20), which allowed the plotting of water sorption isotherms (Figure A3-10). The accuracy of the values was lower than 4%.

$$M_{eq} = \frac{m_{eq} - m_d}{m_d} \cdot 100 \quad (\text{Eq. 2-20})$$

With,  $m_{eq}$  the film mass at equilibrium.



**Figure A3-10** Plotting of water vapor sorption isotherms

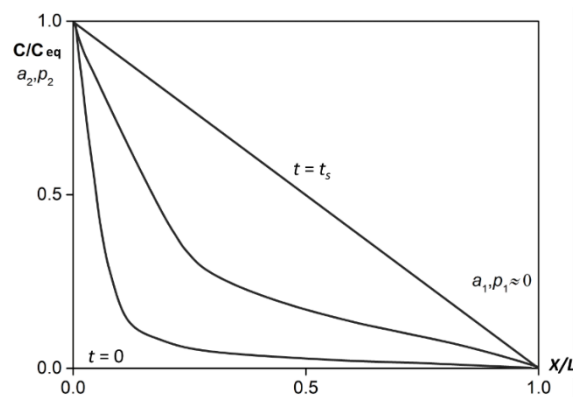
### A3.11.2 Permeation

#### A3.11.2.1 Description of permeation

Permeation diffusion phenomena follow the Fick's laws ((Eq. 2-4) and (Eq. 2-5)). The two interfaces are located at  $x=0$  and  $x=L$ , which correspond respectively to the upstream and downstream. The same hypotheses as for the sorption are used. The permeation boundary conditions are:

$$\begin{aligned} t=0, \quad C(x,0) &= 0 & \forall x \in ]0,L[ \\ x=0, \quad C(0,t) &= C_0 & \forall t \\ x=L, \quad C(L,t) &= 0 & \forall t \end{aligned} \quad (\text{Eq. 2-21})$$

When  $D$  is considered constant, the concentration profile in the film can be schematized as Figure A3-11.



**Figure A3-11** Concentration profiles from  $t = 0$  to  $t = t_s$  (stationary state) with constant  $D$  and reduced scales

Permeation measurements were performed by using a two compartments system. When a certain concentration of penetrant (water or gas) was applied to the upstream, the penetrant molecules diffuse from the upstream to the downstream. Depending on the penetrant, two types of permeation set-up were used. For water (vapor or liquid), differential permeation measurement was used, where the downstream is continuously swept by a carrier gas and the variation of the downstream flux  $J(L,t)$  is measured versus time (Figure A3-12(1)). For gases, the integral permeation measurement system was used where the downstream initially under vacuum accumulated the penetrant quantity  $Q_t$  versus time (Figure A3-12(2)). In both cases, transitory and stationary states can be observed.

With the differential permeation measurement, the amount of penetrant reduced to the unit surface of the film defines the density of downstream permeation flux,  $J_d$ , hereinafter called downstream flux.  $J_d$  remains zero for the first period, then increase stepwise until a plateau, where the flux becomes stationary  $J_{st}$  (Figure A3-12(1)). In this case,  $P$  can be calculated by the stationary flux  $J_{st}$  and the upstream water activity ( $a_w$ ) (if the downstream  $a_w$  is negligible):

$$P = \frac{J_{st} \cdot L}{a_w} \quad (\text{Eq. 2-22})$$

In integral permeation measurement, the quantity of penetrant  $Q_t$  accumulated versus time ( $t$ ) in the downstream can be calculated from:

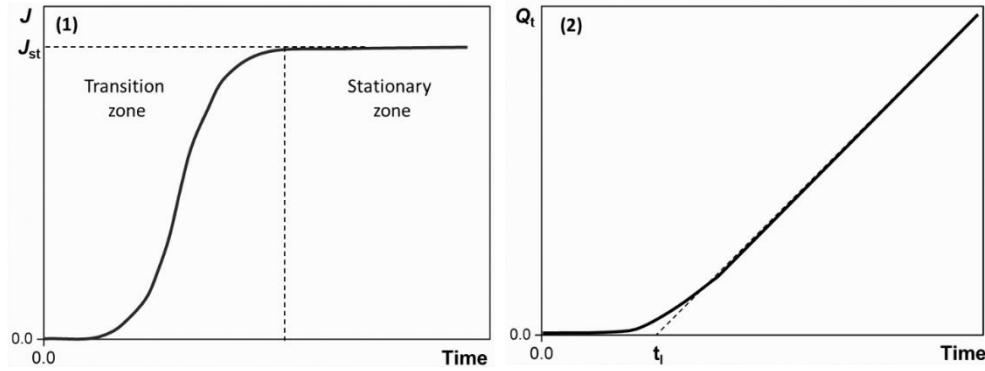
$$Q_t = A \int_{t=0}^t J(L, t) dt \quad (\text{Eq. 2-23})$$

Where,  $A$  is the surface of the film exposed to the permeation.

Over time,  $J(L,t)$  increases stepwise to a steady state ( $J_{st}$ ), where  $J_{st}$  can be related to penetrant quantity  $Q_t$

$$Q_t = A \cdot J_{st} \cdot (t - t_l) \quad (\text{Eq. 2-24})$$

With  $t_l$  delay time for the diffusion or “time lag” (Figure A3-12(2)).



**Figure A3-12** Typical curves obtained from permeation: differential (1) and integral (2)

When processing the experimental data, we will suppose two cases: one with a constant diffusion coefficient (Fickian type 1) as described before and the other with a  $D$  depending on the concentration (Fickian type 2). This latter case can be introduced as follows.

When  $D$  depends on the concentration, there are several dependency laws ( $D = f(C)$ ). It should be noticed that the determination of  $D$  is based on the hypothesis of homogeneous polymer matrix.

In a general case, the diffusion coefficient increases with the concentration when the increase of the penetrant concentration is sufficient to modify the interactions between the macromolecular chains. This phenomenon is often observed when there is plasticization of the polymer matrix by the penetrant [9]. Under this circumstance, an exponential law will be used:

$$D = D_0 \cdot e^{\gamma \cdot C} \quad (\text{Eq. 2-25})$$

where  $D_0$  is the diffusion coefficient when the concentration  $C$  of the penetrant tends to 0 and  $\gamma$  is the plasticization coefficient. This law is generally applied to penetrants with a strong plasticizing effect (*i.e.* water and toluene type hydrocarbons).

Then an integral diffusion coefficient can be calculated as:

$$\bar{D} = \frac{D_0 \cdot [e^b - 1]}{b} \quad (\text{Eq. 2-26})$$

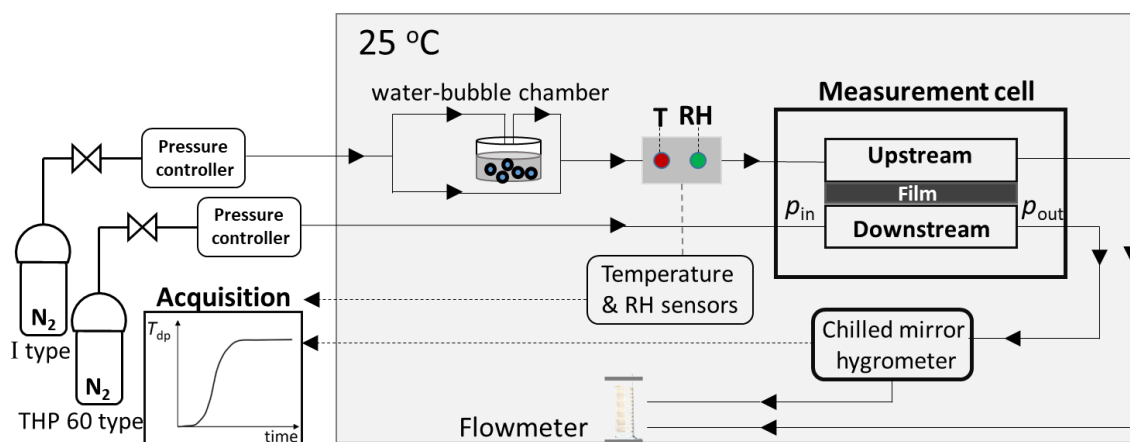
with  $b = \gamma \cdot C_{eq}$ . According to the basis of the  $D$  increases with the concentration, the kinetics of permeation can be simulated by (Eq. 2-25).

### A3.11.2.2 Water vapor permeation

The water vapor permeation coefficients were determined by differential permeation measurement based on the measurement of the accumulation rate of the penetrant into a downstream closed compartment after diffusion through a membrane.

#### Experimental set-up

The experiments were conducted in a thermoregulated measuring cell consisting of two compartments separated by the film to be tested (surface of the film  $A = 3.6 \text{ cm}^2$ ) (Figure A3-13) [9]. Before the measurement, a purge step (dry nitrogen at  $5.8 \text{ cm}^3 \cdot \text{s}^{-1}$ ) was carried out to dry the film and the cell as much as possible. The measurement began when the nitrogen in the upstream compartment was replaced by vapor water (wet  $\text{N}_2$  circulating at  $9.3 \text{ cm}^3 \cdot \text{s}^{-1}$  in a water-bubble chamber with MilliQ<sup>®</sup> water). In the downstream compartment, the nitrogen humidity signal was detected by a chilled mirror hygrometer from General Eastern (M4Dp model equipped with a four stages sensor). The probe signal is proportional to the dew point temperature  $T_{dp}$  that gives the exact water vapor concentration of a gas. The signal is transmitted to the acquisition system ( $T_{dp} = f(t)$ , accuracy  $\pm 0.5 \text{ }^\circ\text{C}$ ). The pressure of downstream was maintained at 1 atm during the whole measurement. The measurement lasted until the downstream humidity signals became constant, which corresponded to a steady state ( $J = J_{st}$ ). Experimental runs were repeated several times for different water activities on each film.



**Figure A3-13** Experimental setup of water vapor permeation measurement (RH for relative humidity)

### **Permeation coefficient ( $P$ )**

The sweeping nitrogen in the downstream compartment receives the water vapor molecules that diffused through the film and carries them to a mirror hygrometer. Consequently, the downstream pressure increases from  $p^{\text{in}}$  to  $p^{\text{out}}$  (Figure A3-13). The flux of water vapor  $J(L, t)$  ( $\text{mmol}\cdot\text{cm}^{-2}\cdot\text{s}^{-1}$ ) through the film can be calculated from the following equation [9]:

$$J(L, t) = \frac{f}{A} \cdot \frac{(p^{\text{out}} - p^{\text{in}})}{R \cdot T} \quad (\text{Eq. 2-27})$$

Where,

$f$ , the flow rate of dry gas ( $9.3 \text{ cm}^3\cdot\text{s}^{-1}$ );

$A$ , the effective surface of the film exposed to diffusion ( $3.6 \text{ cm}^2$ );

$R$ , the constant of ideal gas ( $0.082\cdot\text{atm}\cdot\text{cm}^3\cdot\text{K}^{-1}\cdot\text{mmol}^{-1}$ );

$T$ , the experimental temperature ( $298\text{K}$ );

$p^{\text{in}}$  and  $p^{\text{out}}$ , the inlet and outlet water vapor pressure of the downstream compartment.

$p^{\text{out}}$  value can be indirectly obtained from  $T_{\text{dp}}$  of the downstream carrier gas according to the Clapeyron–Clausius relation [12]:

$$\frac{d(\ln p_s(T))}{d(1/T)} = -\frac{\Delta H_v(T)}{R} \quad (\text{Eq. 2-28})$$

With  $p_s(T)$ , the saturated vapor pressure,  $R$ , the gas constant and  $\Delta H_v(T)$ , the molar vaporization enthalpy at temperature  $T$ .

When  $\Delta H_v(T)$  is considered constant at temperature  $T$ :

$$p = \exp\left(-\frac{B}{T} + C\right) \quad (\text{Eq. 2-29})$$

Knowing that  $p_{\text{out}}$  becomes  $p_s$  when  $T = T_{\text{dp}}$ . Then the water vapor concentration ( $x$ ) in ppmV can be used instead of  $p$ , with  $x_{\text{ppmV}} = 10^6 p/p_t$ , the total pressure  $p_t$  and partial pressure  $p/p_t$ . There is:

$$x_{\text{ppmV}} = 10^6 \cdot \exp\left(-\frac{B}{T} + c\right) / p_t \quad (\text{Eq. 2-30})$$

Where  $B = 6185.66$ ,  $c = 31.38$  and  $T$  in K.

Then (Eq. 2-27) can be deduced into:

$$J(L, t) = 10^{-6} \cdot \frac{f}{A} \cdot \frac{x^{out} - x^{in}}{R \cdot T} \cdot p_t \quad (\text{Eq. 2-31})$$

Due to the downstream total pressure  $p_t$  is usually maintained at 1 atm,

$$J(L, t) = 10^{-6} \cdot \frac{f}{A} \cdot \frac{x^{out} - x^{in}}{R \cdot T} \quad (\text{Eq. 2-32})$$

When the equilibrium is obtained  $J(L, t) = J_{st}$ , according to (Eq. 2-1), we have:

$$P = \frac{J_{st} \cdot L}{\Delta a_w} \quad (\text{Eq. 2-33})$$

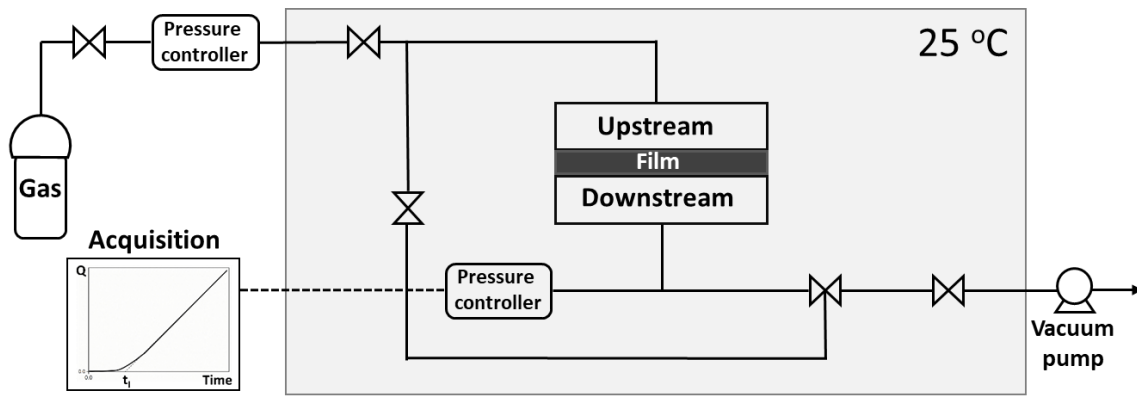
With,  $\Delta a_w$  the difference in water activity between the upstream and the downstream compartment.  $P$  was expressed in  $\text{g} \cdot \text{m}^{-1} \cdot \text{d}^{-1}$  or barrer.

### **A3.11.2.3 Gas permeation**

The gas diffusion coefficient ( $D$ ) and permeation coefficient ( $P$ ) were obtained by a variable-pressure constant-volume method, i.e. the “integral permeation” method based on the continuous monitoring of the amount of diffusing gas through a membrane into a closed vessel.

#### **Experimental set-up**

The gas permeation measurements were conducted at 25 °C on our home-made apparatus shown in Figure A3-14. First, a vacuum ( $10^{-3}$  mbar) environment was applied to the measurement cell for a period at least a duration time twice of the measurement. Then, the upstream compartment was applied a certain pure gas ( $\text{N}_2$ ,  $\text{O}_2$ ,  $\text{CO}_2$ ) pressure ( $p_1=3$  bar), while the downstream was still under vacuum ( $10^{-3}$  mbar). The pure gas permeated through the film from the upstream to downstream, which led to a pressure increase ( $p_2$ ) in the downstream. The increase of the downstream pressure with time was measured by a manometer (0–10 mbar, Druck AW 10 T4) that connected to an acquisition system. The measurement last until the downstream pressure reached a constant value, which indicates the stationary state ( $J_{st}$ ) of the permeation process.



**Figure A3-14** Gas permeation measurement setup

### Diffusion coefficient ( $D$ )

When the steady state is reached, the diffusion coefficient  $D$  is assumed to be constant. It can be calculated from the time-lag  $t_l$  value obtained from the extrapolation of the steady-state asymptote to the time axis (Figure A3-12) [12].

$$D = \frac{L^2}{6t_l} \quad (\text{Eq. 2-34})$$

$D$  expressed in unit  $\text{cm}^2 \cdot \text{s}^{-1}$ .

### Permeation coefficient ( $P$ )

The permeation coefficient  $P$  (expressed in barrer unit) can be calculated by the accumulated gas quantity  $Q$  versus time according to:

$$P = \frac{L \cdot V}{A \cdot R \cdot T \cdot \Delta P} \frac{dQ_t}{dt} \quad (\text{Eq. 2-35})$$

with  $L$  and  $A$ , thickness and surface ( $11.34 \text{ cm}^2$ ) of the film;  $V$ , downstream volume ( $98.13 \text{ cm}^3$ );  $R$ , ideal gas constant ( $0.082 \text{ atm} \cdot \text{cm}^3 \cdot \text{K}^{-1} \cdot \text{mmol}^{-1}$ );  $T$ , experimental temperature ( $298 \text{ K}$ );  $\Delta p$ , the pressure difference between the two sides of the film ( $4 \text{ bar}$ );  $dQ/dt$ , the slope of the experimental curve at stationary state.

$P$  was expressed in barrer ( $1 \text{ barrer} = 10^{-10} \cdot \text{cm}^3 \cdot (\text{STP}) \cdot \text{cm} \cdot \text{cm}^{-2} \cdot \text{s}^{-1} \cdot \text{cmHg}^{-1}$ ).



### Selectivity coefficient ( $\alpha_{A/B}$ )

The gas selectivity coefficient ( $\alpha_{A/B}$ ) was calculated to explain the difference in permeability of the film for two different gases A and B. It was defined as the ratio of the more permeable gas  $P_A$  to the less permeable  $P_B$  as:

$$\alpha_{A/B} = \frac{P_A}{P_B} = \frac{D_A \cdot S_A}{D_B \cdot S_B} \quad (\text{Eq. 2-36})$$

### A3.11.3 Index

Permeation coefficient ( $P$ ) can be expressed in different units, depending on the preference of the authors, which makes comparisons complicated. Thus, units must be unified. Table A3-1 lists the multiplication factors of different units to barrer.

**Table A3-1** Converting  $P$  from different units to barrer

Units	$P \times 10^{-10}$ (barrer) <sup>a</sup>
[mL(STP) cm cm <sup>-2</sup> s <sup>-1</sup> (cm Hg) <sup>-1</sup> ]	1.0
[mL(STP) mm cm <sup>-2</sup> s <sup>-1</sup> (cm Hg) <sup>-1</sup> ]	$1.00 \times 10^{-1}$
[mL(STP) cm cm <sup>-2</sup> s <sup>-1</sup> Pa <sup>-1</sup> ]	$1.33 \times 10^2$
[mL(STP) m m <sup>-2</sup> s <sup>-1</sup> Pa <sup>-1</sup> ]	$1.33 \times 10$
[m <sup>3</sup> (STP) m m <sup>-2</sup> s <sup>-1</sup> Pa <sup>-1</sup> ]	$1.33 \times 10^7$
[mL(STP) cm cm <sup>-2</sup> s <sup>-1</sup> bar <sup>-1</sup> ]	$1.33 \times 10^{-2}$
[mL(STP) cm m <sup>-2</sup> d <sup>-1</sup> bar <sup>-1</sup> ]	$1.54 \times 10^{-11}$
[mL(STP) $\mu$ m m <sup>-2</sup> d <sup>-1</sup> bar <sup>-1</sup> ]	$1.54 \times 10^{-15}$
[mL(STP) cm cm <sup>-2</sup> s <sup>-1</sup> atm <sup>-1</sup> ]	$1.32 \times 10^{-2}$
[mL(STP) mm cm <sup>-2</sup> s <sup>-1</sup> atm <sup>-1</sup> ]	$1.33 \times 10^{-3}$
[mL(STP) cm m <sup>-2</sup> d <sup>-1</sup> atm <sup>-1</sup> ]	$1.52 \times 10^{-11}$
[mL(STP) mm m <sup>-2</sup> d <sup>-1</sup> atm <sup>-1</sup> ]	$1.52 \times 10^{-12}$
[mL(STP) $\mu$ m m <sup>-2</sup> d <sup>-1</sup> atm <sup>-1</sup> ]	$1.52 \times 10^{-15}$
[mL(STP) mil m <sup>-2</sup> d <sup>-1</sup> atm <sup>-1</sup> ]	$3.86 \times 10^{-15}$
[mL(STP) mil 100 in <sup>-2</sup> d <sup>-1</sup> atm <sup>-1</sup> ]	$6.00 \times 10^{-10}$
[mL(STP) mm 100 in <sup>-2</sup> d <sup>-1</sup> atm <sup>-1</sup> ]	$2.36 \times 10^{-8}$
[in <sup>3</sup> (STP) mil 100 in <sup>-2</sup> d <sup>-1</sup> atm <sup>-1</sup> ]	$9.83 \times 10^{-10}$
[mL(STP) mm m <sup>-2</sup> d <sup>-1</sup> kPa <sup>-1</sup> ]	$1.54 \times 10^{-10}$
[mL(STP) $\mu$ m m <sup>-2</sup> d <sup>-1</sup> kPa <sup>-1</sup> ]	$1.54 \times 10^{-13}$
[kg m m <sup>-2</sup> s <sup>-1</sup> Pa <sup>-1</sup> ] for O <sub>2</sub>	$9.34 \times 10^6$
[kg m m <sup>-2</sup> s <sup>-1</sup> Pa <sup>-1</sup> ] for CO <sub>2</sub>	$6.79 \times 10^6$
[kg m m <sup>-2</sup> s <sup>-1</sup> Pa <sup>-1</sup> ] for N <sub>2</sub>	$10.67 \times 10^6$
[kg m m <sup>-2</sup> s <sup>-1</sup> Pa <sup>-1</sup> ] for H <sub>2</sub> O	$16.60 \times 10^6$

<sup>a</sup>The data of  $P$  in barrer were extracted from [13], 1Pa =  $7.5 \times 10^{-4}$  cmHg, 1bar = 75 cmHg, 1atm = 76 cmHg, 1 mil =  $2.54 \times 10^{-3}$  cm, 1 in = 2.54 cm

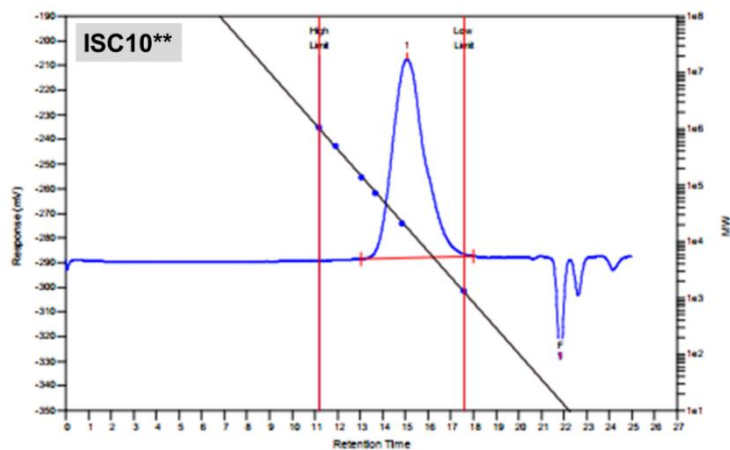
---

## References

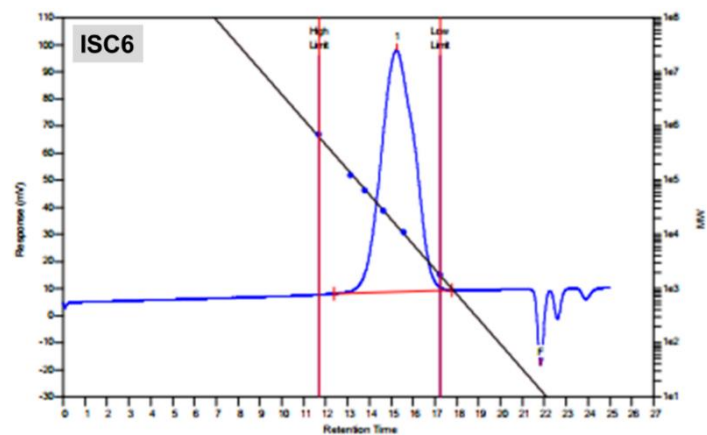
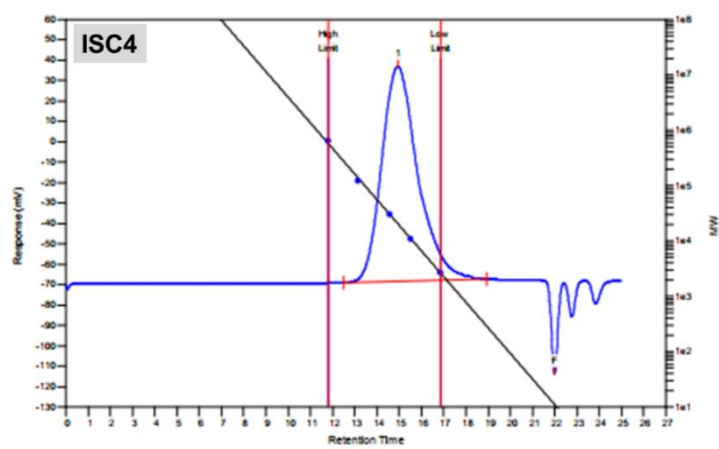
- [1] T.M. Khan, M. Zakria, M. Ahmad, R.I. Shakoor, Optoelectronic study and annealing stability of room temperature pulsed laser ablated ZnSe polycrystalline thin films, (2013).
- [2] D.K. Owens, R.C. Wendt, Estimation of the surface free energy of polymers, *J. Appl. Polym. Sci.* 13 (1969) 1741–1747.
- [3] J. Crank, G.S. Park, *Diffusion in polymers*, London and New York: Academic Press, 1968.
- [4] J. Crank, *The mathematics of diffusion*, 2nd ed, New York: Oxford University Press, 1975.
- [5] H.L. Frisch, The time lag in diffusion, *J. Phys. Chem.* 61 (1957) 93–95.
- [6] C.E. Rogers, Solubility and diffusivity, *Phys. Chem. Org. Solid State.* (1966) 509–635.
- [7] S. Brunauer, P.H. Emmett, E. Teller, Adsorption of gases in multimolecular layers, *J. Am. Chem. Soc.* 60 (1938) 309–319.
- [8] G.S. Park, Transport principles-solution, diffusion and permeation in polymer membranes, in: *Synth. Membr. Sci. Eng. Appl.*, Springer Netherlands, Dordrecht, 1986: pp. 57–107.
- [9] S. Marais, M. Metayer, M. Labbe, Water diffusion and permeability in unsaturated polyester resin films characterized by measurements performed with a water-specific permeameter: analysis of the transient permeation, *J. Appl. Polym. Sci.* 74 (1999) 3380–3395.
- [10] M.H. Cohen, D. Turnbull, Molecular transport in liquids and glasses, *J. Chem. Phys.* 31 (1959) 1164–1169.
- [11] H. Fujita, Diffusion in polymer-diluent systems, *Fortschritte Der Hochpolym.* 3 (1961) 1–47.
- [12] M. Métayer, M. Labbé, S. Marais, D. Langevin, C. Chappey, F. Dreux, M. Brainville, P. Belliard, Diffusion of water through various polymer films: A new high performance method of characterization, *Polym. Test.* 18 (1999) 533–549.
- [13] Robertson, G. L, *Food packaging-Principles and practice*, 3rd ed., Taylor & Francis, 2013.

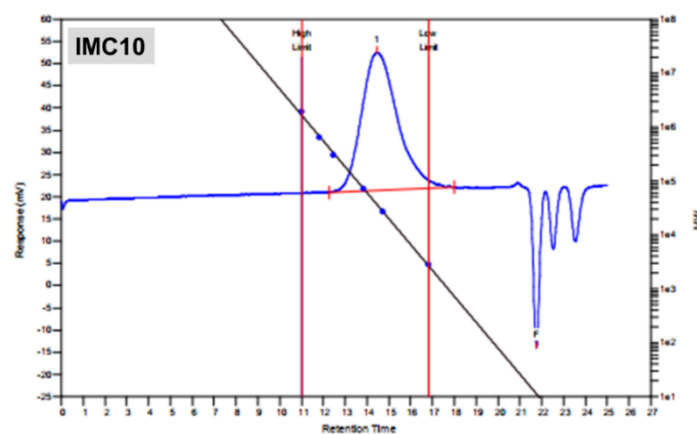
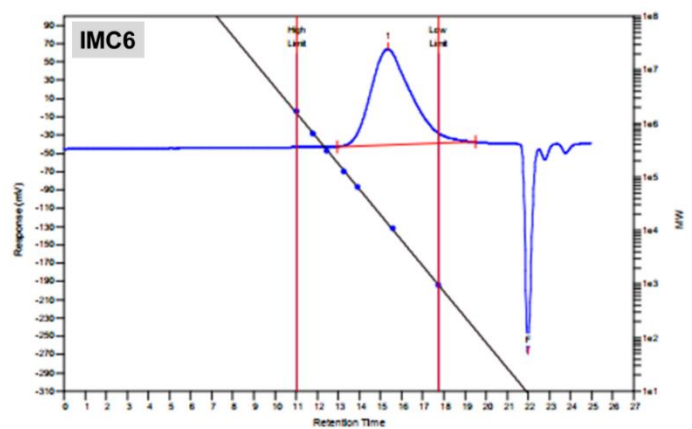
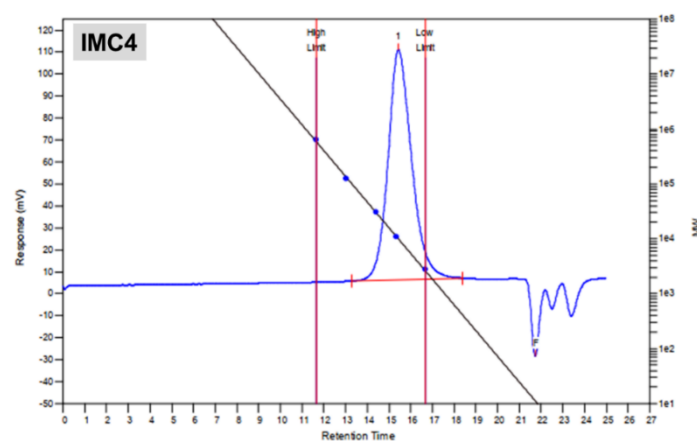
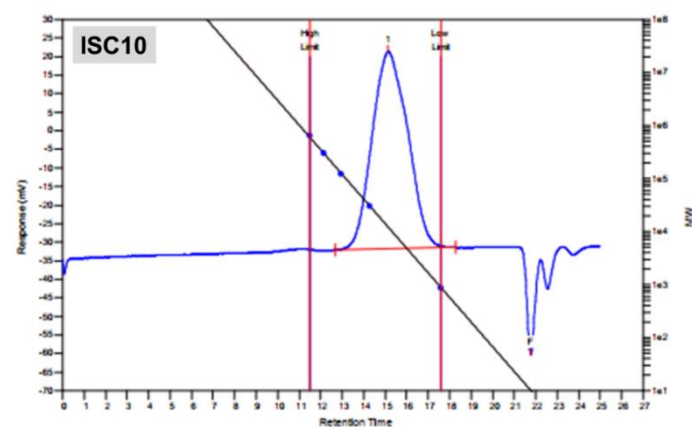
## Annex 4 SEC

### 2.1 Synthesis

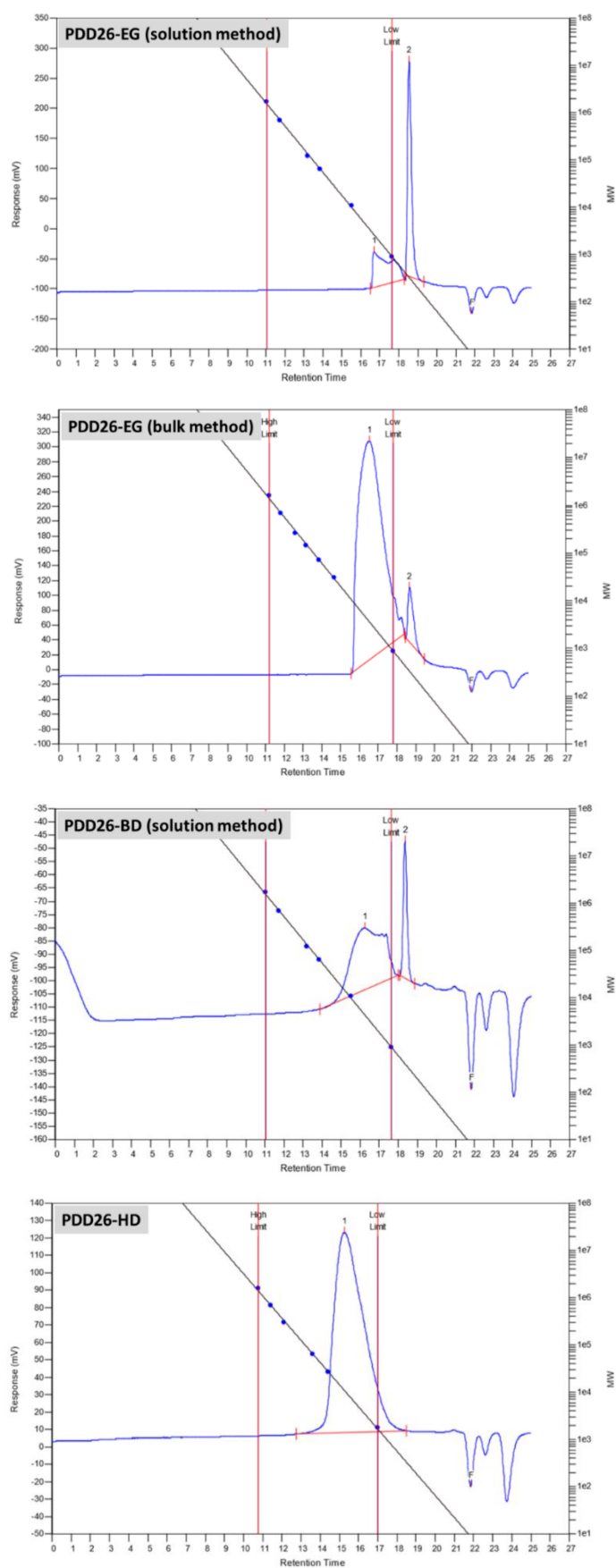


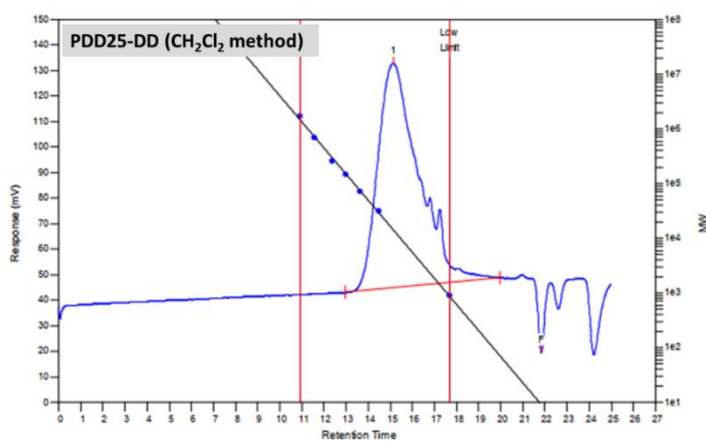
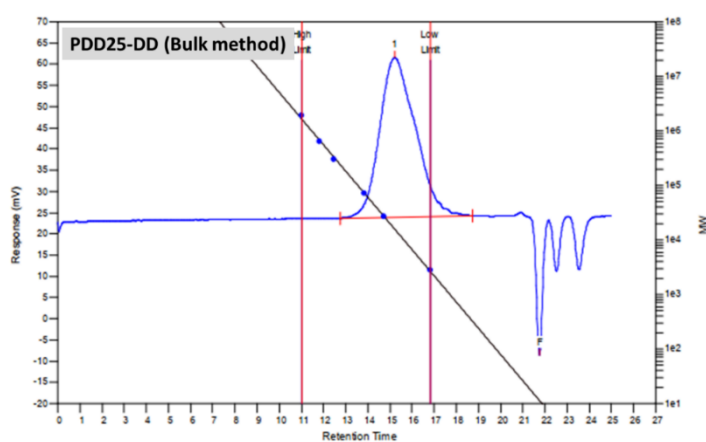
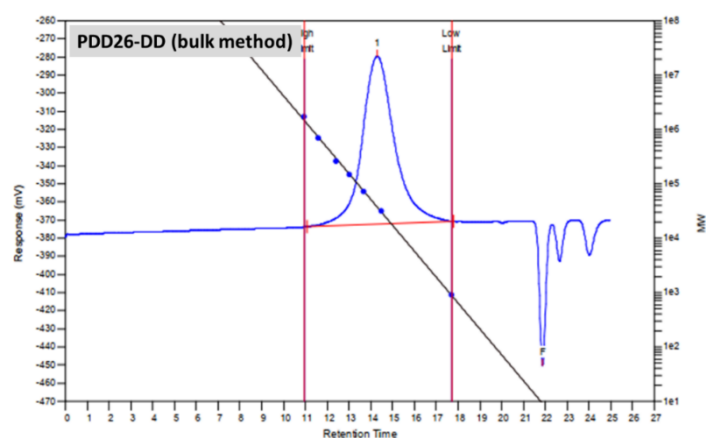
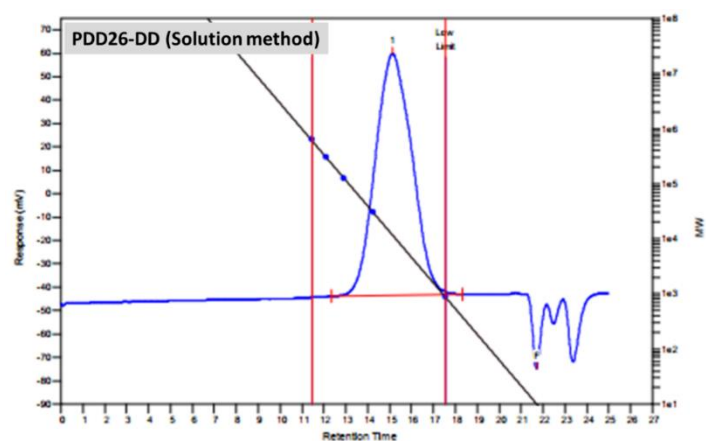
### 2.2.2 Molar masses and yields

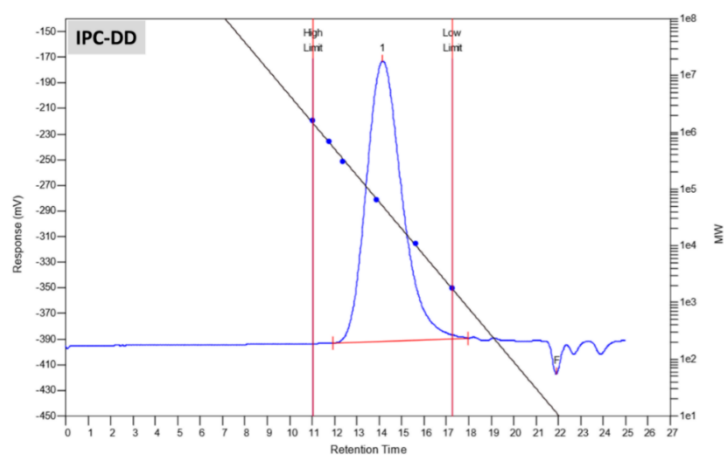
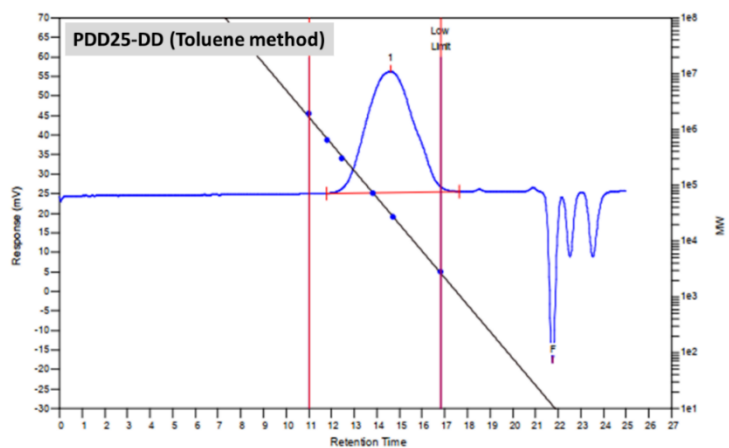




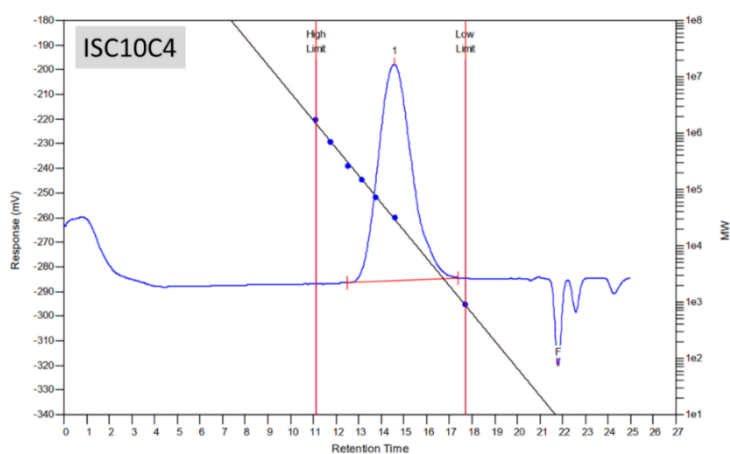
### 3.1.2 Synthesis of polyesters

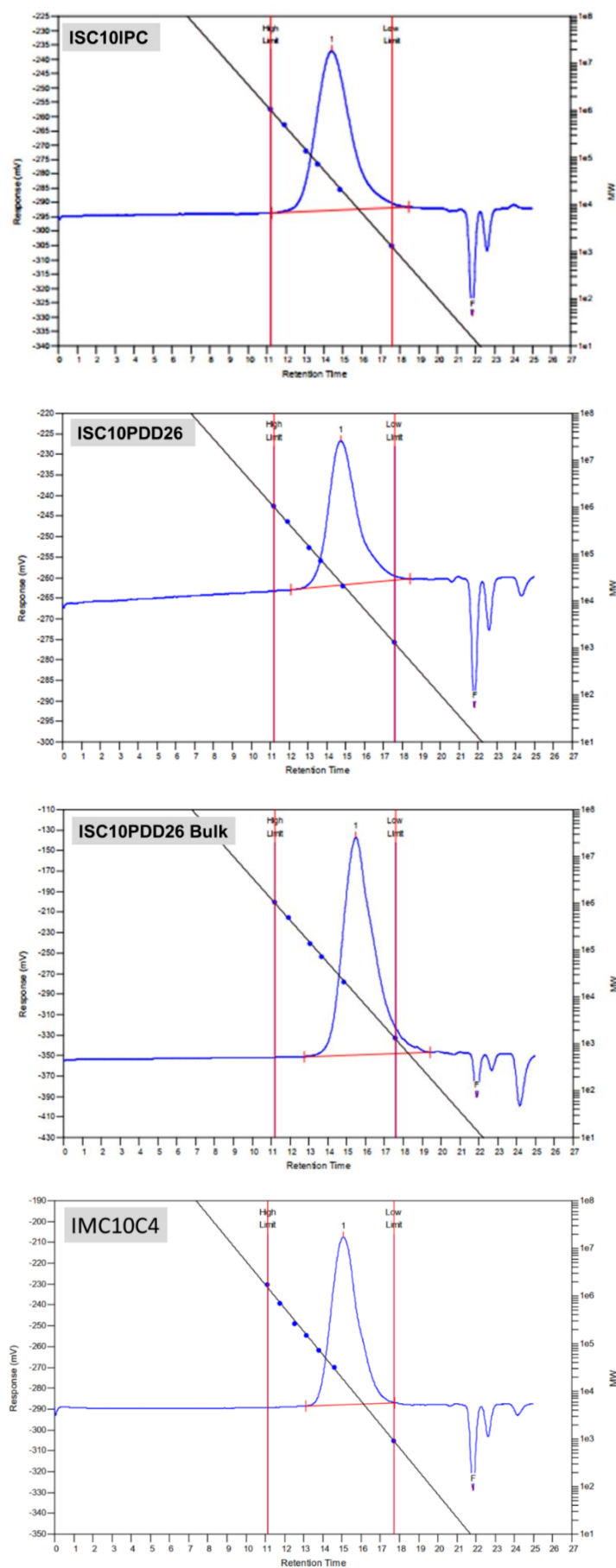




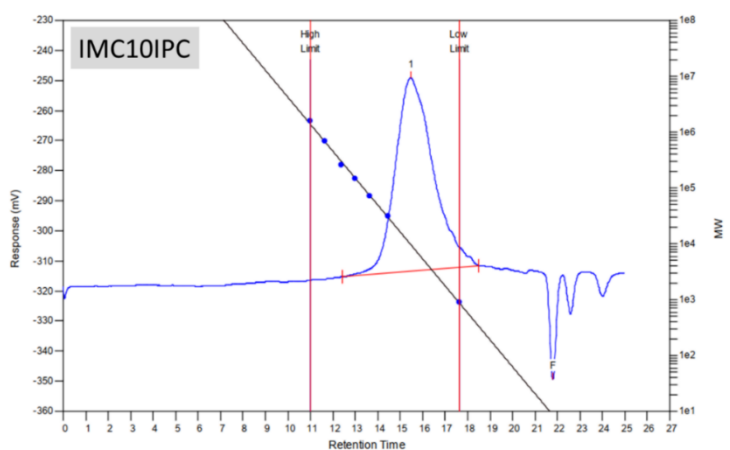
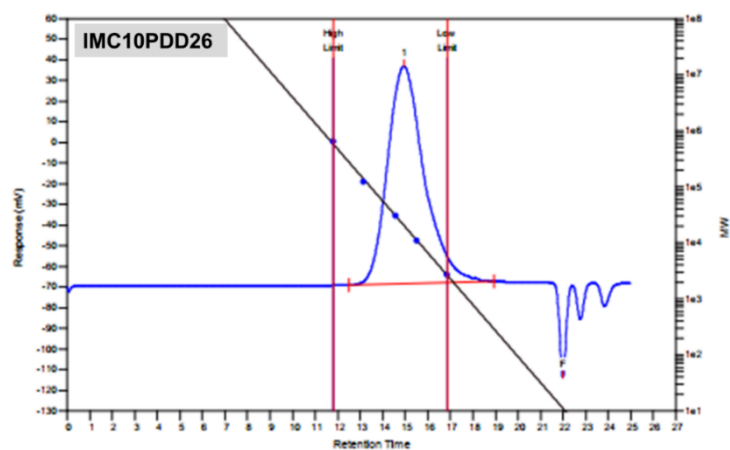


#### 4.I.1 Synthesis

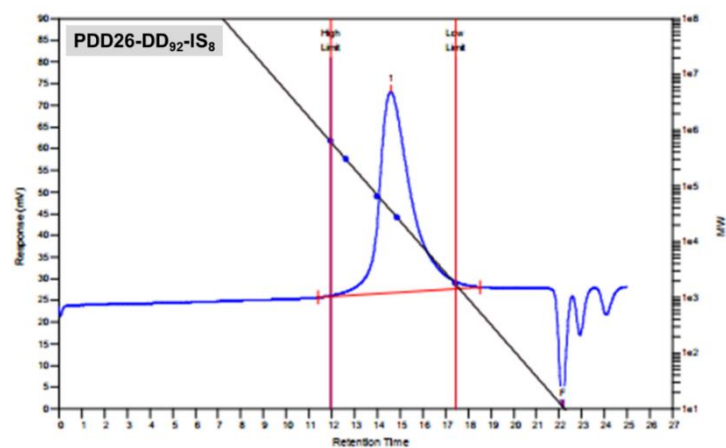


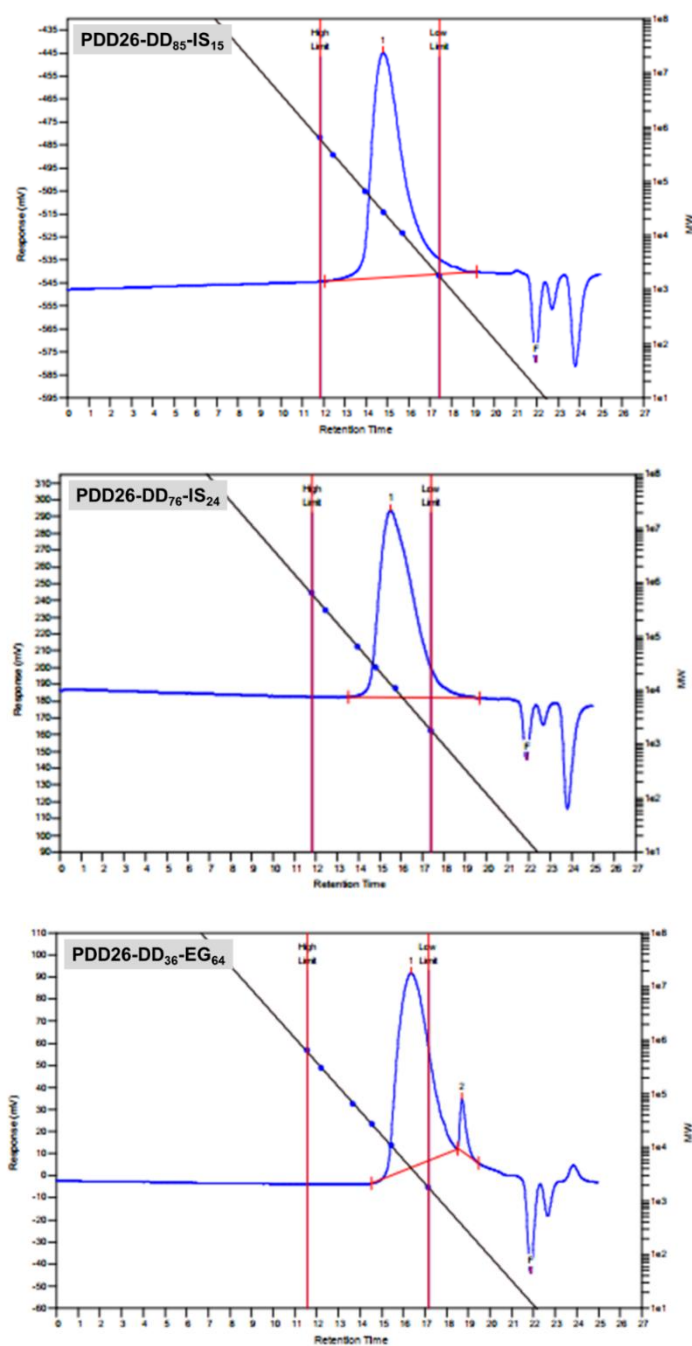






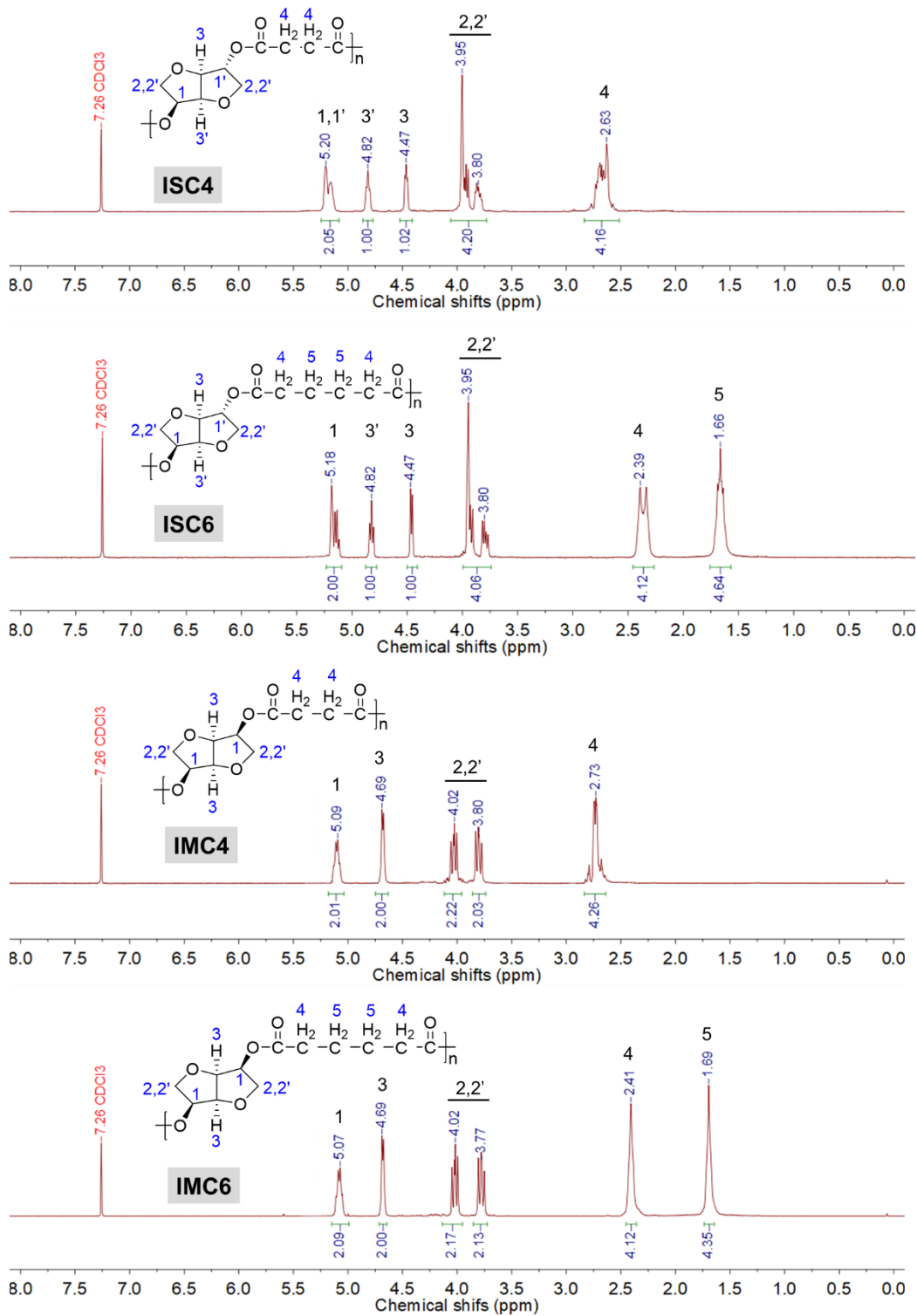
#### 4.2.II.3 SEC analysis

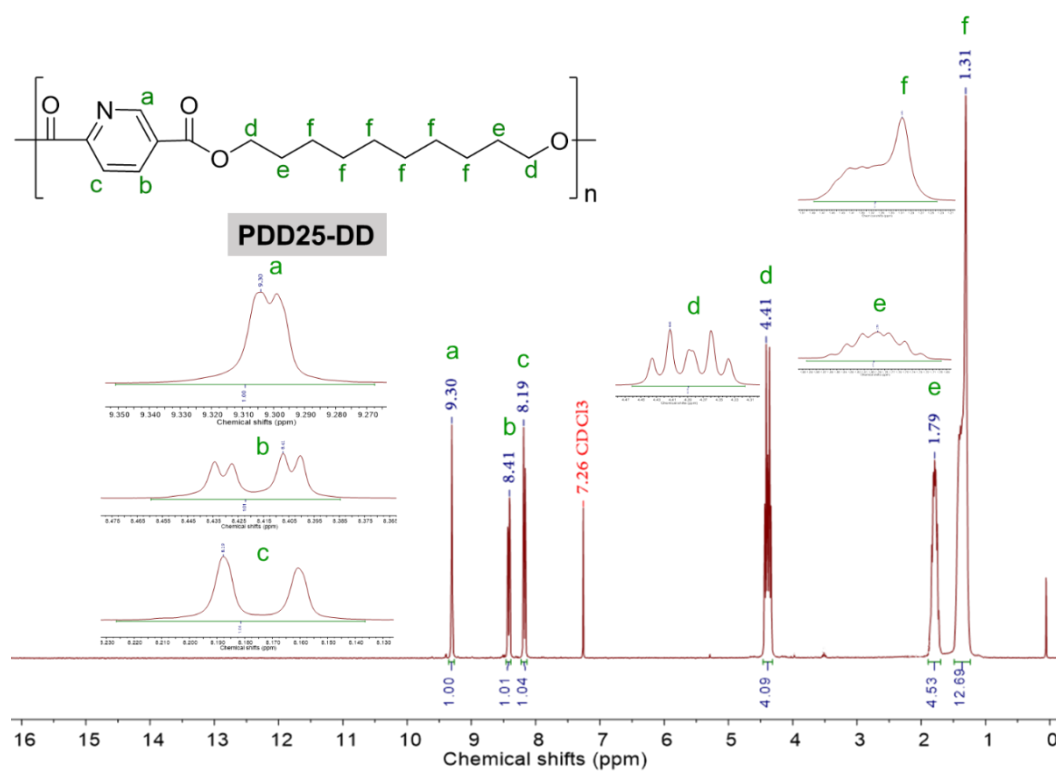
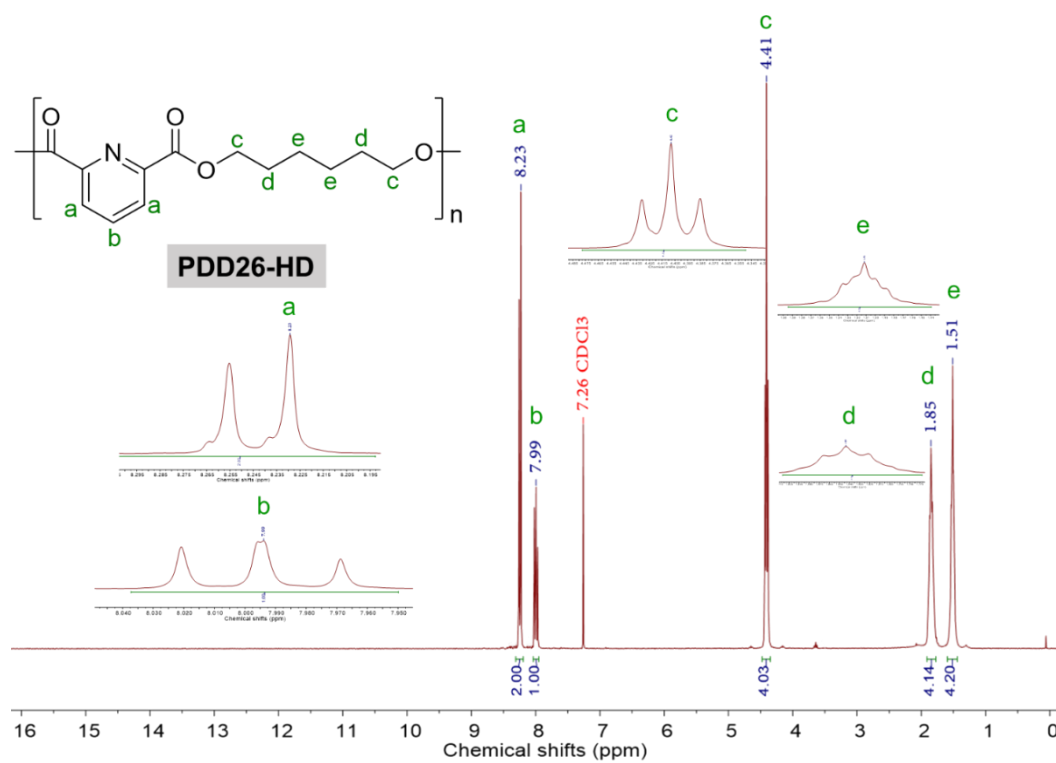


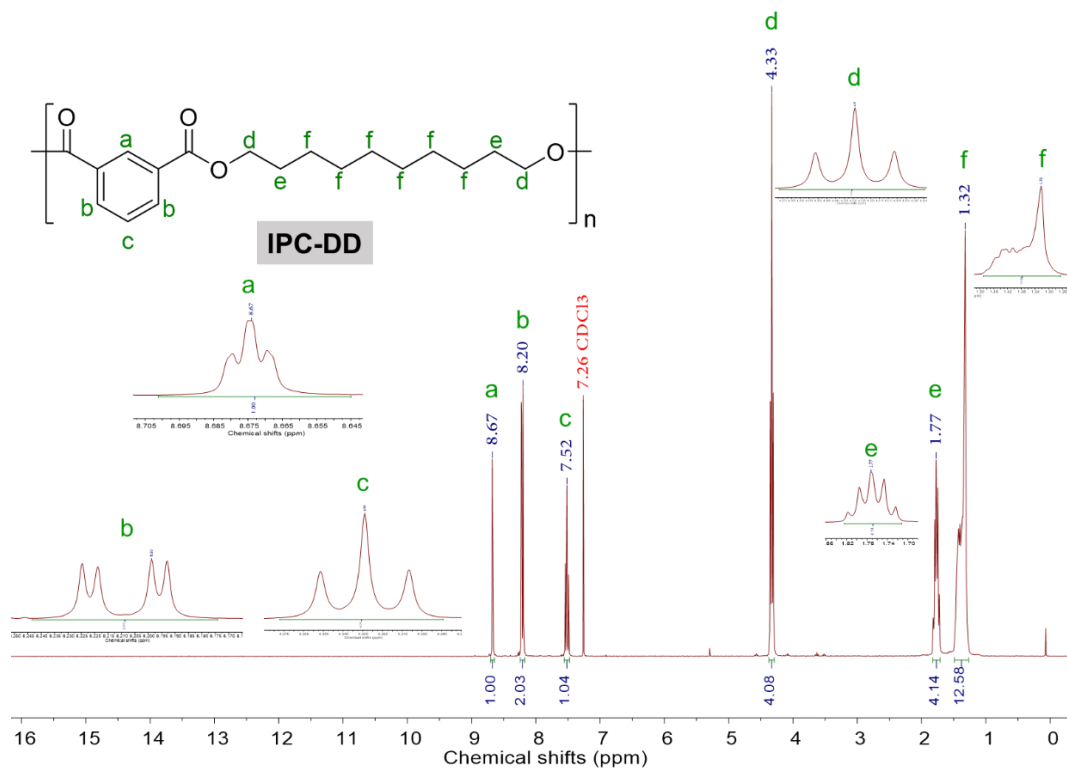


## Annex 5 NMR

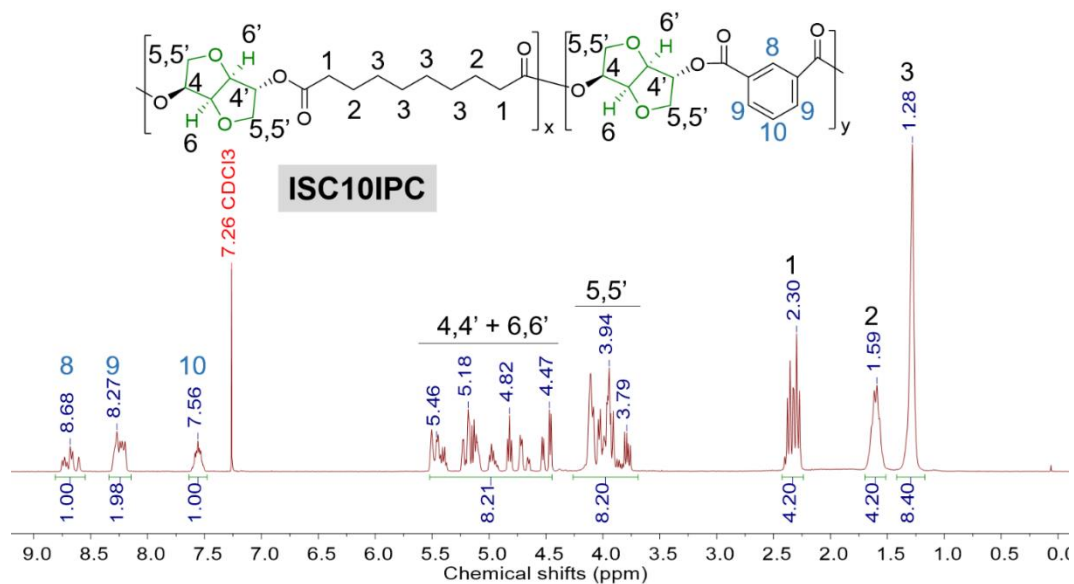
### 2.2.1 IS and IM aliphatic polyesters

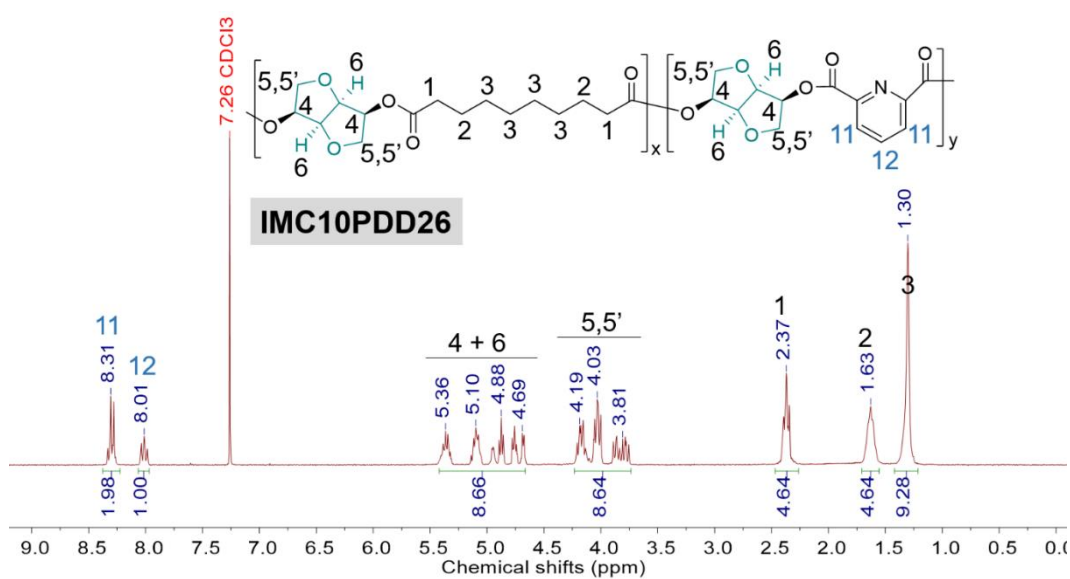
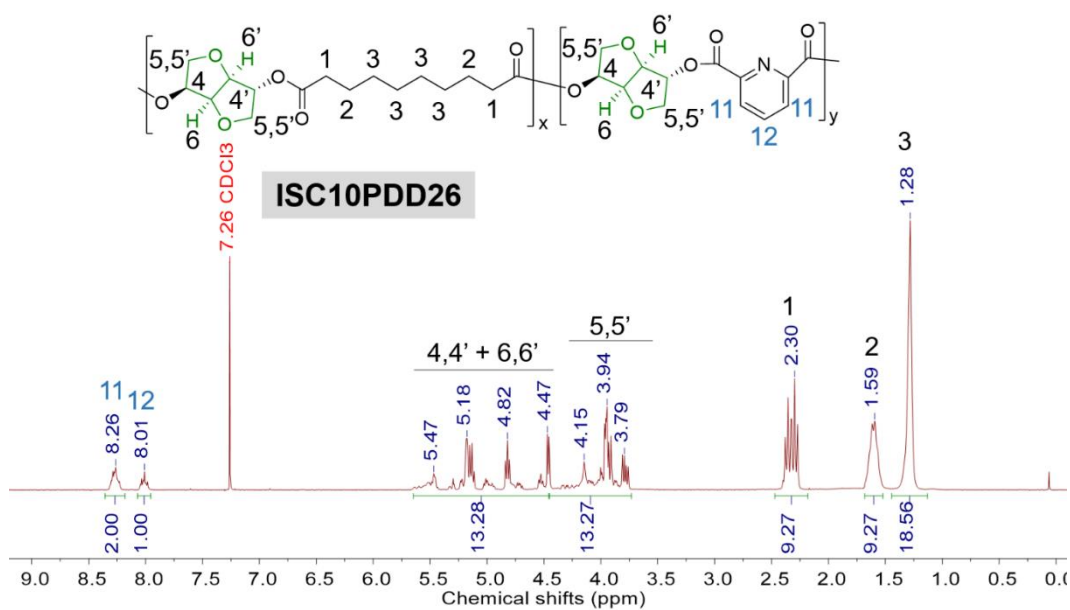
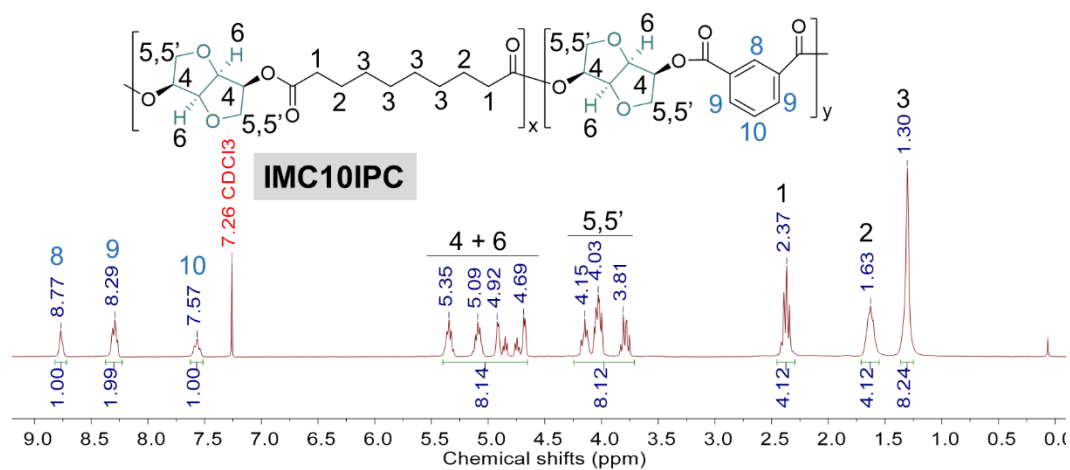


3.2.1.2  $^1\text{H}$  NMR analysis



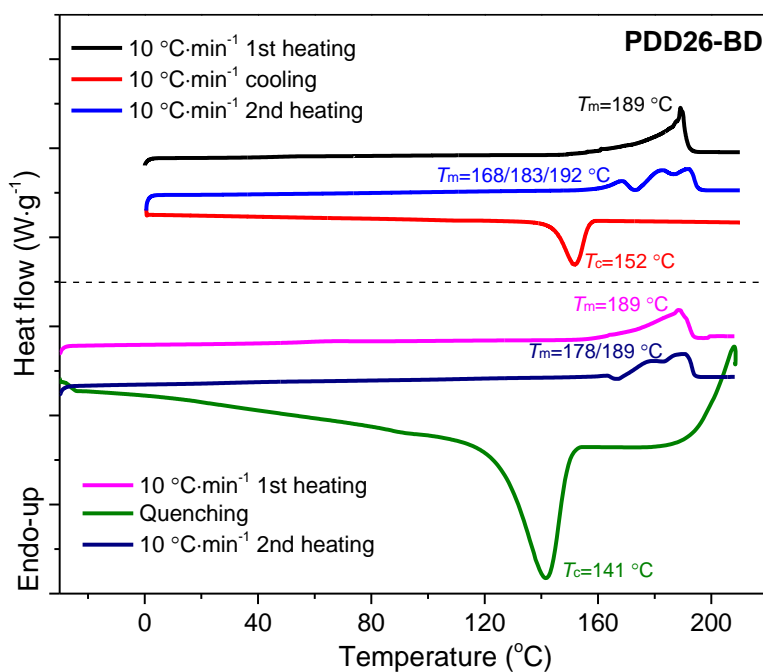
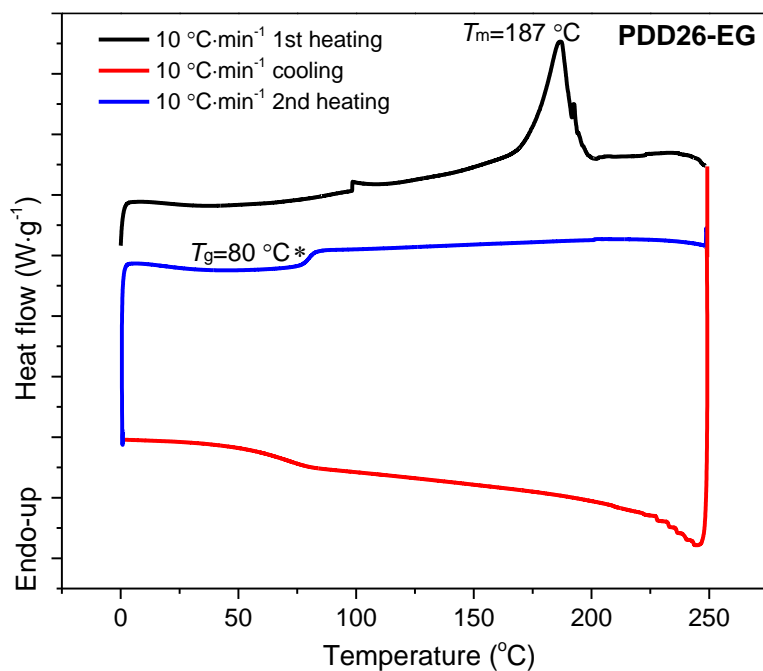
#### 4.I.2.1.1 <sup>1</sup>H NMR analysis

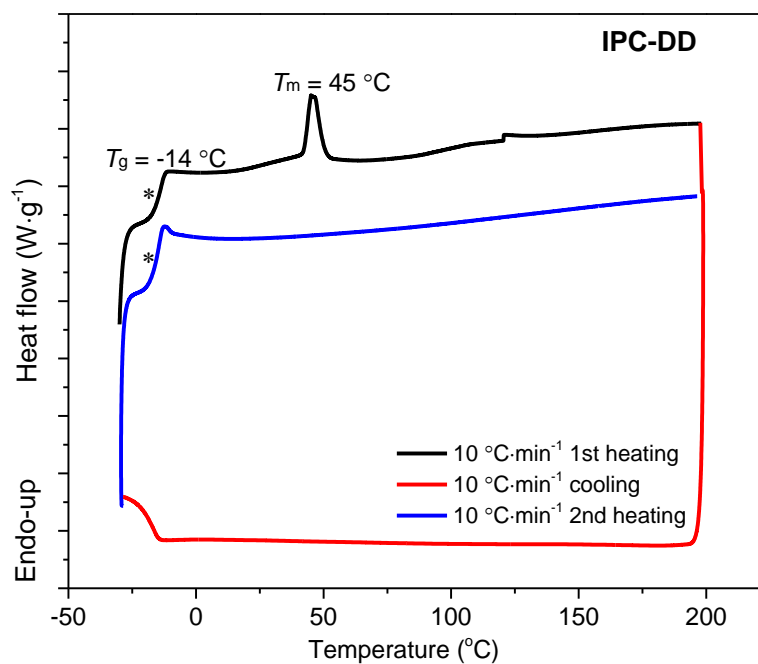
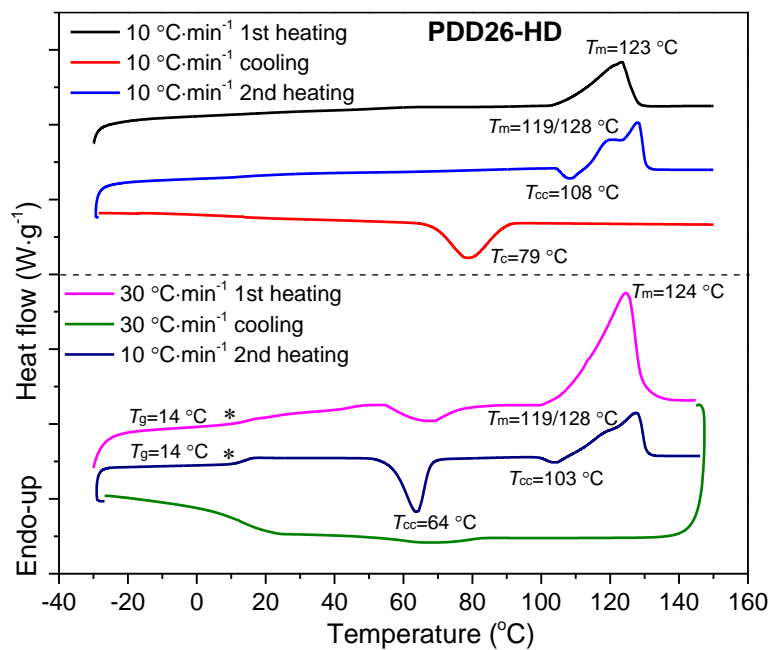




## Annex 6 DSC

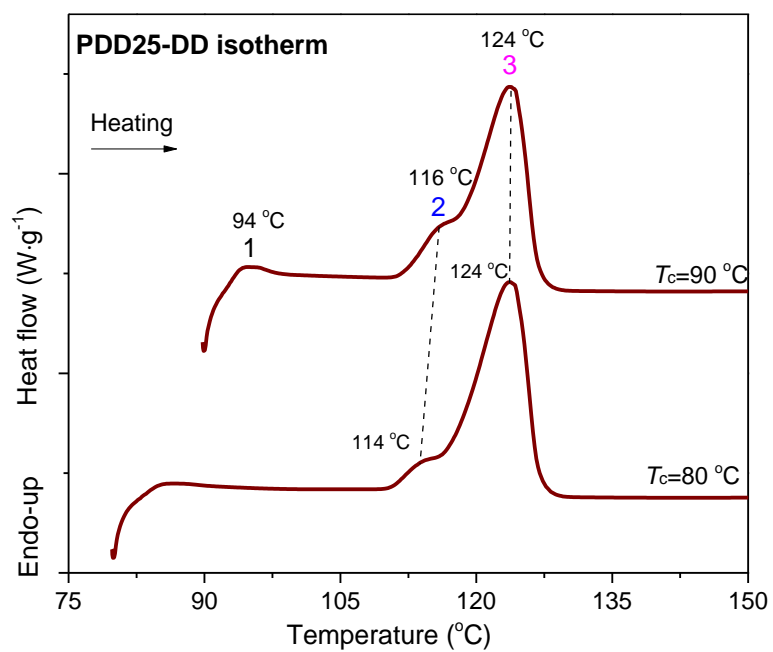
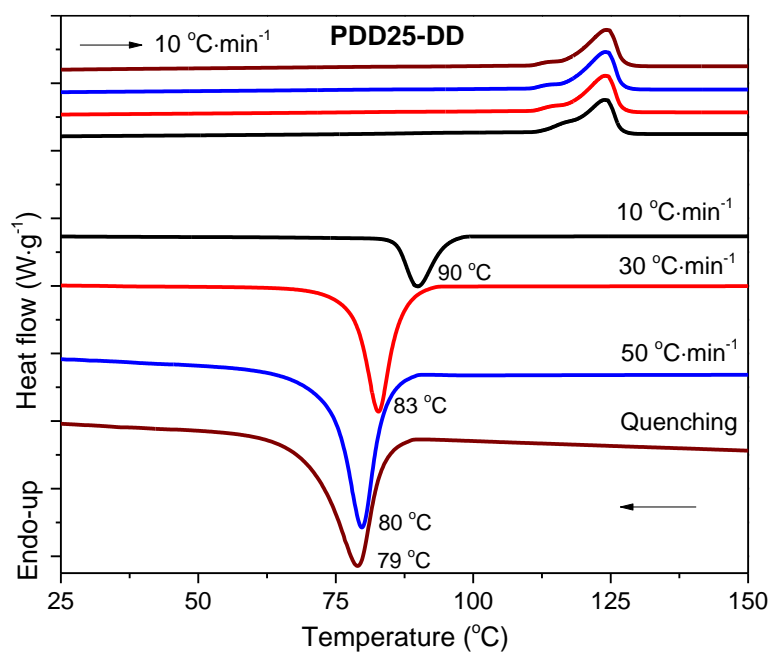
### 3.2.3 Differential scanning calorimetry (DSC)



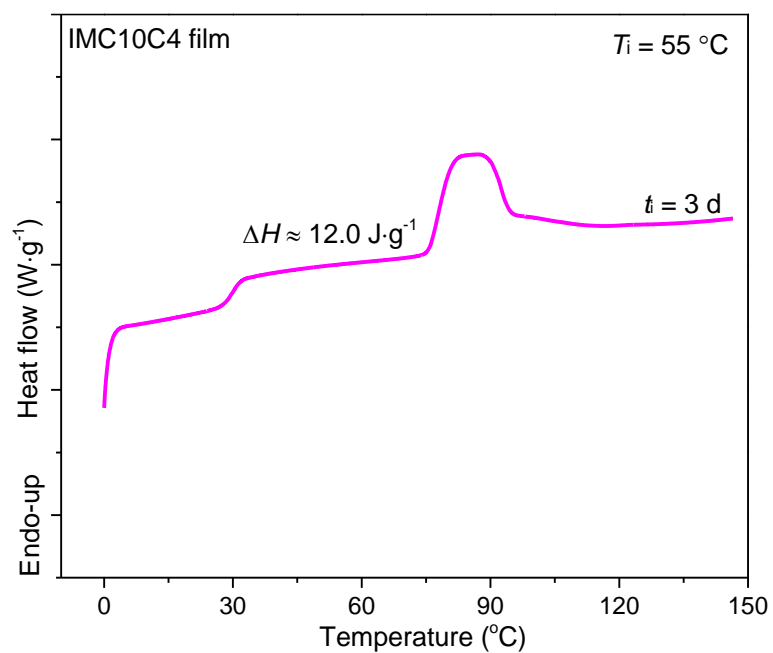




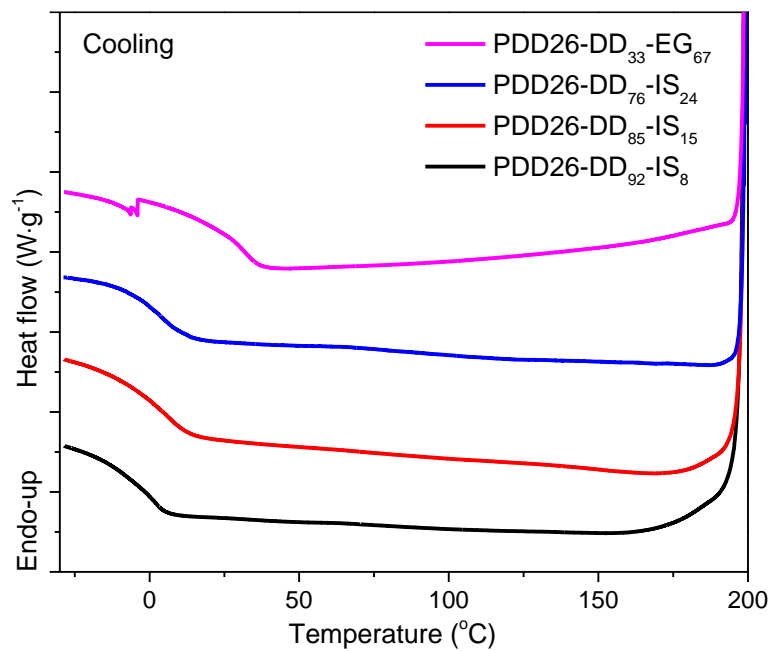
### 3.2.3.2 PDD25-DD crystallization properties investigation



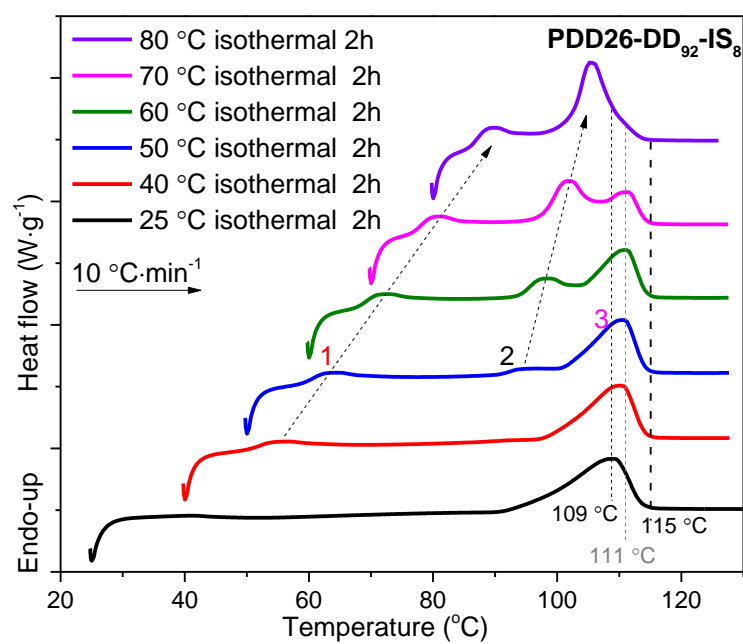
### 4.I.3.1 Hot pressing



### 4.II.2.5 Differential scanning calorimetry (DSC)



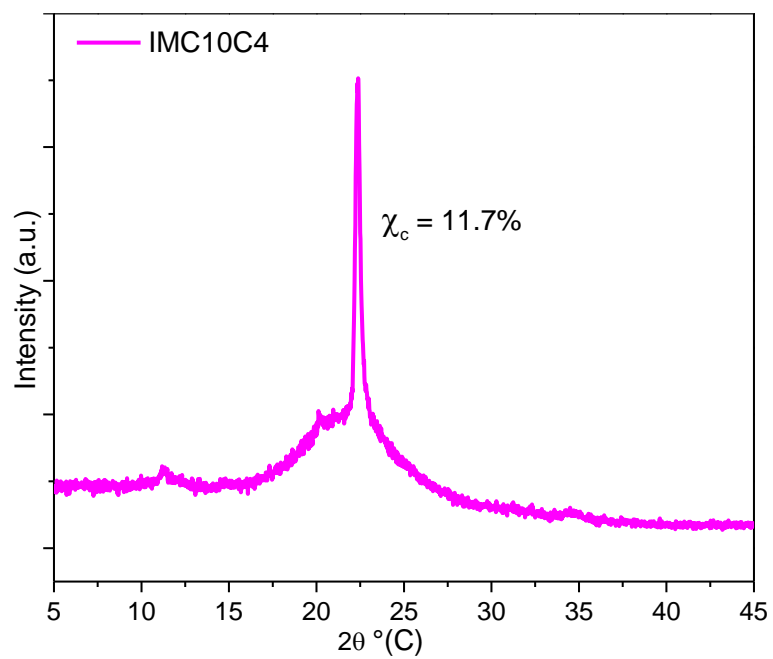
### 4.II.3.2 Crystallinity of films



---

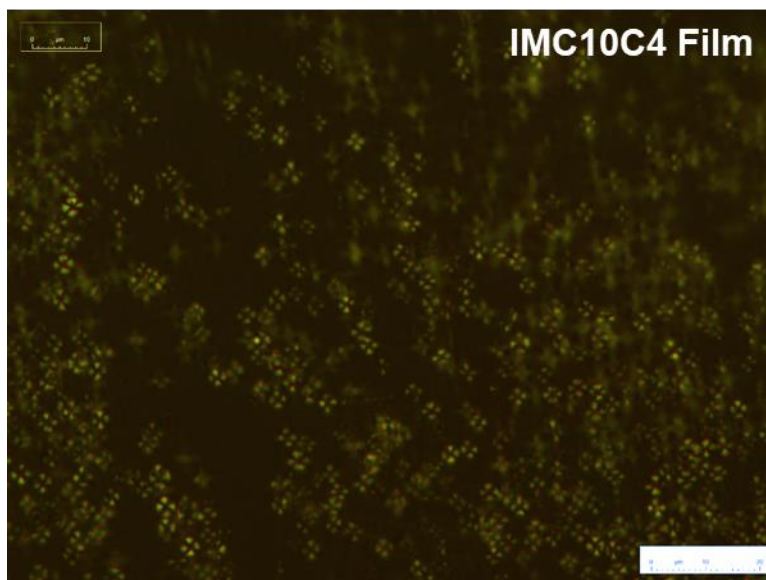
## Annex 7 XRD

### 4.I.3.1 Hot pressing



## **Annex 8 POM**

### **4.I.3.1 Hot pressing**



---

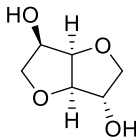
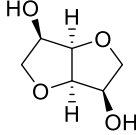
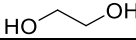
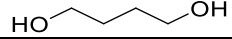
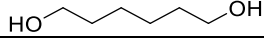
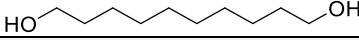
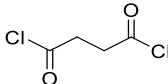
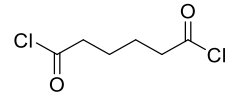
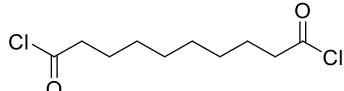
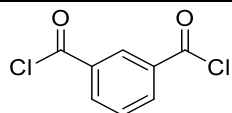
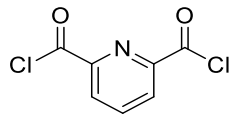
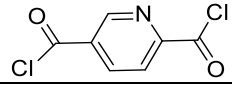
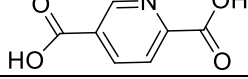
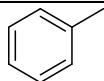
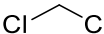
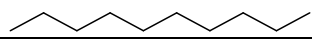
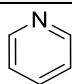
## Annex 9 Reagents

Isosorbide (98%), isomannide (95%), succinyl chloride (95%), adipoyl chloride (98%), sebacoyl chloride ( $\geq 95\%$ ), 2,6-pyridinedicarbonyl dichloride (97%), ethylene glycol ( $>99\%$ ), 1,4-butanediol ( $\geq 99\%$ ) and decane ( $>99\%$ ) were purchased from Sigma-Aldrich. Isophthaloyl chloride (98%) were obtained by Alfa Aesar. 1,10-decanediol ( $\geq 98\%$ ) was supplied by Merck. 1,6-hexanediol (97%), dry toluene (99.85%), dry dichloromethane (99.8%), dry pyridine (99.5%) and dry triethylamine ( $\text{EtN}_3$ , 99.7%) were obtained from ACROS Organics. Dichloromethane ( $\text{CH}_2\text{Cl}_2$ , reagent grade) was provided by Fisher Scientific. Methanol ( $\text{CH}_3\text{OH}$ , reagent grade) was supplied by VWR. All reagents were used as received without further purification.

Gases used for gas and water vapor permeation were  $\text{N}_2$  ( $> 99.99\%$ ),  $\text{CO}_2$  ( $> 99.99\%$ ),  $\text{O}_2$  ( $> 99.99\%$ ). They were purchased from Messer France S.A.S. and used as received.

The short names used in the manuscript, chemical structures and CAS numbers of the reagents are gathered in Table 2-1. Their physical information is given in Table 2-2, and the safety information in Table 2-3.

**Table A9-1** Short name, chemical structure and CAS number of the reagents

Reagent	Short name	Chemical structure	CAS
Diols			
Isosorbide	IS		652-67-5
Isomannide	IM		641-74-7
Ethylene glycol	EG		107-21-1
1,4-Butanediol	BD		110-63-4
1,6-Hexanediol	HD		629-11-8
1,10-Decanediol	DD		112-47-0
Acid dichlorides			
Succinyl chloride	C4		543-20-4
Adipoyl chloride	C6		111-50-2
Sebacoyl chloride	C10		111-19-3
Isophthaloyl chloride	IPC		99-63-8
2,6-pyridinedicarbonyl dichloride	PDD26		3739-94-4
2,5-pyridinedicarbonyl dichloride	PDD25		5620-35-9
2,5-pyridinedicarboxylic acid	PDA25		100-26-5
Solvents			
Toluene	toluene		108-88-3
Dichloromethane	CH <sub>2</sub> Cl <sub>2</sub>		75-09-2
Decane	decane		124-18-5
Catalyst			
Pyridine	Py		110-86-1

**Table A9-2** Physical information of the reagents

Reagent	$M^a$ (g·mol <sup>-1</sup> )	Appearance	$T_m^b$ (°C)	$T_b^b$ (°C)	Densit <sup>c</sup>
Diols					
IS	146.14	Colorless flakes	61-64	160 (10 mmHg)	-
IM	146.14	Colorless crystals	80-85	118	-
EG	62.07	Colorless liquid	-12.9	197.3	1.1135
BD	90.12	Clear liquid	20.2	228	1.0171
HD	118.17	Colorless crystals	38-42	250	0.96
DD	174.28	White flakes	71-75	305.4	-
Acid dichlorides					
C4	154.98	Light yellow liquid	15-18	190	1.407
C6	183.03	Light brown liquid	-	105-107 (2 mmHg)	1.259
C10	239.14	Light yellow liquid	-5~-3	168 (12 mmHg)	1.121
IPC	203.02	Colorless crystals	43-44	276	-
PDD26	204.01	Yellow-green crystals	56-58	284	-
PDA25	167.12	White powder	242-247(dec.)	-	-
Solvents					
Toluene	92.14	Colorless liquid	-95	110.6	0.87
CH <sub>2</sub> Cl <sub>2</sub>	84.93	Colorless liquid	-96.7	39.6	1.33
Decane	142.28	Colorless liquid	-30	174.1	0.73
Catalysts					
Py	79.10	Colorless liquid	-42	115.2	0.98










<sup>a</sup> Molecular weight; <sup>b</sup> at standard atmospheric pressure unless specified, melting point and boiling temperature, respectively; <sup>c</sup> at room temperature.



**Table A9-3** Chemical safety information of the reagents

Reagent	GHS	H statement	P statement
Diols			
IS	-		
IM	-		
EG	GHS07	H302	P264, P270, P301+P312, P330, and P501
BD	GHS07	H302, H336	P261, P264, P270, P271, P301+P312, P304+P340, P312, P330, P403+P233, P405 and P501
HD	GHS07	H315, H319, H335	-
DD	Not a hazardous substance or mixture according to the GHS		
Acid dichlorides			
C4	GHS05	H314	P260, P264, P280, P301+P330+P331, P303+P361+P353, P304+P340, P305+P351+P338, P310, P321, P363, P405, and P501
C6	GHS05	H314	P260, P264, P280, P301+P330+P331, P303+P361+P353, P304+P340, P305+P351+P338, P310, P321, P363, P405, and P501
C10	GHS05, GHS07	H302, H314	P260, P264, P270, P280, P301+P312, P301+P330+P331, P303+P361+P353, P304+P340, P305+P351+P338, P310, P321, P330, P363, P405, and P501
IPC	GHS05, GHS06, GHS07	H312, H314, H315, H317, H318, H319, H331, H335	P260, P261, P264, P271, P272, P280, P301+P330+P331, P302+P352, P303+P361+P353, P304+P340, P305+P351+P338, P310, P311, P312, P321, P322, P332+P313, P333+P313, P337+P313, P362, P363, P403+P233, P405, and P501
PDD26	GHS05	H314	P260, P264, P280, P301+P330+P331, P303+P361+P353, P304+P340, P305+P351+P338, P310, P321, P363, P405, and P501
PDA25	GHS07	H315 H319 H335-	P302 + P352 P305 + P351 + P338 -
Solvents			
Toluene	GHS02, GHS07, GHS08	H225, H304, H315, H336, H361, H373, H402	P210, P260, P280, P301 + P310, P370 + P378, P403 + P235
CH <sub>2</sub> Cl <sub>2</sub>	GHS07, GHS08	H302, H315 + H320, H351	P281, P305 + P351 + P338
Decane	GHS02, GHS08	H226, H304	P210, P233, P240, P241, P242, P243, P280, P301+P310, P303+P361+P353, P331, P370+P378, P403+P235, P405, and P501
Catalysts			
Py	GHS02, GHS07	H225, H302, H312, H332	P210, P233, P240, P241, P242, P243, P261, P264, P270, P271, P280, P301+P312, P302+P352, P303+P361+P353, P304+P312, P304+P340, P312, P322, P330, P363, P370+P378, P403+P235, and P501

## GHS Pictograms

		
Explosives GHS01	Flammables GHS02	Oxidizers GHS03
		
Compressed Gases GHS04	Corrosives GHS05	Acute Toxicity GHS06
		
Irritant GHS07	Health Hazard GHS08	Environment GHS09

## Hazard Statements (H-codes)

Physical hazards

H200	Unstable explosive	H240	Heating may cause an explosion
H201	Explosive; mass explosion hazard	H241	Heating may cause a fire or explosion
H202	Explosive; severe projection hazard	H242	Heating may cause a fire
H203	Explosive; fire, blast or projection hazard	H250	Catches fire spontaneously if exposed to air
H204	Fire or projection hazard	H251	Self-heating; may catch fire
H205	May mass explode in fire	H252	Self-heating in large quantities; may catch fire
H220	Extremely flammable gas	H260	In contact with water releases flammable gases which may ignite spontaneously
H221	Flammable gas	H261	In contact with water releases flammable gas
H222	Extremely flammable aerosol	H270	May cause or intensify fire; oxidizer
H223	Flammable aerosol	H271	May cause fire or explosion; strong oxidizer
H224	Extremely flammable liquid and vapour	H272	May intensify fire; oxidizer
H225	Highly flammable liquid and vapour	H280	Contains gas under pressure; may explode if heated
H226	Flammable liquid and vapour	H281	Contains refrigerated gas; may cause cryogenic burns or injury
H227	Combustible liquid	H290	May be corrosive to metals
H228	Flammable solid		
H229	Pressurized container may burst if heated		
H230	May react explosively even in the absence of air		
H231	May react explosively even in the absence of air at elevated pressure and/or temperature		

Environmental hazards

H400	Very toxic to aquatic life	H412	Harmful to aquatic life with long-lasting effects
H401	Toxic to aquatic life	H413	May cause long-lasting harmful effects to aquatic life
H402	Harmful to aquatic life		
H410	Very toxic to aquatic life with long-lasting effects	H420	Harms public health and the environment by destroying ozone in the upper atmosphere
H411	Toxic to aquatic life with long-lasting effects		

**Health hazards**

H300	Fatal if swallowed	H361	Suspected of damaging fertility or the unborn child
H301	Toxic if swallowed	H361d	Suspected of damaging the unborn child
H302	Harmful if swallowed	H361f	Suspected of damaging fertility
H303	May be harmful if swallowed	H362	May cause harm to breast-fed children
H304	May be fatal if swallowed and enters airways	H370	Causes damage to organs
H305	May be harmful if swallowed and enters airways	H371	May cause damage to organs
H310	Fatal in contact with skin	H372	Causes damage to organs through prolonged or repeated exposure
H311	Toxic in contact with skin	H373	May cause damage to organs through prolonged or repeated exposure
H312	Harmful in contact with skin	H300+H310	Fatal if swallowed or in contact with skin
H313	May be harmful in contact with skin	H300+H330	Fatal if swallowed or if inhaled
H314	Causes severe skin burns and eye damage	H310+H330	Fatal in contact with skin or if inhaled
H315	Causes skin irritation	H301+H311	Toxic if swallowed or in contact with skin
H316	Causes mild skin irritation	H301+H331	Toxic if swallowed or if inhaled
H317	May cause an allergic skin reaction	H311+H331	Toxic in contact with skin or if inhaled
H318	Causes serious eye damage	H302+H312	Harmful if swallowed or in contact with skin
H319	Causes serious eye irritation	H302+H332	Harmful if swallowed or if inhaled
H320	Causes eye irritation	H312+H332	Harmful in contact with skin or if inhaled
H330	Fatal if inhaled	H300+H310+H330	Fatal if swallowed, in contact with skin or if inhaled
H331	Toxic if inhaled	H301+H311+H331	Toxic if swallowed, in contact with skin or if inhaled
H332	Harmful if inhaled	H302+H312+H332	Harmful if swallowed, in contact with skin or if inhaled
H333	May be harmful if inhaled		
H334	May cause allergy or asthma symptoms or breathing difficulties if inhaled		
H335	May cause respiratory irritation		
H336	May cause drowsiness or dizziness		
H340	May cause genetic defects		
H341	Suspected of causing genetic defects		
H350	May cause cancer		
H351	Suspected of causing cancer		
H360	May damage fertility or the unborn child		

**Precautionary Statements (P-codes)****General precautionary statements**

P101	If medical advice is needed, have product container or label at hand
P102	Keep out of reach of children
P103	Read label before use

**Prevention precautionary statements**

P201	Obtain special instructions before use	P235	Keep cool
P202	Do not handle until all safety precautions have been read and understood	P240	Ground/bond container and receiving equipment
P210	Keep away from heat, hot surfaces, sparks, open flames and other ignition sources. No smoking	P241	Use explosion-proof electrical/ventilating/lighting/.../equipment
P211	Do not spray on an open flame or other ignition source.	P242	Use only non-sparking tools
P220	Keep/Store away from clothing/.../combustible materials	P243	Take precautionary measures against static discharge
P221	Take any precaution to avoid mixing with combustibles	P244	Keep valves and fittings free from oil and grease
P222	Do not allow contact with air	P250	Do not subject to grinding/shock/.../friction
P223	Do not allow contact with water	P251	Do not pierce or burn, even after use
P230	Keep wetted with ...	P260	Do not breathe dust/fumes/gas/mist/vapours/spray
P231	Handle under inert gas	P261	Avoid breathing dust/fumes/gas/mist/vapours/spray
P232	Protect from moisture	P262	Do not get in eyes, on skin, or on clothing
P233	Keep container tightly closed	P263	Avoid contact during pregnancy/while nursing
P234	Keep only in original container	P264	Wash ... thoroughly after handling

- P270 Do not eat, drink or smoke when using this product  
 P271 Use only outdoors or in a well-ventilated area  
 P272 Contaminated work clothing should not be allowed out of the workplace  
 P273 Avoid release to the environment  
 P280 Wear protective gloves/protective clothing/eye protection/face protection  
 P282 Wear cold insulating gloves/face shield/eye protection  
 P283 Wear fire/flame resistant/retardant clothing

- P284 In case of inadequate ventilation, wear respiratory protection  
 P231+232 Handle under inert gas. Protect from moisture  
 P235+410 Keep cool. Protect from sunlight

#### **Response precautionary statements**

- P301 IF SWALLOWED  
 P302 IF ON SKIN  
 P303 IF ON SKIN (or hair)  
 P304 IF INHALED  
 P305 IF IN EYES  
 P306 IF ON CLOTHING  
 P307 IF EXPOSED  
 P308 If EXPOSED or concerned  
 P309 IF EXPOSED or if you feel unwell  
 P310 Immediately call a POISON CENTER/doctor/...  
 P311 Call a POISON CENTER/ doctor/...  
 P312 Call a POISON CENTER/ doctor/.../if you feel unwell  
 P313 Get medical advice/attention  
 P314 Get medical advice/attention if you feel unwell  
 P315 Get immediate medical advice/attention  
 P320 Specific treatment is urgent (see ... on this label)  
 P321 Specific treatment (see ... on this label)  
 P330 Rinse mouth  
 P331 Do NOT induce vomiting  
 P332 If skin irritation occurs  
 P333 If skin irritation or a rash occurs  
 P334 Immerse in cool water/wrap in wet bandages  
 P335 Brush off loose particles from skin  
 P336 Thaw frosted parts with lukewarm water. Do not rub affected areas  
 P337 If eye irritation persists  
 P338 Remove contact lenses if present and easy to do. Continue rinsing  
 P340 Remove person to fresh air and keep comfortable for breathing  
 P342 If experiencing respiratory symptoms  
 P351 Rinse cautiously with water for several minutes  
 P352 Wash with plenty of water/...  
 P353 Rinse skin with water/shower  
 P360 Rinse immediately contaminated clothing and skin with plenty of water before removing clothes  
 P361 Take off immediately all contaminated clothing  
 P362 Take off contaminated clothing  
 P363 Wash contaminated clothing before reuse  
 P364 And wash it before reuse  
 P370 In case of fire  
 P371 In case of major fire and large quantities  
 P372 Explosion risk in case of fire  
 P373 DO NOT fight fire when fire reaches explosives  
 P374 Fight fire with normal precautions from a reasonable distance

- P375 Fight fire remotely due to the risk of explosion  
 P376 Stop leak if safe to do so  
 P377 Leaking gas fire - do not extinguish unless leak can be stopped safely  
 P378 Use ... to extinguish  
 P380 Evacuate area  
 P381 Eliminate all ignition sources if safe to do so  
 P391 Collect spillage  
 P301+310 IF SWALLOWED: Immediately call a POISON CENTER/doctor/...  
 P301+312 IF SWALLOWED: Call a POISON CENTER/doctor/.../if you feel unwell.  
 P302+334 IF ON SKIN: Immerse in cool water/wrap in wet bandages  
 P302+352 IF ON SKIN: Wash with plenty of water/...  
 P304+312 IF INHALED: Call a POISON CENTER or doctor/physician if you feel unwell  
 P304+340 IF INHALED: Remove person to fresh air and keep comfortable for breathing.  
 P306+360 IF ON CLOTHING: Rinse immediately contaminated clothing and skin with plenty of water before removing clothes  
 P308+311 If exposed or concerned: Call a POISON CENTER/ doctor/...  
 P308+313 If exposed: Call a POISON CENTER or doctor/physician  
 P332+313 If skin irritation occurs: Get medical advice/attention  
 P333+313 If skin irritation or a rash occurs: Get medical advice/attention  
 P335+334 Brush off loose particles from skin. Immerse in cool water/wrap in wet bandages  
 P337+313 If eye irritation persists get medical advice/attention  
 P342+311 If experiencing respiratory symptoms: Call a POISON CENTER/doctor/...  
 P361+364 Take off immediately all contaminated clothing and wash it before reuse  
 P362+364 Take off contaminated clothing and wash it before reuse  
 P370+376 In case of fire: Stop leak if safe to do so  
 P370+378 In case of fire: Use ... to extinguish  
 P370+380 In case of fire: Evacuate area  
 P301+330+331 IF SWALLOWED: Rinse mouth. Do NOT induce vomiting  
 P303+361+353 IF ON SKIN (or hair): Take off immediately all contaminated clothing. Rinse skin with water/shower

## Annex 9

- P305+351+338 IF IN EYES: Rinse cautiously with water for several minutes. Remove contact lenses if present and easy to do –continue rinsing
- P370+380+375 In case of fire : Evacuate area. Fight fire remotely due to the risk of explosion

- P371+380+375 In case of major fire and large quantities : Evacuate area. Fight fire remotely due to the risk of explosion

### **Storage precautionary statements**

- P401 Store ...
- P402 Store in a dry place
- P403 Store in a well ventilated place
- P404 Store in a closed container
- P405 Store locked up
- P406 Store in a corrosive resistant/... container with a resistant inner liner
- P407 Maintain air gap between stacks/pallets
- P410 Protect from sunlight.
- P411 Store at temperatures not exceeding ...°C ... °F
- P412 Do not expose to temperatures exceeding 50°C /122°F
- P413 Store bulk masses greater than ... kg/... lbs at temperatures not exceeding ...°C ... °F
- P420 Store away from other materials

- P422 Store contents under ...
- P402+404 Store in a dry place. Store in a closed container
- P403+233 Store in a well ventilated place. Keep container tightly closed
- P403+235 Store in a well ventilated place. Keep cool
- P410+403 Protect from sunlight. Store in a well-ventilated place
- P410+412 Protect from sunlight. Do not expose to temperatures exceeding 50°C /122°F
- P411+235 Store at temperatures not exceeding ...°C ... °F. Keep cool

### **Disposal precautionary statements**

- P501 Dispose of contents/container to ... [... in accordance with local / regional / national / international regulation (to be specified)].